ADDITIVE MANUFACTURED BRANCHED COLUMN CONNECTION

TILEN LEBAN

Additive Manufactured Branched Column Connection

Master (MSc) Thesis

February 29, 2024

Author
Tilen Leban

Thesis committee
Prof.dr.ir. Christian Louter (Chair)
Dr. Trayana Tankova (Daily supervisor)
Dr. Ir. Marcel Hermans (Daily supervisor)

Delft University of Technology
Faculty of Civil Engineering and Geoscience

ACKNOWLEDGEMENT

This dissertation, entitled "Additive manufactured branched column connection" represents the completion of my year long research efforts. It serves as the fulfillment of the graduation criteria for the MSc degree in Civil Engineering, specializing in Structural Design within the Building Engineering track, at Delft University of Technology, Faculty of Civil Engineering and Geosciences.

I acknowledge that the work I present in this thesis would not have been possible without the help of many people.

First and foremost, I wish to express my deep appreciation to the esteemed members of my committee. Prof.dr.ir. Christian Louter, in his role as the chair, merits special recognition for his unwavering guidance and support throughout the entirety of my master's thesis studies. His guidance has been crucial from start to finish, helping me with various questions and keeping me on track throughout the research process. Dr. Trayana Tankova and Dr. Ir. Marcel Hermans also deserve heartfelt thanks for generously sharing their extensive technical knowledge on additive manufacturing. Their advice, support, and encouragement were indispensable in navigating the complexities of this research journey.

Beyond the committee, I would like to extend my gratitude to José Galán Argumedo for his pivotal role in facilitating an enlightening additive manufacturing lab excursion and providing invaluable assistance during the lab work. His expertise and support were crucial to the success of the practical aspects of this research.

Furthermore, I am deeply thankful for the unwavering support of my friends and family, whose encouragement has been a constant source of strength throughout my academic journey. I especially appreciate my parents for their unwavering beliefs and encouragement, which have been a key factor in my success.

Thank you for taking the time to read and engage with my thesis.

Tilen Leban
January 2024

ABSTRACT

An investigation into the application of additive manufacturing to the production of structural joints was conducted for this thesis. The main goal was to determine all necessary aspects that someone needs to consider when designing a structural part that is intended to be printed with additive manufacturing. As an example, the branched column connection was selected due to its inherent limitations, which can be effectively addressed through the integration of additive manufacturing techniques.

The advent of Industry 4.0 has ushered in a wave of new manufacturing methodologies, prominently among them being additive manufacturing. Within the construction realm, wire arc additive manufacturing (WAAM) stands out as particularly advantageous due to its ability to yield high mechanical properties comparable to conventionally manufactured materials, coupled with a high deposition rate. WAAM operates by melting a continuous wire feed through an electric arc, layering metal systematically to construct intricate 3D structures. As with any manufacturing process, WAAM operates within certain constraints dictating the types of objects feasible for production.

To ensure compatibility with WAAM while achieving desired structural and aesthetic benchmarks, three laboratory tests were conducted. These tests scrutinized the impact of input process parameters, overhang, and overlapping on the quality of the build. Factors such as travel speed, wire feed speed, voltage, and current were examined for their influence on welding bead dimensions and quality. Additionally, an investigation into how the percentage of overlap affected print quality was done. Among the constraints, the most pivotal one was the overhang limitation, determining the minimum allowed overhang angle in perpendicular and parallel directions depending on the direction of the print. The calculated values of the minimum overhang angle in perpendicular and parallel directions were 43.5° and 48.2° respectively.

The primary objective in designing the connection was to reduce the necessary material for the branched column connection's manufacture. Topology optimization (TO) played a crucial role in achieving this goal. Various models were constructed, each differing in TO input parameters to find the model with the lowest required mass while maintaining adequate structural performance. These models varied based on TO objectives (equivalent von Mises stress, compliance, mass, and volume) and TO constraints (either mass retain percentage or maximum stress), while also integrating manufacturing constraints obtained from lab tests. Ultimately, the model that offered the lowest mass and satisfactory structural performance focused on compliance as its objective, while retaining 15% of its initial mass. This signifies the discovery of the most optimized topology model. Additionally, engineering solutions for connecting the columns and branches and on site assembly were proposed, catering to both wooden and steel profiles.

Based on the above explained research a design guideline could be proposed and includes all necessary steps and considerations that someone needs to take into account when designing a connection manufactured with WAAM. The steps of the guideline include: 1. Selection of additive manufacturing process; 2. Material selection; 3. Determination of additive manufacturing process manufacturing limitations; 4. Design phase including TO with the proposed input parameters.

In illustrating the advantages and limitations of WAAM in the construction industry and proposed design guideline, a case study involving a comparative analysis between a steel plate and a WAAM branch column connection was done. This study centered on the real life project, 6 Bevis Marks in London. The findings showcased a notable reduction in the required material, plummeting from an initial 136 kg to 81.5 kg through the implementation of TO and WAAM. However, the limitations of this approach were apparent in the increased manufacturing time and costs. Manufacturing time increased from 7.5 hours to 12.9 hours, accompanied by a rise in costs from 718 € to 1141 €.

TABLE OF CONTENT

LIST OF FIGURES

LIST OF TABLES

NOMENCLATURE

ABBREVIATIONS

3D	Three dimensional
AM	Additive manufacturing
WAAM	Wire arc additive manufacturing
BJ	Binder jetting
DED	Direct energy deposition
ME	Material extrusion
MJ	Material jetting
PBF	Powder bed fusion
SL	Sheet lamination
VATP	VAT photopolymerization
CAD	Computer aided design
CAM	Computer aided manufacturing
GMAW	Gas metal arc welding
TIG welding	Tungsten inert gas welding
GTAW	Gas Tungsten Arc Welding
PAW	Plasma arc welding
HT	Heat treatment
SP	Shot peening
AFM	Abrasive flow Machining
LSP	Laser shock peening
FSP	Friction stir processing
YS	Yield strength
US	Ultimate strength
EC	Eurocode
TO	Topology optimization
ETFE	Ethylene tetrafluoroethylene
SLS	Selective laser sintering
LCA	Life cycle assesment
EIC	Environmental impact categories

SYMBOLS

TS	Travel speed
WFS	Wire feed speed
HI	Heat input
I	Current
V	Voltage
h	Weld bead height
w	Weld bead width
h/w	Weld bead form factor
u	Thermal efficiency
Δd	Offset distance

INTRODUCTION

1. INRODUCTION

1.1 PROBLEM RELEVANCE

In recent years, sustainability has gained a lot of attention, especially due to rising global warming awareness. The construction industry is one of the biggest natural resource consumers and contributors to air pollution, accounting for 50 % of raw material resource consumption, 40 % of energy consumption, and 20 % of greenhouse gas emissions [1.1]. Therefore, big improvements can and should be done to lower these impacts and increase the overall sustainability of the construction. Futhermore the desire to improve efficiency, and thus increase productivity, lower costs and lower production time is of course also present. All these aspects are pillars of the so called Industry 4.0, which is revolutionizing the way companies manufacture, improve and distribute their products.

One of the measurements that have already been considered and implemented into the international and national legislation (e.g. Netherlands Integral Circular Economy Report 2021) [1.1] is circular construction, where recyclability and reusability are the main focal point of this methodology. Circular construction is an approach that implements sustainability and circularity with the purpose to reduce the environmental impact of construction projects. This means that structures are designed in a way that materials and resources are kept in use for as long as possible, and waste and emissions are minimized. With this, the usage of raw materials is minimized or zero. The main goal of circular construction is to not only construct buildings that are environmentally friendly but also economically and socially sustainable, and thus provide long term benefits for both people and the planet. Dutch government vowed to reach fully circular economy by 2050 and at least halve the use of primary abiotic raw materials by 2030.

Based on the MSc thesis of Tim Vonck - An Eco-Effective Structure [1.2], there are 10 circular design strategies that can contribute to lowering the environmental footprint and/or circularity of construction. These strategies are material selection, material minimization, durability, waste minimization, maintenance, reusability, disassembly, recyclability, adaptability, and flexibility. Some of these strategies can be conflicting, so it is important to evaluate them depending on the purpose of the construction. In the thesis, some of the stated strategies (material selection, material minimization, waste minimization, reusability, etc.) will be taken into the consideration and implemented in the design.

Another important development, that has gained popularity in recent decades is off site construction, also known as modular construction or prefabricated construction. This refers to construction where structural elements are produced in a location that is different from their final installation location. Because of that structural elements can be considered as standardized products, which leads to increased productivity, and therefore rising popularity of the method. With recent developments, modular construction has become a cost effective and essential construction approach. Based on research done by McKinsey [1.3] implementation of modularity into the construction process can halve the time and cut the project costs by 20 %.

One of the newer inventions that include both aspects (circularity and modularity) is a so called additive manufacturing (AM), also known as 3D printing. It is a new manufacturing technique used to make three dimensional solid objects from a digital model. Because this technique allows almost complete freedom of shape of the printed objects, different circular design strategies like material minimization, waste minimization, and disassembly can be easily achieved. Additive manufactured elements are also completely prefabricated, allowing for the production of

innovative and complex elements (structures) without time consuming traditional forming and assembly process. Different materials, namely plastic, metal, and composite, can be used for different manufacturing methods. For now, most of the research has been carried out on the 3D printing of concrete, with the purpose of reducing the need for formwork and construction time. One of the more commonly used methods for the 3D printing of metals is so called wire arc additive manufacturing (WAAM), which uses a welding process to build metal parts layer by layer. Compared to other 3D printing techniques, it is relatively fast and efficient since it allows for fast production while also achieving high characteristics of printed products. For now, the usage of additive manufacturing is in the construction industry still very much limited mostly due to the unavailability and price of (large scale) 3D printers. Nevertheless, its development and increased popularity can be in the next decades expected, since it aligns with the guidelines of Industry 4.0, which is inevitable.

1.2 RESEARCH OBJECTIVE

AM is in the construction industry compared to other industries (aerospace, dental, medical, automotive, etc.) still very rarely used (figure 1.1). This is mostly due to a lack of research done and a habit of using already well established design models. As explained in the introduction there is a big push for the implementation of circularity and modularity into the construction industry, and thus move closer to the desired ''Industry 4.0''. Therefore, it is expected that additive manufacturing will be one of the emerging technologies in the next years. [1.4]

The research objective of this master's thesis is to explore the potential of additive manufacturing (more specifically WAAM) in revolutionizing the design and production of branch column connections in the construction industry. This study aims to assess the feasibility of WAAM in construction, optimize connection designs for WAAM, and conduct comparative analyses with traditional manufacturing methods. The concluding section of the thesis will present the advantages and limitations associated with the utilization of additive manufacturing for the production of structural components.

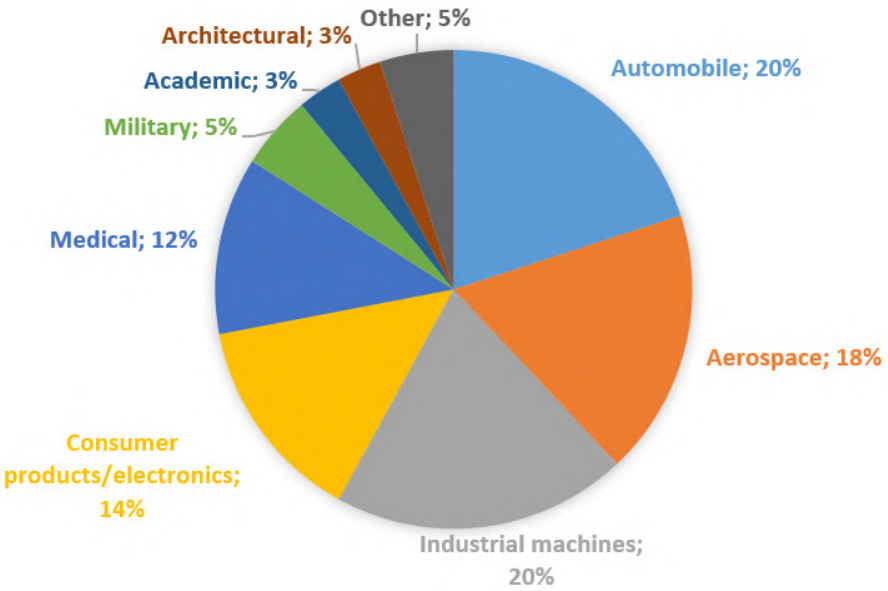

Figure 1.1: Additive manufacturing by industry sectors [1.5]

1.3 RESEARCH QUESTIONS

What strategies and considerations are involved in integrating additive manufacturing into the construction industry, and what specific advantages and limitations characterize its application?

Sub questions:
- What are the existing applications of additive manufacturing in structural connections within the construction industry?
- What kind of additive manufacturing processes and materials are available?
- Which additive manufacturing limitations need to be consider in the design of the connections?
- How to minimize the material consumption in the design of the connections?
- How to lower the complexity of the connection‘s design and on site assembly?

1.4 METHODOLOGY

The work in the thesis can be split into four parts/phases, where research questions from subchapter 1.3 are answered. Each phase refers to the previous phase.

- Phase 1

In the first phase, the literature review on additive manufacturing will be done, where the basics of 3D printing will be explained. To get a better overview of additive manufacturing, seven different printing processes will be shown and elaborated based on their usage, materials and their mechanical properties, and build costs. The selected process i.e. WAAM will be further explored in more detail. Relevant material properties of the WAAM produced objects will be also stated.

- Phase 2

In the second phase the continuation of the first phase, with more emphasis on the manufacturing limitation of the WAAM process will be done. WAAM has as any other manufacturing technology, constraints within which objects can be manufactured. To design an object that is able to be manufactured with WAAM and at the same time achieve the desired structural and aesthetical performance, it is important to carefully examine these constraints. To do so, an additional literature review will be conducted on three main manufacturing limitations, namely input process parameters, overhangs, and overlaps. To verify and complement the existing research, individual lab experiments will be completed from which the limit manufacturing values could be gathered.

- Phase 3

Phase three will start with the state of the art on the existing projects where additive manufacturing was used to produce structural connections. Based on this the selection of branch column connection and the explanation of its structural behaviour with an emphasis on advantages and limitations will be done. The main part of this phase is the topology optimization of the two branch connection. Here the influence of different topology optimization input parameters will be examined and the selection of the most optimal design will be done. The selection will be done based on structural validation and material minimization. The engineering solutions will also be proposed, which include the integration of the designed connection with branch and column profiles and the on site assembly procedure.

- Phase 4

Phase four includes a case study where findings from the analysis that was conducted throughout the thesis will be implemented on a real life project. The selected project is 6 Bevis Marks in London where five branch column connections were manufactured by welded steel plates. These conventionally manufactured connections will be recreated by using WAAM technology. Both connections (conventionally manufactured and WAAM manufactured) will then be compared based on the required amount of material, manufacturing time, and manufacturing costs.

1.5 REFERENCES

[1.1] Hanemaaijer. A., Kishna. M., Brink. H., Koch. J., Gerdien Prins A., Rood. T. 2021. Netherlands Integral Circular Economy Report 2021. PBL Netherlands Environmental Assessment Agency. Available at: https://www.pbl.nl/sites/default/files/downloads/2021-pbl-icer2021_english_summary-4228.pdf

[1.2] Vonck, T. 2019. An Eco-Effective Structure: A qualitative approach into eco-effective structural design perspectives, criteria, and strategies both in theory as in practice. Master's Thesis Delft University of Technology. Available at: http://resolver.tudelft.nl/uuid:42e532da-e578-4cd0-8288-b40867b8366e

[1.3] McKinsey & Company. 2019. Modular Construction: From Projects to Products. Available at: https://www.mckinsey.com/business-functions/operations/our-insights/modular-construction-from-projects-to-products

[1.4] Pasco, J.; Lei, Z.; Aranas, C., Jr. 2022. Additive Manufacturing in Off-Site Construction: Review and Future Directions. Buildings. Available at: https://doi.org/10.3390/buildings12010053

[1.5] Vafadar. A., Guzzomi. F., Rassau. A., Hayward. K. 2021. Advances in Metal Additive Manufacturing: A Review of Common Processes, Industrial Applications, and Current Challenges. Applied Science. Available at: https://doi.org/10.3390/app11031213

ADDITIVE MANUFACTURING

2. ADDITIVE MANUFACTURING - STATE OF THE ART

2.1 ADDITIVE MANUFACTURING

Additive manufacturing, widely known also as 3D printing is a fast emerging technology that uses computer aided design (CAD) drawings to produce a physical object. It is a layer by layer fabrication technology, which allows the easy production of complex shapes. Even though the first commercialized 3D printing process was developed already in 1980 by Charles Hull [2.1], AM is still considered a fairly new and undeveloped technology. Considering that AM allows opportunities and possibilities for companies to increase manufacturing efficiency, while also following the guidelines of circularity, and thus sustainability, big development and increased usage of this technology in the next years can be expected. Nowadays, 3D printing technology is mostly used for the production of elements with smaller dimensions and complex geometries. It is especially useful in agriculture, healthcare, automotive, and aerospace industries, where complex details are present and high accuracy is needed. In other industries, for example in construction, AM is yet to be regularly used.

Manufacturing companies all around the World thrive toward fully automated production lines and revolutionization of the whole manufacturing process. AM is a key part of this change since it increases production speed while also reduce costs. Another big advantage is that it allows consumers to have a greater influence on the final product's design so that the element will fit their specific requirements. This is due to the almost complete freedom of shape of the products that AM machines can produce. Traditional mass production methods are replaced by small batches of customized products that comply with specific criteria. Products can be manufactured on demand, meaning that response time is shortened, there is no need for big storage space, delivery costs are lowered, and individual parts can be easily replaced. This is possible due to direct production from CAD models, meaning that there is no need for additional tools or molds. As explained in the introduction two important aspects of the future developments for ''Industry 4.0'' are circularity and modularity. AM is proven to be able to provide a number of sustainable advantages. Waste minimization is achieved with the capability to optimize products in a way that the minimum amount of material is needed, and thus light weight is achieved. Most of the materials used in AM (mostly metals) have a high ability to reuse waste material (e.g. metal powders are 95 – 98 % recyclable [2.2]).

Even though AM seems like a perspective manufacturing process, it is still in the early stages of its development, and thus has several disadvantages. The biggest one is the price of the 3D printer itself. At the moment the machine price per part is still the biggest component of the total cost of the product, making them relatively unavailable. Because of that most AM technologies are currently only available for low volume production. It can be predicted that the price will fall with further development and normalization of AM technology. This might still take some time since the whole thinking process behind the approach of AM in many ways differs from traditional production methods (in AM the material is not taken off, but added where needed). There is also a big lack of globally accepted technical legislations regarding the AM. This can cause quite a lot of problems since technologies and materials without proper standardization can not be qualified. There are multiple organizations currently working on developing technical

standards for AM, like International Organisation for Standardisation (ISO), American Society for Testing and Materials (ASTM), Deutsches Institut für Normung (DIN), British Standards Institution (BSI), etc. Another drawback is that the size of the product is limited to the size of the printer. For the medical industry for example this is not a concerning problem, since most of the elements are small. On the other hand, limiting element sizes have in the construction industry big impact. Besides that, most AM technologies need some kind of post processing to reduce printing errors such as lack of fusion and porosity. Post processing will increase the quality of the product, but will at the same time increase already high production costs. [2.8]

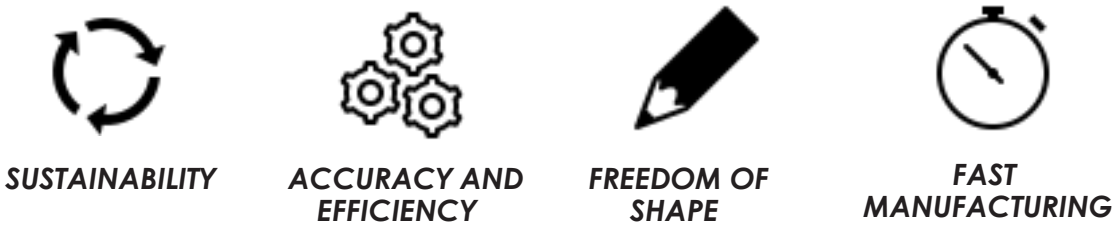

Figure 2.1: Advantages of additive manufacturing

2.1.1 3D PRINTING MATERIALS

Like any other manufacturing process, 3D printing requires materials that meet the specifications needed to build high quality products. With the further development of AM more and more different materials, with specific characteristics are becoming available. There is a wide range of materials available, namely metals, concrete, polymers, composites, and other smart materials. Another advantage of AM concerning material usage is the possibility of implementing integrity into the design. This means that products that consist of various parts with different materials can be replaced by one integrated assembly. This type of manufacturing can significantly reduce costs, time, and quality problems. Materials listed below were conducted from the research paper of Shahrubudin et al. [2.3].

- Metals

3D printing of metals is mostly used in the aerospace, automobile, and medical industry, where big accuracy and manufacturing of complex details is needed. There are different types of metals available for different types of AM technology, namely aluminum alloys, cobalt-based alloys, nickel-based alloys, stainless steel, and titanium alloys.

- Polymers

The biggest advantage of these materials is their low cost, low weight, and processing flexibility, making them important in biomaterials production and medical device production. Polymers in a liquid state or with a low melting point are generally used. These are polylactic acid (PLA), acrylonitrile butadiene styrene (ABS), polypropylene (PP), or polyethylene (PE).

- Concrete

Additive manufactured concrete is mostly used in the construction industry for the design of complex shaped elements. It can improve construction efficiency by eliminating the need to erect formwork and improve construction safety by removing humans from hazardous working environments. Special types of concrete with different admixtures must be used.

- Composites

Composite materials have been mostly used in high performance industries. These materials can reach high versatility, low weight, and can be produced with tailored characteristics. The two most common composites used in AM are carbon fiber reinforced polymer composites and glass fiber reinforced polymer composites.

- Smart materials

These are materials that have the capability of changing their geometry and shape based on external conditions like heat and water. Two examples of smart materials are shape memory alloys and shape memory polymers.

- Special materials

Besides manufacturing, 3D printing can also be used for the production of food such as chocolate and meat. The textile and jewelry industry has also implemented AM into their production process.

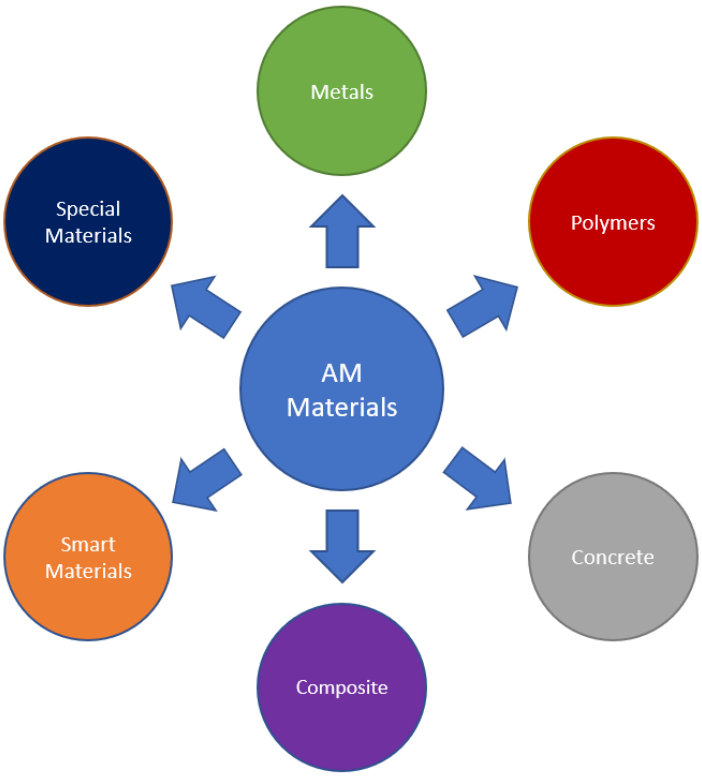

Figure 2.2: Classification of available AM materials

2.1.2 3D PRINTING TECHNOLOGIES

Although AM encompasses several processes, the term "3D printing" is commonly used to refer to them all. Types of AM processes differ depending on machine technology, method of layered manufacturing, materials, and other aspects described in the following paragraphs. To make the distinction between different AM products easier, the American Society for Testing and Materials (ASTM) has determined a set of standards that propose 7 categories of AM technologies. [2.4] These are binder jetting, direct energy deposition, material extrusion, material jetting, powder bed fusion, sheet lamination, and VAT photopolymerization. In the next paragraphs, each technology will be briefly explained, while also their usage and possible materials will be provided. References were takane from study done by Loughborough University [2.5] and article: 7 Families of Additive Manufacturing [2.6].

- Binder jetting (BJ)

In BJ a thin layer of finely crushed material (powder) is spread across the table platform. To distribute material more equally across the platform powder rollers are used. A liquid binder material is then inserted into the powder particles in the shape of the desired object. Liquid binder bonds individual particles, hardens, and thus creates the shape of the product. For each layer, the process is repeated, where the platform is able to be lowered, and therefore a new layer of powder can be added. After the whole object is complete and the liquid binder is fully solidified, the 3D printed product is removed from the platform and any excess powder is cleaned off. In binder jetting, a temporary binder holds the shape and is removed during debinding, while sintering fuses powder particles below the melting temperature.

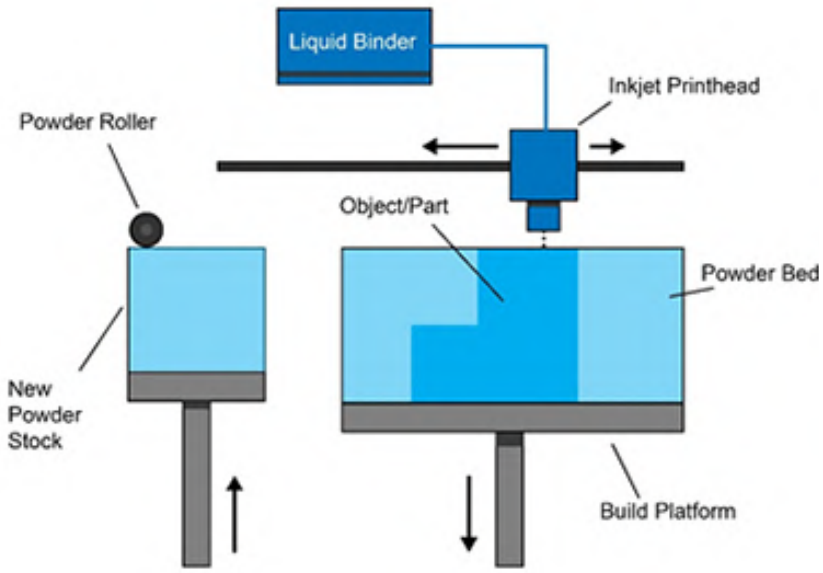

Figure 2.3: Binder jetting process [2.5]

The BJ process is suitable for metals (stainless steel), polymers (ABS, PA, PC), and ceramics (glass), while also allowing colour printing. This is two material approach so different characteristics of individual product parts can be achieved, by changing the binder-powder ratio or properties of the individual materials. The process is compared to other AM technologies normally faster and can be further quickened by adding additional print heads that deposit binder material simultaneously. Since it can produce objects with complex geometries, high resolution, and a good surface finish, it is generally used for creating prototypes or small parts and components. The characteristics of the final products are usually not sufficient enough to be used as structural elements due to the method of binding. Post processing is generally required to increase the mechanical and structural properties of the powder and binder material.

- Direct energy deposition (DED)

DED is compared to other processes much more complicated and is commonly used to repair or add additional material to existing elements. It uses energy source, such as lasers, electron beams, or plasma arcs to melt and merge feedstock material into the desired shape. Feedstock material is usually provided in the shape of wire or powder and is distributed through a nozzle. Wires are generally in comparison to powder less accurate, but more efficient since there is no waste of material. The energy source melts the feedstock material, which is then deposited into the final position and then cooled down, and thus hardened. The nozzle is able to move in multiple directions and is not fixed to a specific axis, allowing for the feedstock material to be more equally melted and shaped.

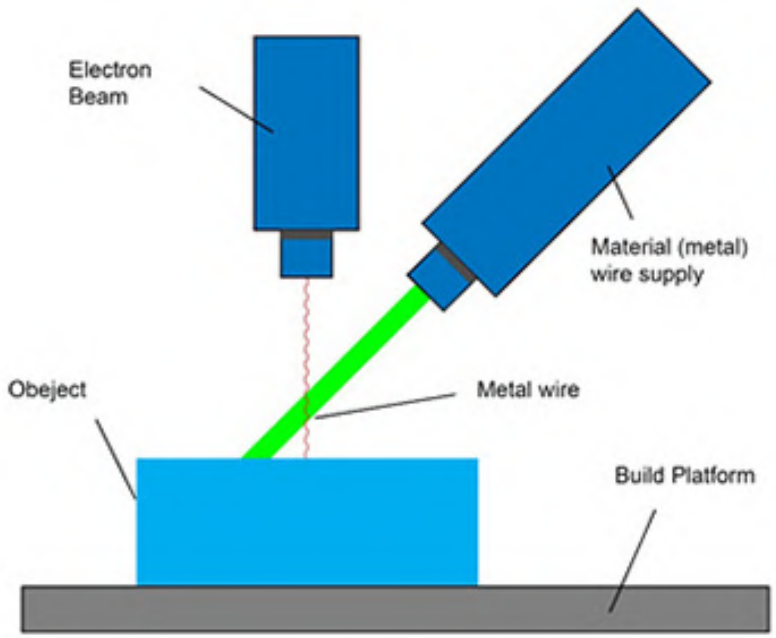

Figure 2.4: Direct energy deposition process [2.5]

The number of possible materials used in DED is in comparison to other AM processes reasonably low since in most cases only metals and metal alloys are used. The most common metals are steel, titanium, nickel, aluminium, and copper. It is important for the material to have a very fast cooling time (typically between 1000 and 5000 °C s^{-1}) since this will have a big impact on the final grain structure of the deposited material. There are several types of DED processes that are used in additive manufacturing. Some of the most common types of DED processes are laser-based DED, electron beam melting, plasma arc welding, and gas tungsten arc welding.

The biggest advantage of DED is the ability to control grain structure to a high degree, and thus create high quality products that are suitable for the structural element under high loads. During the manufacturing process, it is important to balance the production speed with the surface quality. Nevertheless, post production surface treatment will be in most cases needed.

- Material extrusion (ME)

The most common example of ME process is fused deposition modeling (FDM), which is because of its low price commonly used for inexpensive, domestic, and hobby 3D printers. It is usually used for creating prototypes, small production components, and functional parts made out of polymers, namely thermoplastics, thermoplastic elastomers, and some composite materials. The material is deposited through a nozzle, where is heated up and in a liquid state placed layer by layer in the desired shape. The nozzle is able to move in x, y, and z directions, allowing for complex and irregular shapes. During the manufacturing process, it is important to keep constant temperature and pressure in the nozzle. Steady and constant temperature and speed of production will provide high quality products and accurate results.

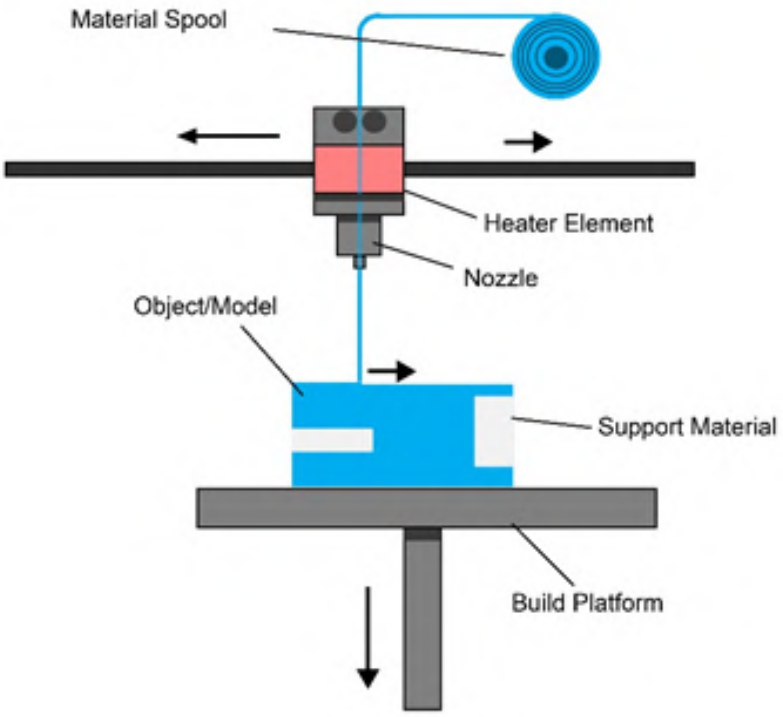

Figure 2.5: Material extrusion process [2.5]

The biggest advantage of ME is the low price and use of easily available materials, making it a very economical process perfect for low volume production. However, ME has also quite a few disadvantages and is thus rarely used in the manufacturing industry. The round shape of the nozzle will influence the final characteristics of the printed model. Compared to other AM processes the speed of production and quality of the final products are reasonably low. ME is also limited to only using polymers, which can not reach high strengths, and are thus not suitable structural elements under high loads. Layer by layer approach may result in a rough surface and inaccurate design, therefore post processing is in a lot of cases used. There are different methods available that help to improve the visual appearance of printed models. The most common methods are increased temperature during printing or the use of resin in the material mixture.

- Materials jetting (MJ)

MJ is AM process where objects are created by depositing droplets of material onto the manufacturing platform in the desired shape. There are multiple available methods of MJ processes, the most common are continuous or drop on demand approach. The material is placed on the platform through a nozzle, which can move horizontally, while the platform moves vertically. When the material is deposited onto the desired location it is cured and hardened with the help of ultraviolet lights. Other AM processes mostly use a continuous stream of material, while MJ uses droplets, which means that material is deposited only when needed.

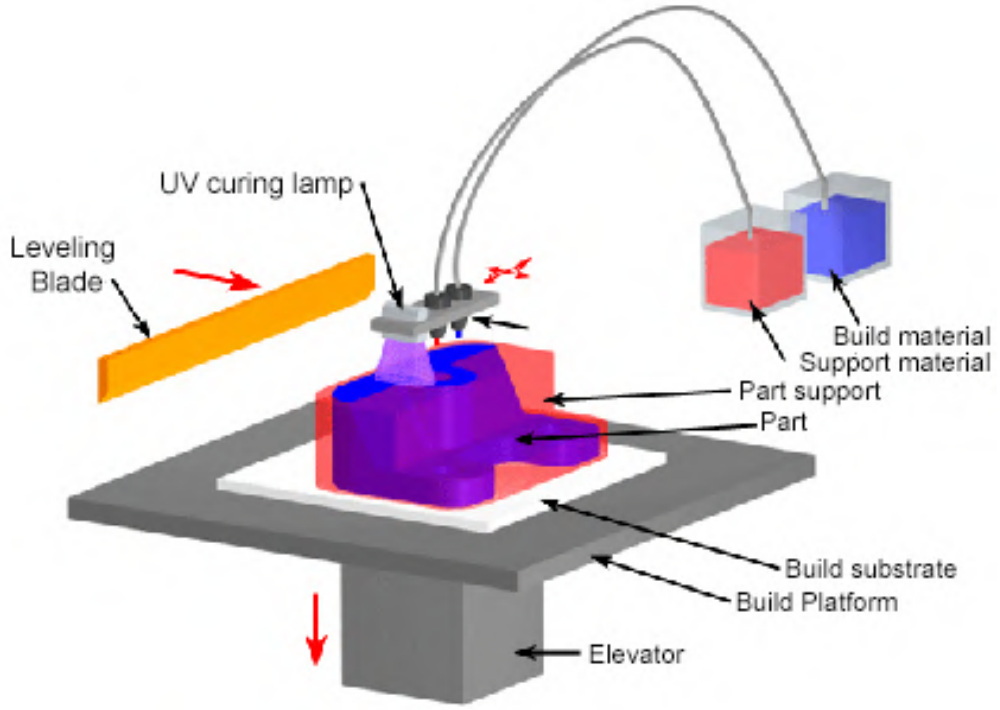

Figure 2.6: Material jetting process [2.5]

The use of droplets for production limits the number of suitable materials. In most cases, polymers and waxes are used due to their viscosity and ability to form drops. As explained drops are deposited only when needed, which means that the waste is minimized, while also high accuracy can be achieved. Moreover, material that was not used can be completely recycled and reused. MJ also allows for fast change of material, which enables products to be built out of multiple materials with different characteristics. Due to the liquid state of the material in most cases, a support material is needed. The support material is put around the printed object and holds the material in place until it is fully hardened. After the manufacturing stage, the support material is removed with the help of sodium hydroxide or a water jet. Because MJ can already in the printing stage, due to UV curing achieve reasonably high quality and accuracy, post processing is in most cases not required. The process has the ability to achieve high fine finishes and resolution, making it perfect for the production of objects with complex geometries or details. Because of that it is mostly used in the medical and aerospace industry. However, MJ is in comparison to other AM processes in general more expensive since it requires specialized equipment and materials.

- Powder bed fusion (PBF)

PBF method created a 3D model by melting and fusing material powder together. The powder is firstly spread across the platform in a thin layer and then heated up and melted by either a laser or electron beam, which is able to move horizontally. The process is each layer repeated by adding new material and lowering the platform. To increase the strength of the final product different considerations can be implemented. The most common one is so called hot isostatic pressing where a vacuum chamber is used. The vacuum makes the temperature and pressure rise, which causes the increase of density and thus strength of the element. The powder is stored in the reservoir next to the manufacturing machine and is spread across previous layers with the help of rollers or blades. Excess powder also called powder bed act as an integrated support structure, which keeps the model in position until it is fully hardened. PBF includes multiple different printing techniques: direct metal laser sintering, electron beam melting, selective heat sintering, selective laser melting, and selective laser sintering.

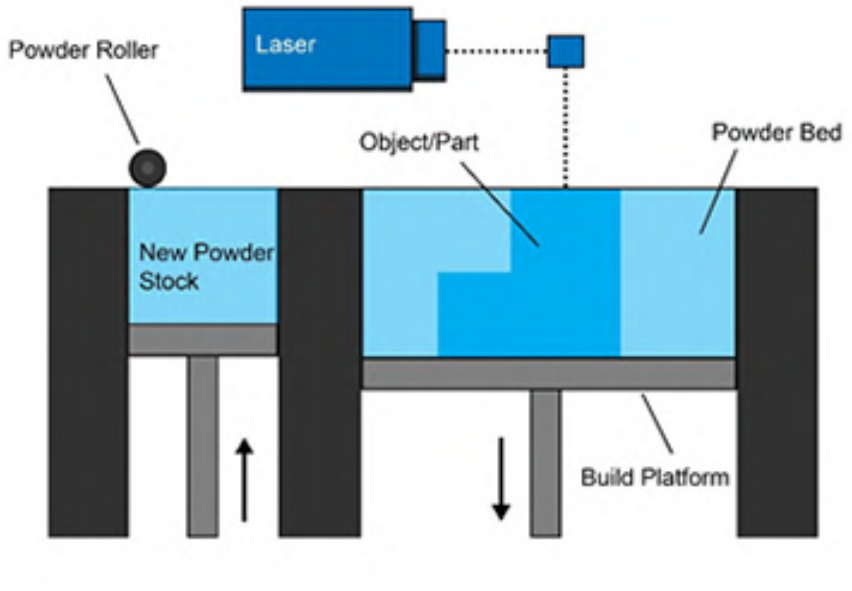

Figure 2.7: Powder bed fusion process [2.5]

PBF can use all kinds of materials as long as they are provided in powder form, most commonly metals and polymers. The production process is in comparison to other AM methods fairly simple, which makes it also inexpensive. The biggest disadvantage of PBF is its low production speed and limited size of 3D printed models. In addition, the materials in most cases lack structural properties and are thus not suitable for elements under high loads. The whole process also has high power usage.

The smoothness of the finish depends on the grain size of the powder material. In most cases, post processing is required to remove excess powder and further clean the model. With the post processing method, we try to increase the density and therefore improve the structural performance of the element.

- Sheet lamination (SL)

SL is a 3D printing process where thin sheets of material are placed on top of each other and bonded together to produce the final product. There are two main types of SL that mostly differ in the types of material that can be used. Ultrasonic additive manufacturing uses individual metal plates that are connected to each other by ultrasonic welding. Unwanted parts of the metal sheet can be removed before the bounding happens (each individual sheet is cut) or after the lamination process (CNC machining). The most used metals are aluminium, copper, stainless steel, and titanium. Another type of SL is called laminated object manufacturing. The process uses the same layer by layer approach, but instead of metal uses paper sheets. Instead of welding, paper sheets are bounded together by adhesive connection. After the lamination process, we again need to remove the excessive paper. This can be done by knife or laser. The third option is called sheet fusion deposition modeling where plastic or metal sheets are bonded together by increased temperature and pressure. After the lamination process model is again cut into the desired shape with a CNC machine.

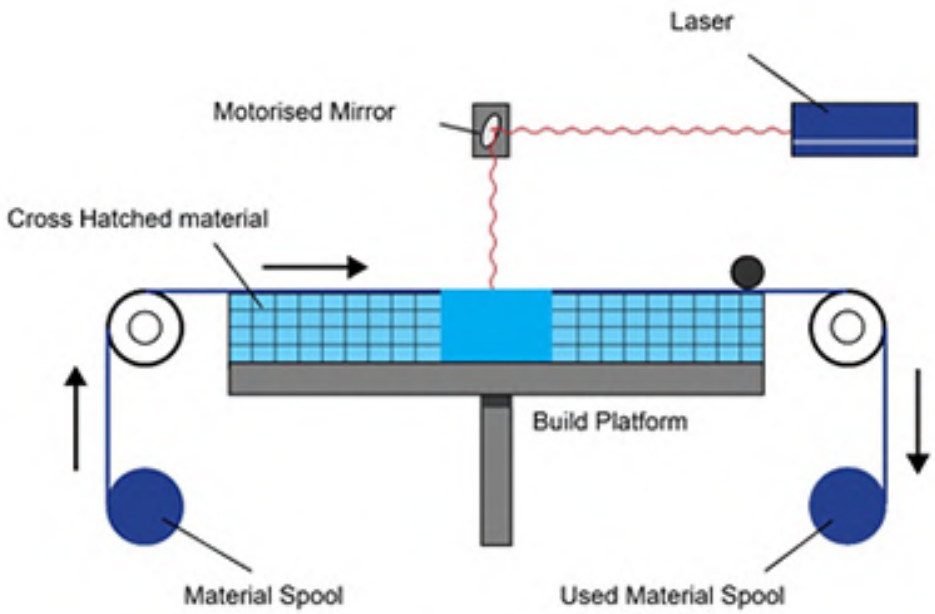

Figure 2.8: Sheet lamination process [2.5]

SL can combine sheets made out of different materials, thus creating a more optimized model. Lamination requires relatively little energy as the material, unlike in other AM methods is not melted, but instead uses a combination of ultrasonic frequency and pressure or adhesive. The process is fast and relatively cheap. This is due to the fact that only the outline shape needs to be cut, instead of the entire cross section area. Laminated elements are not yet used for the structural design, but instead used more for aesthetic and visual models. The strength of the final model in most cases depends on the characteristics of the bonding material. In most cases, post processing is needed to improve the appearance, as well as further machining. This is usually done by adding adhesive, paint, or sanding. Compared to other AM processes SL has a lower resolution and can not reach high accuracy and complexity. Moreover, the choice of materials is fairly limited.

- VAT Photopolymerization (VATP)

The most common VATP process is called stereolithography, where objects are built out of liquid photopolymer. Photopolymers are raw materials sensitive to light and are able to change their properties when exposed to a specific wavelength of light. In most cases, a UV light source (laser) is used to cure and harden the layer of the material. The UV laser solidifies the liquid material in the desired pattern creating the designed shape of the object. When the layer of the material is hardened the build platform moves down allowing the pouring of the new liquid layer. The process is repeated until the whole object is built. Before each layer is poured blades or recoating blades scan the previous layer for any possible defects, such as air gaps. All defects need to be refilled with material to ensure a quality product. Because the raw material is liquid there is a need for a support structure during the curing process. The support structure will keep the material in position until it is fully hardened.

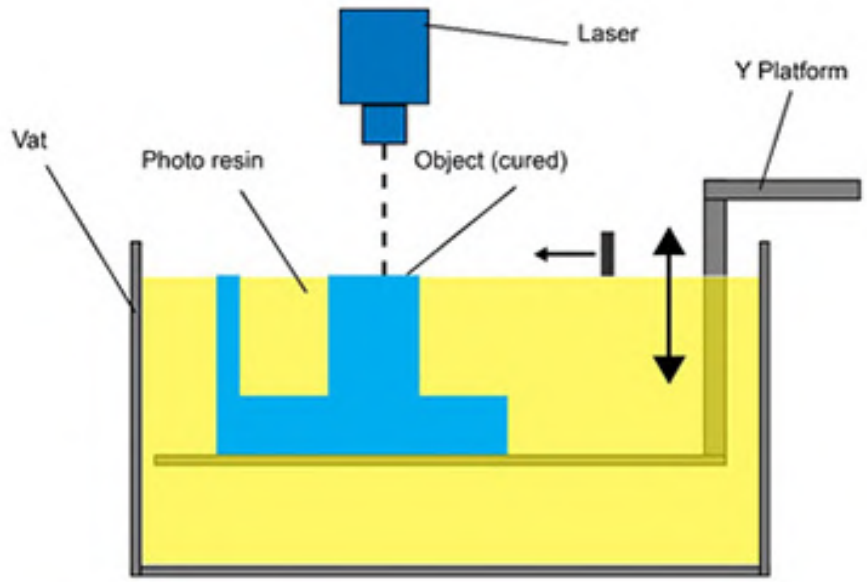

Figure 2.9: VAT Photopolymerization process [2.5]

Post processing is in most cases required to remove the excess material from the model. This can either be done by mechanically removing or using an alcohol rinse. The process might be lengthy but crucial to achieve desired surface quality. The VATP process can produce objects with a high level of accuracy and a good smooth finish. It is usually used to produce high quality complex elements used in the medical, aerospace, and jewelry industries. It is also a relatively fast process that can build larger objects. On the other hand, it is very expensive and has a lengthy post processing. It also requires a specific set of materials that might not be always accessible.

Table 2.1: Overview of AM processes [2.6], [2.7]

AM Type	Description	Advantages	Materials	Mechanical properties	Build costs
Binder jetting	A liquid binder is deposited onto a powder material layer by layer creating a solid object.	Full colour printing High productivity Wide range of materials	Polymers, metals, glass, ceramics	Low	$
Direct energy deposition	A focused energy source (laser, arc, or electron beam) melts feedstock material layer by layer.	High mechanical properties Multiple materials in single part High deposition rate	Metals, cheramics	High	$ $
Material extrusion	Through a nozzle melted material is deposited layer by layer. Material solidifies quicky.	Cheap and economical Full colour printing Good structural properties	Polymers	Low	$
Material jetting	Droplets of liquid material are deposited onto the platform and solidified with UV lights.	High accuracy Full colour printing Multiple materials in single part	Polymers, waxes	Medium	$ $
Powder bed fusion	A laser or electron beam melts powder material layer by layer.	High complexity Powder acts as support Wide range of materials	Polymers, metals, ceramic powder	Medium	$ $
Sheet lamination	Thin sheets of material are cut and bond together layer by layer.	High volume print Low cost Multiple materials in single part	Metals, polymers, paper	Low	$
VAT Photopoly-merization	Liquid photopolymer is cured by UV lights into a 3D object.	High accuracy and complexity Smooth surface Large building areas	Liquid photopolymers	Medium	$ $ $

2.2 WIRE ARC ADDITIVE MANUFACTURING

WAAM is a term that includes all AM processes, which use arc welding as a basis for their 3D build. It is a part of the DED manufacturing family, which in 2020 represented about 16 % of all AM used in the market. [2.9] The first ideas of WAAM technology date back to the 1930s when the process was called shape welding and was only used for the manufacturing of larger objects. Figure 2.11 shows the shape welding machine from the Thyssen factory on the left and the shape welded reservoir on the right. Due to the high development in computational design, robotics, and new welding techniques, the variety of designed and manufactured products has drastically increased.

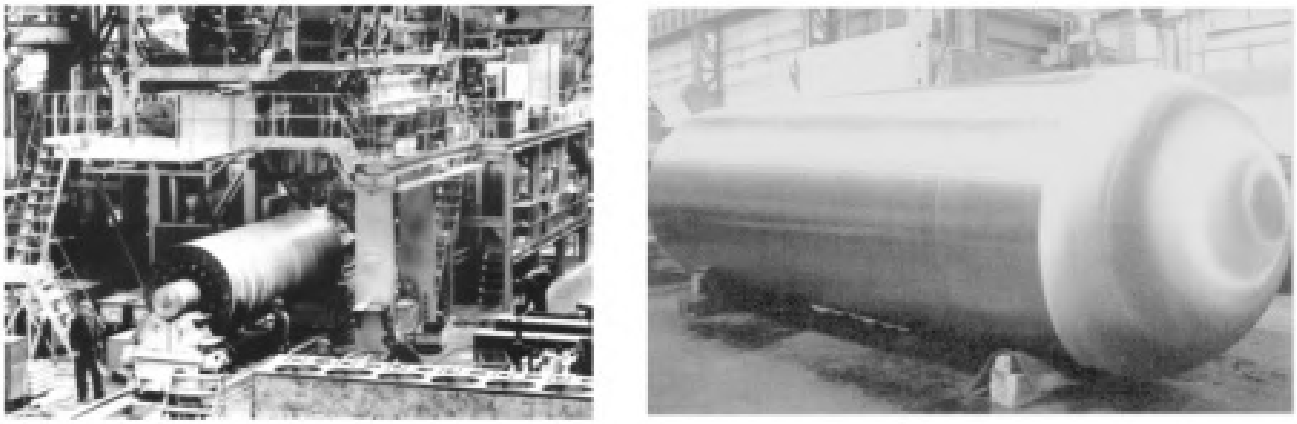

Figure 2.10: Shape welding machine (left) and shape welded reservoir (right) [2.10]

The WAAM technology is nowadays used to produce complex geometry elements from many different disciplines, including aerospace, automotive, shipbuilding, medical, architecture, and also structural. Some specific products manufactured with WAAM are ship propellers, water power plant turbines, car engine parts, etc. Because this technology can compared to other AM processes achieve products with higher strength properties it is also suitable in the construction industry. The most famous example, where WAAM was used for the design of a big structural product is The MX3D Bridge in Amsterdam manufactured by the company MX3D.

WAAM is a reasonably cost effective AM production process and is compared to PBF much cheaper. This is due to the more available and developed technology and the fact that wire feedstock costs only 10 % of the powder price. [2.10] Fast production is one of the most important WAAM features and is achieved due to its high deposition rate, making it perfect for the production of larger parts. Based on tests WAAM can reach a 4 – 9 kg/h deposition rate, while for comparison PBF only 50 g/h. Another advantage of using a wire feedstock is high material utilization, meaning that material waste is minimized. A wire is also preferable because it is easier to store and is less likely to oxidised or be contaminated compared to powder feedstock. Theoretically, there are no size limitations when using WAAM, but geometric inaccuracy and distortions need to be taken into the account. AM produced objects (especially WAAM) are subjected to high residual stresses, which increase with the size of the object. Higher residual stresses mean bigger geometry imperfections. [2.11]

WAAM and therefore AM can produce the final product relatively fast. To go from a digital model to the final product few steps are needed, which will be quickly explained in the following paragraph and presented in figure 2.12. Firstly, a digital 3D model is made in Computer Aided Design (CAD), where its outside geometry is determined. The CAD file needs to be converted into a format that the AM machine can read. Computer Aided Manufacturing (CAM) is used to handle machine tools used in the manufacturing of modules. Before the build process, the AM machine needs to be appropriately set, meaning material constraints, wire supply, manufacturing input parameters etc. are in line with the desired outcome. Once the product is fully complete it can be removed from the machine. Inspection, either visually or with a computer scan is done to detect any possible errors and dimension imperfections. In most cases, post processing is necessary not only to remove the excess print but also to possibly improve the surface quality or strength of the product. [2.12]

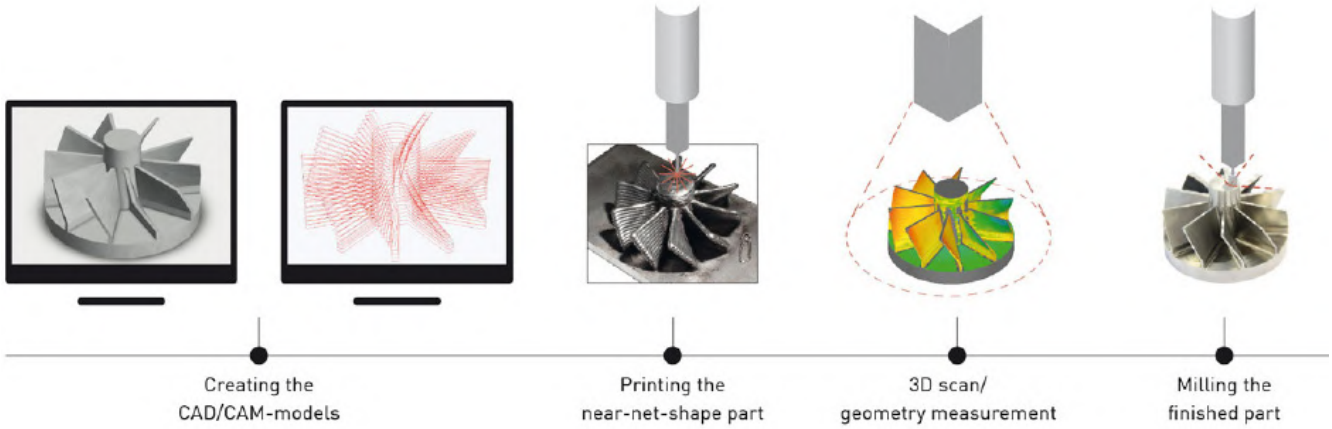

Figure 2.11: Process chain for WAAM [2.12]

2.2.1 PROCESS

The WAAM process is based on the concept of using arc welding to build up metal elements layer by layer. The main difference between ''normal'' arc welding for joints and WAAM is in the thermal conductivity, which depends on the dimensions and shape of the solid metal part. The energy loss to solid metal in joint welding and WAAM is presented in figure 2.13. It can be seen that thermal conductivity in joint welding takes place in more dimensions than in WAAM, where heat is dispersed in one direction only. This is due to the thin walled structures that WAAM produces. Another difference lays in the amount of heat needed for each process. Arc welding melts and connects two metal parts together, thus high heat input is needed. Besides this, better control over the melt pool is possible. On the other hand, WAAM melts and places feedstock layer by layer, for which lower heat is needed. This makes WAAM in comparison to arc welding more energy and cost effective. [2.10]

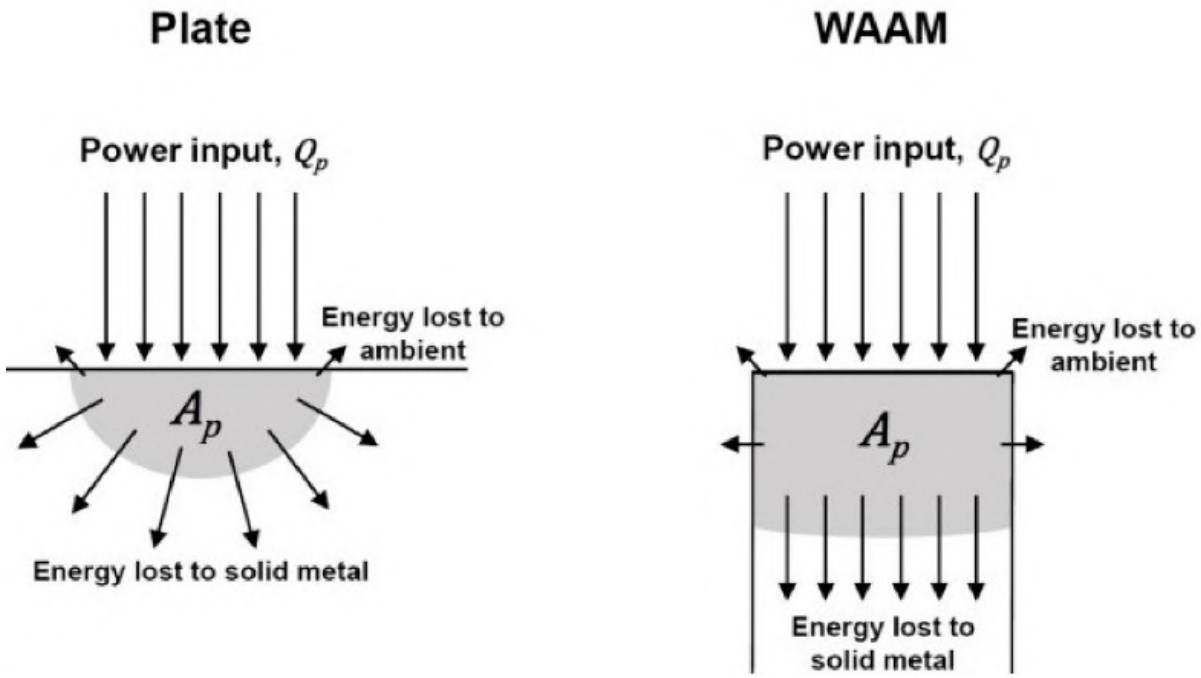

Figure 2.12: Energy transfer in joint welding and WAAM [2.13]

2.2.1.1 TYPES OF ELECTRIC ARC

All WAAM processes are based on the previously explained concept of arc welding. There are a couple of different welding types that can be used in the WAAM build. Depending on the desired material selection, dimensions of the product, wall thickness, welding speed, and quality the specific type can be used. Three more commonly used arc welding techniques, namely gas metal arc welding (GMAW), tungsten inert gas welding (TIG welding), and plasma arc welding (PAW) will be explained in the following paragraphs. References were taken from research paper: The Current State of Research ofWire Arc Additive Manufacturing (WAAM): A Review [2.10] and Comprehensive review of wire arc additive manufacturing: Hardware system, physical process, monitoring, property characterization, application and future prospects [2.14].

- Gas metal arc welding (GMAW)

GMAW, commonly known as metal inert gas welding (MIG), is a prevalent arc welding technology extensively employed in Wire Arc Additive Manufacturing (WAAM) for decades, serving purposes in additive manufacturing, surfacing, and cladding. Recent advancements in arc welding power control systems, particularly modern controlled short arc systems, prove advantageous for AM due to their lower energy input compared to traditional short arc processes. In GMAW, a welding gun feeds a wire electrode, melted by an electric arc, depositing liquid material onto the previously laid layer. Notably, GMAW is often referred to as metal active gas welding (MAG), where the welding gun not only supplies a wire electrode but also a shielding gas. This shielding gas protects the weld pool from oxidation and improves wetting. GMAW, suitable for larger products due to its high deposition rate, supports a variety of metals like steel, stainless steel, aluminum, and copper. However, rapid heating and cooling in GMAW can lead to high residual stresses, impacting the final part's geometry and causing warping. Various measures, such as controlling welding gun speed, wire feed rate, and shielding gas composition, can mitigate these stresses.

- Gas Tungsten Arc Welding (GTAW)

GTAW also known as TIG welding is a welding process where two metal parts are joined together by an arc created by a tungsten electrode. In WAAM, the GTAW welding torch with an arc melts metal wire feedstock into the weld pool. When the wire is melted it is deposited onto the previous layer, and thus the 3D product is made. Inert gas is necessary to prevent oxidation of the tungsten electrode, as oxidation leads to evaporation and subsequent erosion of the electrode.
Compared to other WAAM methods GTAW is able to produce high quality welds with high accuracy and a low possibility of errors. The electrode used in GTAW is non-consumable meaning that the risk of contamination of material is low. However, the process has also some limitations. The most noticeable is the low production speed, which limits the production of big scale elements. Moreover, the GTAW process is much more complex and requires a highly trained operator.

- Plasma arc welding (PAW)

PAW can also be used in WAAM where metal feedstock is fused to the existing parts. A plasma arc is created with a combination of electric current and gas (in most cases argon), which is forced through an opening under high pressure. With the plasma arc feedstock material is melted into a weld pool, which is then deposited and solidified in the desired location. Because of high pressure gas, the plasma arc can achieve high temperatures (temperature ranges from 15000 to 20000 °C) allowing for feedstock material to be either wire or powder.
PAW is a good welding process for WAAM since it can produce precise, high-quality welds at relatively high speeds. The biggest advantage of PAW is the ability to precisely control heat input, which lowers the possibility of distortions. Moreover, the high energy density of the arc can achieve deep penetration of welds, and thus creating strong connections between individual layers. Because of this PAW is a good option for manufacturing big and complex metal parts while at the same time achieving high geometric accuracy and mechanical properties.

2.2.1.2 POST PROCESSING

Even though AM and WAAM show many benefits in regard to the new manufacturing style and Industry 4.0, there are still many limitations that prevent AM processes to be regularly applied in industrial applications. WAAM produced objects in most cases show defects due to high heat accumulation and therefore thermal deformation. During the manufacturing process temperature of individual layers constantly changes, because of repeated melting and cooling. Because of that a coarse grain structure, porosity, and high amount of residual stress will appear, which will then cause deformations and geometry imperfections. A coarse grain structure applies to the microstructure of a material with large grain sizes. This phenomenon can result in reduced material strength, toughness, and ductility. Porosity refers to holes and voids within the material due to not properly fused and deposited material during the manufacturing process. Porosity can significantly limit the quality and performance of the product, thus lowering its strength and increasing the risk of cracking and failure. The product is also less prone to corrosion and other environmental factors.

To lower the impact of defects on the performance of the final products many different post processing techniques have been tested and implemented into the production process. Below different techniques will be explained, namely heat treatment, shot peening, abrasive flow machining, laser shock peening, and friction stir processing. References were taken from science papers titled A review on post processing techniques of additively manufactured metal parts for improving the material properties [2.15] and Post-Processing Techniques to Enhance the Quality of Metallic Parts Produced by Additive Manufacturing. [2.16]

- **Heat treatment (HT)**

There are many studies done on the impact that HT has on the characteristics of 3D printed objects. Many different approaches have been considered differentiating mainly in the temperature and length of the exposure. In general, HT is used to reduce residual stresses accumulated in the material during production and lower the impact of the porosity. This improvement of the material properties happens mostly because of the homogenization of the microstructure, meaning that differences in characteristics in different building directions are neutralized (material becomes more isotropic). Because of reduced residual stresses, there is an increase in yield and ultimate tensile strength.

- **Shot peening (SP)**

SP process includes pounding of the surface of the 3D printed product with the small metal or ceramic particles. Small particles are directed at the product's surface and can vary in size, shape, and velocity depending on the desired outcome of the process. Particles are usually made out of steel, ceramic, or other material. After the small particles hit the surface of the product, a thin compressive layer is created, which increases fatigue resistance, by countering the tensile stresses that accumulate during use. SP can also increase the surface quality, and thus increasing mechanical properties (strength and ductility) and environmental impact resistance (corrosion).

- **Abrasive flow Machining (AFM)**

AFM is a specialized machining/polishing post process where surface defects are reduced. It uses specially designed abrasive media that removes a thin top layer of the product, resulting in a smoother finish and more precise dimension tolerances. This is especially beneficial in WAAM when the products' surface is often rough and dimension tolerances are not exact. Different studies suggest that AFM can improve surface roughness anywhere from 40 % to even 75.5 %. It is however worth noticing that with AFM a part of the object is removed (there is a mass loss), which can lead to a change of dimensions and also the shape of the object.

- **Laser shock peening (LSP)**

LSP is a post process surface treatment to increase surface quality and overall characteristics of the product. It uses a high energy laser that creates shockwaves which cause plastic deformation in the material. These deformations will create compressive stresses in the surface (formation of tensile stresses in the surface is an important limitation), thus improving its mechanical and physical properties. The risk of cracking and other forms of failure will be reduced, especially in high stress areas. Besides that, resistance to fatigue will increase. The only downside is the high price.

- **Friction stir processing (FSP)**

FSP is a post processing method that uses a rotating tool to mix the material in controlled conditions. Rotation can modify a product's microstructure, and thus improve its mechanical properties. In most cases, grain size is lowered creating a more homogenous material. This then improves material strength, ductility, and toughness. Based on some studies FSP can also lower porosity and reduce residual stresses.

2.2.2 MATERIAL

A wide variety of metals can be used for the production of WAAM elements. The microstructure and characteristics of these materials vary significantly due to aspects explained further below and can be similar to that of welds. The most common metals are steel, titanium, aluminum, nickel-based alloys, and copper. The choice of material will depend on the desired application. Steel is generally the most used material in the construction and manufacturing industry, and is therefore also the most studied metal for WAAM production. Steel materials can be divided into two major groups, namely high and low alloy steels, differentiating mostly in the microstructure. The high alloy steel group includes stainless steel and heat resistant steel. Titanium is a very light material with a very good strength to weight ratio. Different titanium alloys are commonly used in the aerospace industry. Because of its high price, it is desirable to use titanium in AM only where the sufficiency of material usage is high. Aluminum is also a lightweight material widely used in lightweight construction with reasonably high strength. Due to aluminum's high thermal expansion and therefore high residual stresses the geometry accuracy is not the best. Also, aluminum has a Young's modulus one-third that of steel, meaning that if greater stiffness is needed, the design must incorporate larger dimensions. Nickel is in most cases used in high temperature and corrosive environments. [2.17]

The structural performance of a material depends on its characteristics, namely microstructure, Young's modulus, yield and ultimate strength, ductility, and fatigue resistance. In the conventionally produced elements, these material properties have been determined and implemented into well known guidelines and codes. On the other hand, for WAAM there are no established design parameters, due to the high characteristics variability of materials. The most important parameters that influence the characteristics are heat input during prefabrication, post processing techniques, and angle of testing in comparison to building direction.

As stated before the material characteristics of WAAM products are significantly affected by microstructure, which can to some degree be compared to welds. The difference lies in the grain growth direction, which is in welds towards the center of the melt pool while WAAM is more upright. Due to the layer by layer production process, different lamellar microstructures varying from the top to the bottom of the manufactured parts have been recorded. Therefore, the anisotropic mechanical behavior of the WAAM material could appear. [2.18] This suggests that the object could behave differently depending on the direction of the print and the direction of the applied load. The orientation of the printed direction is shown in Figure 2.13.

Many studies have been conducted in regard to the anisotropic behavior of the WAAM parts, mostly to determine the mechanical properties of a material in different built orientations. In the following paragraphs, the four most important mechanical properties will be explained, namely strength, elastic modulus, ductility, and hardness. For each, values are proposed, which were taken from the research paper written by Tankova et al. [2.18]. Proposed values refer to the

feedstock ER70S-6, which is a carbon steel wire and is commonly used in WAAM production. In the study, samples were printed in three different directions, namely 0°, 45°, and 90°, as shown in Figure 2.13. Besides that, the impact of the post processing on the magnitude of the mechanical properties was also considered.

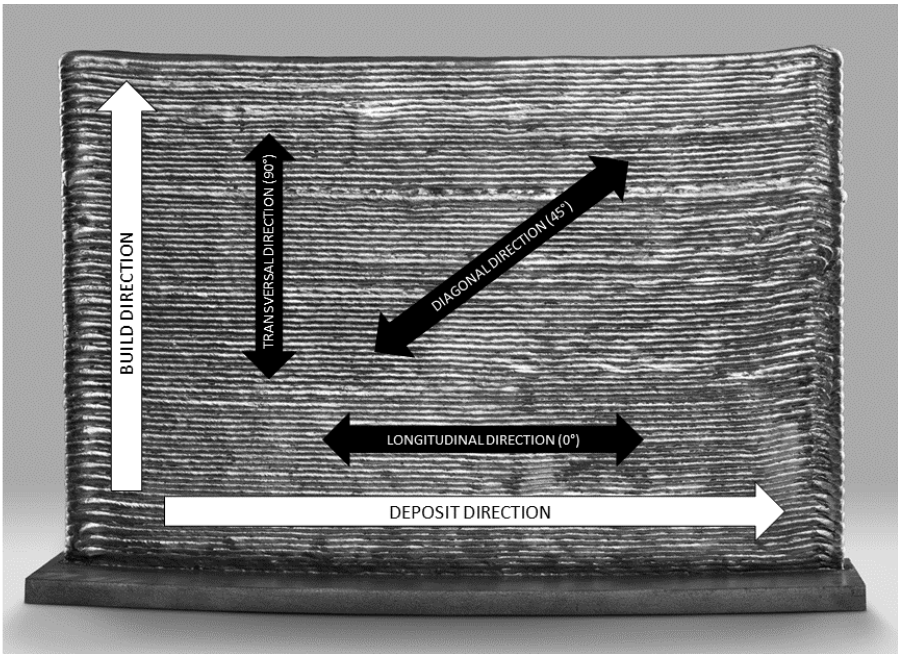

Figure 2.13: Built orientation

- **Yield strength (YS) and ultimate strength (US)**

The average values of the YS and US for all samples printed in the experiment are shown in Figure 2.14. For the as built samples, strength was determined based on their average cross sectional area. It is possible to conclude that post processing (in this case samples were machined) in all cases increases the strength, no matter on the direction of the build. On average, the post processing increased YS by 18,3 %, while the US increased by 13,7 %. Built orientation did not have a major impact on the strength of the specimens. Changing the production angle in the case of as built samples, resulted in variations of 10 % and 5 % for the YS and US. For the machined samples, the variations were even lower with 2,7 % for YS and 2,4 % for US. The presented results show the isotropic behavior, with negligible influence of the built orientation. The differences in values are present most likely due to manufacturing process defects.

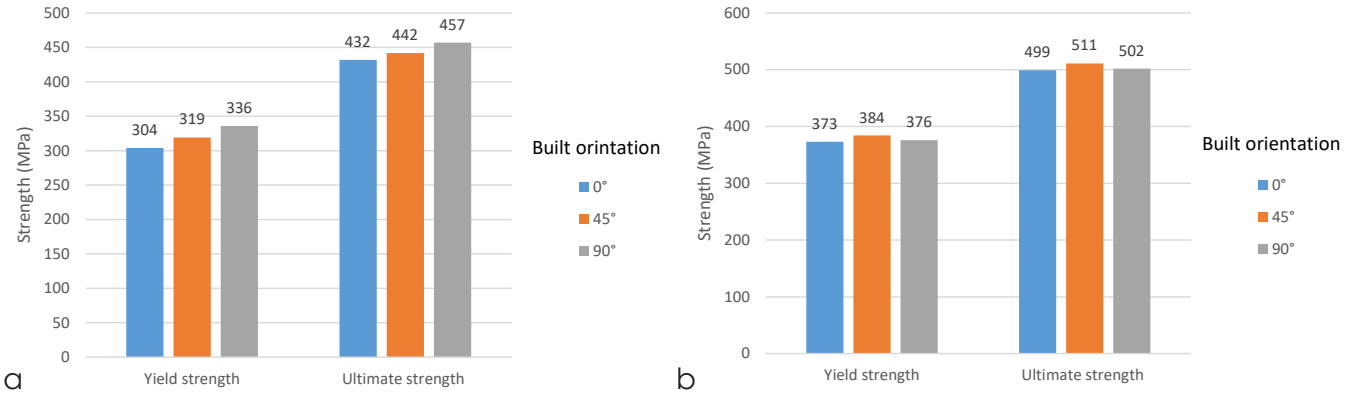

Figure 2.14: Impact of built orientation on the YS and US: a) as built, b) machined [2.18]

- **Ductility**

Ductility is for the structural steel one of the most important properties, as it prevents brittle failure. Ductility can be measured by reading the strain value at the fracture point on the stress strain curve. Fracture strains from [2.18] for the individual samples are presented in Figure 2.15. Values of the as built samples vary a lot with the 45° print experiencing the highest strain and 90° the lowest. For the machined samples, the values are higher, while also the variation is smaller with only a 5 % difference between the highest and lowest value. This happens due to the reduced number of surface defects that are present in machined samples compared to as built ones.

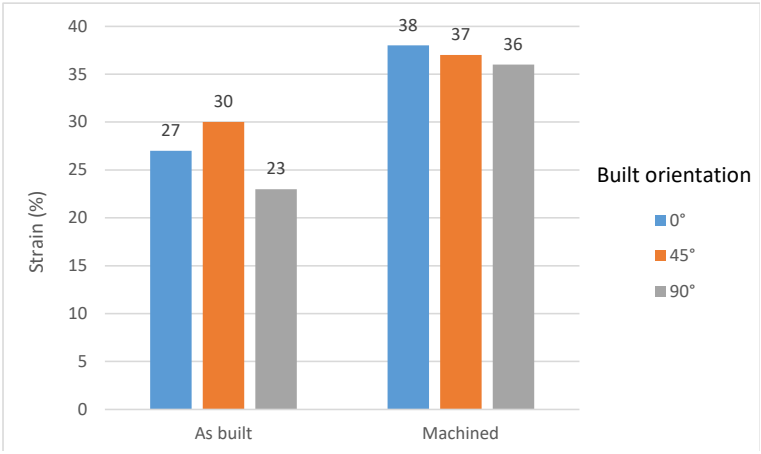

Figure 2.15: Impact of built orientation on ductility [2.18]

Based on the test of tensile strength and elastic strain it is possible to conclude that printed material resembles steel grade S275 for as built samples and S355 for machined samples. This means that WAAM is capable of producing high quality products with similar mechanical properties as traditionally produced elements.

- **Elastic modulus**

Elastic modulus determines the material resistance to elastic deformation under a specific load and can be calculated by dividing the stress by the corresponding strain. In the study [2.18] the elastic modulus was calculated to be 214 GPa, which goes in line with the average values of conventional steel.

2.3 CHAPTER CONCLUSION REMARKS

To conclude this chapter, a concise summary of the literature review on additive manufacturing (AM) is provided. This overview guides the selection of suitable AM processes and materials crucial for the subsequent stages of the research.

In Chapter 2, titled "Additive Manufacturing – State of the Art," referencing the American Society for Testing and Materials [2.4], a comprehensive review of seven AM process types is presented. These include binder jetting, direct energy deposition, material extrusion, materials jetting, powder bed fusion, sheet lamination, and VAT Photopolymerization. Each process was examined in terms of technology, advantages, potential materials and their mechanical properties, and associated costs, forming the key criteria for process selection based on the requirements of the project. In the Introduction of the thesis, the objective was presented, which includes integrating AM into the construction industry through the design of a branch column connection. Since the branch column connection will be a part of the load bearing structure, high loading acting on it can be expected. This requires the printed material to be able to achieve high mechanical properties, thus providing a sufficient structural performance of the model. Using this example provides the requirements and constraints, which narrow down the choice of AM processes quite significantly.

Steel is the predominant material for load bearing frame structures due to its exceptional strength, durability, and versatility, while achieving high tensile strength allows for the creation of slender and efficient designs, ensuring long term structural integrity. Therefore, steel will also be used in this thesis for the design of a structural connection. Among the seven presented AM processes four of them are capable of printing steel (or other metals), namely binder jetting, direct energy deposition, powder bed fusion, and sheet lamination. Between the four listed AM processes, DED manufacturing family can print steel with significantly higher mechanical properties than other processes. Wire arc additive manufacturing is a subset of the DED family. As part of DED, WAAM uses an electric arc to melt a continuously fed metal wire, allowing for layer by layer deposition and efficient production of large scale components. This technique showcases WAAM's versatility within the broader DED manufacturing approach. Notably, WAAM demonstrates comparable mechanical properties to conventionally manufactured steel parts. This was shown in Chapter 2.2.2 Material where mechanical properties of WAAM welding wire ER70S-6 are presented. It is shown that the presented values of yielding strength, ultimate strength, ductility, and elastic modulus are comparable to conventional steel. Depending on the included post processing the mechanical properties of WAAM object printed with welding wire ER70S-6 can be compared either to S275 or S355, which are the two more commonly used structural steel. Due to layer by layer nature of the WAAM process an isotropic material behaviour could be suspected. Based on the provided data shown in Figure 2.14 and Figure 2.15 it is visible that the built orientation will have an influence on the magnitude of the mechanical properties, but the influence is small and can thus be neglected. The influence of built orientation can further be lowered with the introduction of post processing. Therefore, the isotropic material behaviour can be assumed in the design phase.

Beyond impressive mechanical properties, WAAM boasts a high deposition rate, ranging from 4 to 9 kg/h, far surpassing alternatives like Powder Bed Fusion (50 g/h). This attribute is particularly advantageous for large scale prefabrication, ensuring faster printing of objects with greater dimensions. Moreover, the WAAM process demonstrates lower manufacturing costs compared to other metal printing techniques, attributed to its more economical feedstock material.

Taking into account the achieved high mechanical properties, rapid deposition rate, and cost-effectiveness, WAAM emerges as the optimal AM process for advancing the research into the design of the branch column connection within the construction industry. Besides the process itself, the selection of appropriate material is needed. Using the welding wire ER70S-6 should provide us with sufficient structural performance, as high mechanical properties are achieved.

2.4 REFERENCES

[2.1] Holzmann. P., Breitenecker. R. J., Soomro. A. A., Schwarz. E. J. 2017. User entrepreneur business models in 3D printing. Journal of Manufacturing Technology Management, Vol. Available at: www.emeraldinsight.com/1741-038X.htm

[2.2] Ford. F., Despeisse. M. 2016. Additive manufacturing and sustainability: an exploratory study of the advantages and challenges. Journal of Cleaner Production. Available at: https://doi.org/10.1016/j.jclepro.2016.04.150

[2.3] Shahrubudina. N., Leea. T.C., Ramlana. R. 2019. An Overview on 3D Printing Technology: Technological, Materials, and Applications. ScienceDirect. Available at: https://doi.org/10.1016/j.promfg.2019.06.089

[2.4] ASTM F2792-12a, Standard terminology for additive manufacturing technologies. 2012. ASTM International. West Conshohocken, PA.

[2.5] The Additive Manufacturing Research Group (AMRG). 2023. About Additive Manufacturing. Loughborough University. Available at: https://www.lboro.ac.uk/research/amrg/about/the7categoriesofadditivemanufacturing/

[2.6] Hybrid Manufacturing Technologies. 2020. 7 Families of Additive Manufacturing. Available at: https://hybridmanutech.com/resources/

[2.7] Xu. A., Langefeld. B., Erharter. M., Kourkejian. V. 2020. Market, machines and materials – The new playground for large chemical companies. Available at: https://www.rolandberger.com/en/Insights/Publications/Polymer-additive-manufacturing-Market-today-and-in-the-future.html

[2.8] Vranić. A., Bogojević. N., Ćirić Kostić. S., Croccolo. D., Olmi. G. 2017. Advantages and drawbacks of additive manufacturing. IMK-14 - Istrazivanje i razvoj. Available at: 10.5937/IMK1702057V

[2.9] Vafadar. A., Guzzomi. F., Rassau. A., Hayward. K. 2021. Advances in Metal Additive Manufacturing: A Review of Common Processes, Industrial Applications, and Current Challenges. Applied Science. Available at: https://doi.org/10.3390/app11031213

[2.10] Treutler. K., Wesling. V. 2021. The Current State of Research of Wire Arc Additive Manufacturing (WAAM): A Review. Applied Science. Available at: https://doi.org/10.3390/app11188619

[2.11] Evans. S. I., Wang. J., Qin. J., He. Y., Shepherd. P., Ding. J. 2022. A review of WAAM for steel construction – Manufacturing, material and geometric properties, design, and future directions. Structures. Available at: https://doi.org/10.1016/j.istruc.2022.08.084

[2.12] FMA Communications. 2019. Gefertec and research partners to study gas used for 3D printing. Available at: https://www.thefabricator.com/additivereport/news/additive/gefertec-and-research-partners-to-study-gas-used-for-3d-printing-

[2.13] Mohebbi. M. S., Kühl. M., Ploshikhin. V. 2020. A thermo-capillary-gravity model for geometrical analysis of single-bead wire and arc additive manufacturing (WAAM). The International Journal of Advanced Manufacturing Technology. Available at: https://doi.org/10.1007/s00170-020-05647-6

[2.14] Li. Y., Su. C., Zhu. J. 2021. Comprehensive review of wire arc additive manufacturing: Hardware system, physical process, monitoring, property characterization, application and future prospects. Results in Engineering. Available at: https://doi.org/10.1016/j.rineng.2021.100330

[2.15] Shiyas. K.A., Ramanujam. R. 2021. A review on post processing techniques of additively manufactured metal parts for improving the material properties. Materials Today: Proceedings. Available at: https://doi.org/10.1016/j.matpr.2021.03.016

[2.16] Mahmood. M. A., Chioibasu. D., Rehman. A. U., Mihai. S., Popescu. A. C. 2022. Post-Processing Techniques to Enhance the Quality of Metallic Parts Produced by Additive Manufacturing. Metals. Available at: https://doi.org/10.3390/met12010077

[2.17] Srivastava. M., Rathee. S., Tiwari. A., Dongre. M. 2022. Wire arc additive manufacturing of metals: A review on processes, materials and their behaviour. Materials Chemistry and Physics. Available at: https://doi.org/10.1016/j.matchemphys.2022.126988

[2.18] Tankova. T., Andrade. D., Branco. R., Zhu. C., Rodrigues. D., da Silva. L. S. 2022. Characterization of robotized CMT-WAAM carbon steel. Journal of Constructional Steel Research. Available at: https://doi.org/10.1016/j.jcsr.2022.107624

WAAM MANUFACTURE LIMITATIONS

3. WAAM MANUFACTURE LIMITATIONS

WAAM has as any other manufacturing technology, constraints within which objects can be produced. To design an object that is able to be manufactured with WAAM and at the same time achieve the desired structural and aesthetical performance, it is important to carefully examine these constraints. Besides that, the outcome of the WAAM products highly depends on the input that was provided. Therefore, proposing the appropriate manufacturing parameters can influence the manufacturability and quality of the prints, especially in the case of complex geometries (for example topology optimized shapes).

In this chapter, the two of most important manufacturing constraints will be presented, namely overhang and overlap. Besides that, the relevant process parameters will be elaborated and their influence on the weld bead geometry will be shown. For each limitation, a short literature review will be done, where relevant findings from the previous studies will be presented. To verify and complement the existing research, individual experiments will be completed from which the limit manufacturing values could be gathered. Some of these limitations will be then in the next chapter used to design the shape of the connection that is not only optimized for structural performance and mass minimization but also shape that is able to be produced by WAAM manufacturing technique.

3.1 PROCESS PARAMETERS - STATE OF THE ART

As stated before WAAM has in recent years gained significant attention for its potential in producing large scale metallic components. However, like any manufacturing process, WAAM also has its limitations and unknowns that need to be further researched. The main limitations of WAAM that are worth considering and will be elaborated on in this chapter are:

- **Surface Finish**

WAAM often produces rougher surface finishes compared to other additive manufacturing techniques such as powder bed fusion. The layer by layer nature of the process, combined with the deposition of molten metal, can result in visible build lines and rough surface textures. Additional post processing steps, such as machining or grinding, may be required to achieve the desired surface finish. [3.1]

- **Resolution and Accuracy**

While WAAM can produce large scale structures, its resolution and accuracy are relatively lower compared to some other AM processes. The wire diameter used in WAAM can limit the achievable level of detail and intricacy. Smaller features or fine geometries may not be accurately reproduced, which can restrict the application of WAAM for certain components. [3.2]

- **Residual Stresses and Distortions**

The rapid heating and cooling cycles inherent in WAAM can result in the generation of residual stresses and distortions in the fabricated parts. These stresses and distortions can affect the dimensional accuracy and mechanical properties of the printed components. Proper design considerations and post processing techniques, such as heat treatment or stress relief, may be necessary to mitigate these effects. [3.1]

- **Process Complexity**

WAAM involves the interaction of multiple process parameters that can have a significant influence on the quality of the 3D print. Optimizing and controlling these parameters can be complex, requiring careful adjustment and calibration. [3.3]

To consider these limitations and try to lower their impact, thus optimizing material characteristics and build quality, it is important to properly determine the input factors of the WAAM process. The most relevant input process parameters include travel speed [TS] (the velocity at which the welding torch moves along the deposition path), wire feed speed [WFS] (the rate at which the consumable wire electrode is fed into the welding arc), and heat input (depends on current [I] and voltage [V] of the welding arc). [3.3]

Throughout the years many experiments in regard to the impact of process parameters on the geometry and size of the weld bead have been conducted. Lambiase et al. [3.3] explored how different combinations of travel speed and wire feed speed influence the bead's height (h) and width (w) (Figure 3.1). The results of the experiment can be seen in Figure 3.2 a-c.

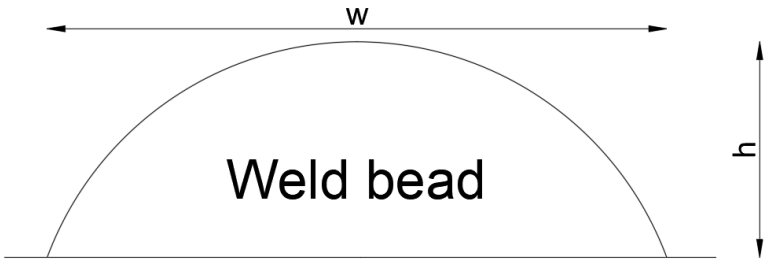

Figure 3.1: Weld bead geometry and dimensions

In Figure 3.2 a, the relationship between h, WFS, and TS is depicted. The measurements demonstrate that increasing the WFS and decreasing the TS result in a consistent increase in the weld height. This can be predicted since the increase in the WFS and the decrease in the TS leads to a higher amount of material deposited per unit length (represented as RWT and calculated by dividing the WFS by the TS). The effect of the processing conditions on w is shown in Figure 3.2 b. We can see that the reduction of TS causes the increase of w, which is again predictable since more material is deposited at the same time. The influence of WFS on w is not as straightforward and requires more attention. Prints where lower values of WFS were used (for example 0.3, 0.5, and 0.7 m/min), w experienced an increase with the increase of WFS. The peak value of w is reached when WFS is about 10 m/min (the exact peak value differs depending on TS). If WFS is increased above 10 m/min, then w will continue to decrease. Figure 3.2 c shows the influence of TS and WFS on h/w ratio. This ratio is called the weld bead form factor and helps characterize weld beads by shape (low h/w means flat weld, while high h/w means slender weld). The weld bead form factor is mostly influenced by WFS, where h/w exponentially increases with the increase of WFS. Changing TS did not significantly influence h/w.

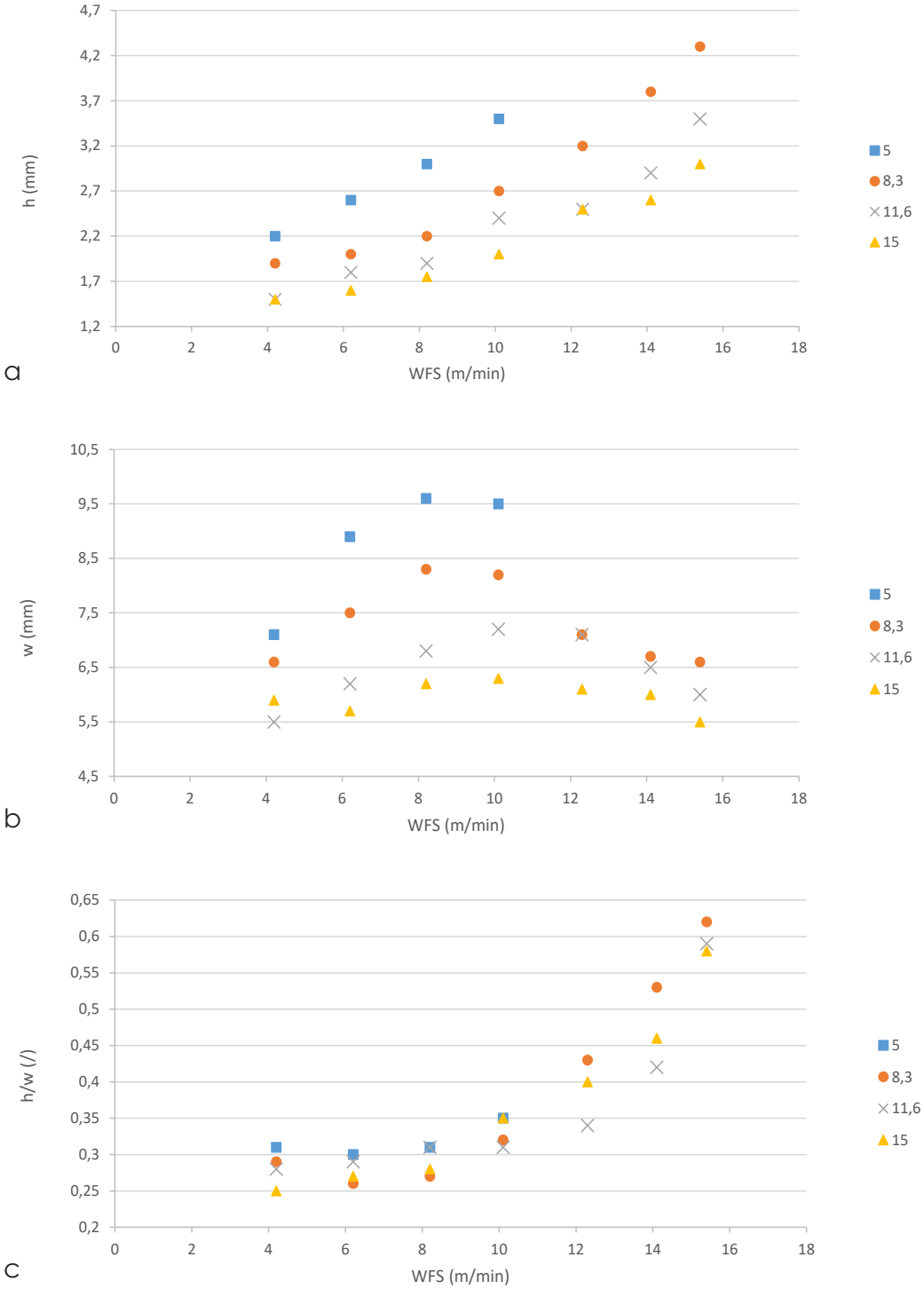

Figure 3.2: Influence of process parameters on bead geometry [3.3]

Dinovitzer et al. [3.4] also explored the impact of process parameters on weld bead size and quality. For the purpose of the research 16 specimens were printed that differentiate in WFS, TS, I, and argon flow rate. The experiments showed that h increases with the increase of WFS, while w experienced a decrease when WFS reached above 0.23 m/min. TS did not have a significant effect on the h, while the increase of TS caused the increase of w.

3.2 PROCESS PARAMETERS - LAB TESTS

A small experiment was conducted, where 5 single layer weld beads were printed. Specimens were fabricated at the Additive Manufacturing Laboratory of the Delft University of Technology at the Faculty of Mechanical, Maritime and Materials Engineering. During the experiment WAAM machine ''Fanuc M710iC/12 L series robot'' was used. The feedstock material was welding wire ER70S-6, with a diameter of 1 mm. Table 3.1 shows the chemical composition of the feedstock material as provided by the manufacturer. During the process, a shielding gas was used, which composition is shown in Table 3.2.

Table 3.1: Chemical composition of feedstock material ER70S-6 (wt%)

Wire type	C	Mn	Cr	Ni	Mo	V	P	Fe
ER70S-6	0,05-0,15	1,40-1,85	0,15 max	0,15 max	0,15 max	0,03 max	0,025 max	Bal.

Table 3.2: Chemical composition of shielding gas

Gas type	Ar	CO_2
	85%	15%

As stated before 5 single layer weld beads were printed and are presented in Figure 3.2. Two of the beads had the same process parameters, while the other 4 differ in WFS, TS, I, and E. For the purpose of this experiment two input parameters needed to be determined, namely WFS and TS. The WAAM machine could then based on these two provided parameters determine the most optimal heat input (HI), thus setting the appropriate I and E. Table 3.3 shows the provided process parameters for each of the individual weld beads. First 4 parameters presented in Table 3.3, namely TS, WFS, I, and E were read out directly from the WAAM machine. HI presented in column 6 from Table 4.3 could then be calculated with the below shown formula, where μ is the thermal efficiency and is assumed to be 0,9.

$$HI = \frac{\mu * E * I}{TS} \qquad (1)$$

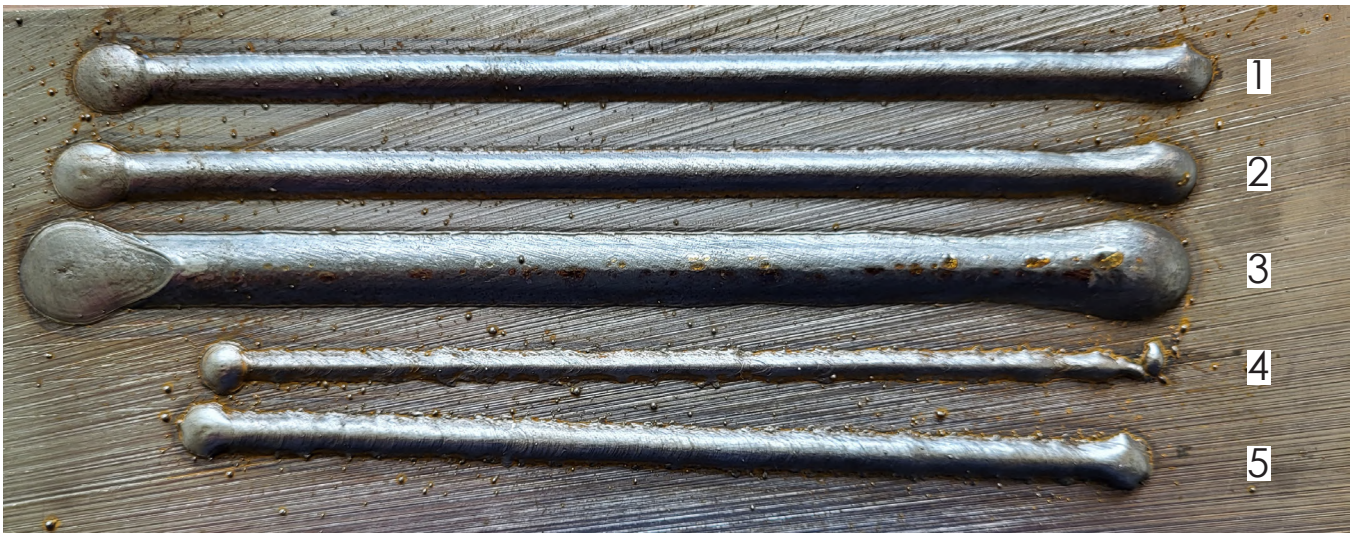

Figure 3.2: Single layer samples

Table 3.3: Process parameters for individual single layer samples

Specimen	TS (mm/s)	WFS (m/min)	I (A)	E (V)	HI (J/mm)
1	10	5	135	21,7	263,7
2	10	5	135	21,7	263,7
3	10	10	271	28,2	687,8
4	10	2	60	16,2	87,5
5	5	2	70	18,3	230,6

To evaluate the results and determine the size of the welds beads, 3D scans of the test specimens were done from which the accurate dimensions could be read. The h and w of the individual weld beads are presented in Table 3.4. In the following paragraphs, the results will be evaluated. To make the measurements more accurate three dimensions are presented, one at the start, one at the middle, and one at the end of the weld bead. The average of the three measurements is then calculated.

- **Specimen 1 and 2**

For the first two specimens, TS of 10 mm/s and WFS of 5 m/min were chosen, which means that the optimal HI was added to 263,7 J/mm. The size of the weld bead was compared to other specimens average, with the h being 1,89 – 1,90 mm and w being 6,87 – 6,98 mm. The quality of the weld itself was good and there were no noticeable defects. The surface of the weld was smooth without visible waviness and discontinuity.

- **Specimen 3**

For specimen 3 the TS was kept the same at 10 mm/s, while WFS was increased to 10 m/min, which means that compared to the previous print twice as much material is deposited at the same rate. The increase of WFS caused the increase in weld bead size, both in w and h. This is in agreement with the experimental findings reported in [3.3] and [3.4]. The quality of the weld is again high, without noticeable defects or discontinuity.

- **Specimen 4**

For the print of specimen 4, TS was again kept at 10 mm/s, while WFS was decreased to only 2 m/min. As predicted and stated in [3.3] and [3.4], a decrease in WFS will cause a decrease in weld bead size. Even though the printed specimen has small dimensions the problem occurs in the quality of the weld. There are multiple visible defects present, especially at the start and end of the print. The surface of the weld is not smooth but wavy and noticeable discontinuity is present. Defects are visible in Figure 3.3.

Figure 3.3: Welding defects (waviness, discontinuity, low accuracy at the start and end of the print) in sample 4

- **Specimen 5**

Specimen 5 was printed with WFS of 2 m/min and TS of 5 mm/s. Compared to specimen 4 the decrease of TS caused the increase of dimensions of weld bead, which aligns with [3.3] and [3.4]. Due to the bigger size of the weld bead, its quality also increased. Even though the surface quality is compared to the first three specimens still reasonably bad, it increased compared to specimen 4. The present defects are also not as noticeable as for specimen 4. The close up look of the weld bead surface of specimen 5 is shown in Figure 3.4.

Figure 3.4: Welding defects (waviness) in sample 5

Table 3.4: Bead geometry of individual single layer samples

Specimen	Width (mm)	Average width (mm)	Height (mm)	Average height (mm)	Weld bead form factor
1	7,13	6,98	1,78	1,90	0,27
	6,83		1,96		
	6,98		1,95		
2	6,94	6,87	1,86	1,89	0,28
	6,83		1,84		
	6,84		1,97		
3	10,60	11,18	2,30	2,47	0,22
	11,40		2,52		
	11,53		2,60		
4	5,10	4,75	1,16	1,16	0,24
	4,53		1,11		
	4,61		1,20		
5	6,41	6,00	1,89	1,91	0,32
	5,74		1,82		
	5,84		2,02		

3.3 OVERHANG - STATE OF THE ART

Due to the freeform shape of the objects that are usually manufactured with WAAM, the creation of overhangs is usually needed, which is again another AM constraint. Overhang angles are the angles for which 3D printers can print tilted surfaces without the need for supporting structures. In WAAM, using support material is not desirable due to the possibility of penetration of support material into the deposit and the creation of a permanent bond between these two parts, which might require additional post processing. [3.5] Therefore, it is important to accurately examine the maximum allowed overhangs and the impact of the main process parameters on the outcome of the overhang. In the following chapter, the impact of individual process parameters on the manufacturability of the overhang will be shown and the possible accuracy of the overhang build will be presented. At the end the experiment where the overhang capacity for the chosen process parameters will be conducted.

Li et al. [3.6] studied the possible achievable accuracy of the fabricated straight inclined thin walled part. For the purpose of the experiment 5 thin walls were printed, that differ in inclination angle, namely 0°, 22.5°, 45°, 67.5°, and 90°. After the print of each layer was complete, the horizontal and vertical growth was measured. The results are shown in Figure 3.5 and compared to the actual inclination. It can be concluded that the accuracy of the build is reasonably high, with the angle error under 10 %. Therefore we can assume that WAAM is suitable process for the design of the inclined thin walled parts.

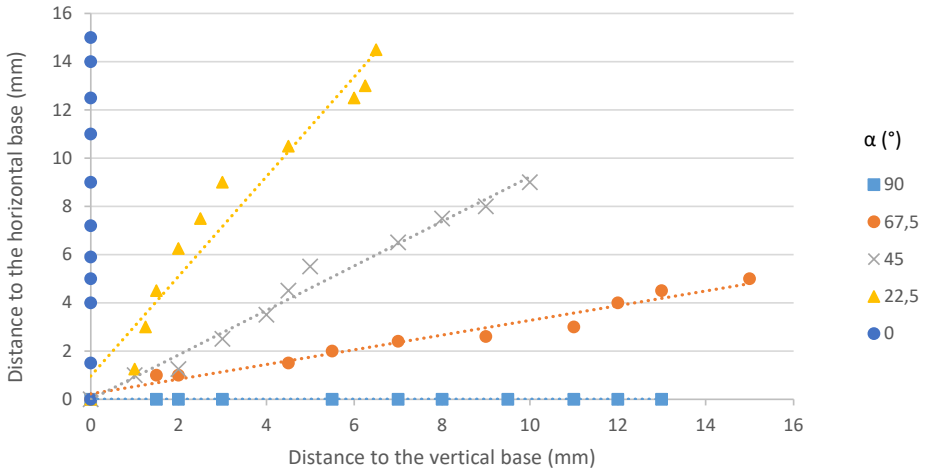

Figure 3.5: Accuracy of inclined thin walled parts [3.6]

Zhao et al. [3.7] explored the impact of WFS, TS, and offset distance (Δd) on the inclined geometrical features, namely inclined angle (a). Δd represents the horizontal distance from the center of the bottom layer to the center of the top layer. Firstly, the influence of WFS was studied. For this, TS was set to 8 mm/s and Δd was set to 1.4mm, while WFS ranged from 3,0 to 5,0 m/min. The results are shown in Figure 3.6 a, from which we can discern that the increase of WFS, will cause a slight decrease of a. For the second test, TS varied from 5,0 to 10,0 mm/s, while other process parameters were kept constant. Results of this test are shown in Figure 3.6 b and propose that TS and a increase/decrease simultaneously. Finally, the influence of Δd is examined (Figure 3.6 c), where TS and WFS are set constant and Δd changes from 1,2 to 1,8 mm. It was shown that the increase of Δd will cause the increase of a.

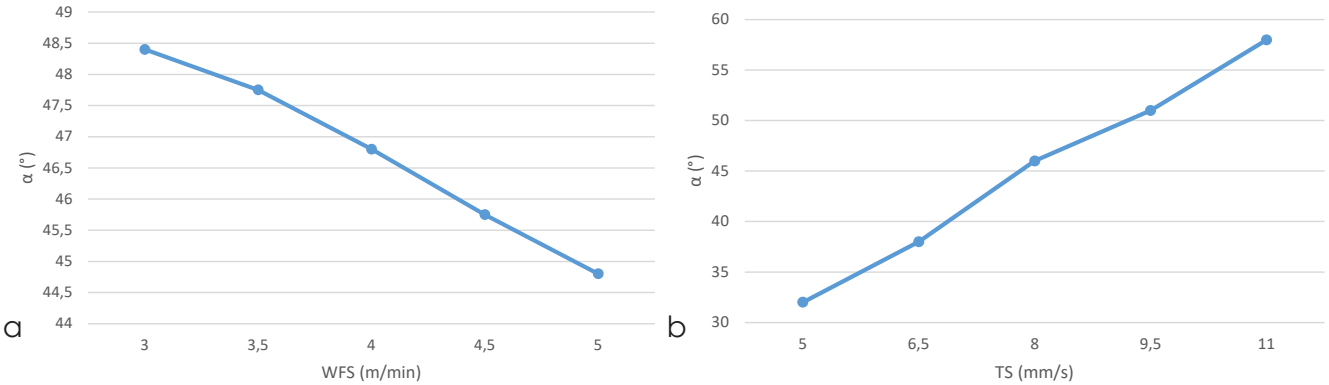

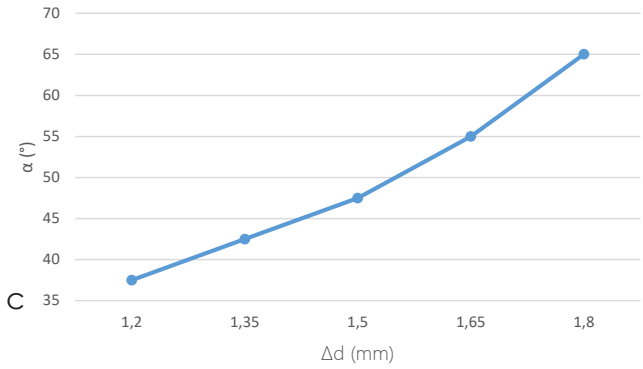

Figure 3.6: a) Effect of the WFS on inclined angle, b) Effect of the TS on the inclined angle, c) Effect of the Δd on the inclined angle [3.7]

3.4 OVERHANG - LAB TESTS

To determine the maximum allowed offset distance between individual layers and validate the overhang so the print is still stable, two experiments were conducted. Both experiments include the build of the thin walled wall inclined in either a parallel or perpendicular direction depending on the direction of the print. The material used for the print was welding wire ER70S-6, with a diameter of 1 mm. The chemical composition of the used material and shielding gas is shown in Table 3.1 and Table 3.2 respectively. The welding parameters are shown in Table 3.5 and are constant during both experiments, while the distance between the torch and weld beads was kept at 10 mm. Depending on the chosen process parameters the size of the weld beads can be read from Table 3.4.

Table 3.5: Chosen process parameters

Ts (mm/s)	Wfs (m/min)	I (A)	E (V)	HI (J/mm)
10	5	135	21,7	263,7

The overhang was created by linearly increasing the Δd each layer, thus creating the parabolic shape of the overhang. To create a more stable build each layer consist of two weld beads with the same Δd, meaning that every two weld beads Δd increased. The chosen deposition strategy is shown in Figure 3.7, where the bottom weld bead (black colour) begins at the start and finishes at the end, while the top weld bead (red colour) begins at the end and finishes at the start. The explained deposition strategy was implemented to lower the impact of the possible defects that usually occur at the start and end of the WAAM weld beads. The common defects include lack of fusion, lack of penetration, and improper bead geometry. The example can be seen in Figure 3.3. Between the print of the individual weld beads there was a pause to allow for the temperature of the weld to drop under 100 °C. This is very important due to the high heat accumulation of the surrounding materials. If the next layer is added before this accumulated heat dissipates, it can lead to excessive heat buildup and can negatively affect the subsequent weld, causing defects like porosity, cracks, or lack of fusion. In addition, it is important to wait for the molten pool to solidify, thus preventing distortion, warping, or other issues that may arise if subsequent layers are added before sufficient solidification.

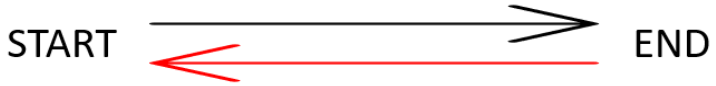

Figure 3.7: Deposition strategy

3.4.1 OVERHANG IN PERPENDICULAR DIRECTION

The overhang was done by increasing Δd each layer in a perpendicular direction depending on the direction of the print. The schematic representation of the printed overhang is shown in Figure 3.7. Each layer the Δd increased for 0,2 mm (meaning that layers 3 and 4 have Δd of 0,2 mm; layers 5 and 6 have Δd of 0,4 mm; layers 7 and 8 have Δd of 0,6 mm; and so on). All Δd corresponding to individual layers are presented in Table 3.6.

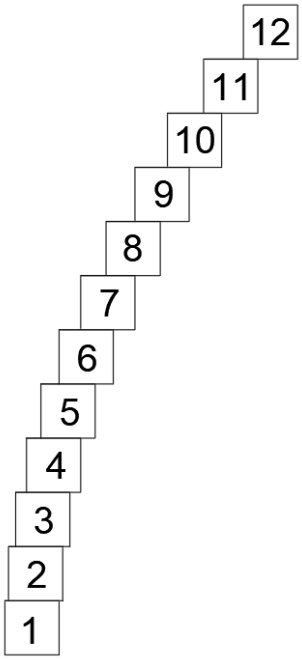

Figure 3.7: Schematic representation of the overhang in perpendicular direction

Table 3.6: List of Δd corresponding to individual layers

Layer	1	2	3	4	5	6	7	8	9	10	11	12
Δd (mm)	0	0,2	0,4	0,6	0,8	1,0	1,2	1,4	1,6	1,8	2,0	2,2

In total 12 layers (24 weld beads) were printed. The progress of the print is shown in Figure 4.8, where each picture represents the individual Δd. The last stable layer is layer 11 with the Δd of 2,0 mm which is shown in Figure 3.8 11. When Δd was in Layer 12 increased to 2,2 mm the weld bead collapsed and the print became unstable. This means that the Δd was too big and the molten pool did not have time to solidify and thus overflew (Figure 3.9). Therefore, it can be assumed that for the set process parameters the maximum allowed Δd while creating an overhang in perpendicular direction is 2,0 mm. The quality of the print was throughout the experiment high without noticeable defects, with an exception in layer 7. Figure 3.8 7 shows the overflow of the mentioned layer at the end of the weld bead. Even though the end of that particular weld bead collapsed, it did not have an influence on the overall stability of the overhang. The accuracy of the designed overhang turns out to be reasonably high. Figure 3.9 shows the 3D scan of the overhang with the comparison with the desirable shape (presented with red line).

1

2

3

4

5

6

7

8

9

10

11

Figure 3.8: The progress of the print of the overhang in perpendicular direction

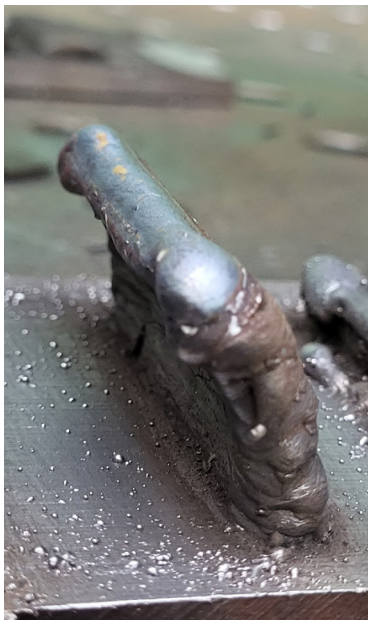

Figure 3.9: Overflow of the weld pool in layer 12

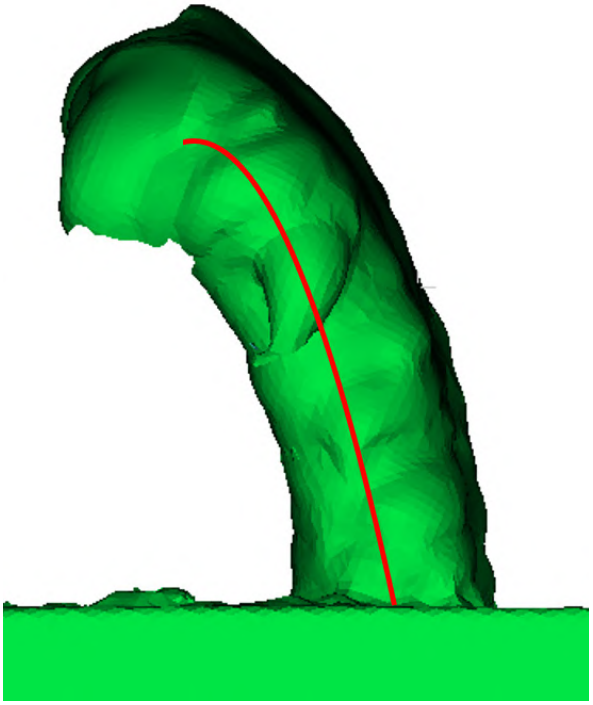

Figure 3.10: Accuracy of the printed overhang

It is important to notice that the welding torch was during the whole print always positioned vertically. The stability of a welding pool depends on the resultant of the 5 main forces, namely the gravity G, the droplet impact force Fd, the arc force Fa, the normal force from the solidified part F_N, and surface tension σ. All the mentioned forces are shown in Figure 3.11 depending on the orientation of the welding torch. Fd and Fa, which are two primary forces contributing to the stability of the molten pool, are believed to direct toward the solidification section in line with the welding torch direction. When the torch aligns with the inclined thin walled part (as depicted in Figure 3.10 b), it enhances the loading condition of the molten pool compared to the perpendicular torch position strategy (as illustrated in Figure 3.10 a). This improvement reduces the likelihood of molten pool overflow and benefits the overall fabrication process. [3.6] Based on this it can be assumed that the maximum allowed Δd where the print is still stable can be increased by aligning the welding torch in accordance with the inclined angle of the printed wall.

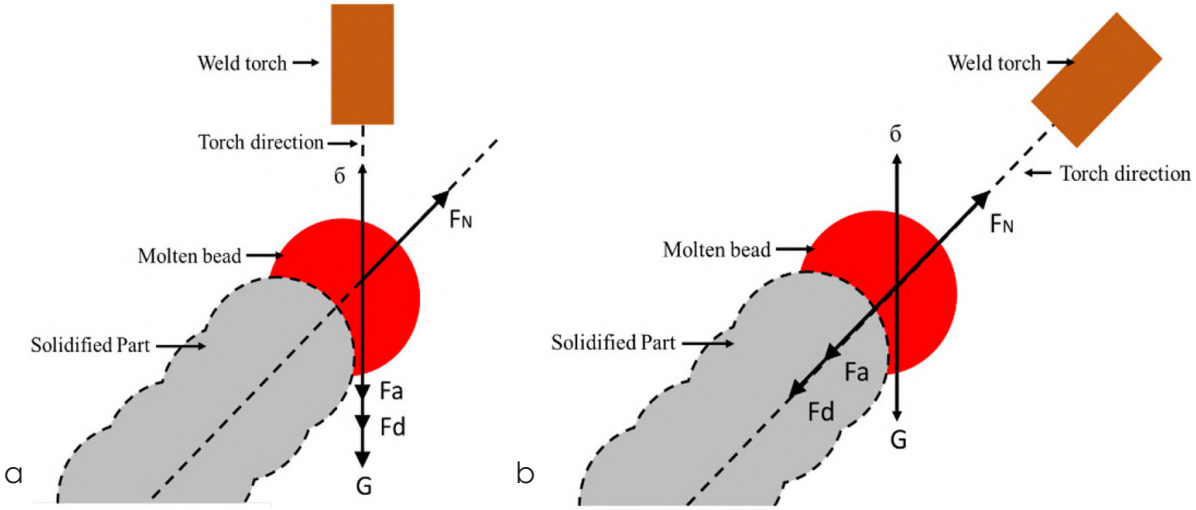

Figure 3.11: The force model of the weld bead of a thin walled part [3.6]

3.4.2 OVERHANG IN PARALLEL DIRECTION

The overhang in a parallel direction depending on the direction of the print was done by increasing the length of the individual weld beads. The schematic representation of the overhang in a parallel direction is shown in Figure 3.12. To create a stronger base and increase heat accumulation, the first 4 weld beads were printed without any Δd. After that, the Δd was for each layer implemented as shown in Table 3.7.

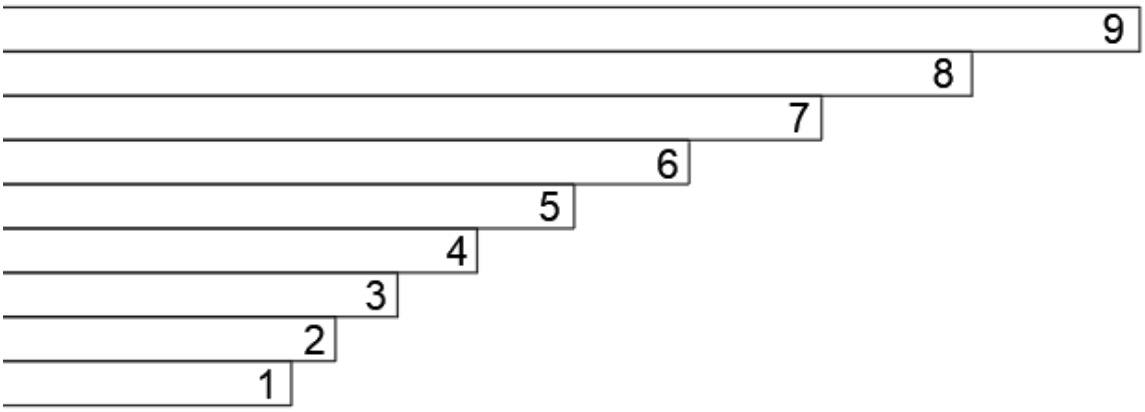

Figure 3.12: Schematic representation of the overhang in parallel direction

Table 3.7: List of Δd corresponding to individual layers

Layer	1	2	3	4	5	6	7	8	9
Δd (mm)	0	0,5	0,7	0,9	1,1	1,3	1,5	1,7	1,9

In total 9 layers were printed. The progress of the print is shown in Figure 3.13, where each picture shows the individual Δd. The last stable layer was layer 8 with the Δd of 1,7 mm. In layer 9 the Δd of 1,9 mm was applied and as shown in Figure 3.14 the layer collapsed. From this, it can be assumed that for the chosen process parameters and print conditions the maximum achievable overhang in parallel direction is 1,7 mm. Figure 3.15 shows the 3D scan of the overhang with the comparison with the desired shape (red line). Even though the overhang in a parallel direction is achievable its accuracy is reasonably low, especially in comparison with the overhang in perpendicular direction.

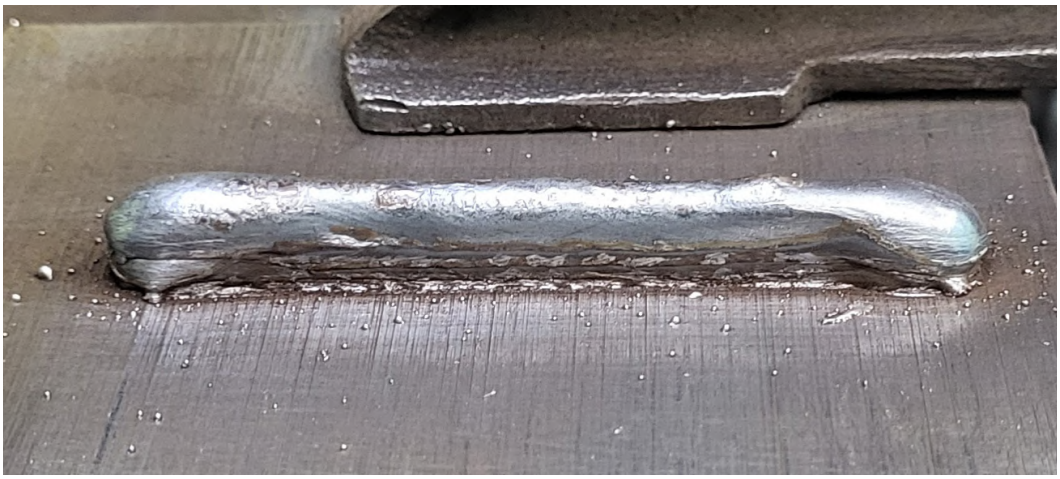

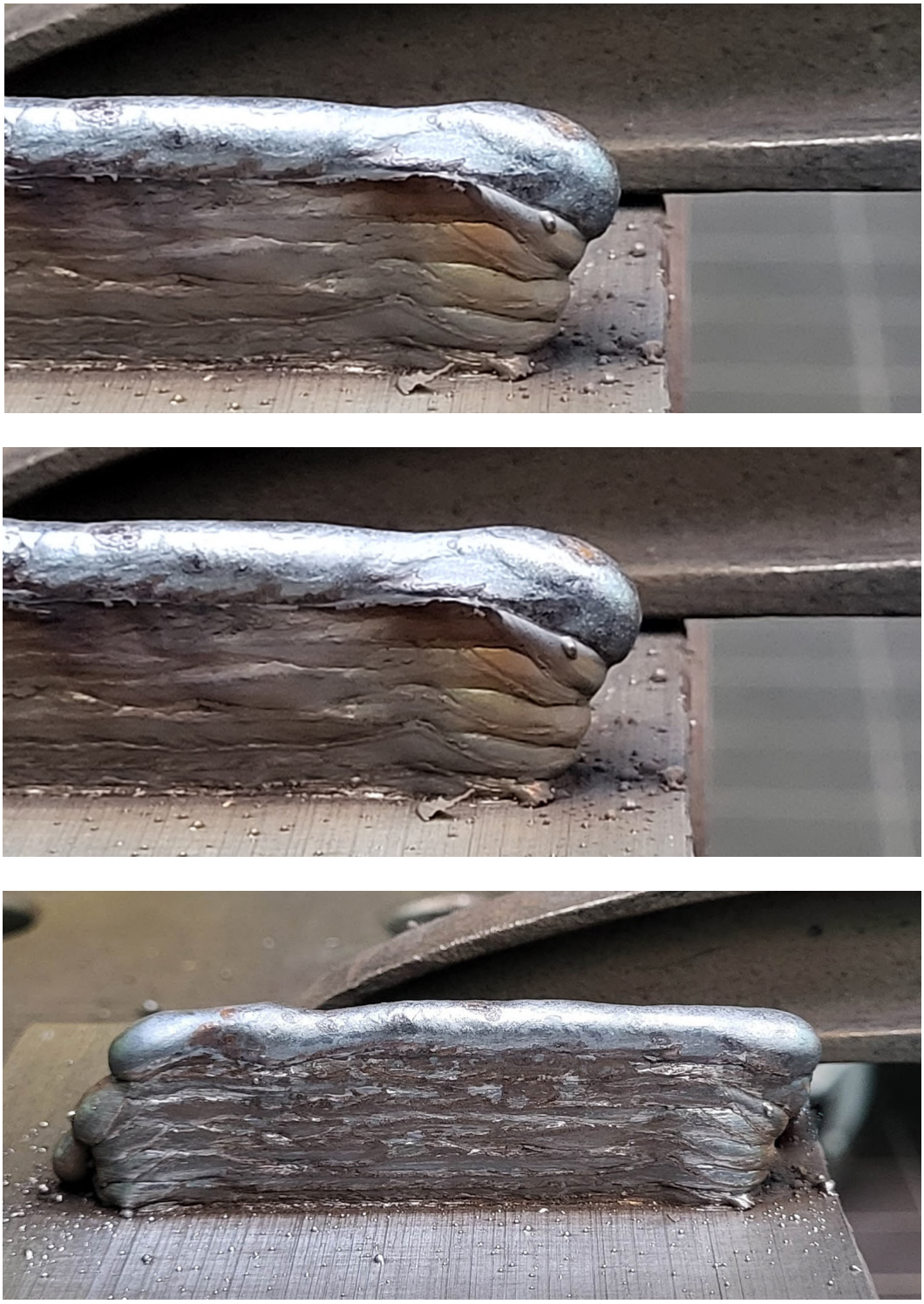

Figure 3.13: The progress of the print of the overhang in parallel direction

Figure 3.14: Overflow of the weld pool in layer 9

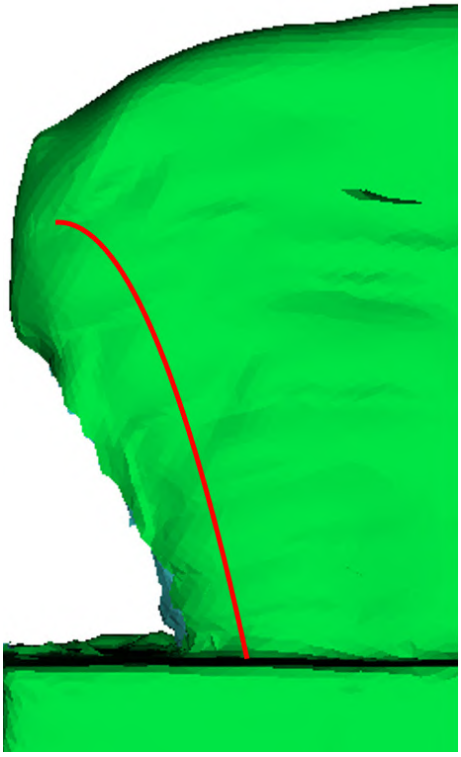

Figure 3.15: Accuracy of the printed overhang

3.5 OVERLAPPING - STATE OF THE ART

In WAAM, it is crucial to employ a parameter set that ensures the desired mechanical properties of the manufactured parts. To ensure the consistent performance of the printed material, it is recommended to use a single parameter set for the print of the whole object. However, complex parts, such as force flow optimized structures made with TO, often exhibit continuously changing wall thickness along the build up direction. Accommodating these thickness variations requires more than just adjusting the number of weld beads per layer, it also necessitates modifying the distance between individual beads. This is referred to as an overlap (Figure 3.16) and can be calculated with the following formula, where d represents weld bead distance and w weld bead width. [3.8]

$$Overlap\ (\%) = \left(1 - \frac{d(mm)}{w(mm)}\right) * 100 \qquad (2)$$

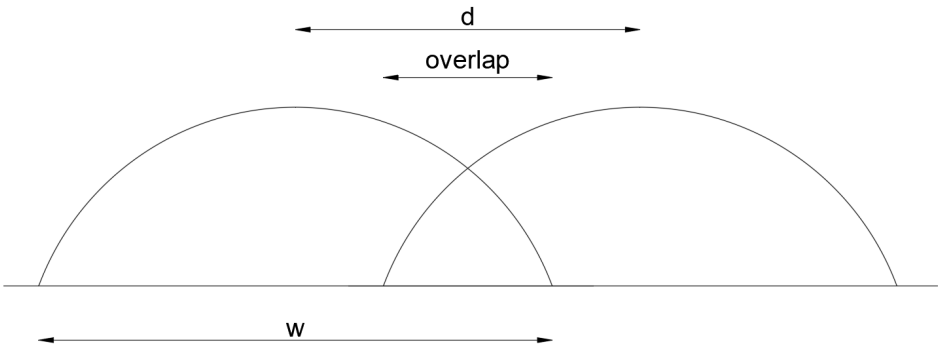

Figure 3.16: Scheme for the definition of overlap

To ensure the high quality print it is important to properly determine the optimal overlap percentage. If the distance between weld beads is too large, it can result in an uneven surface on the layer being deposited. This unevenness can further lead to a lack of fusion between the subsequent layer and the previous one, compromising the overall integrity of the part. Conversely, if the distance between weld beads is too small, it can cause the electric arc to be deflected toward the previously deposited weld bead. Consequently, the penetration into the previously welded layer may not be sufficient, and this can lead to an interlayer lack of fusion. Insufficient fusion in WAAM negatively impacts the quality of printed parts. It leads to structural weakness, reduced mechanical strength, porosity, inconsistent material properties, compromised surface finish, and dimensional inaccuracies. [3.8] Maintaining proper fusion between layers is crucial for achieving reliable, high quality results in WAAM. Therefore, finding the appropriate distance between weld requires striking a delicate balance where the distance is neither too large nor too small, allowing for consistent and effective fusion between layers, thereby producing parts with optimal strength and quality.

Ding et al. [3.9] developed a fitting function based on which the most optimal overlap distance can be determined. Based on this research the overlap distance is calculated as a percentage of the total width of the weld bead. The optimal overlap percentage was predicted to be 73,8 %. Cao et al. [3.10] studied a similar effect and also predicted the most optimal overlap percentage. The result of that study showed that the most optimal overlap percentage is 63,7 %.

Elsokaty et al. [3.11] made an experiment where the impact of different overlap percentages on the mechanical properties of the print was examined, namely hardness and tensile strength. Three samples with the same process parameters and different overlap percentages (30 %, 40 %, and 50 %) were tested. Hardness and tensile strength results are shown in Figure 3.17. It is possible to see that samples with 30 % overlap experienced the highest mechanical properties, while the increase of weld bead distance will result in the lower structural performance of the model.

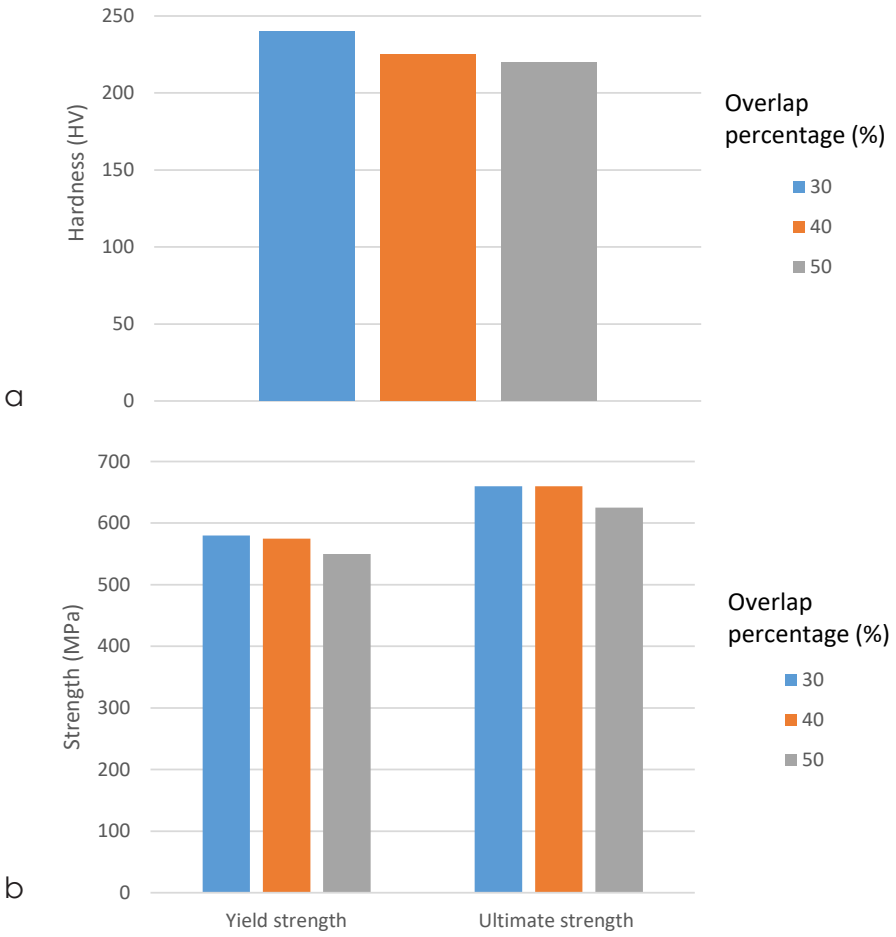

Figure 3.17: Inpact of overlap percentages on the: a) Hardness, b) Tensile strength [3.11]

3.6 OVERLAPPING - LAB TESTS

Above stated cognitions gathered from different research studies include a lot of contradicting information. Therefore, a short experiment was conducted where the visual effect of changing overlap percentage was examined. The material used for the print was welding wire ER70S-6, with a diameter of 1 mm. The chemical composition of the used material and shielding gas was, as shown in Table 3.1 and Table 3.2 respectively. The welding parameters are shown in Table 3.8, while the distance between the torch and weld beads was kept at 10 mm. Corresponding to the chosen process parameters the size of the weld beads can be read from Table 3.4. Multiple single layer weld beads were printed in a deposition strategy shown in Figure 3.18.

Table 3.8: Chosen process parameters

Ts (mm/s)	Wfs (m/min)	I (A)	E (V)	HI (J/mm)
10	5	135	21,7	263,7

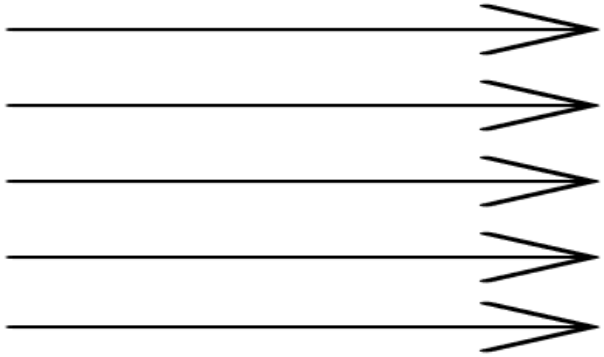

Figure 3.18: Deposition strategy

Three different overlap percentages were selected for the experiment, namely 60 %, 80 %, and 20 %. Corresponding d can be seen in Table 3.9. In the following paragraphs the influence of the different overlap percentages on the quality of the build is elaborated.

Table 3.9: Overlap percentages and bead distances

Test	Overlap (%)	Bead distance (mm)
1	60	2,8
2	80	1,4
3	20	5,6

- **60 % overlap**

Figure 3.19 shows the printed sample where 60 % overlapping was considered. In this case, the distance between individual weld beads was 2,8 mm. It is visible that the quality of the build is high without any noticeable defects. Individual weld beads intertwine nicely, thus creating a high quality homogeneous object, that behaves as one and not as multiple individual weld beads. The top surface is reasonably smooth without a high level of waviness. The occurred imperfections and small amount of waviness can easily be removed with the proper mechanical post processing. In addition, the second layer was printed on top of the first printed layer. This is shown in Figure 3.20. The qulity of the build is again high, without noticeable defects.

Based on this, it is possible assume that 60 % overlap is for the set process parameters good solution, that will provide the desirable outcome.

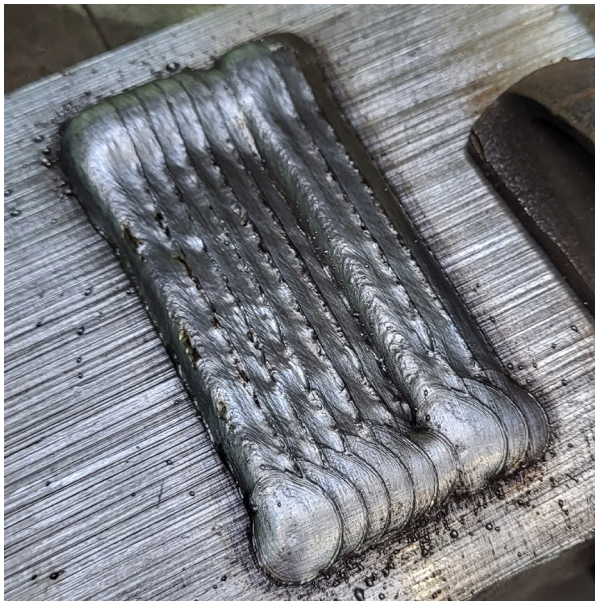

Figure 3.19: 60 % overlap - 1st layer

Figure 3.20: 60 % overlap - 2nd layer

- **80 % overlap**

Secondly, the print was done with an 80 % overlap, where weld bead distances were 1,4 mm. This can be seen in Figure 3.21. The print only continued for 5 layers, due to the collapse of the final weld bead. The overlap percentage was too big, thus the individual weld beads were just placed on top of each other instead of next to each other. The build has very bad quality and the desired shape could not be achieved by the set overlap percentage.

Based on the results, it can be assumed that for the set process parameters the 80 % overlap is to big to achieve the desired high quality object.

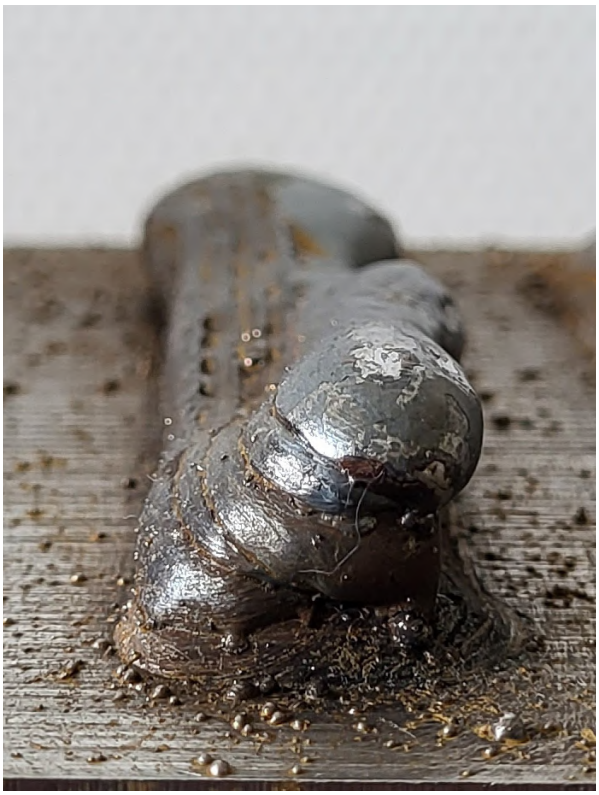

Figure 3.21: 80 % overlap

- **20 % overlap**

Finally, the sample with 20 % overlapping was built, where distances between individual weld beads are 5,6 mm. The print is shown in Figure 3.22. The weld beads are far apart, which creates voids between individual prints. The surface waviness is high, which might cause problems for aesthetic reasons. Besides that, the intertwinement between the individual weld beads is poor, which lowers their connectivity. The problem might occur in case additional layers are printed on top of the existing layers. In that case, the print would create multiple individual thin single bead walls rather than creating one homogeneous object. To solve this problem a new deposition strategy could be adopted, where top layers are placed in between the bottom existing layers, thus guaranteeing the required fusion between weld beads. The explained deposition strategy is shown in Figure 3.23, where the first layer is presented with black colour and second layer with red colour.

Based on the above explained findings assumption that 20 % overlap is too small for the built of the high quality object can be made.

Figure 3.22: 20 % overlap

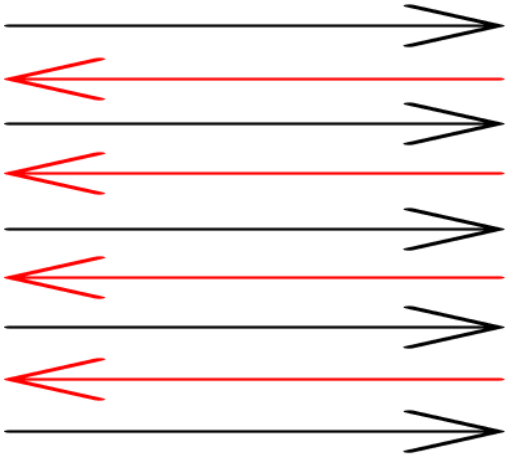

Figure 3.23: Deposition strategy in case weld beads are far apart. The first layer is presented with black colour and second layer (on top of the first one) with red colour.

3.7 CHAPTER CONCLUSION REMARKS

Throughout Chapter 3, manufacturing limitations that need to be considered while designing and printing a WAAM model were presented. In total three limitations were explained, namely the influence of WAAM input process parameters, minimum overhang angle, and optimal overlapping percentage. To conclude the chapter an overview of the presented results gathered from the laboratory tests will be done. These results will also be compared with values collected from the literature review of other research papers. By doing this it is possible to see how consistent and reliable the WAAM laboratory tests are.

- Process parameters

In WAAM, crucial input parameters include travel speed (TS), wire feed speed (WFS), and heat input (determined by welding arc current [I], voltage [V], and TS). TS impacts deposition path velocity, shaping geometry and surface finish. WFS ensures consistent deposition and dimensional accuracy, while heat input influences melt pool size and layer fusion. It is important to properly determine the correct combination of these parameters to enable the production of precise 3D-printed components, showcasing the adaptability of advanced manufacturing technologies.

Through the performed laboratory tests, the influence of TS and WFS on the width and height of the weld bead was examined. Besides this, a visual inspection of the quality of the print was shown. It is possible to conclude that the increase in TS will cause a decrease in the dimensions of the weld bead. Regarding the WFS, its decrease will decrease the weld bead dimensions as well. It was also noticed that with the lower values of WFS, the quality of the print is impacted. The surface of the weld became more wavy compared to previously smooth welds and there are defects present at the start and end of the print. These defects can be seen in Figure 3.3. All used input process parameters and their corresponding weld bead dimensions can be seen in Table 3.3 and Table 3.4 respectively.

In the following tables, the comparison between the results provided by Lambiase et al. [3.3] and results collected from the laboratory tests are displayed. The newly conducted results are presented with red dots. Figure 3.24 a and Figure 3.24 b show the impact on the height and width of the weld bead and present that both tests achieved similar outcomes, thus showing the consistency of the influence of the printing input parameters. In Figure 3.24 c some differences are visible, mostly in the sense that weld beads appeared more flat than those from the [3.3].

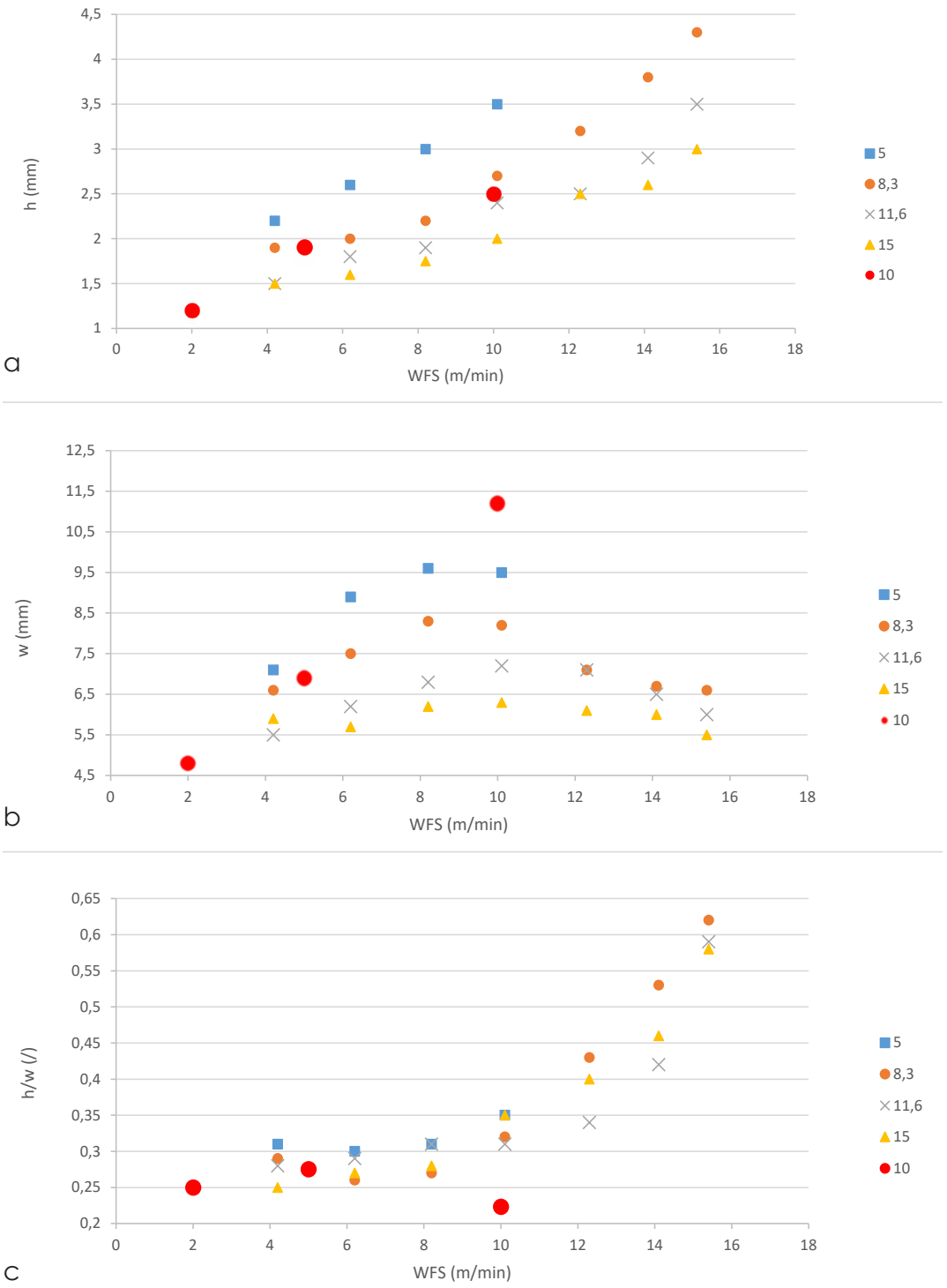

Figure 3.24: Influence of process parameters on bead geometry - results comparison between laboratory tests and literature review [3.3]

The results of the laboratory test showed that by changing the input process parameters not only the dimensions of the weld beads will be affected but also the quality of the print itself. Therefore it is important to select input process parameters so that a high quality build can be achieved. To do so each welding wire type has a so called technical specification sheet where the limit values of some input parameters are stated. For the selected welding wire ER70S-6 such technical specification sheet is shown in Appendix A.

- Overhang

In WAAM, an overhang refers to a portion of the printed object that extends horizontally beyond the previously deposited layers. Printing overhangs can be challenging as the molten metal or wire material may sag or droop due to gravity, potentially leading to geometric distortions or print defects. Specialized support structures or strategies may be employed to ensure the stability and accuracy of overhanging features during the additive manufacturing process. Overhangs are in most cases undesirable due to the possibility of penetration of support material into the deposit and the creation of a permanent bond between these two parts, which might require additional post processing. Because of that, it is important to determine the overhang limitations and consider them in the design phase.

A big factor that will have an influence on the magnitude of the overhang is the position flexibility of the torch. Figure 3.11 shows the force model of the weld bead of a thin walled part. It can be visible that by aligning the torch with the inclined thin walled part the distribution of forces contributes to better stability of the molten pool. Li et al. [3.6] showed by using this method that low overhang angles can be achieved with reasonably high accuracy (Figure 3.5).

During the laboratory tests the inclined torch was not used, meaning that it was constantly throughout the print positioned vertically. The distribution of forces in the weld bead is unfavourable (Figure 3.1). Therefore the stability of the molten pool is limited to the maximum allowed offset distance, which was determined through the performed experiments. Two separate overhangs were printed differentiating in the direction of the overhang depending on the direction of the print, namely perpendicular and parallel. Smaller overhang inclination could be achieved in the perpendicular direction where the last stable layer had an offset distance of 2.0 mm, while for the parallel direction, the maximum overhang was 1.7 mm. Besides this, the accuracy of both overhangs was compared with the conclusion that the overhang in the perpendicular direction achieved much higher precision (Figure 3.10 and Figure 3.15). These differences between the print directions should be considered during the print path programming. Concerning the overhang, its limit values should be taken into account during the design process of the printing model. This will guarantee that no part within the model has a lower inclination then proposed value, thus achieving high quality print.

- Overlapping

Overlapping percentage is an important parameter that needs to be considered during the printing path preparation process (g code) and manufacturing phase. It determines the distance between individual weld beads as presented in Figure 3.16. Considering overlapping in WAAM is crucial for several reasons. First, proper overlapping ensures the structural integrity of the manufactured object by creating strong bonds between successive layers of material. Second, it helps in achieving a uniform and consistent build, reducing the likelihood of defects such as voids or weak points. Additionally, overlapping plays a role in controlling thermal stresses and maintaining dimensional accuracy during the additive manufacturing process, contributing to the overall quality and reliability of the final product.

The overlapping can most easily be presented as a percentage of the weld thickness. During the laboratory tests, three different overlapping percentages were printed, namely 20%, 60%, and 80%, and then visually inspected. Created prints are shown in Figure 3.19, Figure 3.21, and Figure 3.22. Notably, the specimen featuring 20% overlapping encountered challenges in effectively fusing individual welds. This issue poses a potential risk of yielding a nonhomogeneous final part, characterized by uneven material distribution and compromised structural integrity. Rather than one solid part, multiple individual thin walled parts would be created.

Conversely, the scenario of 80% overlapping demonstrated a different set of complications. In this instance, weld beads were stacked on top of each other, ultimately resulting in the collapse of the printed object. This result emphasises how crucial it is to balance overlapping parameters in order to prevent negative effects on the WAAM process's overall printing and structural stability.

In contrast, the test specimen employing 60% overlapping exhibited favorable characteristics. The quality of the print was notably high, featuring high connectivity between individual welds, creating a homogeneous object. Furthermore, the surface waviness of the final part was relatively

minimal, indicating a well executed and successful manufacturing process. This underscores that percentages around the 60% value provide a sufficient high quality print, without any significant defects.

The conclusions of the performed laboratory tests showed similar results as the provided literature review. For example, Ding et al. [3.9] developed a fitting function based on which the most optimal overlap distance can be determined and was 73.8%. Similarly, Cao et al. [3.10] proposed that the most optimal overlapping percentage is 63.7%.

3.8 REFERENCES

[3.1] Jafari. D., Vaneker. T. H. J., Gibson. I. 2021. Wire and arc additive manufacturing: Opportunities and challenges to control the quality and accuracy of manufactured parts. Materials and Design. Available at: https://doi.org/10.1016/j.matdes.2021.109471

[3.2] Xia. C., Pan. Z., Polden. J., Li. H. 2020. A review on wire arc additive manufacturing: Monitoring, control and a framework of automated system. Journal of Manufacturing Systems. Available at: http://dx.doi.org/10.1016/j.jmsy.2020.08.008

[3.3] Lambiase. F., Scipioni. S. I., Paoletti. A. Accurate prediction of the bead geometry in wire arc additive manufacturing process. The International Journal of Advanced Manufacturing Technology. Available at: https://doi.org/10.1007/s00170-021-08588-w

[3.4] Dinovitzer. M., Chen. X., Laliberte. J., Huang. X., Frei. H. 2019. Effect of wire and arc additive manufacturing (WAAM) process parameters on bead geometry and microstructure. Additive Manufacturing. Available at: https://doi.org/10.1016/j.addma.2018.12.013

[3.5] Eyercioglu. O., Atalay. Y., Aladag. M. 2019. Evaluation of overhang angle in tig welding-based wire arc additive manufacturing process. International Journal of Research Granthaalayah. Available at: https://doi.org/10.29121/granthaalayah.v7.i10.2019.393

[3.6] Li. Y., Qin. X., Wu. Q., Hu. Z., Shao. T. 2019. Fabrication of curved overhanging thin-walled structure with robotic wire and arc additive manufacturing (RWAAM). Industrial Robot: the international journal of robotics research and application. Available at: 10.1108/IR-05-2019-0112

[3.7] Zhao. Y., Li. F., Chen. S., Lu. Z. 2019. Direct fabrication of inclined thin-walled parts by exploiting inherent overhanging capability of CMT process. Rapid Prototyping Journal. Available at: 10.1108/RPJ-03-2019-0081

[3.8] Müller. J., Hensel. J. 2023. WAAM of structural components—building strategies for varying wall thicknesses. Welding in the World. Available at: https://doi.org/10.1007/s40194-023-01481-y

[3.9] Ding. D, Pan. Z., Cuiuri. D., Li. H. 2014. A multi-bead overlapping model for robotic wire and arc additive manufacturing (WAAM). Robotics and Computer-Integrated Manufacturing. Available at: 10.1016/j.rcim.2014.08.008

[3.10] Cao. Y., Zhu. S., Liang. X., Wang. W. 2010. Overlapping model of beads and curve fitting of bead section for rapid manufacturing by robotic MAG welding process. Robotics and Computer-Integrated Manufacturing. Available at: 10.1016/j.rcim.2010.11.002

[3.11] Elsokaty. A., Oraby. O., Sadek. S., Salem. H. G. 2022. Influence ofWire Arc Additive Manufacturing Beads' Geometry and Building Strategy: Mechanical and Structural Behavior of ER70S-6 Prismatic Blocks. Manufacturing and Material Processing. Available at: https://doi.org/10.3390/jmmp7010003

CONNECTIONS

4. CONNECTIONS

4.1 ADDITIVE MANUFACTURED CONNECTIONS - STATE OF THE ART

Different strategies for integrating metal 3D printing into the construction sector could result in numerous specialized areas of use. The manufacture of metal components that provide practical answers to construction related problems is one significant possibility. Even though these materials are more expensive, their superior practical qualities can support the economic feasibility of metal 3D printing. With classic low cost building materials, qualities that were previously impossible to integrate are now possible thanks to advances in production technology. Creating specialized geometric shapes is one example. The digitized inventory and decentralized manufacturing made possible by metal 3D printing are another noteworthy benefit. These features result in shortened lead times, lower transportation costs, and easier supply chains. Additionally, this technology enables standard designs to be modified and customized to match regional needs. [4.1]

However, despite metal 3D printing technology's increasing readiness, the construction industry still has difficulties producing large scale structures. The main obstacles inhibiting the broad adoption of metal 3D printing at the moment are the lack of particular design regulations and limited experience. Serial production can cover the costs of experimental validation for high tech industrial items, but this method is impractical for comparatively straightforward civil constructions. Since these buildings are not mass produced, the testing procedures needed for each construction "product" would negate the advantages of metal 3D printing. Within the next ten years, it will be required to update the building rules and standards to completely integrate metal 3D printing into the construction industry. This entails defining particular metal 3D printing parameters (such as material and process) tailored for steel construction applications, analyzing the mechanical and metallurgical characteristics of steel parts produced using compatible 3D printing techniques, and coming up with techniques to precisely assess the structural, economic, and environmental effects of this emerging technology. New codes could be different from the conventional codes now employed in the building industry due to the nature of AM, where each unique product might have its own geometrical features (there is no need for uniform shapes). Therefore, rather than totally replacing it with AM technology, it is crucial to increase the ability to use AM in tandem with traditionally manufactured components. [4.2]

Throughout the years many projects concerning the usage of AM for structural application have been conducted, either as research or as a real life application. One of the more famous projects where AM is used on a bigger scale is the MX3D bridge located in Amsterdam, The Netherlands (Figure 4.1). It shows that WAAM is applicable for the design of not only individual structural elements but also structures as a whole. The integrity of the bridge was guaranteed by comprehensive physical testing and numerical modeling. With this, the required structural performance can be satisfied and the ultimate limit state specified in codes can be achieved. [4.3]

Figure 4.1: MX3D additive manufactured bridge [4.3]

The usage of metal 3D printing has also been explored for tubular elements, which are in the construction industry frequently used, mostly due to the high strength to weight ratio and architectural aesthetics. The biggest problem with tubular cross section is reasonably low buckling resistance of compression members. Recent studies showed that structural optimization can have a significant impact on the performance of tubular elements. Physical conducted tests of models made with PBF technology showed that optimized tubular cross sections with aster and wavy shells can achieve 40 % higher bucking resistance while maintaining the same volume. [4.1]

Besides using AM for the design of the whole element much research has been done on the design of the connections between two or more structural elements. In Figure 4.2, the optimized joint between the I section and the hollow column is made. The objective of the optimization was to maximize the rotational stiffness of the joint. The numerical simulation of the joint showed that structural optimization increased capacity and stiffness compared to traditionally fabricated joints of the same volume. [4.1] Kanyilmaz et. al. [4.4] and Chierici et.al. [4.5] have been exploring the design of the complex tubular nodes as a single element, instead of a multi part assembly (Figure 4.3 a). In their proposed designs the whole joint acts as a separate element to which the profiles are subsequently attached by welded or bolted connection. Using hollow sections for columns might be problematic due to the low bending stiffnesses of the section walls, therefore stiffeners are usually applied. By designing the optimized shape, authors obtained geometry. with already included natural stiffeners, which is shown in Figure 4.3 b.

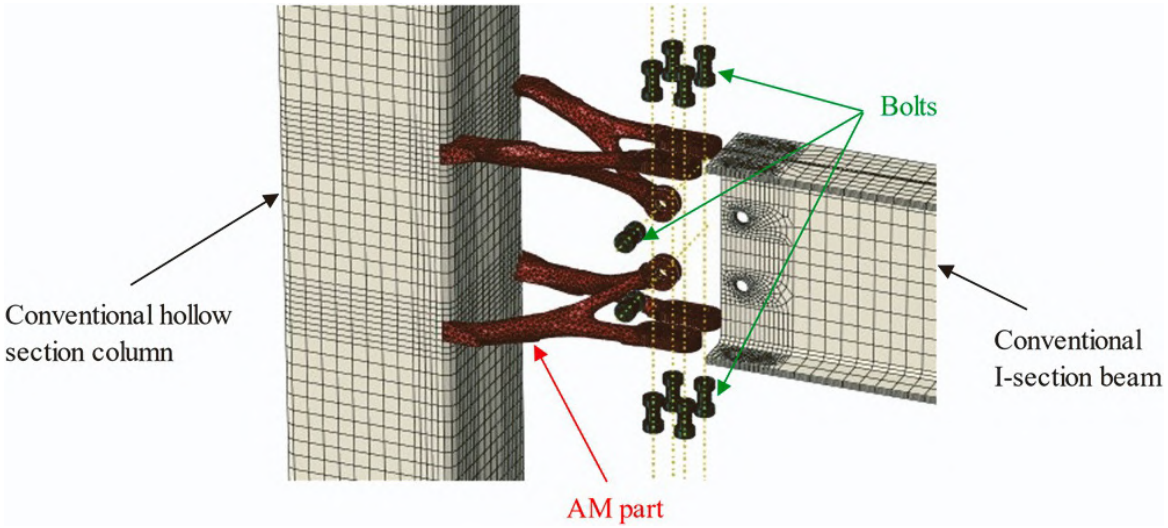

Figure 4.2: Optimized joint between an I-section beam and a hollow section column [4.1]

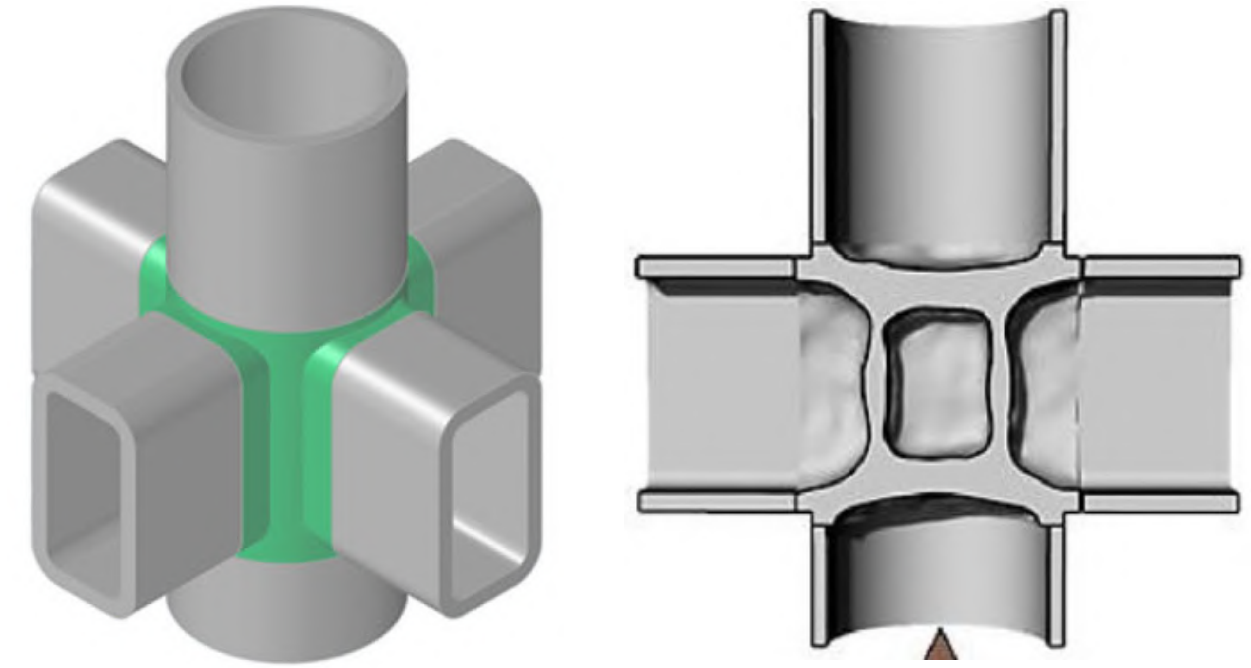

Figure 4.3: a) Node between tubular elements, b) Natural stiffeners [4.4]

A two floor pavilion building located in Massachusetts, USA uses an interestingly shaped façade where glass panels are unevenly placed onto the supporting structure (different distances from the slab edge), which is presented in Figure 4.4 a. AM was used to design TO connections for the façade panels, where each connection was designed and shaped based on individual requirements. This method produced connections that were not labour intensive and aesthetically more pleasing than welded plate design. One connection iteration is shown in Figure 4.4 b. The required structural performance of the connections was proven with physical tests of 3D printed test coupons. [4.6]

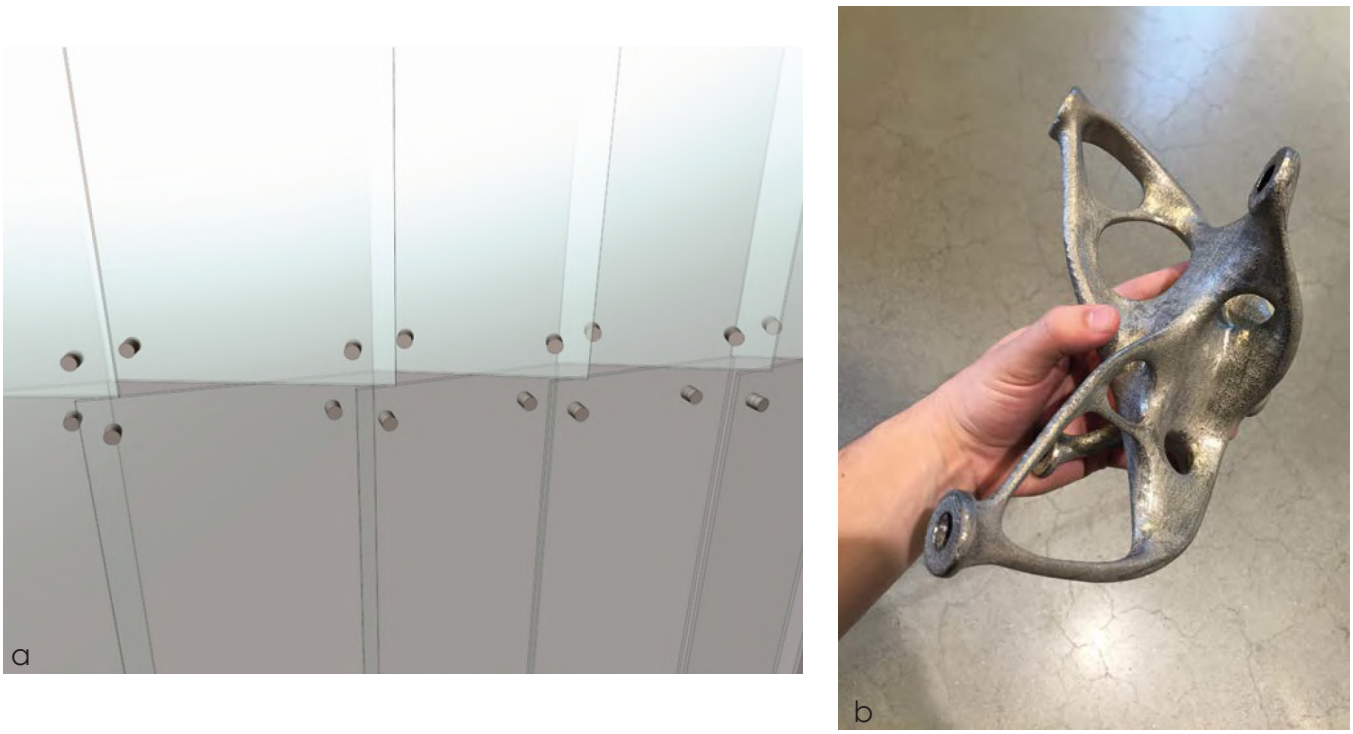

Figure 4.4: a) Close-up of the façade showing geometric variation, b) Optimized AM connection [4.6]

In a research paper written by Lange and Feucht [4.7], multiple different application possibilities of WAAM for structural elements are proposed, especially in a sense of connections where little material is needed and great geometrical variation is present. Their proposal included so called beam hook, which is a substitute for pinned connection between a steel column and beam, for example fin connection (Figure 4.5 a), a stiffener for increased bending and bucking resistance of an I section (Figure 4.5 b), an end plate as a replacement for a T-stub model (Figure 4.5 c), and a node to connect four elements within the space frame (Figure 4.5 d). All of the shown designs are focused on achieving the advantages of AM, which are better dimensional tolerances, simple erection, material efficiency, etc.

a

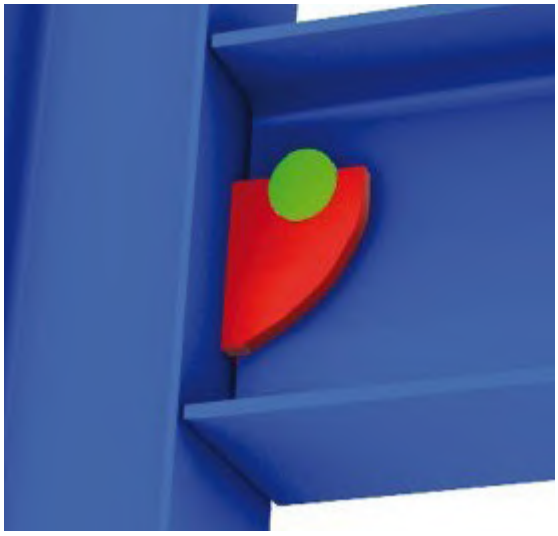

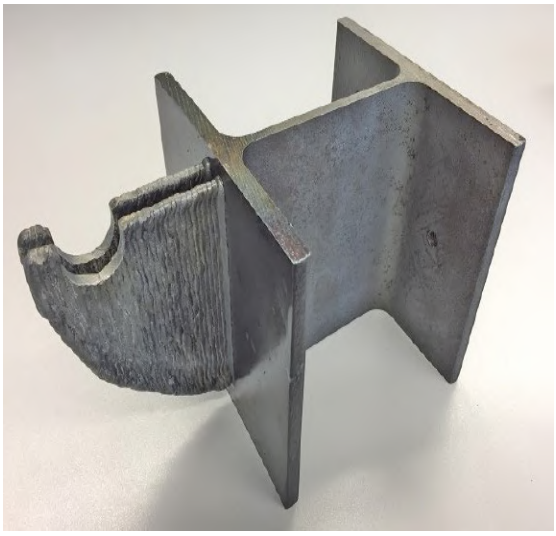

b

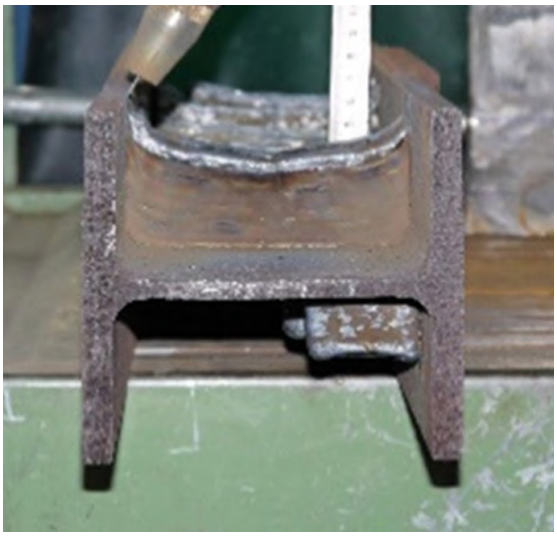

c

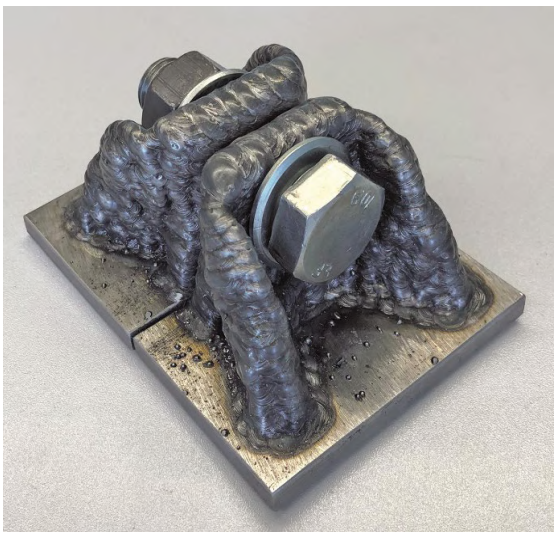

d

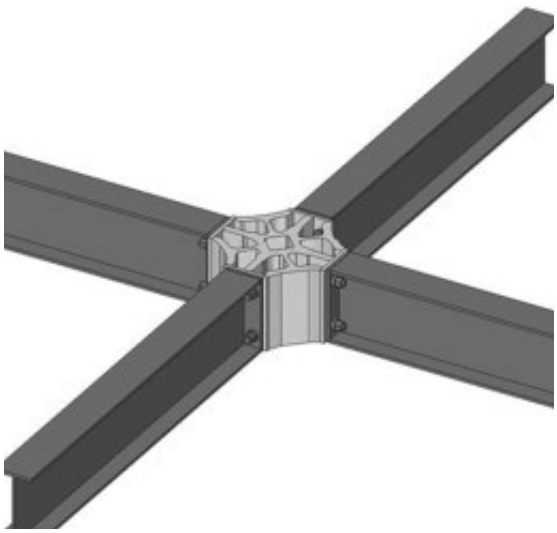

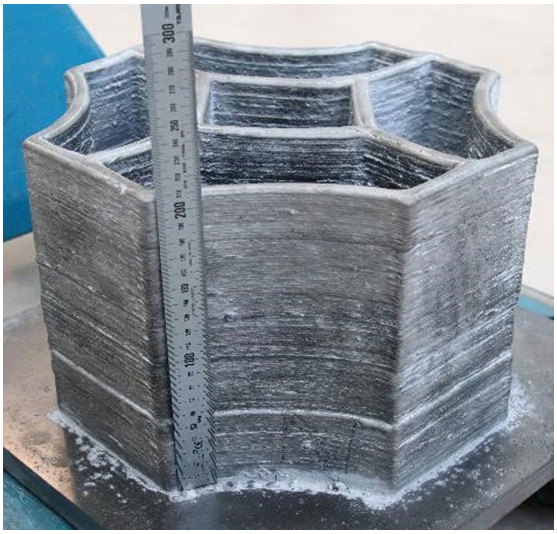

Figure 4.5: a) Beam hook, b) Stiffener, c) End plate, d) Space frame node [4.7]

Takenaka Corporation presented a conceptual design of a free form structural connector that uses 3D printing technology. The joint is connecting a vertical column with multiple branches under arbitrary angles and was further TO. For printing, WAAM technology was used, as it combines good material mechanical properties and reasonably good geometrical accuracy. Destructive testing showed strong and constant structural performance of the joint establishing the relevance of robotic 3D printing to the construction industry. Figure 4.6 shows the designed connection. [4.8]

Figure 4.6: Free form structural connector [4.8]

Swiss company Jansen in corporation with TU Delft, Knippershelbig GmbH, and MG Metalltechnik GmbH studied the possibility of using AM for the design of the free from structures. They used 2 different AM technologies (DED and SLM) to print a free geometry joint that is capable to connect multiple VISS profiles coming from different directions and angles (Figure 4.7). High strength connections allow for the load to be transferred directly through VISS profiles, thus no secondary structure is needed. Besides that, printed nodes ensure an organic homogeneous appearance, which goes along with the free form frame structure. The onsite assembly process is simplified as there is no need for special tools to connect profiles with the joint. [4.9]

a

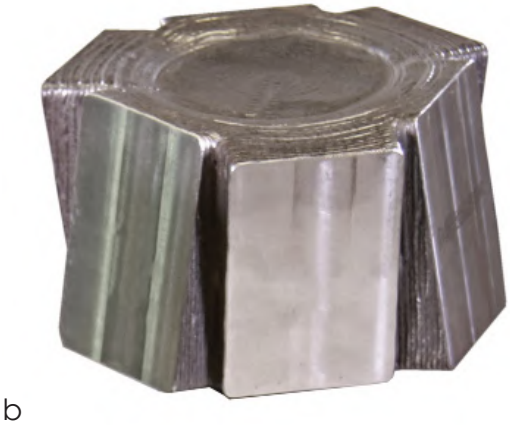

b

c

Figure 4.7: a) Facade structure, b) AM node with DED, c) AM node with SLM [4.9]

SLS has been used in the 6 Bevis Marks building in London by the architect company Flecher Priest and construction firm Skanska. In the project, the addition of 9 floors to the existing building has been done. An interesting part of the building is the roof canopy (Figure 4.8), which consists of a steel framework, made with CHS profiles supported by branched columns and covered by ETFE pneumatic cushions. The canopy is open on both sides and is designed so it wraps around both sides of the structure, thus forming a curved profile. [4.11] In order to obtain an appropriate structural solution that is coherent and integrated with the architecture of the existing structure, a form finding of each structural junction of the roof frame was done, as well as for the pattering of the ETFE pillows. The form finding contributed also to the design of the connections between 8 columns and 45 branches supporting the frame structure. The shape of the connection depends on the number of branches, which is influenced by the location of the column. The number of branches varies from five to seven per column. A complex column-branches node was first intended to be manufactured with individually designed cast steel elements, but construction firm Skanska expressed concerns regarding expense and difficulty. [4.12] The final design of the node consists of multiple individual steel plates that are by welding connected together. The structural connection can be seen in Figure 4.9 a. The aesthetic shape of the node did not coincide with the architect's vision of following the organic shapes of the canopy, therefore sheaths were designed for each individual connection shape (Figure 4.9 b). 3D modeling was used to achieve the desired organic shape of the covering and to get the needed information for the printing machine (Figure 4.9 c). For the manufacturing of the covering SLS process was used, which is in more detail explained in Chapter 2.1.2 3D printing technologies – powder bed fusion. The 3D printing material is a type of nylon that is suitable for exterior applications as it can obtain environmental impacts. [4.10]

Figure 4.8: 6 Bevis Marks in London [4.13]

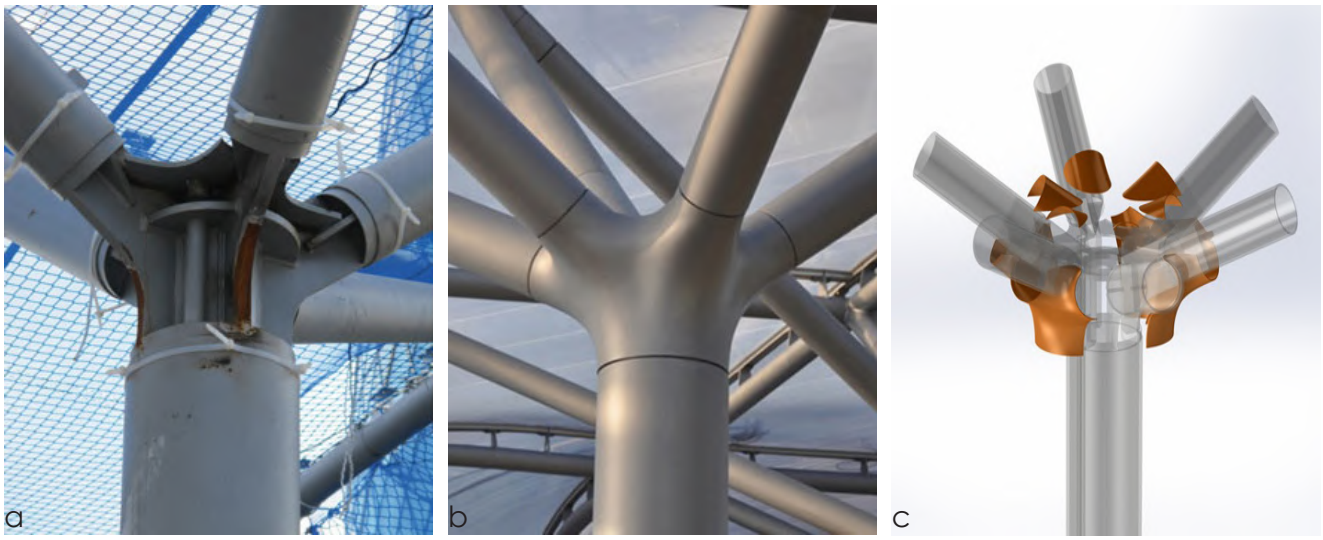

Figure 4.9: a) Structural connection [4.12], b) Final connection design [4.12], c) 3D model of the sheaths [4.14]

4.2 BRANCHED COLUMNS - STATE OF THE ART

For the purpose of this thesis, the possible use of WAAM for the design and manufacture of structural steel connections will be presented for branched columns. Branched columns, also known as branched members or branching columns, are unique and innovative structural elements that have gained attention in the field of engineering and architecture. Unlike traditional single column designs, branched columns split into multiple branches, thus resembling tree shapes. These unique features are employed for specific engineering needs and architectural objectives.

One of the primary reasons branched columns are used is their efficient load distribution. By dividing into multiple branches, they effectively disperse applied forces, reducing stress concentration and enhancing load carrying capacity. This characteristic makes them ideal for supporting heavy vertical loads or complex load patterns, while also allowing bigger distances between individual columns (spans), thus providing space efficiency. Another advantage of branched columns is their inherent redundancy, which contributes to overall structural integrity. In case of localized damage or failures in one branch, the load can be redistributed to neighbouring branches, ensuring the continued stability of the structure. This resilience makes branched columns particularly appealing for safety critical applications. [4.15] Moreover, branched columns provide material efficiency, leading to cost savings in construction. By distributing loads across multiple branches, they require less material compared to traditional single column designs while maintaining structural strength. This advantage makes them cost effective and sustainable if they are properly designed. From an architectural perspective, branched columns offer aesthetic appeal due to their unique branching patterns. The visually striking design adds an artistic touch to buildings and spaces, making them an attractive choice for modern and contemporary architectural projects. If designed properly branched columns can achieve a smooth organic shape, which is a key aspect of modern architecture and design. Besides that, the versatility of branched columns extends to their adaptability. Engineers can customize the number, angle, and positioning of branches to meet specific structural needs or achieve desired aesthetics. This flexibility allows them to accommodate irregular floor layouts and challenging architectural configurations. This means that branched columns are ideal structural elements for the support of complex shaped structures (for example free form roofs). [4.16] An example of the possible use of branched columns for the support of the roof structure is Den Haag Centraal railway station (Figure 4.10).

Figure 4.10: Branched columns in the Den Haag Centraal railway station [4.16]

However, the implementation of branched columns does come with certain challenges. The design and analysis of branched columns can be more complex compared to traditional single column designs. Determining the optimal branching angles, sizes, and positions requires careful engineering calculations and simulations to ensure structural integrity and load distribution. This complexity may add to the overall project cost and time. Additionally, the construction of branched columns may present practical challenges during the fabrication and erection phases. Precise fabrication and welding of the branching connections are critical to ensure that the load transfer occurs as intended. Due to the complex shape of the connection between column and branches its design can not be standardized, which increases the design difficulty. This is also applicable to the manufacturing process, meaning that its manufacturing with conventional technologies is very complex and time consuming.

To solve the above stated problems and complications, one intriguing possibility for manufacturing branched columns is through WAAM. With WAAM, the complex geometry of branched columns can be easily achieved, allowing for precise control and optimization over branching angles and positions. This capability enables engineers to produce customized branched column designs efficiently and accurately while still achieving required structural performnces.

4.3 TOPOLOGY OPTIMIZATION - STATE OF THE ART

Topology optimization (TO) is a process that creates the most optimal material layout of a given 2D or 3D model, based on provided set of rules. It is besides sizing optimization and shape optimization one of the three types of structural optimization and is commonly used in many different industries, such as automotive, aerospace, and construction. The main purpose of the TO is to increase the performance of the element, by designing its shape following the mathematical modeling principles. By introducing advanced algorithms and computation models TO enables engineers to maximize the performance of a design while minimizing its weight, cost, and material usage. The topology optimized shape will differ depending on the design limitations set by the user. The input parameters are external forces, load conditions, boundary conditions, constraints, and material properties. Besides that, the outcome of the TO will also depend on the set objectives. Depending on the whished end result the optimization software can reduce the stiffness-to-weight ratio, increase the strain energy-to-weight ratio, or reduce material volume. [4.18]

TO involves iteratively removing material from non-essential regions while maintaining structural integrity. Two popular approaches to topology optimization are density based topology optimization (DBTO) and level set based topology optimization (LSBTO). Both methods have unique characteristics and advantages, offering engineers valuable tools for creating innovative and efficient designs. DBTO, better known as solid isotropic material with penalization (SIMP) uses a continuous density field to represent the distribution of materials within a design area. According to this method, each design domain point has a density value assigned to it that represents the volume of material that is present there. The densities range from zero to one, and they are repeatedly changed during the optimization process to obtain the desired structural performance. The density values are then mapped to material properties, and regions with low densities (close to zero) represent void or empty space, while regions with high densities (close to one) represent solid material. This strategy is ideal for additive manufacturing because it can transform optimised ideas directly into complex shapes that are challenging to produce using conventional manufacturing techniques. However, the geometries generated with DBTO have in most cases rough and poorly defined geometry, thus post processing and smoothing is required before the object can be manufactured. [4.19] LSBTO is an alternative method that represents the geometry of a design using a level set function. The boundary between the solid and void regions is implicitly defined by the level set function, which assigns various values to various areas of the design domain. To achieve the desired structural performance, the level set function and material distribution within the design domain alter as the optimization process goes on. LSBTO is due to the level set function capable of producing smooth geometries with gradual material transitions. In contrast to DBTO, LSBTO may need more computing power and time because it updates the level set function between iterations by solving partial differential equations. [4.20]

While creating the TO, a certain procedure needs to be followed. [4.21] The steps are described in the following paragraph and presented in Figure 4.11. Firstly the initial geometry needs to be created that coincides with the design space. The user then needs to specify so-called excluded areas (preserved geometry), which are the areas where the element is attached to the supports or where the load is applied. Loads, boundary conditions, and material properties are then defined and applied to the model. To create a FEM model, the mesh needs to be defined and generated. After the model is set, the objective of the optimization needs to be defined, where the user decides what is the purpose of the optimization. After the TO is completed, the optimized geometry can be exported and edited for the purpose of manufacturability. In the end, the optimized design is again analyzed with FEM.

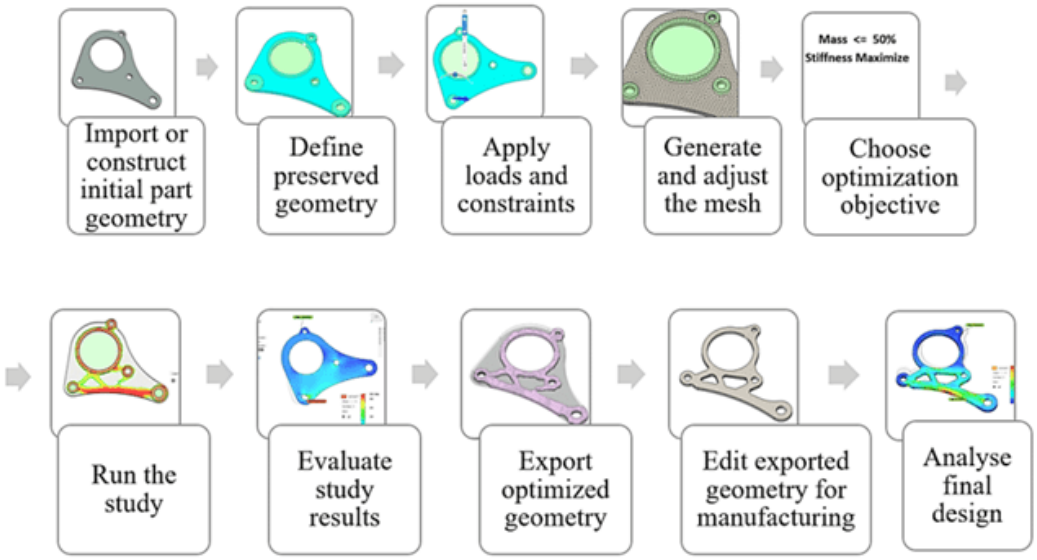

Figure 4.11: Topology optimization procedure

TO is a progressive technique that is revolutionizing the field of engineering design. It provides us with many advantages over traditional design methods, mainly the increased efficiency of the product. Its ability to reduce the amount of unnecessary material and thus increase the stiffness-to-weight ratio will decrease the mass of the products therefore also decreasing the necessary energy consumption. Because of material minimization topology optimized products are much more cost effective and have a lower environmental footprint. [4.21]

An important aspect of TO is that it does not take into account the final shape of the optimized model, as it is only following a mathematically driven design. This means that in most cases the optimized geometry turns out to have a very complex shape, which might not be suitable for production with the traditional manufacturing techniques. For example, the topology optimized organic shapes would be manufactured with subtractive techniques, where unwanted material is removed from the original block. This would cause high material wastage and thus high production costs, while also increasing production time. AM is a perfect tool for the production of TO elements, due to its ability to produce complex geometries. AM and TO thus complement each other in the sense that their usage is not really beneficial without their cooperation. [4.22]

To apply TO into the design, different software packages are available. For the purpose of this assignment, the ANSYS software package will be used. [4.23] ANSYS is a finite element analysis (FEA) software, produced by an American multinational company, that uses advanced solver options (including both above explained TO) to perform structural analysis. Its biggest advantage is that all necessary calculations (modeling, structural analysis, TO, and verification of the design) can be completed within the same workbench. This lowers the possibility of errors while exporting and importing results into different softwares.

4.4 BRANCHED COLUMN CONNECTION - RESULTS

As stated before, the biggest advantage of the branched columns is their freeform and nonstandard shape, which can be adjusted and modified based on the most beneficial design input parameters. This chapter will examine the influence of different TO input parameters, applied loads, boundary conditions, angle of branches, etc. on the TO geometry. The variety of TO geometries will be collected, differentiating in mentioned parameters, and then rated based on relevant output, namely structural validation, mass and volume reduction, and manufacturability. The manufacturability aspect is especially relevant since the connection is intended to be printed with WAAM. To guarantee that the connection's geometry is within the WAAM manufacture limitations, the knowledge collected in Chapter 3 will be considered. Based on this, the most optimal TO input parameters will be determined, which will then be used for further analysis.

To perform the structural analysis a certain material and its material properties needed to be selected, thus ER70S-6 was picked. ER70S-6 is a widely used WAAM welding wire due to its versatility, good weldability, and cost effectiveness. It provides adequate strength, produces high quality welds, and is compatible with carbon and low alloy steels commonly used in WAAM applications. Material properties of the selected wire are stated in Chapter 2.2.2 Material. For further analysis the mechanical properties of the as built samples were considered, meaning that post processing of the connections was not predicted. Besides that the isotropic material behaviour was assumed, meaning that the object have the same mechanical properties in all directions. This means that the yield strength was assumed to be 320 MPa, while elastic modulus is 214 GPa. In the case of post processing the yield strength increases to an average of 375 MPa.

The last part of this chapter will be concerned with the engineering solutions of the proposed connection, where the complexity of the on site assembly will be solved. The necessary adjustments to the TO geometry will be made and the advantages of these solutions will be presented.

To determine the loads acting on the connection, a simple frame structure was assumed as shown in Figure 4.12. The frame model consists of a single column, two branches, and a roof slab that is loaded with a vertical load of 5 kN/m2. Both column and branches are made with circular hollow cross sections, namely CHS 101.6x10 and CHS 114.3x20 respectively. The structure was also modeled in MatrixFrame software [4.24], from which internal forces and moments acting on the connection were determined. To perform TO the initial ''block'' of material needs to be assumed so it enables the optimization process to find globally efficient design and helps to create practical and manufacturable solutions. The geometry and the dimensions of the block are shown in Figure 4.13 a.

4.4.1 TOPOLOGY OPTIMIZATION ANALYSIS SETTINGS

To determine the loads acting on the connection, a simple frame structure was assumed as shown in Figure 4.12. The frame model consists of a single column, two branches, and a roof slab that is loaded with a vertical load of 5 kN/m2. Both column and branches are made with circular hollow cross sections, namely CHS 101.6x10 and CHS 114.3x20 respectively. The structure was also modeled in MatrixFrame software [4.24], from which internal forces and moments acting on the connection were determined. To perform TO the initial ''block'' of material needs to be assumed so it enables the optimization process to find globally efficient design and helps to create practical and manufacturable solutions. The geometry and the dimensions of the block are shown in Figure 4.13 a. The TO block was loaded with the load split into three components, namely horizontal, vertical, and moment load (Figure 4.13 b) with the magnitude of 162.8 kN, 57.7 kN, and 26.6 kNm respectively. To perform TO, a mesh was generated with an element size of 5 mm.

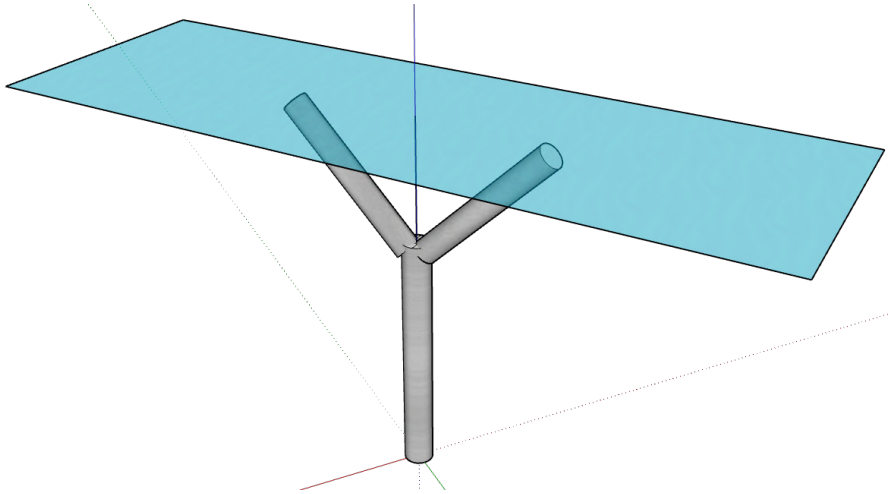

Figure 4.12: Frame structure

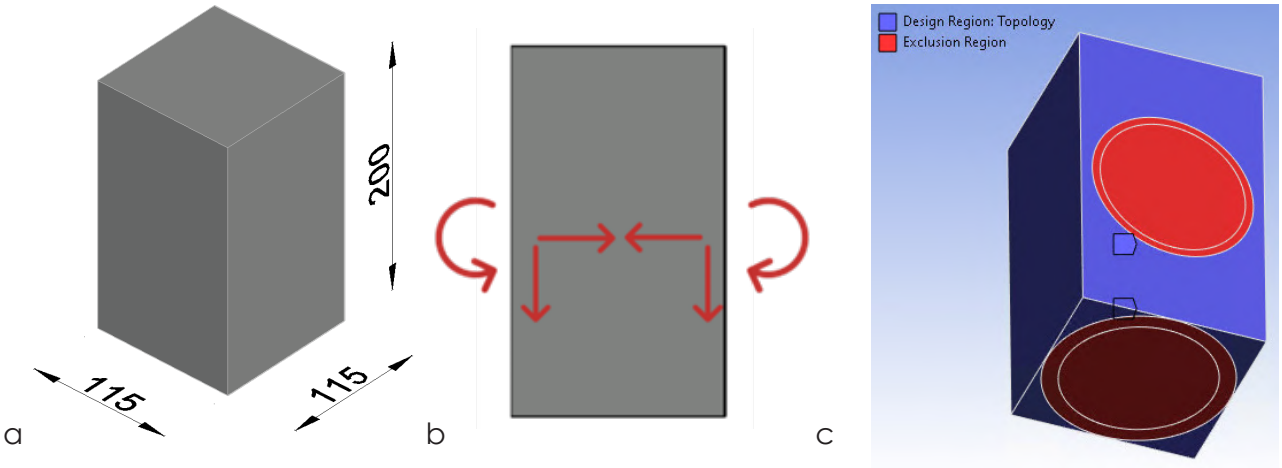

Figure 4.13: a) TO block dimensions, b) Application of loads

In Table 4.1 all more relevant TO analysis settings and model set up information are presented. All TO input parameters can be seen in Appendix B.

Table 4.1: Main topology optimization model set up information

Column profile	CHS 114.3x20
Branch profile	CHS 101.6x10
Vertical loading	5 kN/m^2
Nx	162.8 kN
Vz	57.7 kN
My	26.6 kNm
Mesh size	5 mm

4.4.2 TOPOLOGY OPTIMIZATION INPUT PARAMETERS

Since TO is a complex process with many variables at play, many models must be constructed. These models were created to investigate the interactions between various input parameters and understand how they impact optimization outcomes. The process involves generating a variety of models with distinct TO objectives and constraints, all aimed at enhancing the performance and efficiency of the connection.

The primary objectives in this TO process are compliance, equivalent stress, mass, and volume. The objective of compliance optimization is to strike an optimal balance between structural rigidity and flexibility, ensuring that the structure can deform appropriately to accommodate varying loads or conditions. This enables the structure to perform optimally, absorb stress efficiently, and minimize deformation in critical areas. The primary objective of stress optimization is to distribute material within the model in a way that ensures stress is minimized, particularly in critical regions or areas prone to high stress concentrations. This involves adjusting the topology or layout of the material within the design to ensure that stress is evenly distributed and remains within safe operating limits. Mass optimization focuses on reducing the weight of the connection while maintaining structural integrity, an essential consideration for practical applications. Volume optimization tries to minimize the volume of the required material for the production of the designed shape.

To guide the topology optimization process effectively, specific constraints were incorporated related to each objective. For compliance and stress objectives, mass retain percentage constraints will be imposed. This constraint ensures that during the optimization, the structure's mass does not fall below a certain predefined percentage, preventing excessive material removal that might compromise stability or safety. Additionally, for mass and volume objectives, stress limit constraints will be employed. These constraints ensure that, while optimizing for mass reduction or space efficiency, stress levels within the connection remain within a predefined limit. This is imperative to maintain the structural integrity of the connection, preventing the design from becoming overly fragile or susceptible to failure.

Figure 4.14 shows the overview of the explained TO objectives and constraints, while also providing individual constraint values that were used in this analysis.

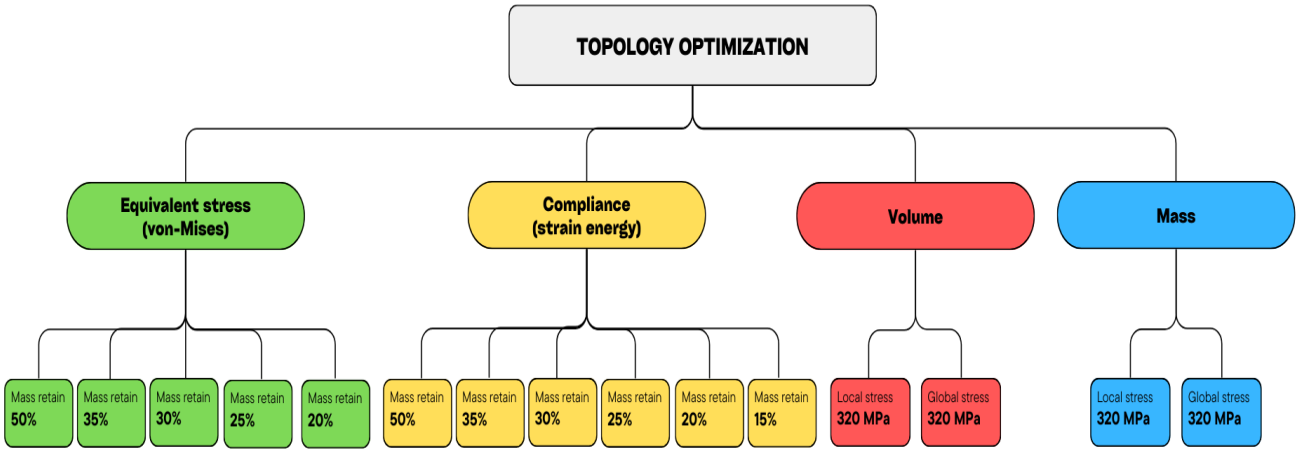

Figure 4.14: Overview of the TO analysis

In the following paragraphs, a total of 15 TO models will be presented. For the objective of equivalent stress, 5 models were generated differentiating in mass retain percentage, namely 50%, 35%, 30%, 25%, and 20%. In case of compliance TO objective 6 models were made with the mass retain percentages of 50%, 35%, 30%, 25%, 20%, and 15%. For volume and mass TO objective, two constraints were implemented, namely local and global stress of 320 MPa, which represents the assumed value of the selected material yield strength.

For the purpose of the structural validation, stress diagrams will be plotted for each model. Overall stresses in the individual models should be lower than the assumed yield strength. Based on this a selection of 4 models (one for each TO objective) that satisfy a structural validation while achieving the lowest required mass will be selected for further analysis.

- **Equivalent stress (von Mises)**

Figure 4.15 a - e shows geometries gathered from the TO with the objective of equivalent stress. The models differ based on the retained mass percentage. From the geometries, it is clear that due to the loading shown in Figure 4.13 b the specific shape is followed. Because of the moment load, which can based on structural mechanics be split into a tension force on the top and compression force on the bottom, an opening in the middle of the connection appear. With the decrease in the retained mass percentage the size of the opening increases. The top part of the connection is connected to the bottom column with so called ''supporting legs''. The decrease in the retained mass percentage causes the supporting legs to shirk, while also change the orientation. In the higher percentages, the legs are orientated in the direction of branches. With the gradual decrease in the percentage the legs start rotating around the vertical central axis of the connection until at 20% reach the location perpendicular to the branches. Due to the fact that in that orientation the supporting legs provide low stability, an additional third supporting leg is created.

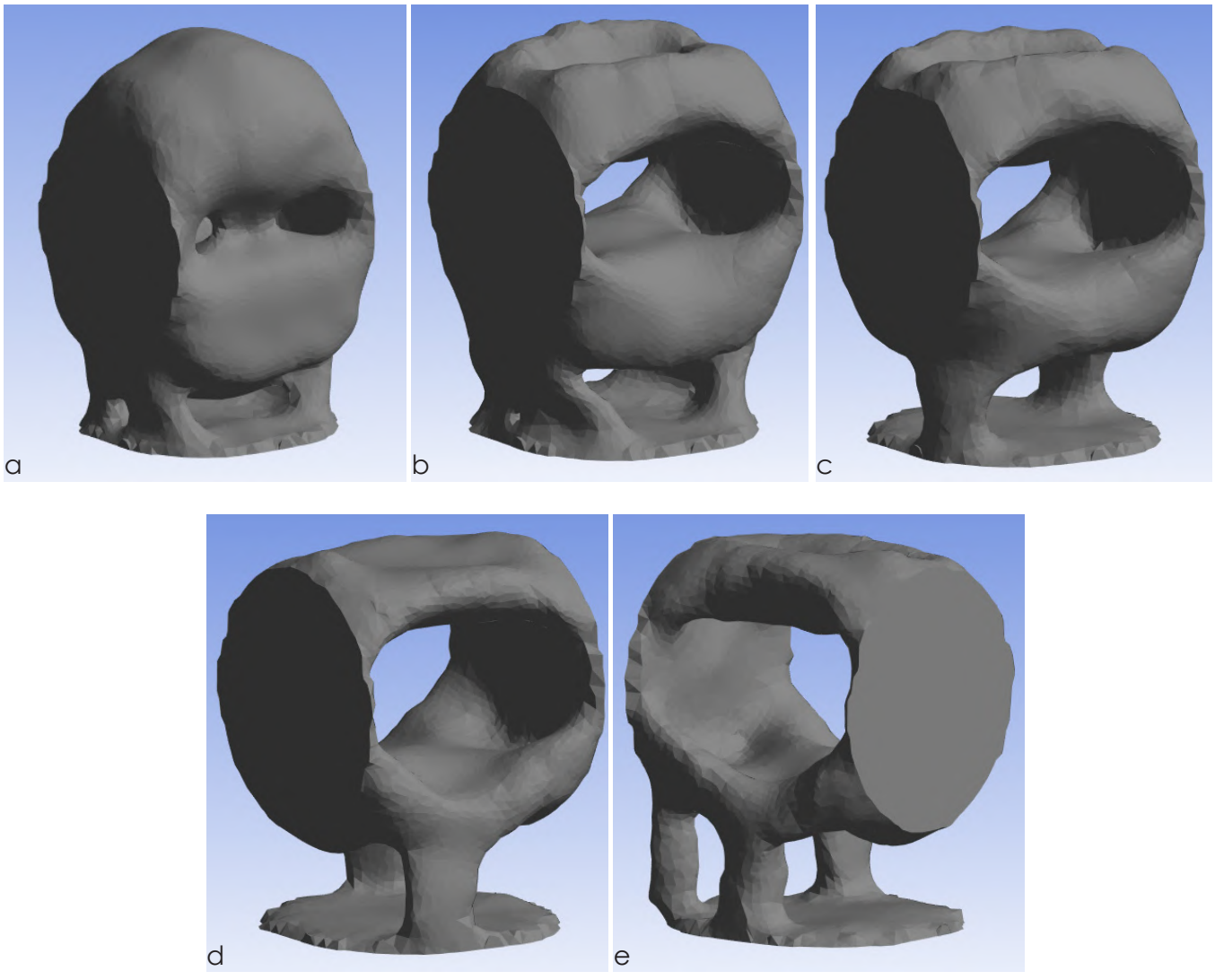

Figure 4.15: Objective of equivalent stress: a) 50%, b) 35%, c) 30%, d) 25%, e)20%

Figure 4.16 a – e shows the plots of the stress diagrams of the geometries shown in Figure 4.15. The red colour on the plots represents stresses higher than the assumed yield strength (320 MPa). For the first three models (50%, 35%, and 30%) the overall stresses are reasonably low, which is visible with a dominant blue colour all over the connection. There are stresses that exceed 320 MPa but can be disregarded due to the very small area that they represent. In addition, these stresses are mostly localized around the location where the loads are applied (where the branches are welded to the connection), thus the additional thickness of the welds can contribute to better stress distribution meaning less concentrated stress peaks.

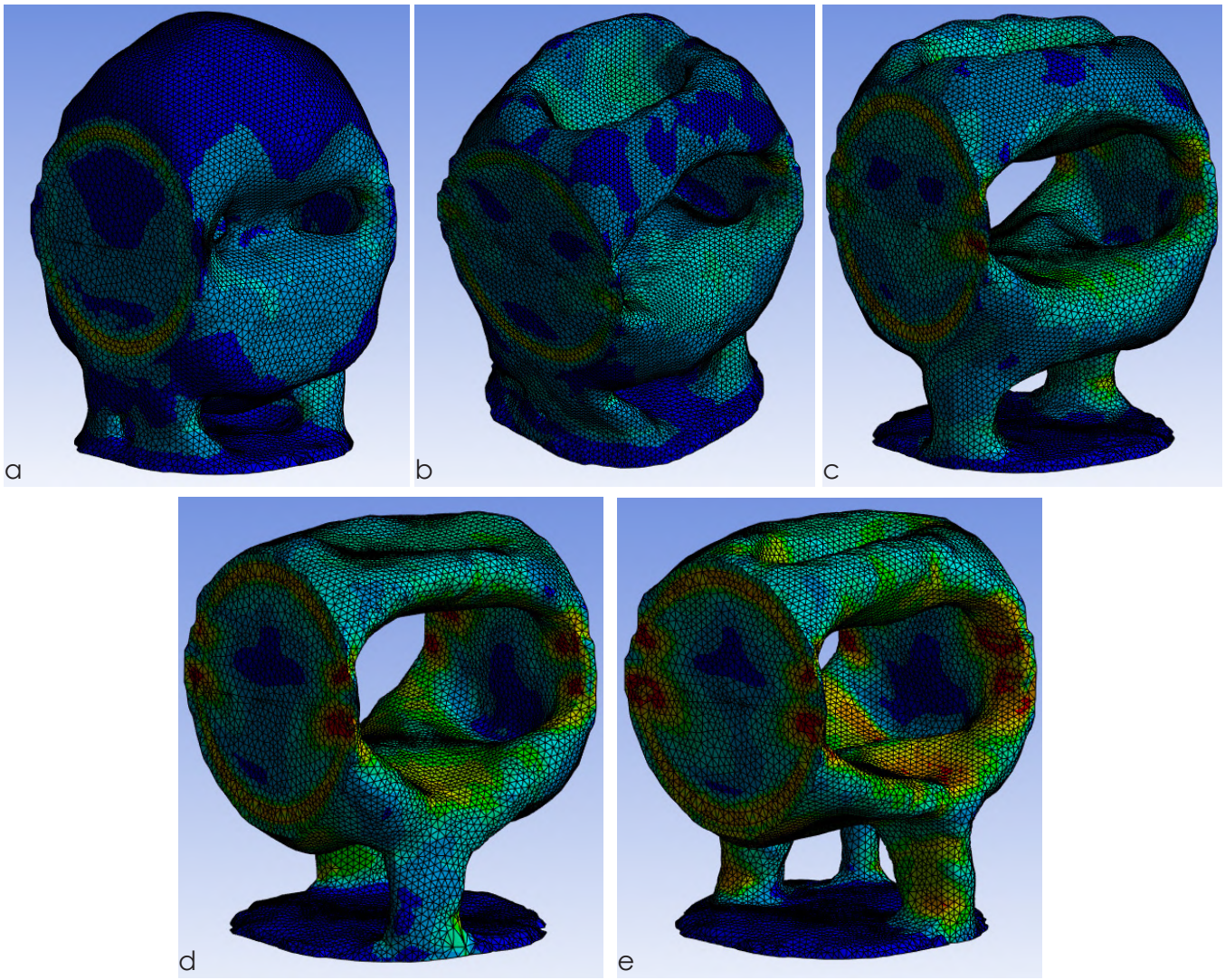

Figure 4.16: Stress diagrams for equivalent stress objective: a) 50%, b) 35%, c) 30%, d) 25%, e)20%

Figure 4.16 d and Figure 4.17 a show the stress distribution for the model with 25% retained mass. It is now visible that patches with stresses higher than 320 MPa (colour red) are more dominant and represent a relevant part of the volume. This means that in the mentioned locations the yielding will occur. The same can be also applied to the model with 20% retained mass and can be seen in Figure 4.16 e and Figure 4.17 b.

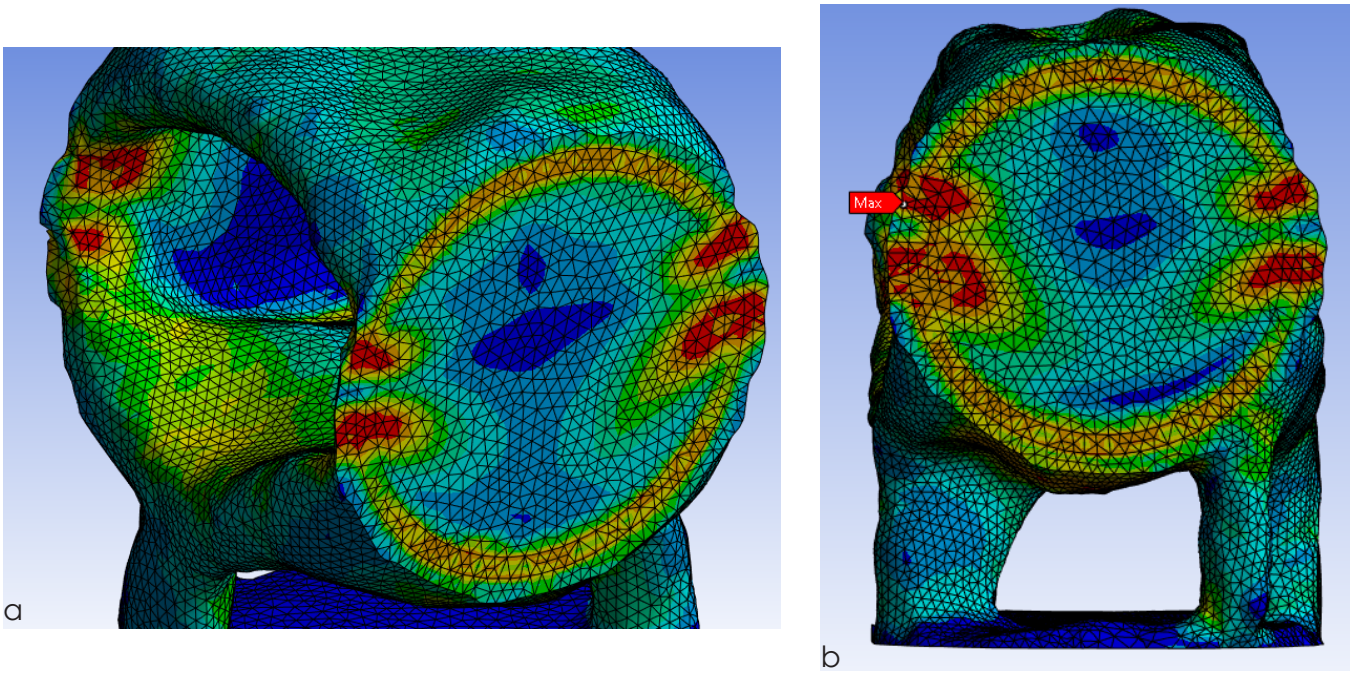

Figure 4.17: Stress distribution: a) 25%, b) 20%

- **Compliance**

Figure 4.18 a - f shows geometries gathered from the TO with the objective of compliance. The shapes are similar to the ones gathered with the previous TO objective. Again, due to the moment load the opening appears in the center of the connection and it gradually increases with the decrease of the mass retain percentage. The main part of the connection is again joined to the bottom column with a two supporting legs. The size of these legs gradually decreases with the decrease of mass retain percentage until 15% where again, for stability reasons the additional supporting leg appears.

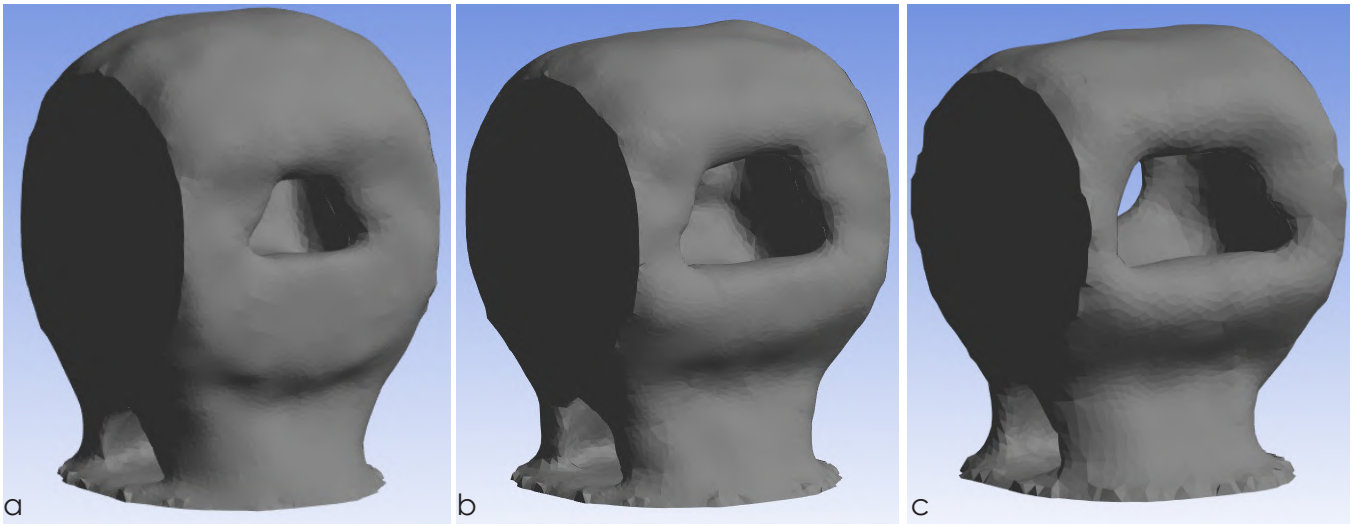

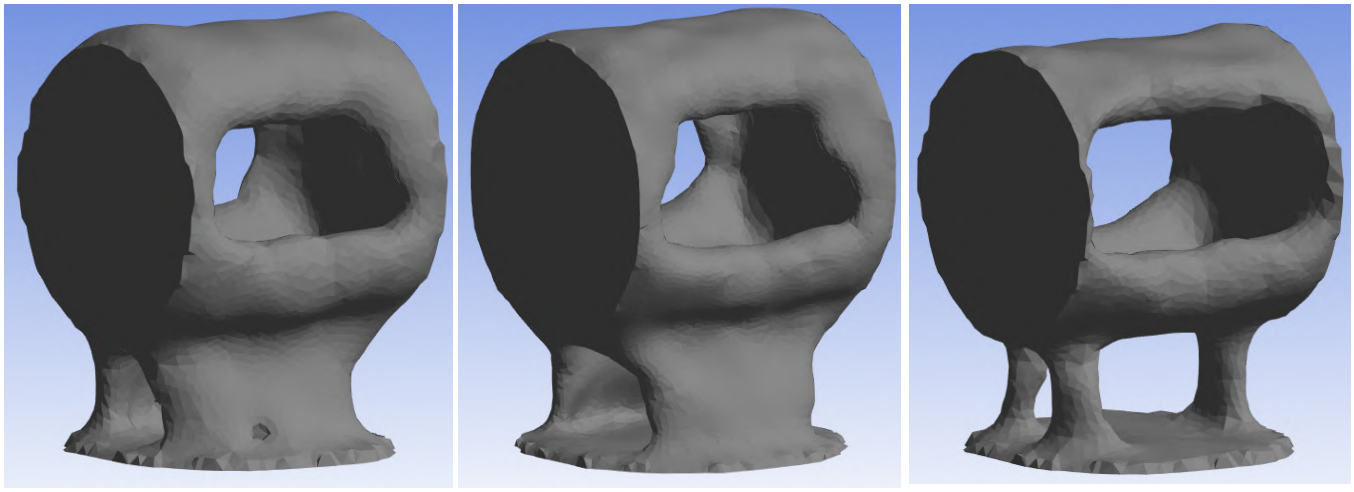

Figure 4.18: Objective of compliance: a) 50%, b) 35%, c) 30%, d) 25%, e)20%, f) 15%

Figure 4.19 a – f shows the plots of the stress diagrams of the geometries shown in Figure 4.18. The first four models with mass retain percentages of 50%, 35%, 30%, and 25%, experience overall stresses that are reasonably low. This can be seen with a dominant blue and green colour. Peak stresses that exceed the assumed yield strength are again localized at the location of the applied load. For the same reason as explained previously, these stresses can be neglected. At the percentage of 20% visible red patches start to appear, indicating that the stresses reached the yield strength at certain points. This can be visible in Figure 4.19 e and Figure 4.20. The same conclusion can be made for the model with a 15% mass retain percentage, where the yielding is even more significant (Figure 4.19 f).

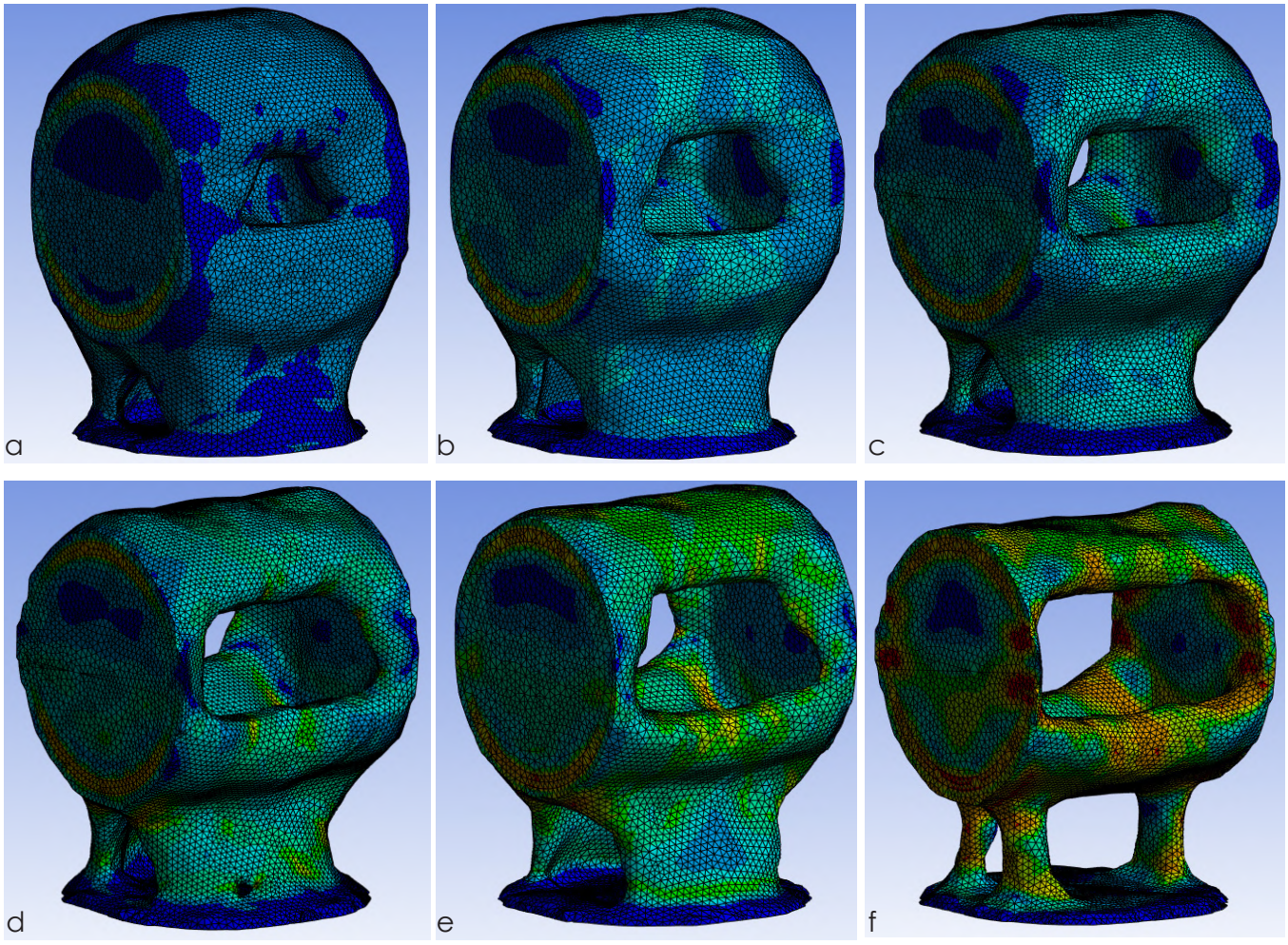

Figure 4.19: Stress diagrams for compliance objective: a) 50%, b) 35%, c) 30%, d) 25%, e) 20%, f) 15%

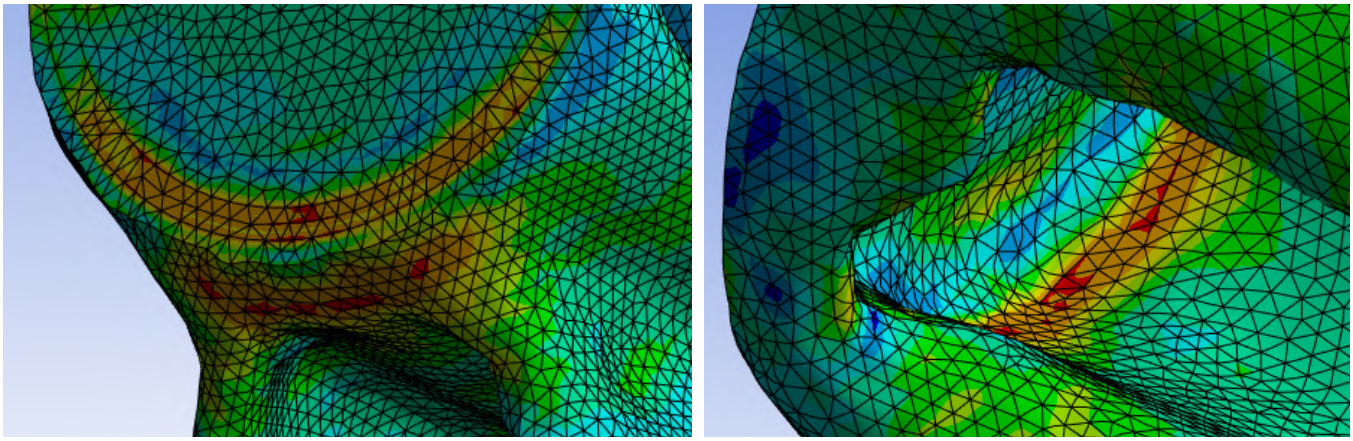

Figure 4.20: Stress distribution: 25%

- **Mass / Volume**

The geometries gathered for the TO objective of mass and volume are the same (or at least very similar), thus they will be presented together. The geometries for the two proposed constraints (local and global stress) are shown in Figure 4.21 a and b. When using local stress as a constraint, the optimization process will tend to focus on reducing stress concentrations or addressing specific critical areas. This results in localized changes in the topology to minimize stress at those specific points while possibly neglecting the overall structural efficiency. Using local stress as a constraint leads to a design that is highly stress optimized at critical points but might not be structurally efficient or cost effective in terms of mass. This can be seen in Figure 4.21 a, which shows that the geometry is fairly robust compared to other models. On the other hand, using global stress as a constraint will prioritize a more even stress distribution across the entire structure. The optimization will aim to achieve a design that minimizes stress across the structure as a whole, potentially leading to a different topology that provides a more balanced stress distribution. Global stress constraints produce a design that balances stress levels throughout the structure, achieving a more efficient design in terms of mass while trying to meet stress requirements. [4.25] The model with the global stress constraint is more slender than the one with the local stress constraint.

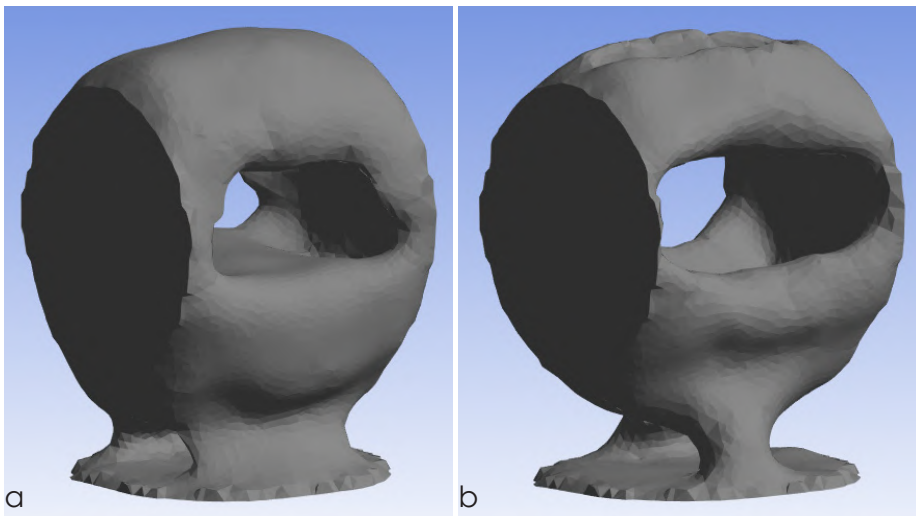

Figure 4.21: Objective of Mass / Volume: a) Local stress, b) Global stress

Figure 4.22 a shows a stress diagram from the model with a local stress constraint. It is visible that the stresses in the models are fairly low, with the exception of localized stresses around the area where the load is applied. On the other hand, the model with a global stress constraint requires lower mass but also experiences higher overall stresses (Figure 4.22 b). Even though the maximum stress constraint was implemented, there are areas where stress reaches the assumed yield strength of the material. These areas though are small and localized.

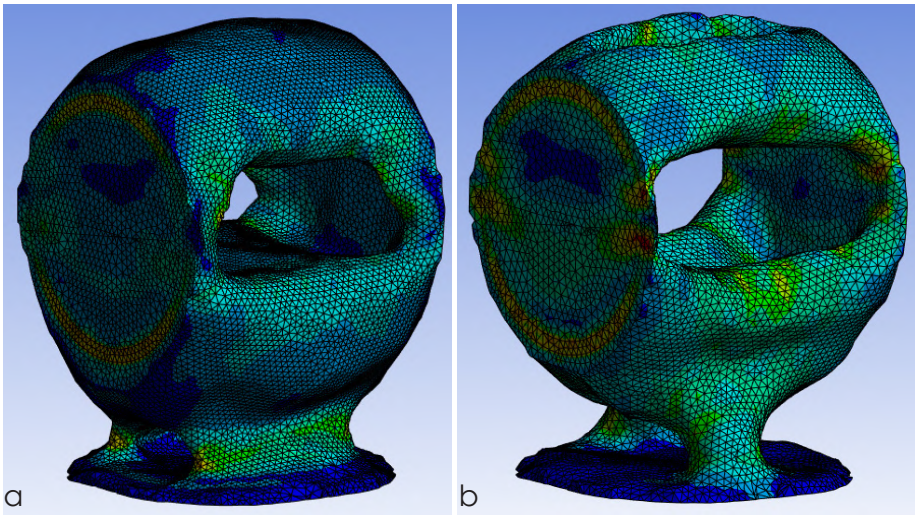

Figure 4.22: Stress diagrams for mass / volume objective: a) Local stress, b) Global stress

In the previous paragraphs, 15 TO geometries were presented and their structural validation was done. Based on this the selection of the most optimal models for each TO objective can be complete, meaning that three models will be used for further analysis. These models were picked based on the presented stress values. If the models include visible areas where stresses exceed the assumed yield strength they do not suffice the structural validation and are thus not sufficient. The selected models are shown in Figure 4.23 a - c and their corresponding TO input parameters are shown in Table 4.1. Figure 4.24 a - c shows for each model the location of the maximum stresses (the location where yielding first appears). It is interesting to see that for the objective of stress and mass/volume, the maximum stresses appear at a similar location, namely at the side of the opening, where the element thickness is the smallest. The TO with the objective of compliance creates geometry with the thicker wall, which contributes to the connection's stiffness and stress reduction at that location. This means that the yielding will first appear at the different location visible in Figure 4.24 b. Because of that, an additional reduction of the mass retain percentage can be applied, meaning that with the objective of compliance lower mass can be achieved. The mass comparison will be additionally presented in the following paragraphs.

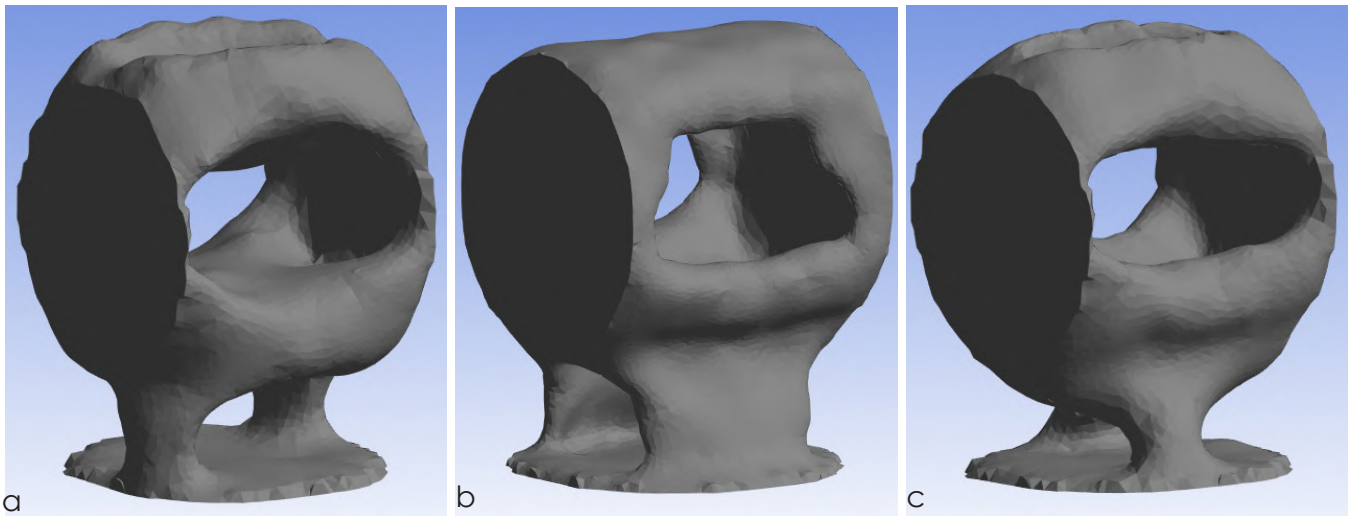

Figure 4.23: Selected models: a) Equivalents stress (30%), b) Compliance (25%), c) Mass / Volume

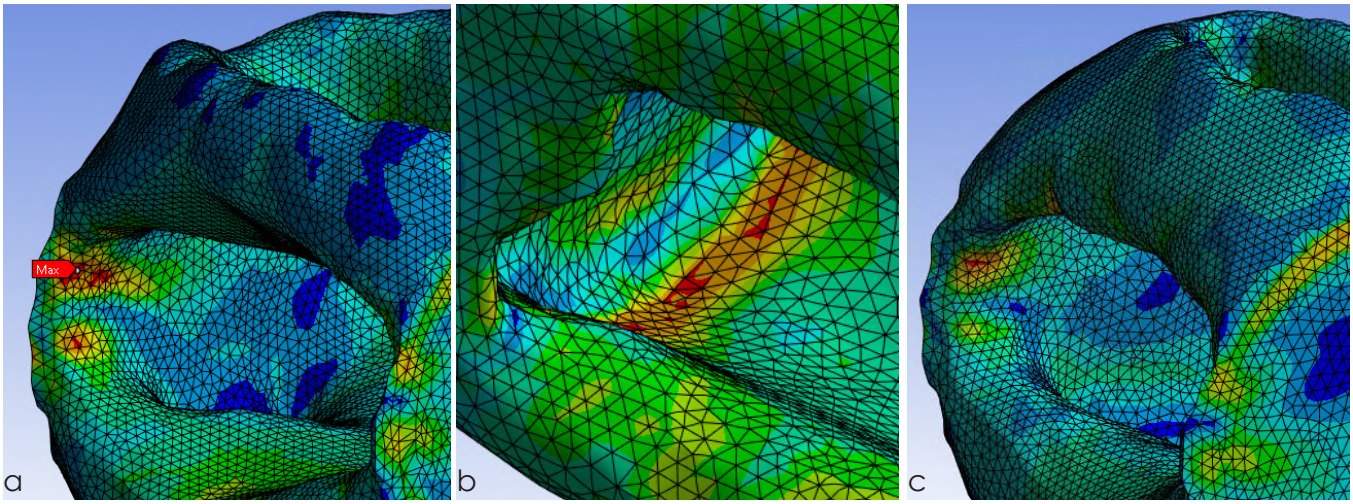

Figure 4.24: Maximum stress location: a) Equivalents stress (30%), b) Compliance (25%), c) Mass / Volume

Table 4.2: TO input parameters of the selected models

	TO objective	TO constraint
Model 1	Equivalent stress	Mass retain 30%
Model 2	Compliance	Mass retain 25%
Model 3	Mass / Volume	Global stress 320 Mpa

4.4.2.1 OVERHANG LIMITATION CONSTRAINT

Since the goal is to manufacture the proposed geometry with WAAM, it is important to consider its manufacturability aspects. To guarantee that the TO geometry has a shape that can be produced with WAAM, manufacturing limitations explained in Chapter 3: WAAM Manufacturing Limitations will be used. In that chapter, the influence of WAAM process parameters, overhang limitations, and overlap limitations were considered. The most important manufacturability limitation that is relevant to be included in the design phase is the overhang limitation. Overhangs, which are regions of an object that extend beyond the vertical axis, present a significant challenge in WAAM due to the nature of the printing process. Because of this, the WAAM process requires specific printing techniques to ensure successful fabrication. Failing to consider overhang constraints in topology optimization may result in designs that are difficult or impossible to print without additional support structures. Incorporating overhang constraints into topology optimization can lead to designs that minimize the need for support material. This is crucial as excessive support material not only increases material waste but also extends printing time and cost. In addition, support material is not desirable due to the possibility of penetration of the support material into the deposit and the creation of a permanent bond between these two parts, which might require additional post processing. By optimizing the design with consideration for overhangs, the need for support structures can be reduced, improving the efficiency of the printing process.

To solve the problem and modify the TO geometry so it aligns with the overhang limit values gathered from the experiment, manufacturing constraints need to be included. Ansys software allows for the option to include the overhang angle limit into the TO solver. This constraint will modify the geometries so that no part will be inclined under the angle limitation. The limit overhang angle can be calculated based on the limit overhang offset distances provided in Chapter 3. The schematic representation of the angle is shown in Figure 4.25, while limit angle values are shown in Table 4.2.

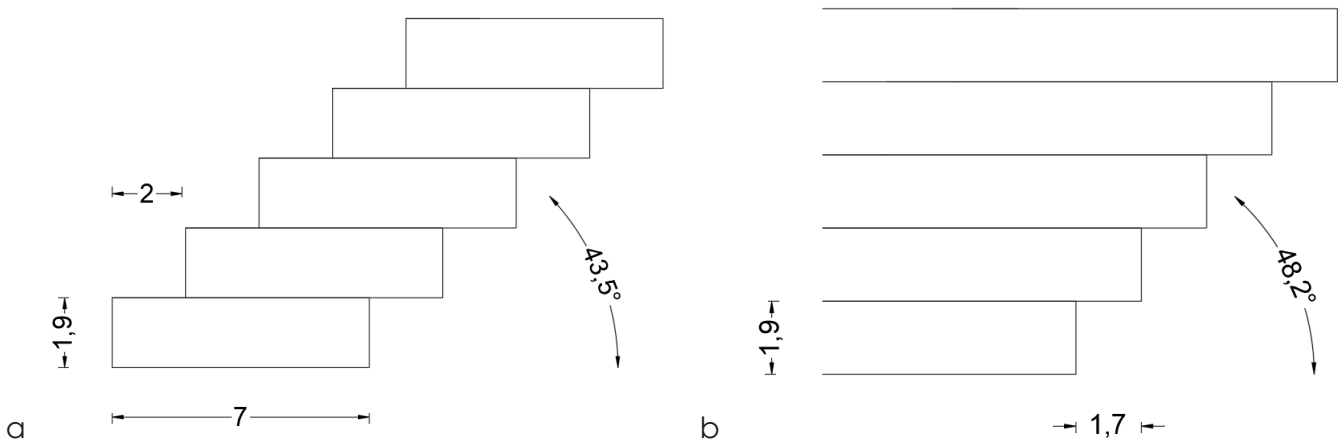

Figure 4.25: Overhang angle: a) Perpendicular direction, b) Parallel direction

Table 4.3: Overhang angle limitation

	Limit overhang angle
Perpendicular direction	43,5°
Parallel direction	48,2°

The overhang experiments were conducted in two directions, perpendicular and parallel direction, thus two different overhang angles are given. To simplify the further analysis, an average angle of 45° will be assumed.

Although WAAM is conventionally associated with a vertical or near vertical orientation during the fabrication process it can also be adapted for a more horizontal printing direction. This can be done by the change of orientation of the printing plane. By tilting the workpiece or applying the welding wire and torch at the correct angle, the layers can be deposited in a manner closer to the horizontal plane. This modification is significant in scenarios where specific geometries or design requirements necessitate a departure from the standard vertical orientation. By allowing for a more horizontal approach, WAAM can meet a variety of design requirements and provide more flexibility when fabricating intricate parts. Even though this might be a sufficient option for the manufacturing of the above proposed models it will not be considered in the scope of this research. Thus, the overhang angle constraints will be implemented into the TO design. This means that the models will be manufactured based on the setup that was used for the lab test conducted and explained in Chapter 3.

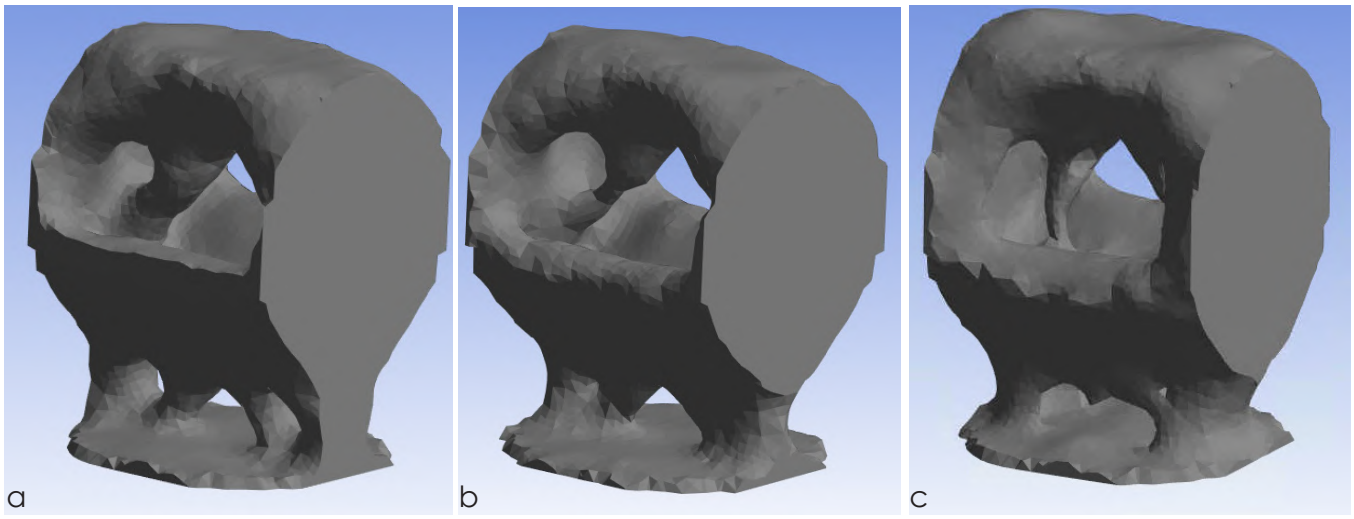

Figure 4.26: Models with the overhang constraint: a) Equivalents stress (30%), b) Compliance (25%), c) Mass / Volume

Figure 4.26 a – c shows models stated in Table 4.1 with the implementation of the overhang angle constraint in the TO. It is visible that the geometries are quite significantly modified and supporting structures need to be built. All of the geometries still follow the same principle of the opening in the top part due to the moment load and supporting legs where the loads are transferred to the bottom column. To limit the overhang angles, supporting structures were designed. These support structures are column lookalike elements that support the printed parts during the build. From Figure 4.27 a – c (plot of the stress diagrams) it is visible that stresses in these support structures are very low (presented with dark blue colour). From this, we can assume that these elements do not provide any significant structural support or contribute to the structural performance of the connection, but rather just serve as a manufacturing tool to avoid overhang angle limitations.

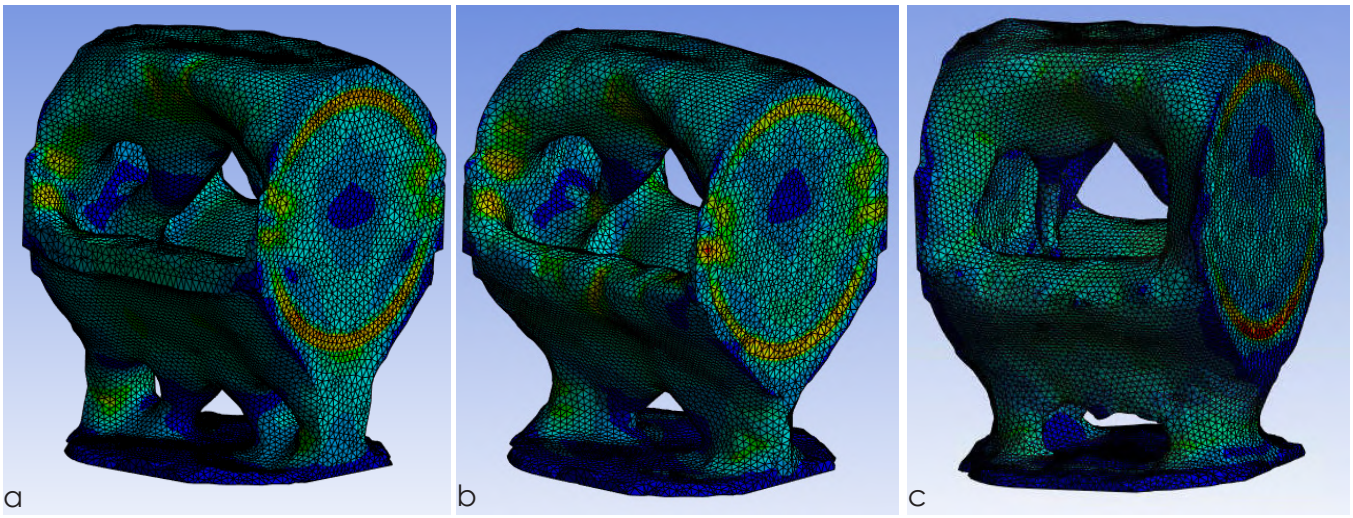

Figure 4.27: Stress diagrams: a) Equivalents stress (30%), b) Compliance (25%), c) Mass / Volume

Table 4.3 shows the values of the mass and volume for the individual models. As explained previously, the best stress distribution can be achieved with the objective of compliance, thus the biggest mass reduction can also be implemented. For model 2 the required mass is reasonably smaller (6 kg) compared to models 1 and 3 where the required mass is 7,1 kg and 7,5 kg respectively.

Table 4.4: Mass and volume values

Model	Objective	Constrain	Mass (kg)	Volume (cm^3)
1	Equivalent stress	Mass (30 %)	7.1	907.2
2	Compliance	Mass (25 %)	6.0	769.9
3	Mass / Volume	Global stress (320 Mpa)	7.5	918.4

Based on the structural validation presented in previous paragraphs and values shown in Table 4.3, the most sufficient model and the most optimal TO parameters can be selected. Based on the fact that with model 2, the geometry with the smallest required mass was achieved, the TO objective of compliance was selected for further analysis.

4.4.3 SENSITIVITY ANALYSIS

Now that the TO input parameters have been determined other aspects of the connection's design can be considered. In this subchapter, the impact of the implemented boundary conditions, type of TO, and angle of branches on the geometry and its performance will be checked. Different models can be compared based on different criteria, and thus a selection can be done.

- **Boundary condition**

To start with the design firstly the appropriate boundary conditions need to be selected. This includes the application of loads onto the model and defining the supports. Set boundary conditions depend on the geometry of the elements in the connection and the desired outcome of the geometry. In this case, three different types of boundary conditions were proposed, which differ in the size of the area where loads and supports are applied. After TO each boundary condition type provides us with a unique geometry.

For the first boundary condition loads and supports were assigned as if the cross section of profiles were full. This type of boundary condition would be applicable in case the column and branches were made out of concrete, wood, or other materials where hollow cross sections are not achievable. The proposed boundary conditions for loads and support are shown in Figure 4.28 a and b respectively. The final geometry of the TO is shown in Figure 4.28 c.

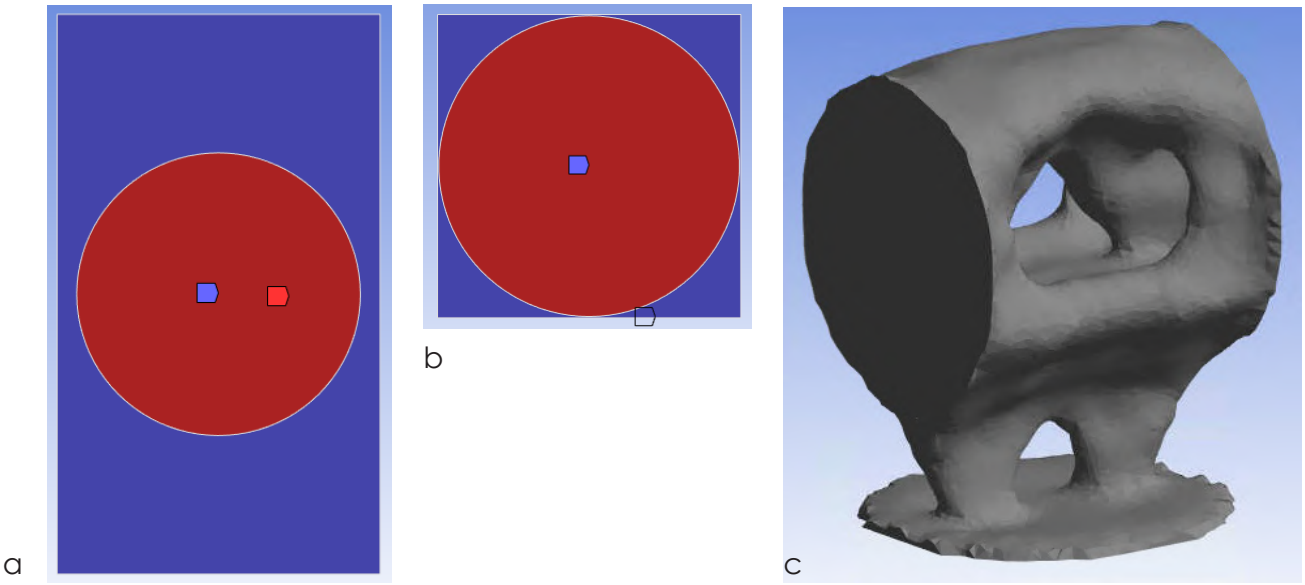

Figure 4.28: Boundary conditions 1: a) Loads, b) Support, c) TO geometry

Second boundary conditions are applied as a hollow cross section, meaning that loads and supports are set only on the edges of the cross section while the inner part is excluded. This type of boundary condition is applicable for steel profiles with hollow cross sections or cross sections with other geometries. The application of the loads and fixed support is shown in Figure 4.29 a and b respectively. Based on provided boundary conditions TO gives us the geometry shown in Figure 4.29 c.

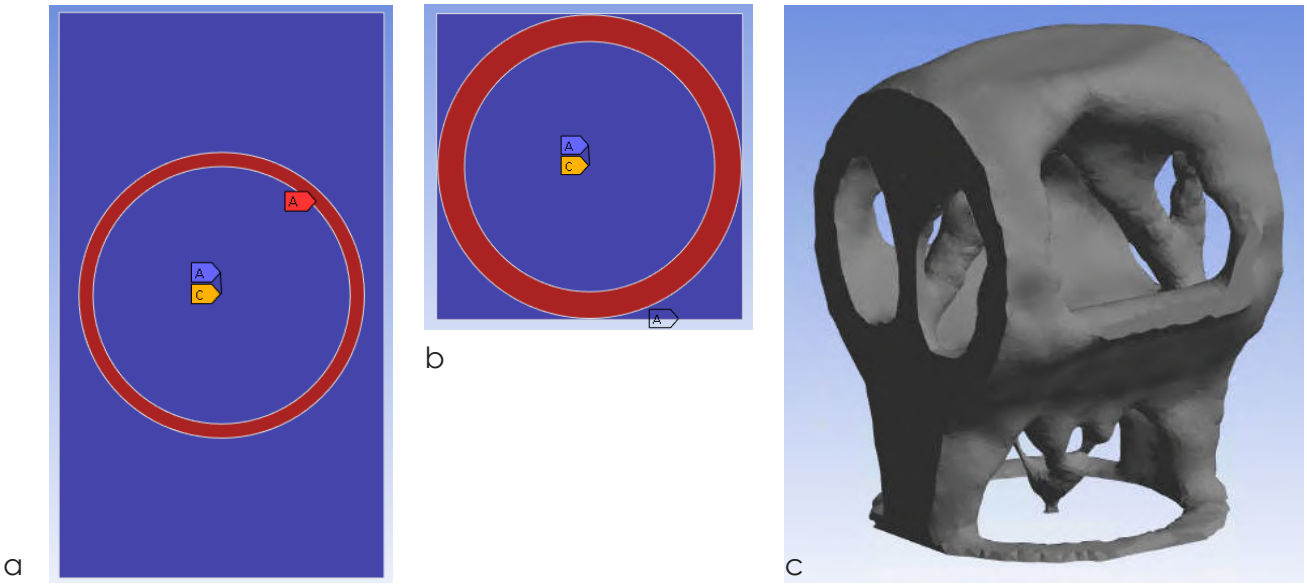

Figure 4.29: Boundary conditions 2: a) Loads, b) Support, c) TO geometry

For the third type of boundary conditions, the combination of the first two was applied. Loads and supports are again applied only on the edges of the profile. The inner part of the profiles (hollow parts) was in the TO set as an excluded region. The excluded region refers to areas within the design domain where material (part of the object) should stay unchanged or should not be removed. The purpose of setting up the excluded regions, in this case, is to close the hollow cross section. Closing hollow cross section offers benefits such as protecting the inner part from environmental impacts, enhancing structural stiffness, and improving safety. The boundary conditions for loads and supports are shown in Figure 4.30 a and b respectively. The final TO geometry is presented in Figure 4.30 c.

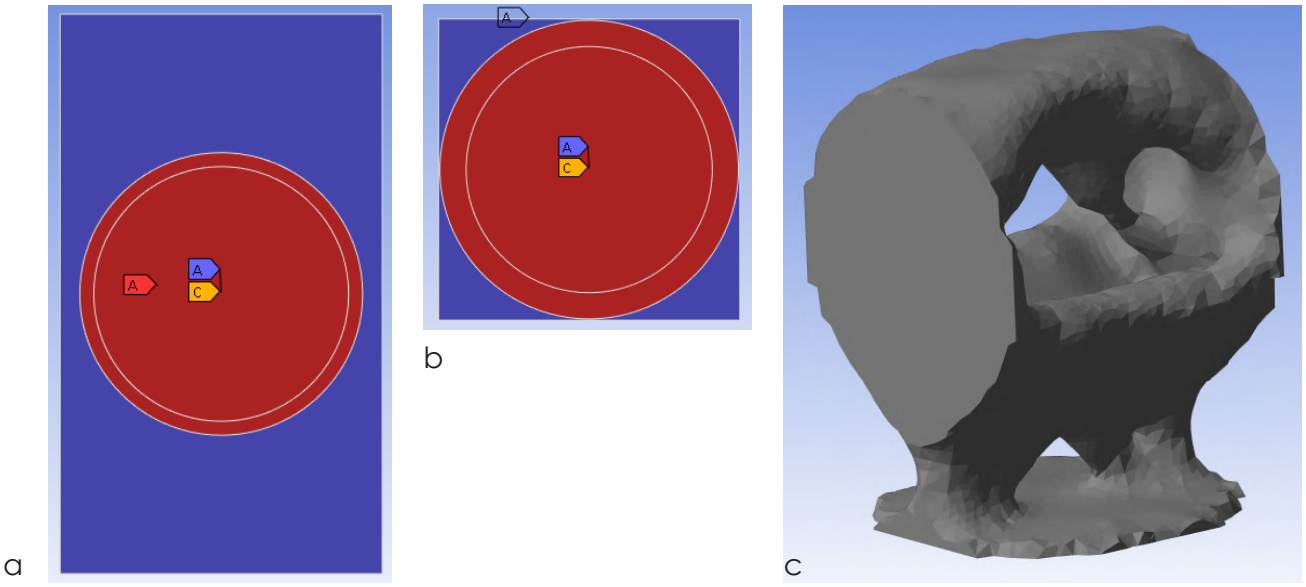

Figure 4.30: Boundary conditions 3: a) Loads, b) Support, c) TO geometry

From Figures 4.28 c, 4.29 c, and 4.30 c the impact of different proposed boundary conditions on the TO geometry can compared. All three geometries follow similar principle with the top part where branches are connected and two supporting legs that transfer the load to the bottom column. The second boundary condition results in complex geometry with many individual thin elements and might present challenges when it comes to production using WAAM. The intricate and thin geometry might pose difficulties for WAAM processes, as they often require more substantial and robust features to be effectively built. The complexity may lead to issues such as poor deposition control, overheating, or warping, which can compromise the structural integrity and functionality of the manufactured part. For the purpose of this thesis, the profiles of branches and column are hollow steel profiles, thus the first boundary condition is not sufficient. Therefore the third boundary condition was selected due to the fact that the optimized geometry does not achieve high complexity. Besides that, the used boundary condition provides a sufficient solution for closing the hollow part of the cross section from the environmental impacts.

- **Angle of branches**

Another parameter that might have an effect on the geometry and performance of the TO connection is the angle of the branches. The schematic representation of how the mentioned angle is measured is shown in Figure 4.31.

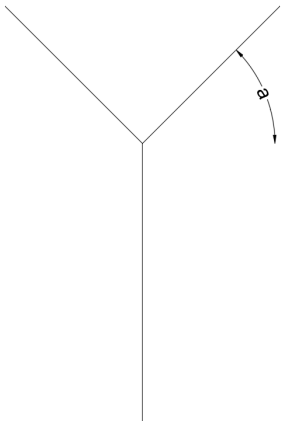

Figure 4.31: Angle of branches

The influence of different angles was considered based on the loads that are acting on the connection. By adjusting the angle of the branches the size of the individual load components also changes. For the purpose of this assignment three different angles were selected, namely steep angle (75°), shallow angle (15°), and average angle (45°). In Table 4.4 sizes of different load components acting on the connection are shown. The increase in the angle causes an increase of the vertical force component and a decrease in axial force and moment. Angle 45° experiences average values of all three components.

Table 4.5: Values of load components for different angle of branches

Angle	Nx (kN)	Vz (kN)	My (kNm)
15°	184,1	27,9	48,8
45°	162,8	57,3	26,6
75°	100,0	84,4	20,3

For the TO of the below presented geometries an objective of compliance and 35% mass retain constraint was used, while overhang angle limitation was also implemented. To analyze the performance of each model structural validation was done, thus stress distribution is shown in Figure 4.32 a – c. It is visible that for the smaller angle (15°) the overall stresses that appear in the connection are much higher, which can be seen with the dominant green and yellow colour. The average stress value hovered around 280 MPa. In the case of higher angles (45° and 75°), the stresses in the connection are much lower (blue colour) and range around 180 MPa value mark.

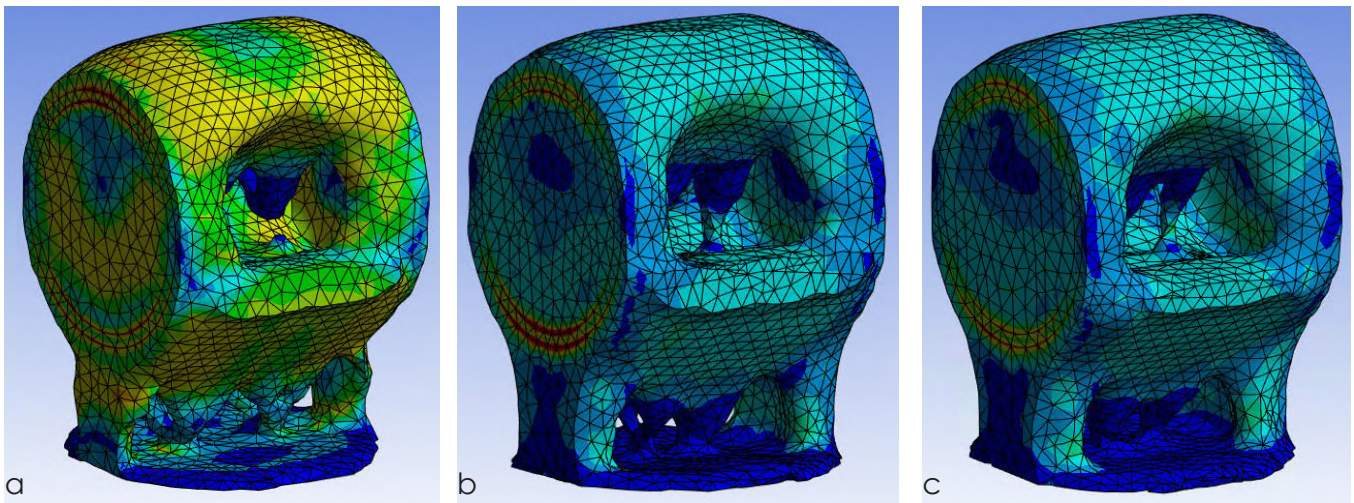

Figure 4.32: Stress diagrams: a) 15°, b) 45°, c) 75°

- **Type of topology optimization**

The last aspect that was considered is the type of TO. In chapter 4.3 Topology Optimization, two types of TO were presented, namely density based and level set based. The geometries gathered with both types are presented in Figure 4.33 a and b respectively. In Table 4.5 both models are compared based on the number of required iterations and required time for the TO analysis. It is visible that the level set based TO process took almost four times longer and required three times more iterations, thus the whole design process extends. The advantage of level set based TO is that the provided geometry is immediately after the TO process smooth and prepared for structural validation, while density based TO provides rougher geometry that requires additional smoothing and shrinkwrapping afterward. Based on available results it can be assumed that the density based method is for this assignment more relevant since it requires less time, while at the same time provides very similar geometries, with similar structural performances.

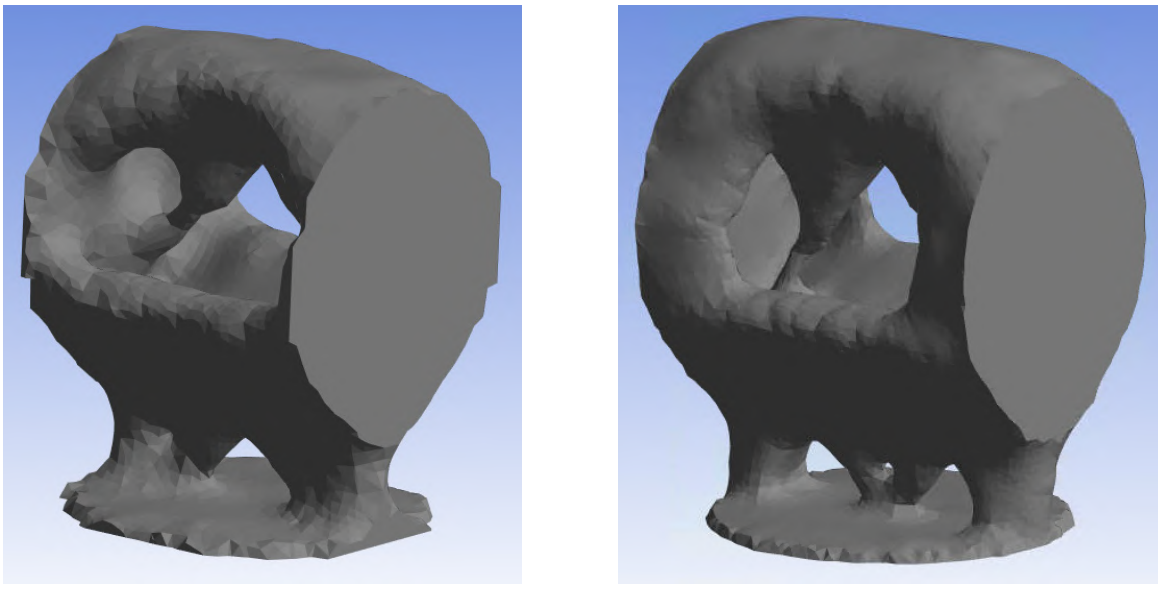

Figure 4.33: a) Density based TO, b) Level set based TO

Table 4.6: Required number of iterations and time for both TO types

TO type	Number of iterations	Time (min)
Density based	24	16
Level set based	68	55

4.4.4 ENGINEERING SOLUTIONS

After the most sufficient TO input parameters are determined the given design should be adapted to become a suitable connection that can be used in the actual construction. To do so a number of problems need to be considered and solved. This includes the solution of how the connection will be joined to the columns and branches, and how can a system be assembled on site. All of the solutions need to be considered and integrated into the design so that the proposed connections will reach the required structural behavior, while also achieving the desired functionality.

In case the picked material for the column and branches is steel and since the connection itself is made out of steel, then the most efficient and easiest solution for joining the printed connection with the profiles is welding. This means that after the connection has been printed out the profiles are directly welded onto it. To be able to weld profiles onto the connection it is firstly important to modify their geometry. Depending on the angle of branches the profiles should be cut at that same angle. This is shown in Figure 4.34. Even though this solution is sufficient, cutting steel profiles at specific angles for welding in connections can be a complex task due to several factors that influence the precision and quality of the resulting joint. One of the primary challenges lies in achieving accurate angular cuts. Even a small deviation from the intended angle can lead to a poorly fitting joint, especially in the TO elements where high accuracy is very important. In case of a lower accuracy, connections might not perform optimally, considering that they were designed for the specific case. Poor accuracy can also have an impact on the quality of the weld, which is crucial for the desired performance of the connection. The characteristics of steel itself present challenges during the cutting process. Steel is a tough and durable material, requiring specialized tools and machinery capable of efficiently and accurately cut through it. Achieving precise cuts at specific angles demands advanced cutting equipment, such as CNC machines or laser cutters, which must be set up and calibrated accurately to ensure the desired angular precision. Moreover, all the additional required modifications will cause an increase in manufacturing costs and time.

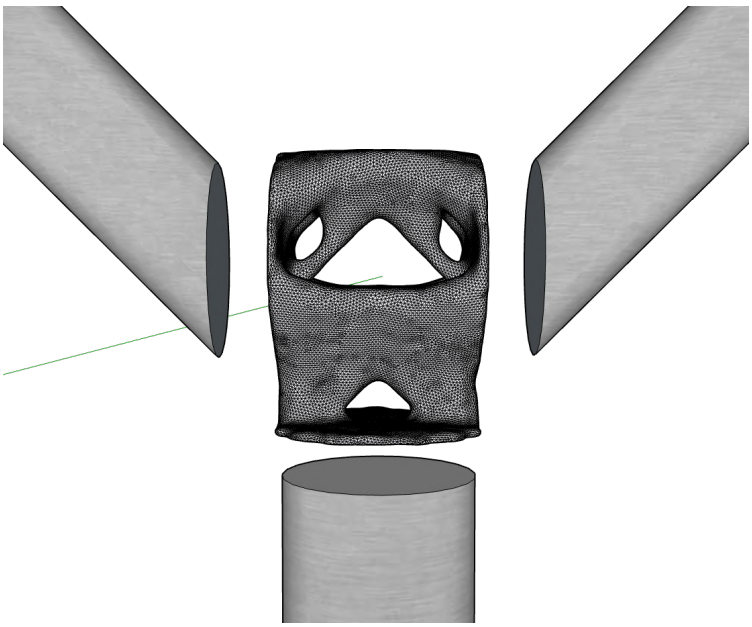

Figure 4.34: Modification and cutting of the branch profiles

To avoid the problem of precise profile cutting and thus lower the complexity of the manufacturability and on site assembly some modifications can be done. To do so a change to the original TO block, which is visible in Figure 4.13 a is needed. The modified TO block with its dimensions is shown in Figure 4.35 a, while the application of loads for the purpose of the TO is shown in Figure 4.35 b. The new block resembles the shape of the house, where the angle of its roof needs to coincide with the angle of the branches. In this case, the branch profiles can be joined with the connection in a perpendicular direction, thus no cutting is needed. For the purpose of this analysis, an angle of branches was selected as 45°, while TO input parameters were selected based on the previously explained research (Table 4.6). Loads acting on the connection are the same as for the previous example, only now they are oriented in the local coordinate system.

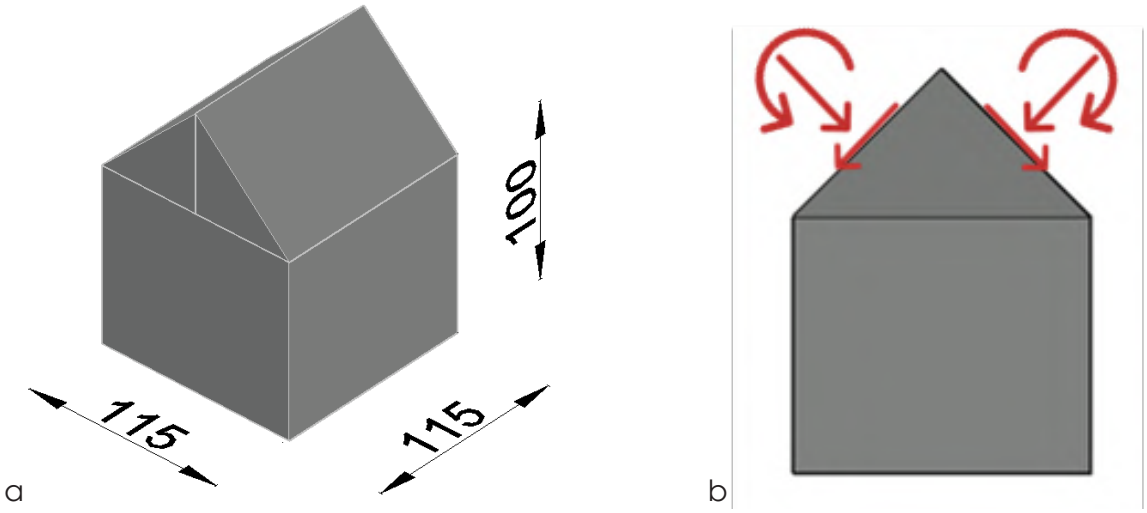

Figure 4.35: a) Modified TO block, b) Dimensions

Table 4.7: TO input parameters

TO objective	TO constraint	Overhang limitation
Compliance	Mass retain 25%	45°

Figure 4.36 a shows the newly obtained geometry from the TO. The shape resembles similarities with the previously obtained geometries where the robust top part accumulates loads coming from the branches and two supporting legs that transfer the loads to the bottom column. For manufacturing reasons, two supporting columns were created, which means that the overhang angle limitation was considered.

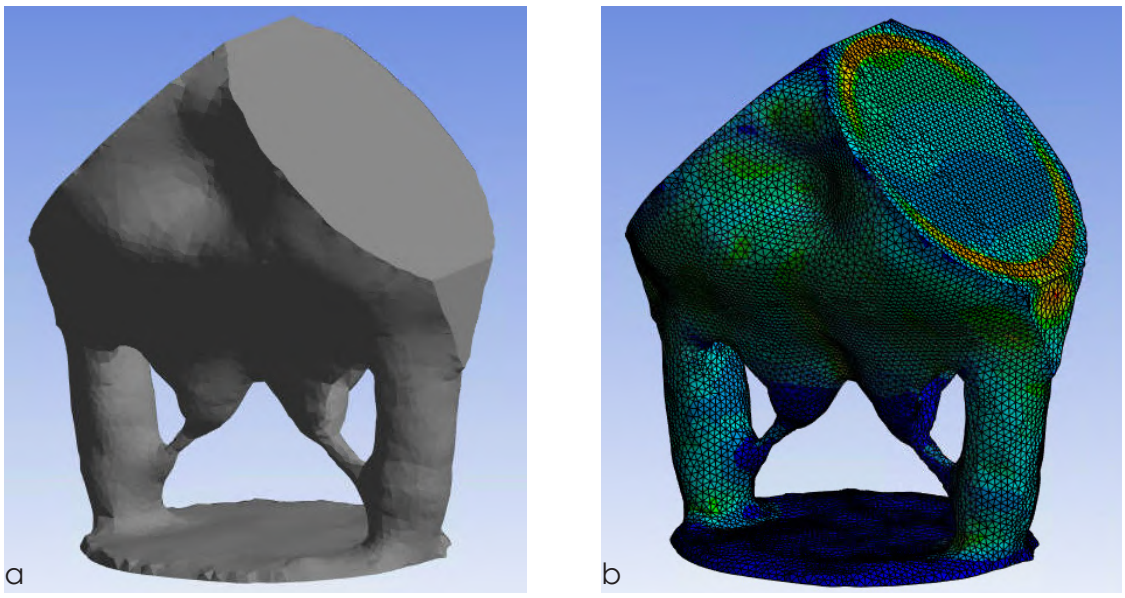

Figure 4.36: a) Updated geometry: 25%, b) Stress diagram of the updated geometry 25%

Figure 4.36 b shows the stress diagram for the provided geometry. It is visible that the overall stresses in the connection are reasonably low (dominant blue and green colour). The areas with the increased stress are localized only at the location of the applied load, which can be disregarded due to the previously explained reasons. Low overall stresses and the fact that there are no areas where stresses are reaching the yield strength suggest that the change in the geometry of the TO block improves the structural performance of the connection. This means that the additional mass reduction can be considered. Since this is the final modification to the design a more accurate analysis of the mass retain percentage was done. To do so a load–strain graph was plotted and is shown in Figure 4.37.

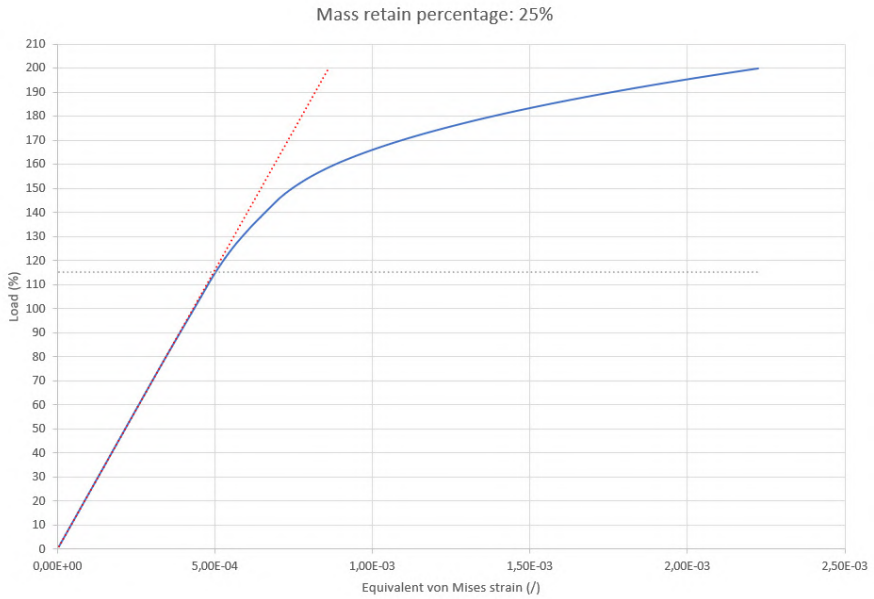

Figure 4.37: Load - strain graph: 25%

On the x axis of the graph, an equivalent von Mises strain was plotted, while on the y axis the load is shown. Load is presented as a percentage where 100% represents the load that is intended to apply to the connection, while 200% is twice as much load as the connection should withstand. The blue line in the graph represents the behaviour of the material. It is visible that around 115% of the load the material starts behaving nonlinearly, meaning that the yield strength is reached. After the 115%, the plastic deformation occurs. From this, we can conclude that the connection is capable of withstanding 15% more load than it was designed for. This can be solved by additionally reducing the mass retain percentage until the yielding occurs at exactly 100% of the applied load.

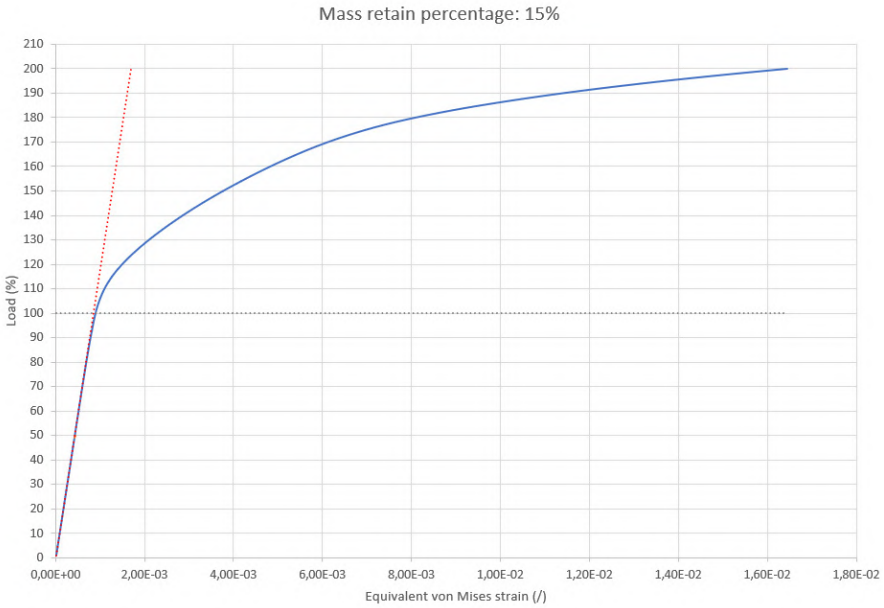

Figure 4.38: Load - strain graph: 15%

The mass retain percentage was gradually decreased until the 15% when the behaviour shown in Figure 4.38 was achieved. From the graph, it is visible that the nonlinear behaviour starts at the load for which the connection was designed. The final design of the connection is shown in Figure 4.39 a and b. Figure 4.39 c presents the location of the maximum stresses (stresses where the yielding has been reached first). This is also the location for which both of the graphs were plotted.

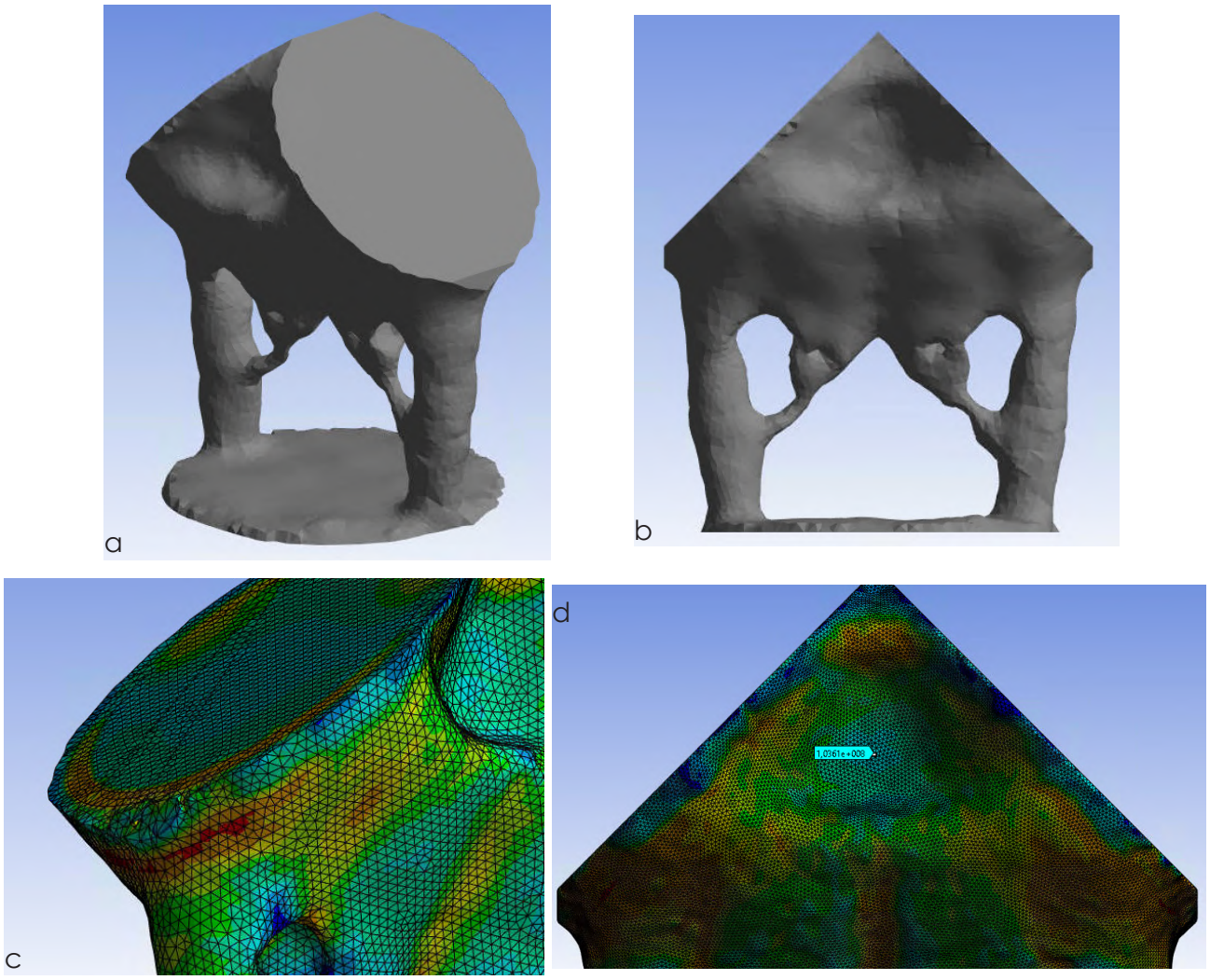

Figure 4.39: a,b) Updated geometry: 15%, c,d) Stress diagram of the updated geometry: 15%

From Figure 4.39 a it is visible that during TO a dent was created in the top part of the connection, which suggests that the stresses in that part are low (this is confirmed in Figure 4.39 d). This means that the additional reduction of mass might be possible and that the TO does not provide the lowest possible mass. To check this hypothesis, three additional designs were made where a hole was created at the location of the dent. The models differ in the size of the hole, which can be seen in Figure 4.40 a - c. The shape of the hole was selected based on the WAAM manufacturing limitation. Due to the overhang angle constraint of 45° the shape of the hole represents an isosceles triangle.

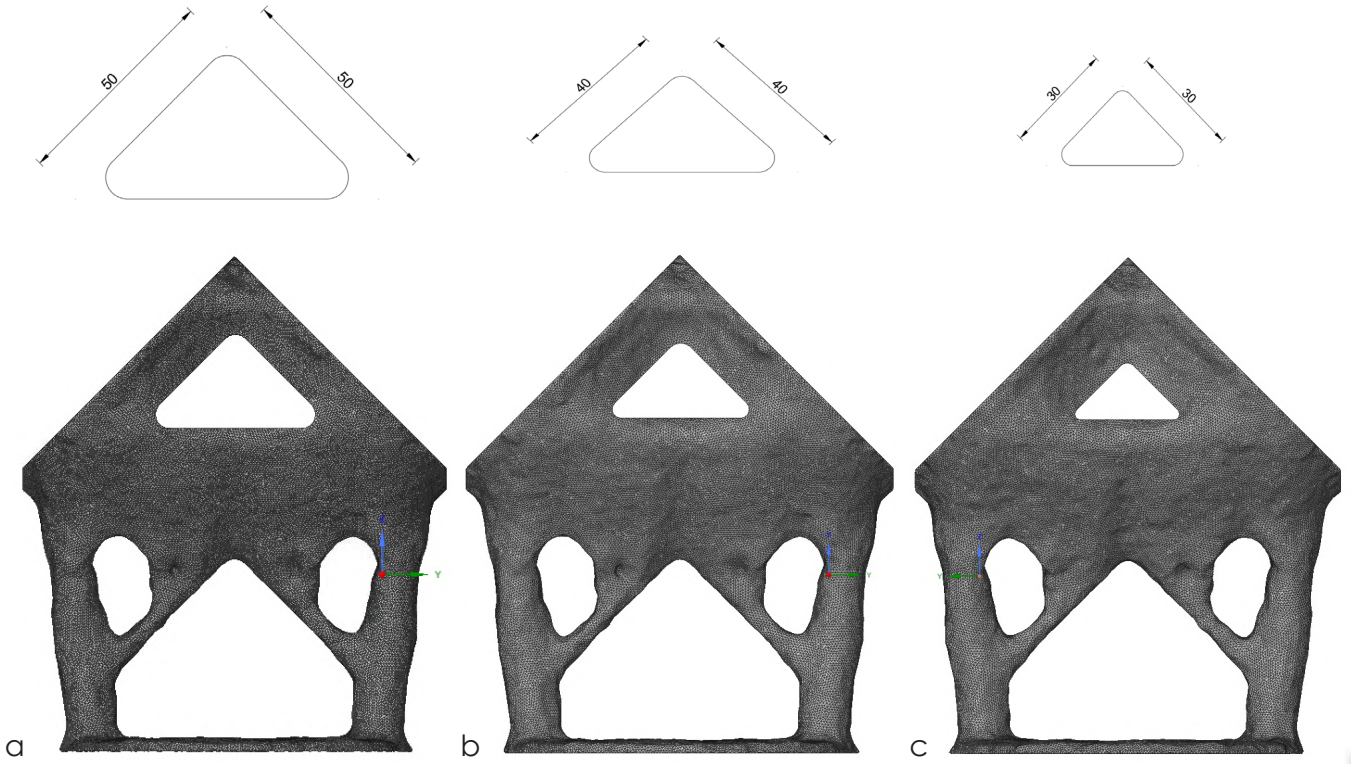

Figure 4.40: Models with additional mass reduction

To see the impact of the additional mass reduction, a stress analysis was conducted and is presented in Figure 4.41 a – c. It is visible that even small modifications to the TO model cause a significant change in the stress magnitude. Areas, where the yielding is reached (presented with a red colour), are very significant, even in the case of the smaller hole. Maximum stresses appear at the same location as for the model without the opening (Figure 4.39 c), but are now more dominant and spread out over a bigger area (Figure 4.41 d). Such a big difference in stress diagrams can be attributed to the fact that the objective of the TO was to optimize compliance, which is directly connected to stiffness (compliance = 1/stiffness). By creating an opening in the model, the overall stiffness of the connection is lowered, which causes bigger deformations, and thus higher stresses. The high stiffness of the top part of the connection is crucial for its performance since this is where the loading is applied and then transferred to the bottom column. This shows that big modifications to the TO models are not possible and can significantly impact the overall efficiency and performance of the connection.

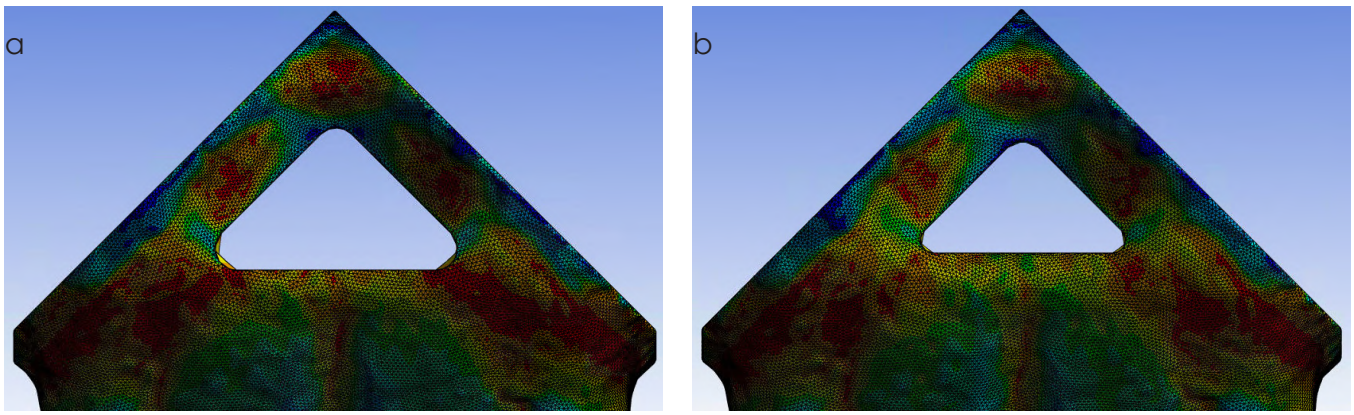

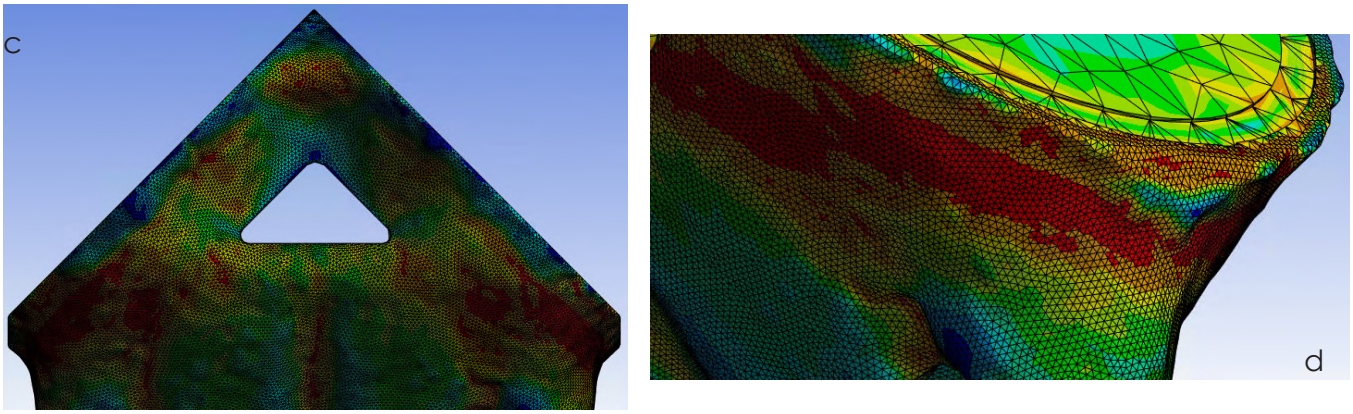

Figure 4.41: Stress diagrams of models with additional mass reduction

4.4.4.1 INTEGRATION OF THE DESIGNED CONNECTION WITH BRANCH AND COLUMN PROFILES AND ON-SITE ASSEMBLY PROCEDURE

In the introduction, the importance of modularity in the progress of Industry 4.0 was explained. It was also stated that AM can significantly influence this progress and contribute to automation in the construction industry. To do so an appropriate system assembly plan is needed, where attention will be paid to increasing prefabrication and facilitating the on site assembly process, thus lowering the construction time and possibility of errors.

The design of the joints between the connection itself and the profiles strongly depends on the material and shape of the profiles. In the next paragraphs, two engineering solutions will be proposed. Firstly, a solution for steel profiles will be presented followed by the solution in the case of timber/concrete profiles.

- **Steel profiles**

In case the picked material for column and branches is steel and since the connection itself is made out of steel, then the most efficient and easiest solution is welding. This means that after the connection has been printed out the profiles are directly welded onto it (Figure 4.42). This is a very simple solution that does not require any significant modifications of the connection or profiles. The calculation and design of the required welds are needed for which the procedure presented in EC3 can be considered. In addition, the use of profile splice can be used. In this case, only a part of a profile is welded onto the connection already in the factory. The whole element is then transferred to the construction site where the onsite assembly includes the connection with the profile splice (Figure 4.43). In Figure 4.44 some possibilities of profile splice for hollow cross sections are presented. To design this connection an appropriate EC3 procedure can be followed. By using this system assembly, higher accuracy on the connection can be achieved, while possible tolerances can be compensated within profile splice connections.

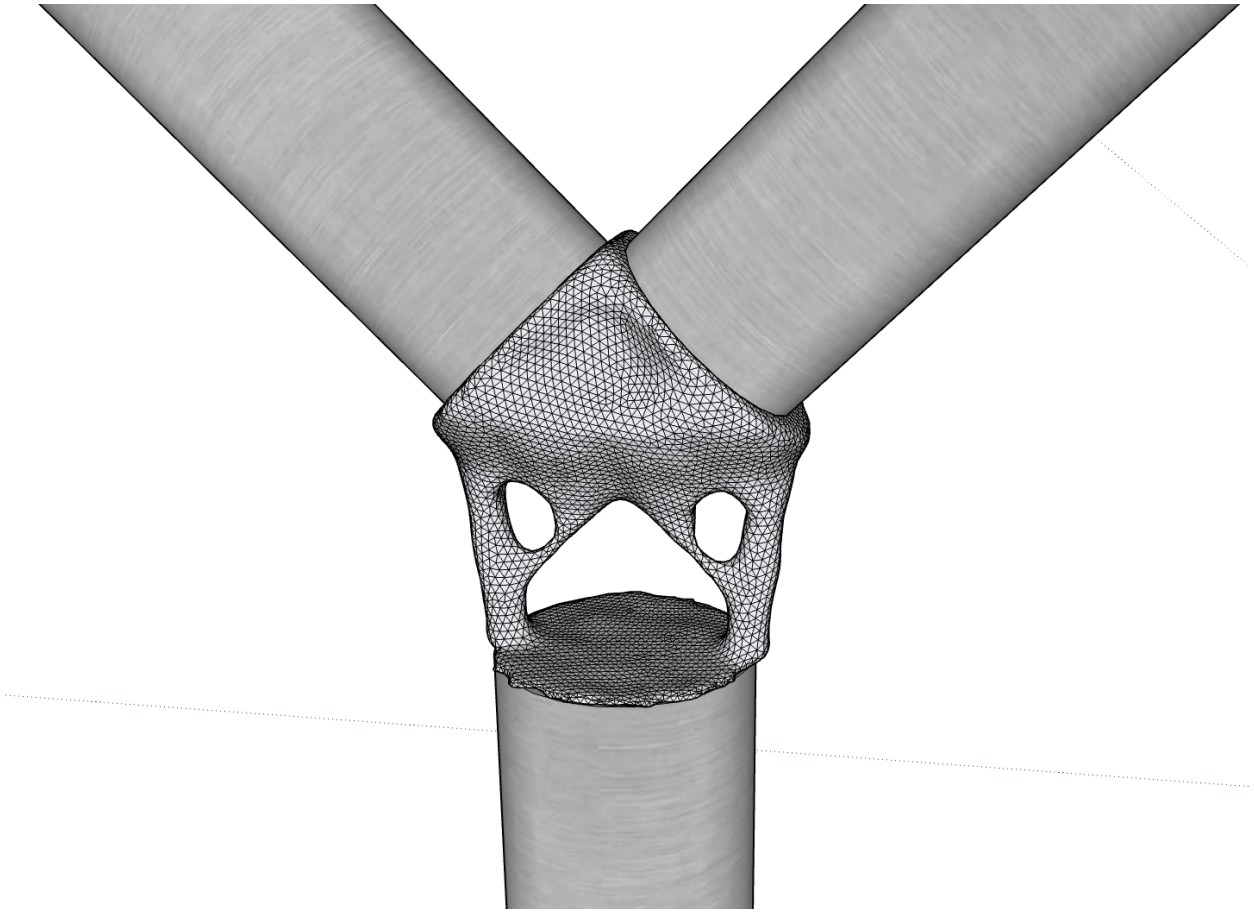

Figure 4.42: Assembly of the steel profiles

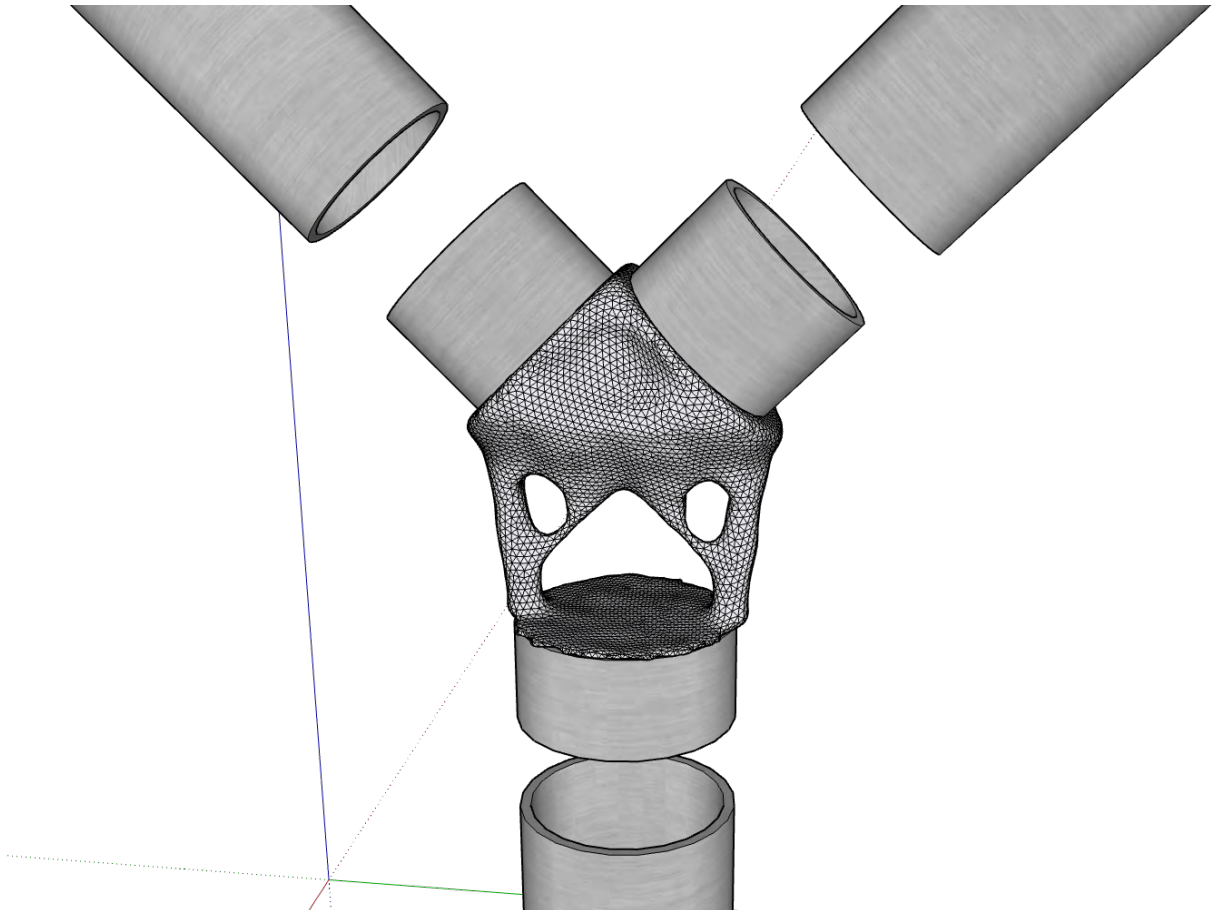

Figure 4.43: On site assembly with profile splice

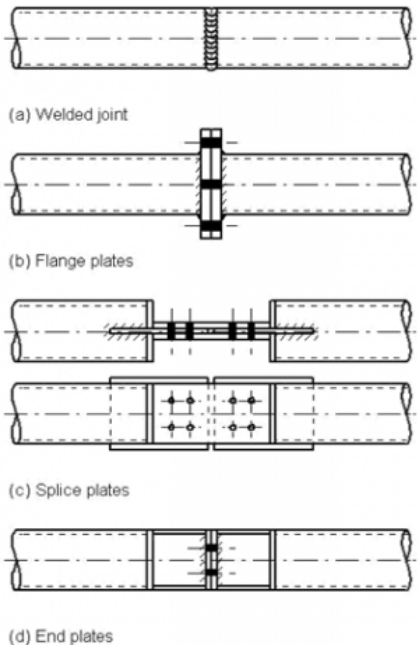

Figure 4.44: Profile splice for hollow profiles

- **Timber / concrete profiles**

In case a branched column is made out of timber, concrete, or other materials where welding is not possible, another engineering solution needs to be implemented. To do so a specific element was designed that allows jointing the profile with the connection by bolting. This element is basically a short steel hollow profile that is welded onto the connection. Column and branch profiles are then inserted into this element and attached by bolts through the predrilled holes. The explained engineering solution is presented in Figure 4.45. To properly design the proposed solution a calculation of required welds and bolts is needed, which can be done based on EC3 procedure. The whole connection is completely prefabricated and then brought to the construction site. The on site assembly includes joining the connection element with profiles by bolting. The assembly is shown in Figure 4.46.

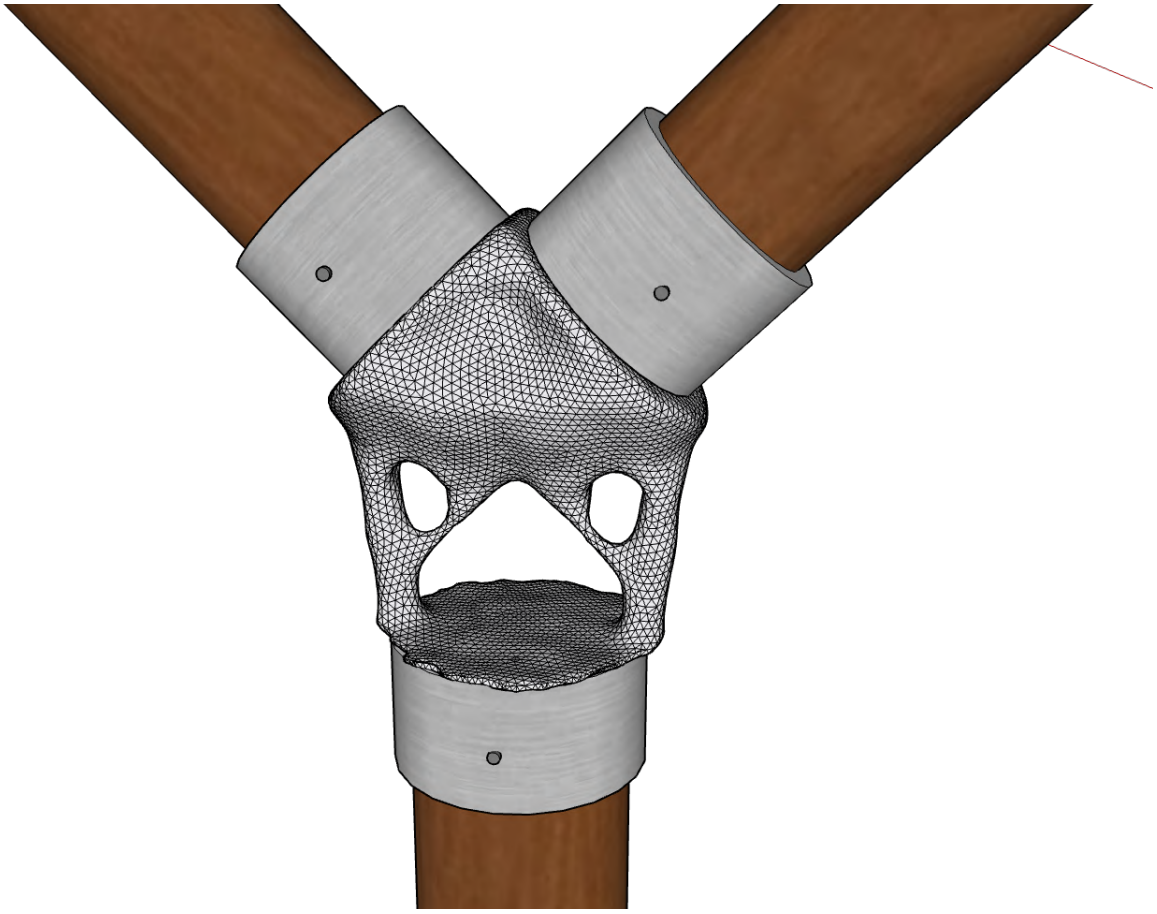

Figure 4.45: Assembly of the timber profiles

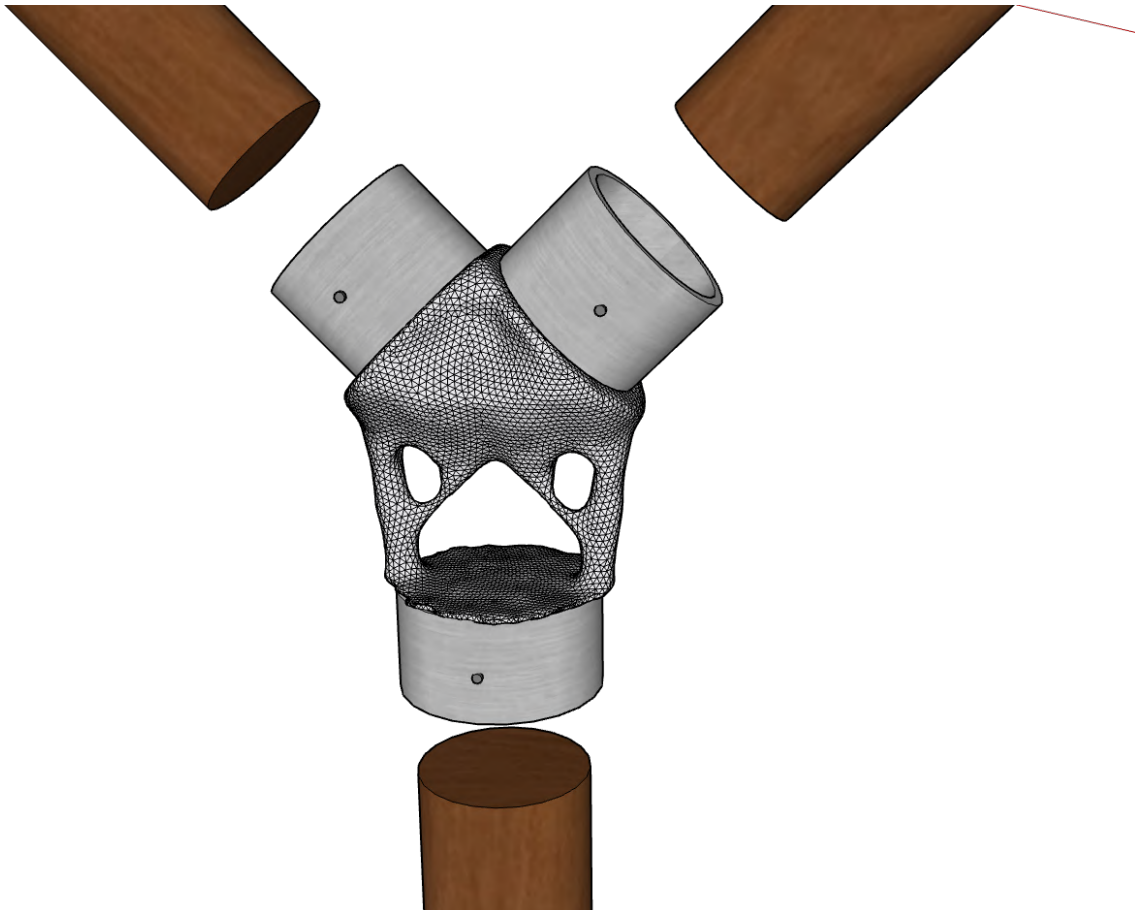

Figure 4.46: On site assembly with timber profiles

4.4.5 ANALYSIS RESULTS OVERVIEW

In the previous paragraphs, an extensive analysis of the TO was done. This analysis examined the impact of different TO input parameters on the connection's performance and geometry. The TO was done to minimize the required material and increase the overall performance of the model. Besides the TO, the engineering solutions (integration of the designed connection with branch and column profiles and on-site assembly procedure) were also proposed. To better understand the provided outcome of the analysis and thus see the difference between different models, the overview of the results will be done in a comparative way. In the following paragraphs, the most important TO input parameters (TO objectives and constraints) and their impact on the required mass, average stress, and deformation will be shown through graphs.

The analysis showed that using different TO objectives provides us with models, which drastically differ in geometry, mass, volume, and structural performance. Based on these four criteria the most optimal TO objective of compliance was selected. For each model, a structural analysis was done to see if the internal stresses align with the assumed yield strength. Models that satisfied the structural performance were then further compared based on the required mass. Figure 4.47 shows the comparison of models with different TO objectives. The comparison is done based on the two most relevant criteria, which are the average stress that appears in the connection and the required amount of material.

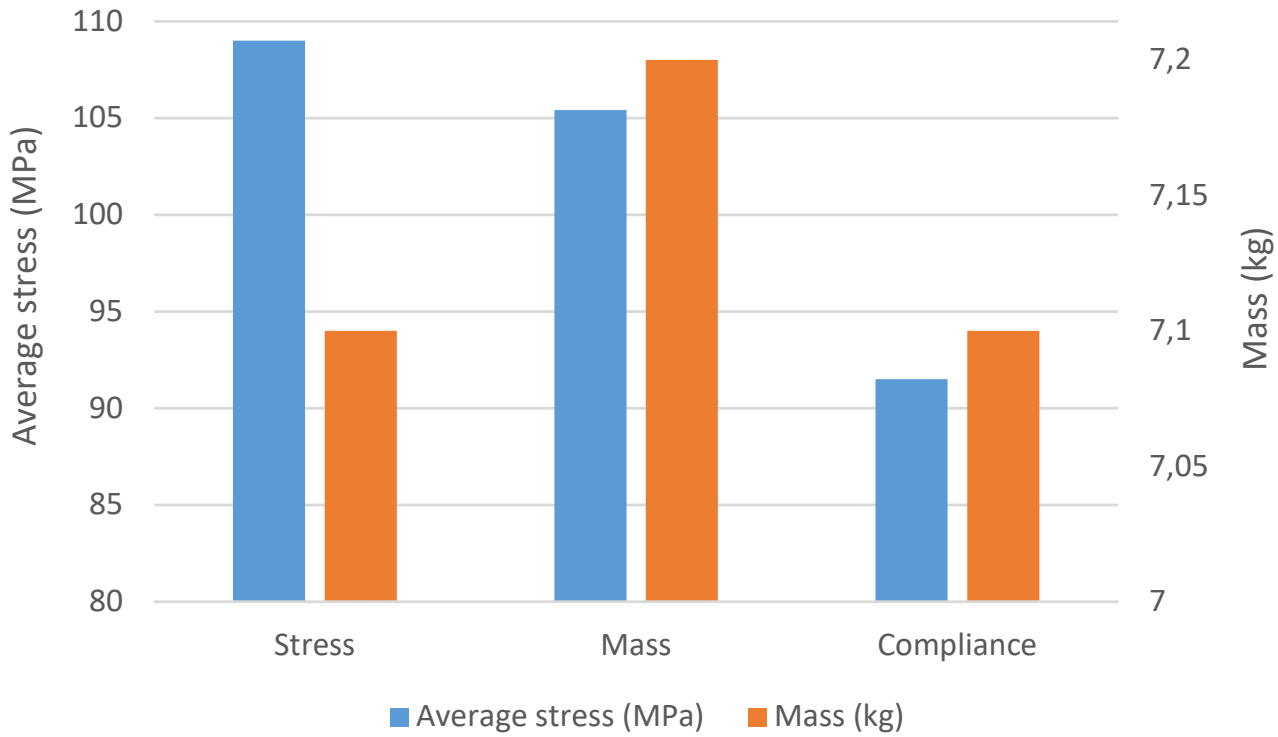

Figure 4.47: Comparison of models with different TO objective based on average stress and mass

Besides the impact of TO objectives, the analysis also examined the influence of the proposed TO constraints. In the case of the TO objective of compliance the mass retain percentage was implemented as a constraint. This constraint blocks the solver from removing more material from the TO block than the proposed value. Therefore, the proposed constraint has a direct link with the mass of the produced model. To examine the impact of the proposed constraint, eight models were created where the mass retain percentage was gradually increased from 15 % to 50 %. The required amount of material for each model corresponding to individual mass retain percentages is presented in Figure 4.48. As predicted the required mass and mass retain percentage are linearly connected. The gradual increase of the percentage will cause a linear increase in the mass. Based on this, it is possible to conclude that the needed material for the production of the model depended on the dimensions of the original TO block and the proposed TO constraint.

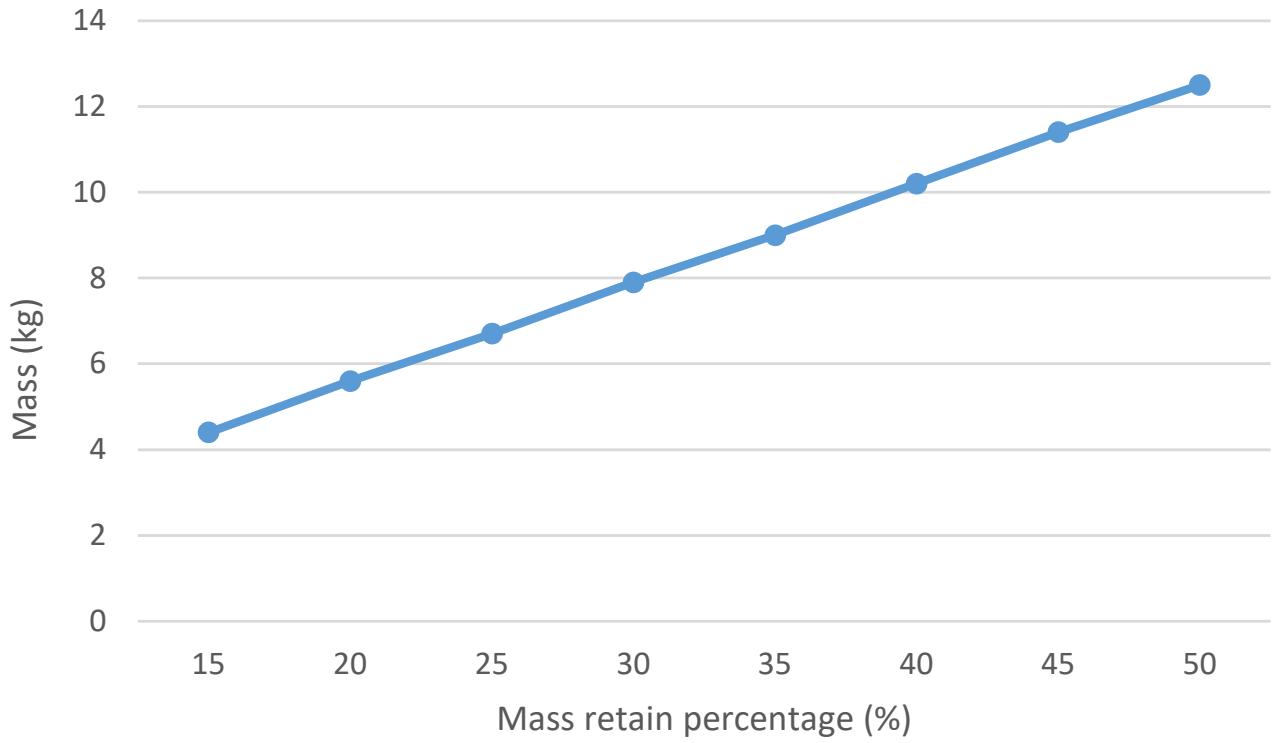

Figure 4.48: Mass of models with different mass retain percentages

As explained, changing the mass retain percentage directly influences the required amount of material needed for the production of the model, which indirectly affects the structural performance of the connection. Larger elements tend to distribute stress more effectively and can thus handle higher loads without failing compared to smaller elements. This is due to a larger cross sectional area that spreads the force over a greater surface, reducing the overall stress within the material. More material generally means greater strength and stiffness, which provides additional resistance to deformation and enhances its ability to withstand stress. Figure 4.49 shows how changing the mass retain percentage (required amount of material) impacts the average stress within the model. The average stress value represents the average stress experienced in the nodes of the entire model. This value is derived from the stress distribution across the finite elements used in the FEM analysis. The average stress provides an overall understanding of stress levels within a model. The value can not be directly used in the dimensioning and design phase, but rather serves as a statistical representation that can give a general idea of the stress magnitude and the overall performance of the model. For design purposes, the maximum stresses should be examined, with a fair amount of caution. In the case of this analysis, maximum stresses in most cases appear at the location where the load is applied (where branch and column profiles are attached to the connection), and their amount is independent of the size of the model. These peak stresses are very localized and can be disregarded, especially if we consider additional weld thickness and thus better stress distribution in those locations. The graph illustrates an exponential decrease in average stress as the model's mass linearly increases. This indicates that the influence of the mass retain percentage on connection performance is more pronounced when the volume is smaller.

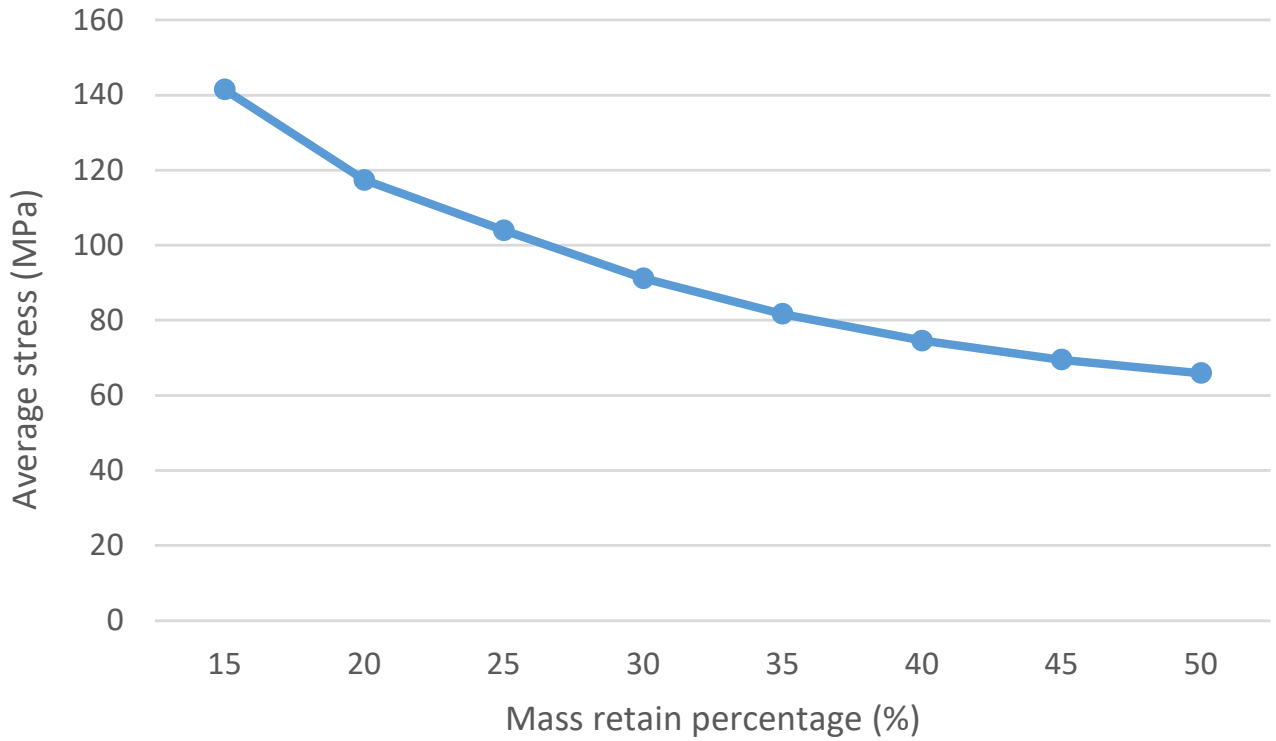

Figure 4.49: Average stress of models with different mass retain percentages

Besides stresses, the important part of the design is also limiting the deformation of the model. The assurance of steel connection integrity is crucial in ensuring the stability and safety of the structures they underpin. Although the examination of deformations in these connections may at first seem irrelevant to the main design factors, their role in supporting structural elements indicates their importance. These connections support critical elements like roofs, beams, or even entire frameworks. The implications of deformations within these connectors are substantial, directly impacting the stability and operational efficiency of the structures they fortify. Consider, for instance, the scenario of connections supporting a roof structure. Any deformation within these connections is not isolated as it resonates throughout the entire system. The subtle shifts or distortions in these connections have the potential to compromise the structural integrity, potentially leading to diminished performance or, in extreme cases, structural failure. This is especially relevant in the case of brittle covering material, for example, glass.

To see how the deformations change depending on the mass retain percentage the graph shown in Figure 4.50 was plotted. The deformations presented in the graph are maximum deformations in the z direction, which is a direction perpendicular to the roof structure. Values used in the graph were taken from the deformation plot diagrams. In Figure 4.51 the plot is shown for the mass retain percentage of 20 %. From the plot, it is visible that the maximum deformations appear at the top of the connection and then gradually decrease towards the bottom. This is because the section at the top of the joint is much smaller than at the bottom, which means less resistance to deformation. Even though the values used in the graph are taken from the top of the connection (maximum values), their magnitude is fairly low (only reaching a few hundredths of millimeters), which suggests also small displacements of the structure that they support. To properly validate the deflections, limit values from EC are shown in Table 4.8.

From Figure 4.50 it is possible see that the magnitude of the maximum deformation decreases with the increase of the mass retain percentage. This is predictable since the increase in the model's mass will increase its robustness (stiffness) and thus lower its deformation. The results from Figure 4.50 also align with the results of the average stress (Figure 4.49). Strain (deformations) and stress are directly connected through Hooke's law. The relationship between directional deformation and mass retain percentage is more or less linear.

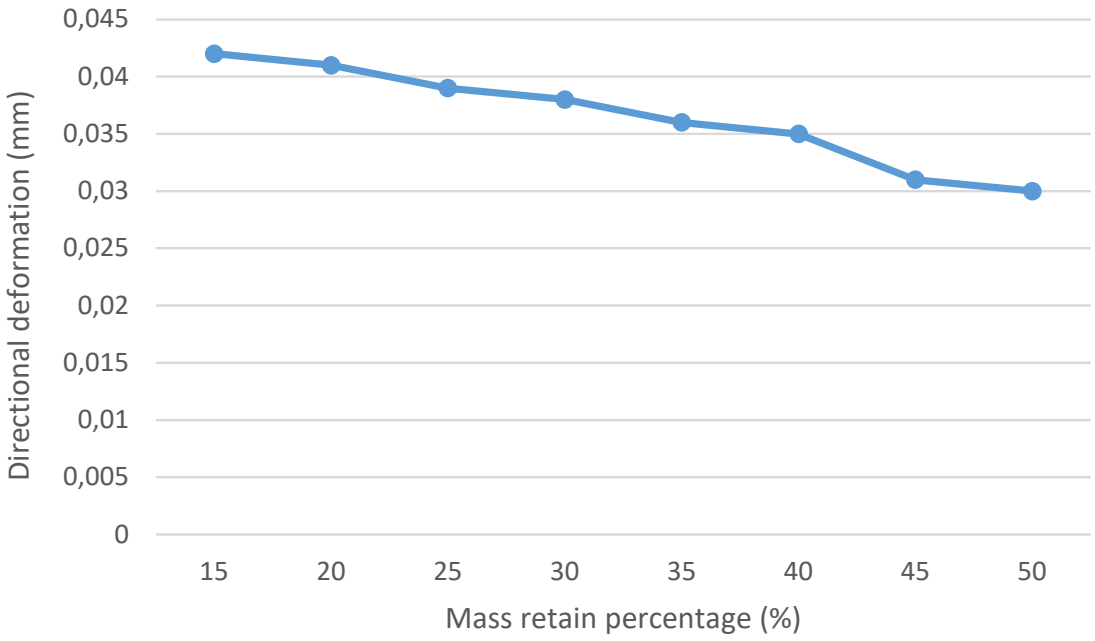

Figure 4.50: Directional deformation of models with different mass retain percentages

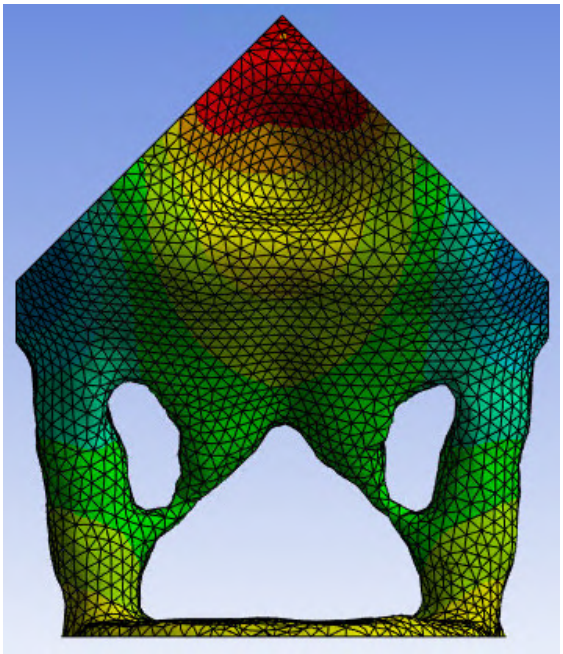

Figure 4.51: Directional deformation plot for model with mass retain percentage of 20 %

Table 4.8: Limit vertical deflection values based on Eurocode [4.26]

	Vertical *total* deflection Calculated from dead + imposed loads
Member supporting partition walls	
• Brittle (not reinforced)	≤ L/500
• Reinforced	≤ L/300
• Removable	≤ L/300
Ceilings	
• Plastered	≤ L/300
• Suspended	≤ L/200
Roofing and Flooring	
• Rigid (e.g. ceramic tiles)	≤ L/500
• Flexible (e.g. flexible floor covering)	≤ L/250

Table 2. ***Vertical deflections: Values from Table 8 of BS 5950-1: 2000***

	Vertical *imposed load* deflection
Cantilevers	≤ L/180
Beams carrying plaster or other brittle finish	≤ L/360
Other beams (except purlins and sheeting rails)	≤ L/200

4.5 REFERENCES

[4.1] Kanyilmaz. A., Demir. A. G., Chierici. M., Berto. F., Gardner. L., Kandukuri. S. Y., Kassabian. P., Kinoshita. T., Laurenti. A., Paoletti. I., du Plessis. A., Razavi. N. 2022. Role of metal 3D printing to increase quality and resource-efficiency in the construction sector. Additive Manufacturing. Available at: https://doi.org/10.1016/j.addma.2021.102541

[4.2] Zhengyao. L., Tsavdaridis. K. D., Gardner. L. 2021. A Review of Optimised Additively Manufactured Steel Connections for Modular Building Systems. Industrializing Additive Manufacturing. Available at: http://dx.doi.org/10.1007/978-3-030-54334-1_25

[4.3] Gardner. L., Kyvelou. P., Herbert. G., Buchanan. C. 2020. Testing and initial verification of theworld's first metal 3D printed bridge. Journal of Constructional Steel Research. Available at: https://doi.org/10.1016/j.jcsr.2020.106233

[4.4] Kanyilmaz. A., Berto. F., Paoletti. I., Caringal. R. J., Mora. S. 2020. Nature-inspired optimization of tubular joints for metal 3D printing. Structural and Multidisciplinary Optimization. Available at: https://doi.org/10.1007/s00158-020-02729-7

[4.5] Chierici. M., Berto. F., Kanyilmaz. A. 2021. Resource-efficient joint fabrication by welding metal 3D-printed parts to conventional steel: A structural integrity study. Fatigue & Fracture of Engineering Materials & Structures. Available at: https://doi.org/10.1111/ffe.13428

[4.6] Lange. J., Feucht. T., Erven. M. 2021. 3D-Printing with Steel - Additive Manufacturing Connections and Structures. Proceedings in civil engineering. Available at: https://doi.org/10.1002/cepa.1258

[4.7] Menges. A., Sheil. B., Glynn. R., Skavara. M. 2017. Fabricate 2017 Rethinking Design and Construction. ULC Press. Available at: https://www.uclpress.co.uk/products/89026

[4.8] MX3D. 2019. Connector for Takenaka. Available at: https://mx3d.com/industries/construction/connector-for-takenaka/

[4.9] Jansen. 2023. Study VISS free-form façade with 3D printed steel nodes. Available at: https://www.jansen.com/en/building-systems-profile-systems-steel/topics/jansen-viss3.html

[4.10] Naboni. R., Paoletti. I. 2015. Advanced Customization in Architectural Design and Construction. Springer briefs in applied sciences and technology. Available at: https://link.springer.com/book/10.1007/978-3-319-04423-1

[4.11] Foundation reuse creates sustainable landmark. NSC. Vol 21 No.5. Sept/Oct 2013. Available at: https://www.newsteelconstruction.com/wp/

[4.12] 3D printing: it's the shape of things to come. 2013. Construction Management. (Accessed on 29.6.2023). Available at: https://constructionmanagement.co.uk/3d-printing-shape-things-come/

[4.13] Skanska. 2023. 6 Bevis Marks. (Accessed on 29.6.2023). Available at: https://www.skanska.co.uk/expertise/projects/57267/6-Bevis-Marks

[4.14] Griffiths. A. 2013. British architect claims "first architectural application" of 3D printing. De zeen. (Accessed on 19.6.2023). Available at: https://www.dezeen.com/2013/12/02/first-architectural-application-of-3d-printing-adrian-priestman-6-bevis-marks/

[4.15] Dekhn. R. C., Shadhan. K. K. 2022. Structural behavior of tree-like steel columns subjected to combined axial and lateral loads. Journal of the Mechanical Behavior of Materials. Available at: https://doi.org/10.1515/jmbm-2022-0030

[4.16] Selçuk. A. S., Gülle. N. B., Avinç. G. M. 2022. Tree-Like Structures in Architecture: Revisiting Frei Otto's Branching Columns Through Parametric Tools. SAGE Open. Available at: https://doi.org/10.1177/21582440221119479

[4.17] Frearson. A. 2016. Benthem Crouwel's new station for The Hague brings light in through a patterned glass roof. De zeen. (Accessed on 28.7.2023) Available at: https://www.dezeen.com/2016/02/17/benthem-crouwel-den-haag-centraal-station-hague-netherlands-patterned-glass-roof/

[4.18] Lundgren. J., Palmqvist. C. 2012. Structural Form Optimisation. Master's Thesis, Chalmers University of Technology, Göteborg, Sweden. Available at: https://publications.lib.chalmers.se/records/fulltext/162939.pdf

[4.19] Herrero-Pérez. D., Picó-Vicente. S. G., Martínez-Barberá. H. 2022. Efficient distributed approach for density-based topology optimization using coarsening and h-refinement. Computers and Structures. Available at: https://doi.org/10.1016/j.compstruc.2022.106770

[4.20] van Dijk. N. P., Yoon. G. H., van Keulen. F., Langelaar. M. 2010. A level-set based topology optimization using the element connectivity parameterization method. Structural and Multidisciplinary Optimization. Available at: DOI 10.1007/s00158-010-0485-y

[4.21] Introduction to Topology Optimization. 2017-2023. Engineering Design Analysis, Product Design Process, Tools and Techniques. (Accessed on: 1.8.2023). Available at: https://engineeringproductdesign.com/knowledge-base/topology-optimization/

[4.22] 3 advantages of topology optimization that your product team can't afford to miss. 2020. Fast Radius a Sybridge Brand. Available at: https://www.fastradius.com/resources/topology-optimization-advantages/#:~:text=Topology%20optimization%20enables%20designers%20to,the%20help%20of%20a%20computer.

[4.23] Ansys. 2023. Computer Software. (Accessed on: 7.8.2023). Available at: https://www.ansys.com/

[4.24] Matrix Software. 2023. Computer Software. (Accessed on: 7.8.2023). Available at: https://www.matrix-software.com/structural-engineers/matrix-frame

[4.25] Han. Y., Xu. B, Duan. Z., Huang. X. 2021. Stress-based topology optimization of continuum structures for the elastic contact problems with friction. Structural and Multidisciplinary Optimization. Available at: https://link.springer.com/article/10.1007/s00158-022-03169-1

[4.26] European Committee for Standardization (CEN). 2005. Eurocode 3: Design of steel structures - Part 1-1: General rules and rules for buildings. EN 1993-1-1. Brussels, Belgium: CEN

DESIGN GUIDELINE

5. DESIGN GUIDELINE

This chapter proposes a design guideline that someone should follow when designing an additive manufactured connection. The design guideline is constructed based on the provided literature review and research results and follows the organization of all until now written chapters in the thesis. It suggests the steps that need to be considered in the preparation for the design phase and shows the criteria based on which the selection of design considerations is based. It also provides some limit or optimal values that were gathered through the thesis. The guideline serves as a comprehensive overview of essential details and components to be considered in the design of the structural connection, intended for manufacturing through AM technology. To better understand the guideline the visual presentation of all the required steps is shown in Figure 5.1.

1. Before starting with the actual design of the connection appropriate AM process needs to be selected. In Chapter 2: Additive Manufacturing – State of the art, many different AM processes were presented. It is important to first determine your project characteristics and requirements and based on this make the selection. The considerations that govern this selection are the desirable material and its required mechanical properties, needed accuracy and allowed dimensional tolerances, dimensions of the AM object, and the available budget. For this thesis, WAAM process was selected.

2. Once the AM process is selected its manufacturing constraints within which objects can be printed need to be determined. Besides this, the material and its properties (yielding strength, ultimate strength, elastic modulus, tangent modulus, and Poisson's ratio) should be selected. As of now, there are no standardized codes available, thus the needed information should be collected from the published research papers. Through this research, the selected material was welding wire ER70S-6, which is one of the more commonly used carbon steel welding wires. Based on the structural validation conducted through the thesis it can be concluded that the achieved mechanical properties of ER70S-6 are sufficient. It is also important to notice that in the thesis as built mechanical properties were assumed, meaning that post processing was not considered. In the case of post processing the value of mechanical properties would increase, this is seen in subchapter 2.2.2 Material.

3. In Chapter 3: WAAM manufacturing limitations some of the research papers presenting the material properties and manufacturing limitations concerned with WAAM technology are shown and can be taken as a reliable reference. It is important to note that the usage of AM is still in the research phase and some of the provided information can be contradicting, thus it should be taken with some consideration.
Regarding the WAAM process, three factors should be considered and used as a constraint either in the design or manufacturing phase. WAAM manufacturing input parameters (travel speed, wire feed speed, and heat input), will have an impact on the dimensions and quality of the weld beads. Overlapping should be considered in the manufacturing phase while overhang limitation needs to be implemented into the design.

4. For the design of the connection TO should be used. The design of the model includes multiple considerations that need to be determined before the TO model can be generated. The design phase is therefore further divided into numerous additional steps.

a) Firstly the loads acting on the connection need to be calculated. This can be done by modeling the frame structure in which the connection is a part. Based on the frame structural analysis, internal forces and moments acting on the connection can be determined.

b) In the next step the selection of boundary conditions is done. The way the loads and supports are applied to the model depends on the shape and size of the elements included in the connection.

c) TO block also needs to be proposed and should resemble the desired geometry of the connection. This is a block of material based on which the TO software will find the most optimal geometry. Previously calculated loads should be applied to the TO based on selected boundary conditions.

d) The input parameters for the TO depend on the desired outcome. In case the goal of the design is to decrease the amount of needed material (as it was in this thesis) the most optimal TO objective is the objective of compliance as it allows for the biggest mass reduction. For the TO constraint the mass retain percentage should be used. The smallest allowed percentage that still creates the geometry with sufficient structural performance is found with a load – strain graph presented in Figure 4.38, which is plotted for the location on the connection where maximum stresses are present. The mass retain percentage should be gradually decreased until the plasticity in the connection is reached at exactly 100% of the applied load. Besides this, manufacturing constraints should also be included in the TO as input parameters. For WAAM process the minimum overhang angle should be limited to the proposed value.

e) The last phase of design should include shrink wrapping and smoothing of the generated TO model. This will increase the manufacturability of the connection and remove possible defects

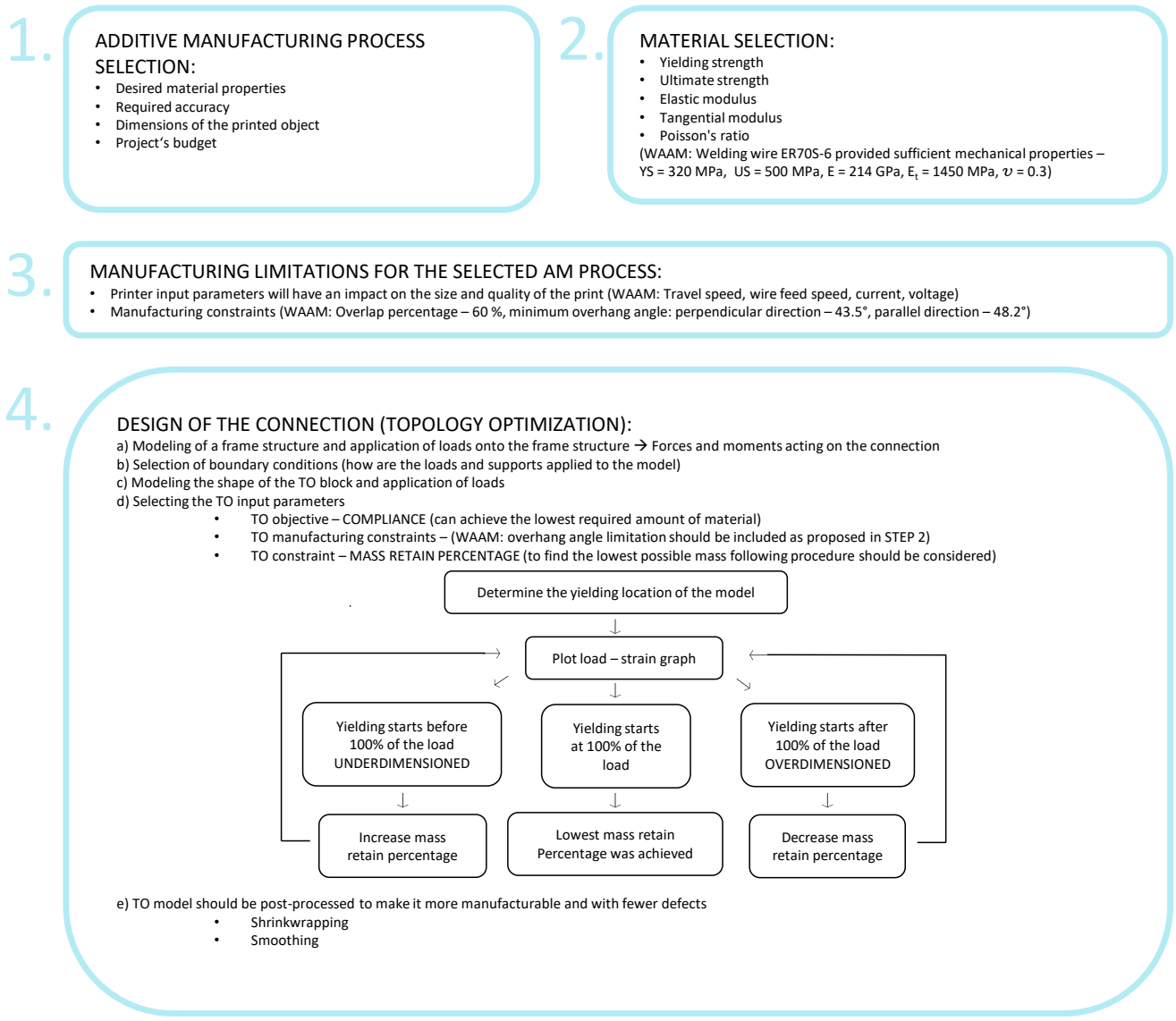

Figure 5.1: Guideline for the design of the additive manufactured connection

CASE STUDY

6. CASE STUDY

The last part of the thesis is dedicated to the case study, meaning that findings from the extensive analysis that was conducted throughout this research will be implemented on a real life project. The selected project is 6 Bevis Marks in London where branched columns were used for the design of the rooftop canopy. The connections between branches and columns were manufactured with the conventional methods i.e. by welding individual steel plates. In this chapter, firstly the description of the selected project will be done, with a more detailed description of the manufacturing methods used for its construction. Most of the attention will be paid to the branched column connections. These connections will then be recreated by using the previously proposed topology optimization and manufacturing techniques. After the design of the connection is completed, the comparison between the conventionally produced connection and the AM connection can be done. This comparison will be based on three essential criteria that closely align with the research questions that have guided this study: the quantity of material required, the time needed for manufacturing, and the associated costs.

The design of the branch column connection for this case study will be done by following the proposed design guideline from Chapter 5: Design guideline. The guideline should include all necessary information that someone needs for the design of an additive manufactured connection.

By scrutinizing these three factors, the goal is to gain in depth insights into the advantages and potential limitations of the proposed AM approach. In essence, this chapter serves as the practical realization of the theoretical and analytical work undertaken in this thesis, offering a demonstration of how the theoretical insights can be translated into real world engineering solutions. This chapter adds to the body of knowledge in the engineering and construction fields in addition to offering useful insights, especially when it comes to innovative production procedures. It also provides information about the practicality and usability of the previously proposed design guideline.

6.1 PROJECT – 6 BEVIS MARKS

6 Bevis Marks is a mixed use building situated in the heart of London's City right next to the infamous Gherkin. With 16500 m2 of usable space and 1100 m2 of terrace space, it provides a sufficient working environment for multiple companies. The building was designed by Fletcher Priest Architects and executed by Skanska. The project's primary focus was the incorporation of a 1980s structure present on the site while adding nine new floors and three private terraces, including the creation of a sky rooftop. Of particular note is the groundbreaking use of AM in the structural system of this building. [6.1] In the following paragraphs, an in depth analysis of the architectural and technological innovations that define 6 Bevis Marks will be explained.

The architectural style of the 6 Bevis Marks blends the historical existing buildings in that area with a modern touch of the newly constructed structures. It successfully pays homage to the rich historical context of London while embracing cutting edge technologies, forms, and materials. The project included the demolition of the existing eight storey steel frame structure with the precast concrete slabs while preserving its piled foundation. Due to the fact that the new design of the building includes an increase in size (16 stories) and preserves the existing foundation, the weight reduction was of great importance. [6.2] This was done with a steel frame structure incorporating composite deck slabs, which are compared to the standard precast slabs much lighter. The composite steel and concrete deck slabs have a thickness of 150 mm and are supported by 600 mm deep fabricated composite steel beams with either circular or rectangular cross section. Besides that, some of the existing retaining walls and basement slabs were also preserved and incorporated into the new building's load bearing structure. This meant that 52 % of the existing building could be preserved, which contributed to carbon savings of approximately 1000 tones and achieving the desired excellent BREEAM rating. [6.3]

a

b

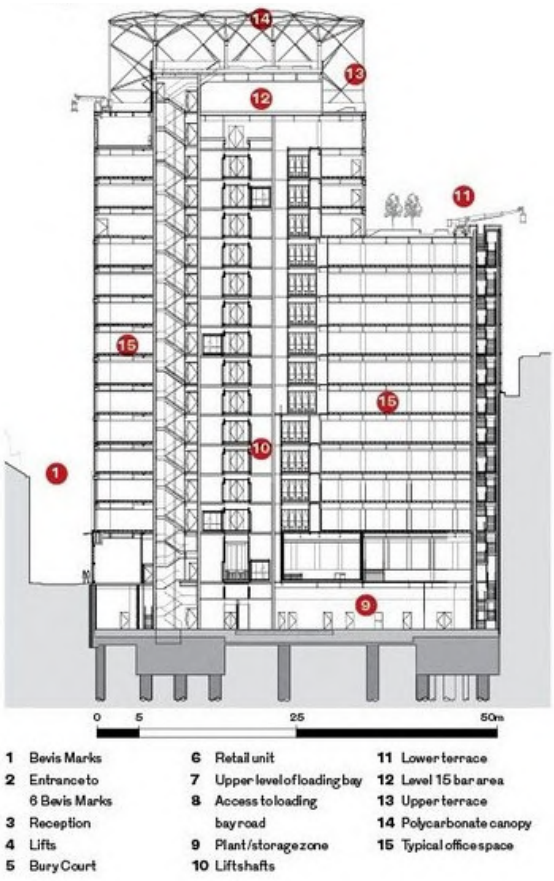

Figure 6.1: a) 6 Bevis Marks [6.1], b) Section of the building [6.3]

At a distance, the most remarkable aspect of the development is the roof canopy, which offers complete weather protection for the sky court, the biggest of the three roof gardens included in the building. The architect designed a rooftop garden that would be perfect for various corporate events as well as an ideal lunch spot for tenants has a footprint of around 33 m by 25 m. The top terrace provides a stunning view of the London financial district and the nearby Gherkin building. The cover is made out of a curved steel frame, which is open at the two ends and wraps approximately 28 m down the south façade. This creates the perfect mixture of the open space feeling, while still providing shade from sun and rain. [6.4] The ETFE (Ethylene Tetrafluoroethylene) roof cladding used in 6 Bevis Marks stands as one of the engineering innovations used in the building. Because of this material's transparency, the interior can receive an abundance of natural light. Dot matrix print patterning on the upper ETFE foil layer aids in shielding against overly intense solar radiation, meaning that a very low g-value can be achieved. Its lightweight nature minimizes structural stress, ideal for intricate rooftop designs as seen in 6 Bevis Marks. ETFE also provides good thermal insulation properties, contributing to energy efficiency, and it endures environmental impacts, maintaining optical clarity over time. Its flexibility in fabrication offers architects and designers the latitude to shape it according to their aesthetic visions, as demonstrated in the steel cladding at 6 Bevis Marks. Beyond its visual appeal, ETFE aligns with environmental concerns through energy efficiency, recyclability, and minimized transportation costs, making it a sustainable choice for modern building design. [6.2]

Figure 6.2: Rooftop terrace and canopy [6.1]

The canopy steel frame is supported by eight individually designed branched columns. The columns are made out of circular hollow sections with 355 mm diameter and connect 45 branches, which are also designed as circular hollow sections with a diameter of 193 mm. Due to the curved freeform shape of the canopy frame, the branched columns differ depending on their location. The difference between them is visible in the number of branches, their orientation, and inclination. [6.1] By modifying the geometry of each column, the most efficient load and stress distribution could be achieved. Originally, eight intricate connections between the branches and columns were planned as cast steel nodes however, Skanska (the main constructor) anticipated significant costs and challenges with this type of manufacturing process. Thus the alternative steel plate option was considered and is shown in Figure 6.3.

Figure 6.3: Steel plate branched column connection [6.2]

Since the architects' primary design focus was to maintain the building's organic shape, the designed connection did not coincide with this vision. Therefore the innovative AM solution was implemented. This approach involved the creation of 3D printed cladding shrouds that were applied around the connection, thus creating a smooth transition between branches and columns. The explained concept is shown in Figure 6.4 a and b. AM was used because of the complex and customized geometries of each individual connection. The selected 3D printing process was a Selective Laser Sintering (SLS), which fused layers of powdered Nylon PA 12 to produce highly detailed shapes. This material is a specific kind of nylon that is resistant to UV light and other environmental impacts, making it ideal for outdoor use. The architect's CAD specifications were transformed into 0.1mm layers, and the SLS machine automatically built up the eight unique cladding shrouds. These approximately 600mm wide and 800mm high nylon shrouds were finished to resemble steel, achieving a similar colour and texture (Figure 6.4 c). [6.5]

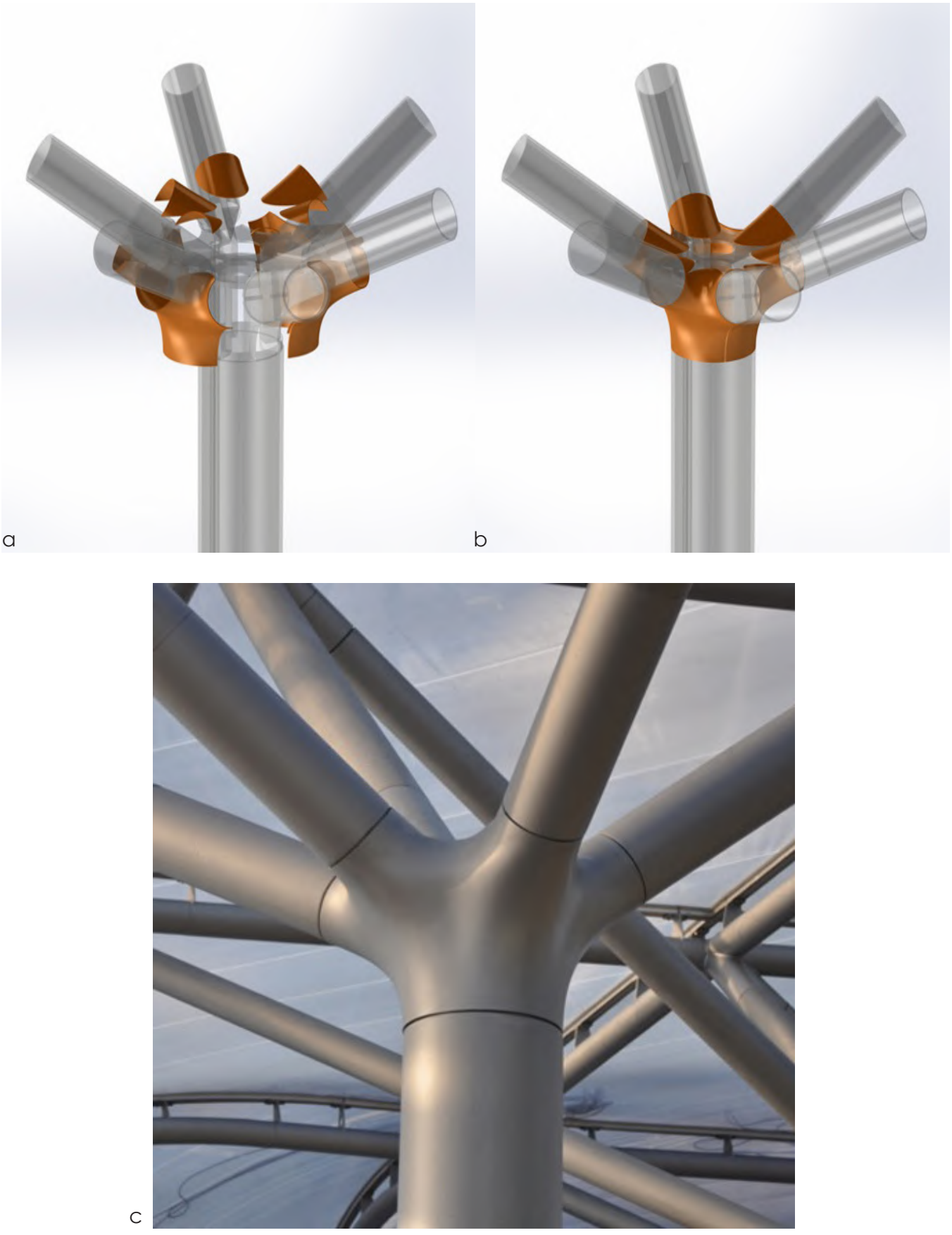

Figure 6.4: 3D printed cladding shrouds [6.2]

6.2 ADDITIVELY MANUFACTURED FIVE-BRANCHED CONNECTION

As above explained, the load bearing part of the connection between the column and branches relies on welding together multiple individual steel plates. Even though the connection's structural performance is sufficient, the proposed design provides quite a few limitations and difficulties that should be considered and improved. Firstly, the geometry does not coincide with the desired aesthetics of the organic architecture but rather has a very robust and industrial look. Therefore, additional applications need to be considered, for example cladding shrouds. Secondly, the design phase of this connection is very complex, as its unique geometry does not resemble any other standard connections. In addition, there are no standardized guidelines proposed in any of the codes, that engineers could follow when dimensioning individual parts of the connection, and thus need to create their own custom solutions, which can have a significant effect on the length of the design process. The complex geometry also has an influence on the manufacturability of the part. Due to the high number of individual parts (steel plates), the manufacturing and on site assembly part can also be complex and lengthy. This might cause dimensional errors, which can have a notable impact on the desired performance of the connection.

To solve the above stated problems, improve the overall performance of the connection, and lower the required amount of material, the system developed throughout the thesis will be implemented. To do so, a couple of assumptions are needed.

In 6 Bevis Marks the number of branches per individual column varies from 5 to 7 depending on its position. For the purposes of this case study the five branched column connection will be recreated, which is shown in Figure 6.3. To design the connection, a structure needs to be created, which will as much as possible resemble the conditions in 6 Bevis Marks. Previously it was mentioned that the footprint of the rooftop canopy is about 33 m times 25 m, which adds up to a total of 825 m2 of area space. The canopy is supported by eight branched columns, which means that each column supports around 103 m2 of the canopy. From Figure 5.3 the angle of branches was assumed to be 30°. The profile diameters are the same as in the original connection, namely 355 mm for the column and 193 mm for the branches. Based on this a simple frame structure can be created and is shown in Figure 6.5.

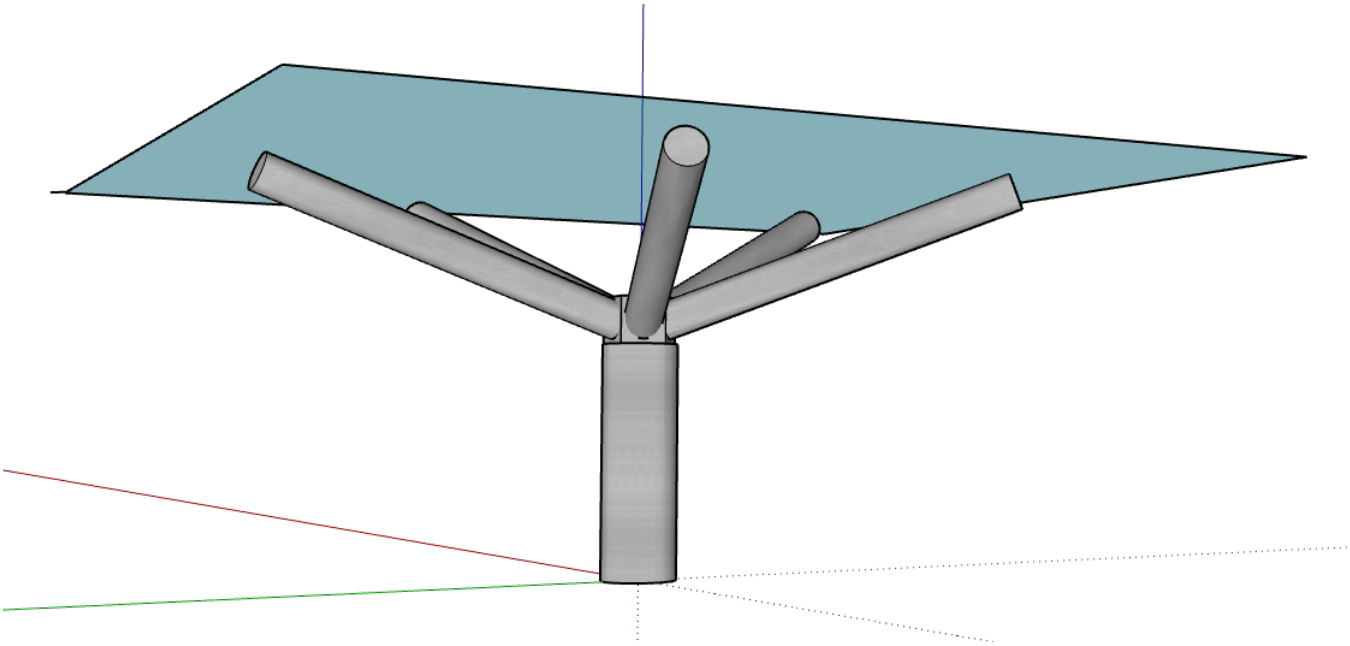

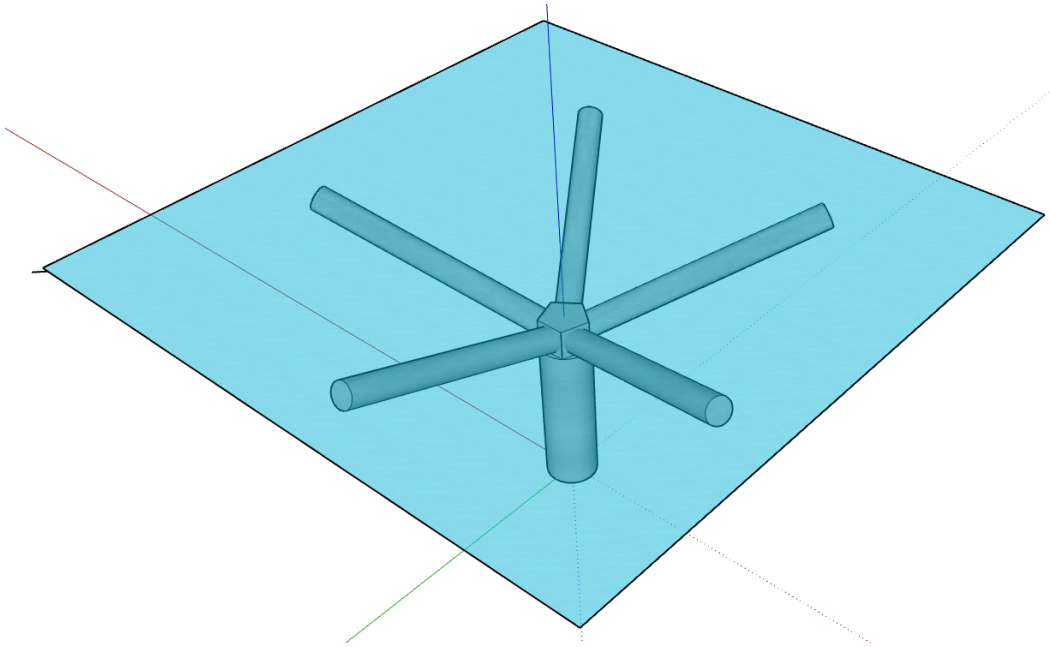

Figure 6.5: Frame structure of a five branch column connection

To perform the topology optimization and structural validation, loads acting on the connection needed to be calculated. Therefore, the frame structure shown in Figure 6.5 was modeled in a Matrix Frame where the structural analysis could be conducted. For the purpose of the case study symmetrical conditions were assumed, thus the structure was loaded by only vertical load. The assumed load was 5 kN/m2, which includes the live load proposed by EC 1 (0,6 kN/m2) [5.6] and the dead load from the canopy steel frame. Loads acting on the connection were again split into three components, namely horizontal, vertical, and moment load. Their values are presented in Table 6.1.

Table 6.1: Load components acting on the connection

Nx	951,2	kN
Vz	473,6	kN
My	350,1	kNm

Besides loads, the TO block also needed to be determined. Since the selected connection includes five branches, the block geometry resembles a pentagonal pyramid placed on top of a 100 mm tall pentagonal prism. The prism side has a length of 315 mm, while the height of the pyramid is 310 mm. The shape of the TO block and its dimensions are shown in Figure 6.6.

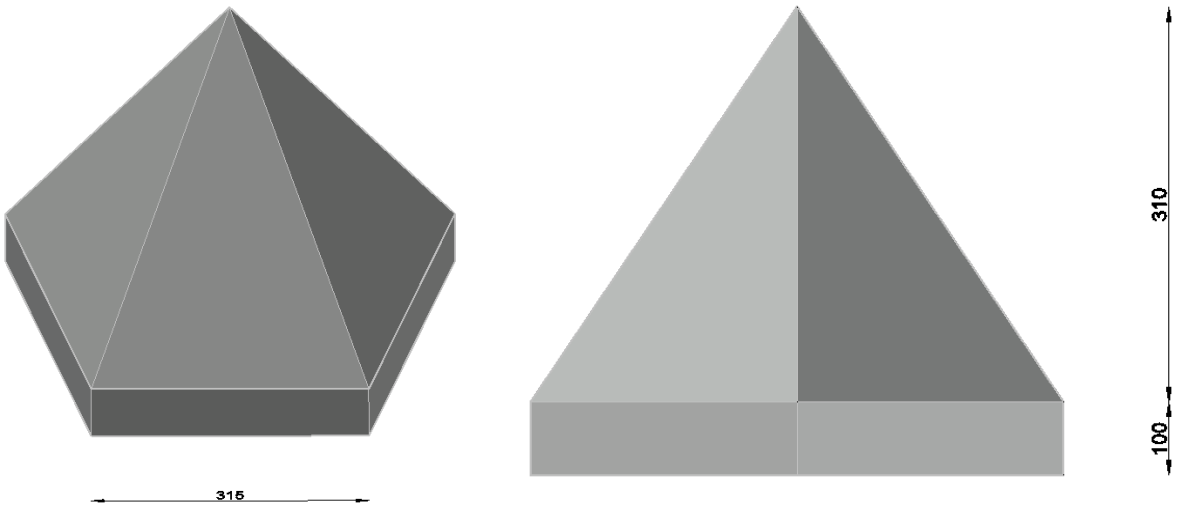

Figure 6.6: TO block for five branch column connection

The application of loads onto the proposed TO block is presented in Figure 6.7. Loads and support are applied as an annulus region on each side of the pyramid presented with red colour. The inner part of the circle was set up as an excluded region, meaning that it was not removed during the TO process.

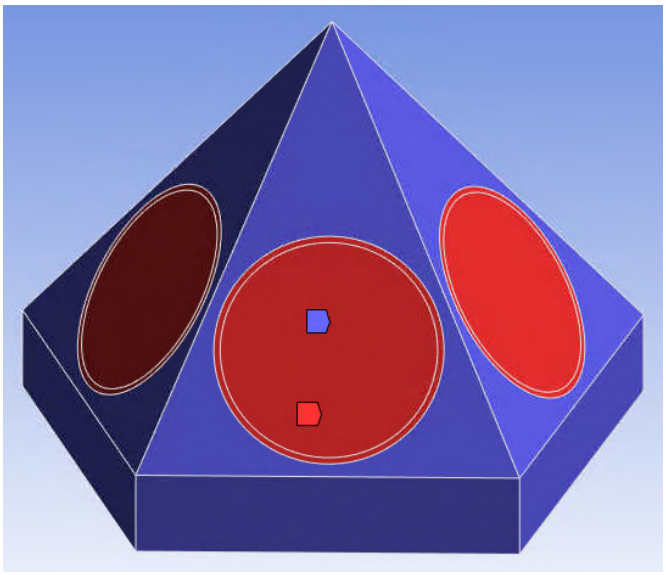

Figure 6.7: Load application onto the TO block

The material used for the case study is the same as it was used for the lab tests and two branched column analysis. The selected WAAM welding wire is ER70S-6 with a diameter of 1 mm. To simplify the analysis, isotropic material properties were assumed, thus a yield strength of 320 MPa, an elastic modulus of 214 GPa, and Poisson's ratio of 0,3 were selected. To perform a plastic structural analysis of the connection a tangential modulus of 1450 MPa was assumed.

For the TO, the appropriate input parameters were selected based on findings from the analysis performed in Chapter 4: Connections. For the TO objective compliance was chosen since it provides a sufficient solution and at the same time achieves the lowest required mass. As a TO constraint, the mass retain percentage of 30% was implemented. The smallest achievable percentage was selected based on structural analysis and an exported load – strain graph, which will be shown in the following paragraphs. To guarantee that the gathered geometry will be manufacturable with WAAM, the overhang limitation was included. This manufacturing limitation was considered with the smallest allowed overhang angle of 45°. Besides that, density based TO was selected as a type of TO.

For printing the connection, process input parameters presented in Table 6.2 were used. The corresponding weld bead dimensions are written in Table 6.3. The chosen process parameters were picked based on the lab tests performed in Chapter 2: WAAM manufacturing limitation, which show that the selected welds experience high quality without major visible defects and have relatively big dimensions.

Table 6.2: WAAM input process parameters

TS (mm/s)	WFS (m/min)	I (A)	E (V)	HI (J/mm)
10	5	135	21,7	263,7

Table 6.3: WAAM weld bead dimensions

Weld height (mm)	Weld width (mm)	Weld bead form factor
1,9	6,9	0,27

The analysis provides us with the optimized geometry, which is shown in Figure 6.8 a – d. The geometry was after the TO process was completed additionally shrinkwrapped (with size of 3 mm) and smoothed (by flattening peaks and with 60° angle threshold). Shrinkwrapping and smoothing TO geometries is for WAAM crucial as it increases its manufacturability by enhancing surface finishing and removing extensive material. TO created a symmetrical geometry with 5 straight surfaces where branches are connected. The bottom part of the geometry is shown in Figure 6.8 d and presents a part where the connection is joined with the main column. Although the connection appears sturdy and solid on the outside, it is actually hollow, which helps to reduce the mass during TO. The cross section of the connection is presented in Figure 6.9 a and b. It is visible that symmetrical voids were generated within the geometry. The holes are located behind the branch and column hollow profiles, while the solid part of the connection is generated where the loads and supports are applied.

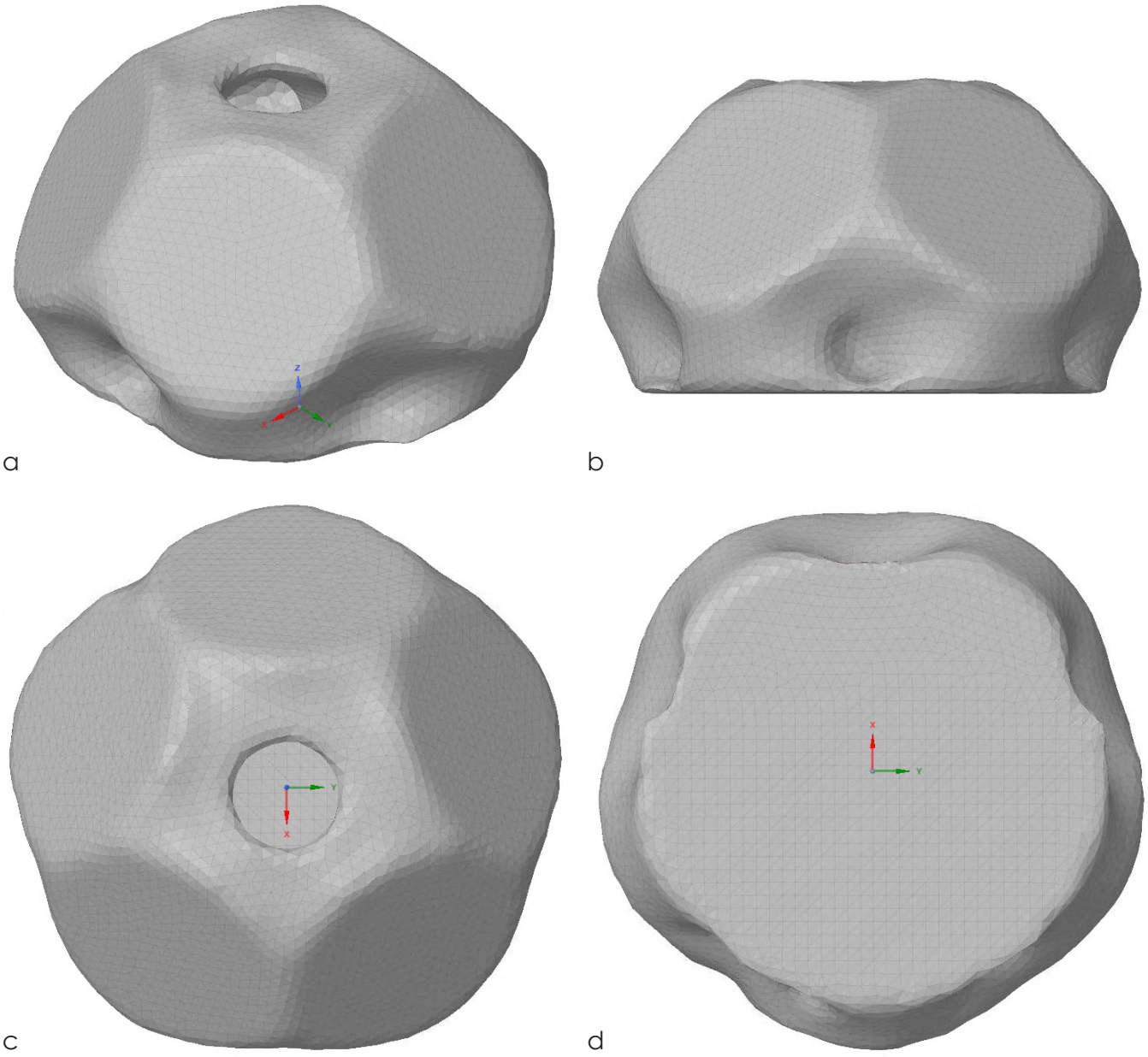

Figure 6.8: TO geometry for five branch connection

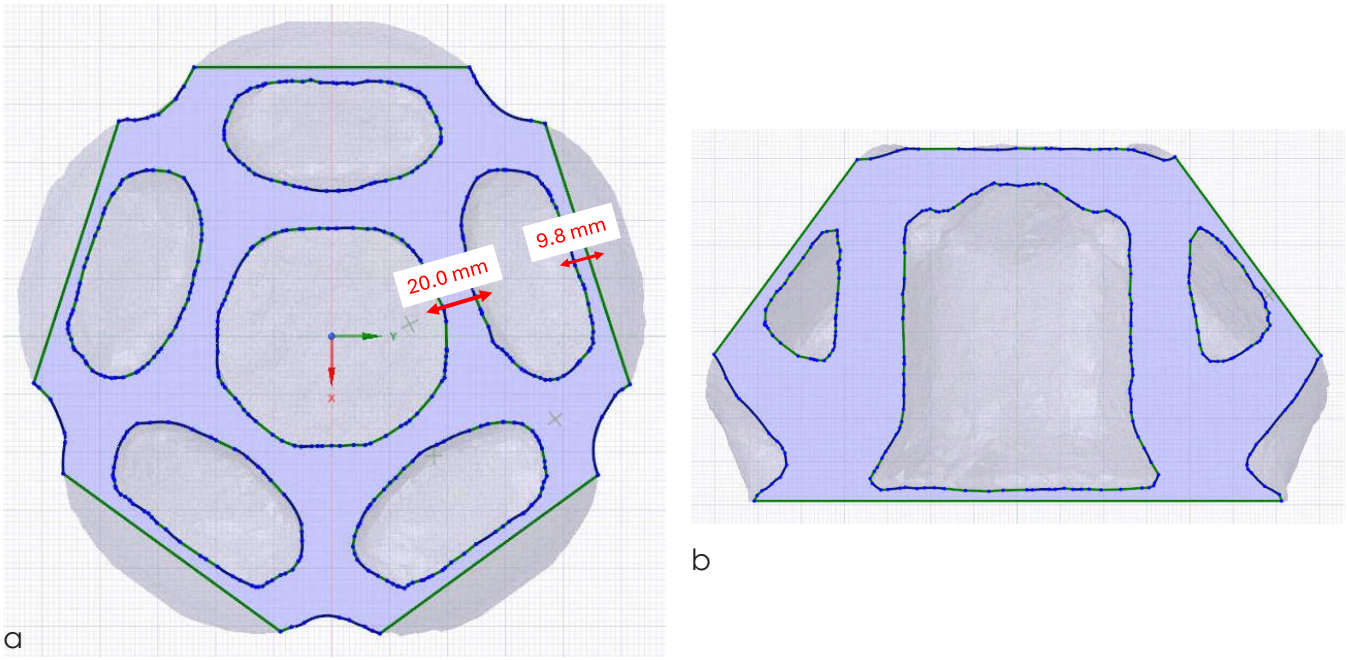

Figure 6.9: Cross section of the TO geometry for the five branch connection

In Chapter 3: WAAM Manufacturing limitations, different overlapping percentages were examined. It turned out that by using 60 % overlapping high quality built can be achieved with good fusion between individual weld beads. When designing a g code for printing the overlap percentage will vary depending on the thickness of the weld bead (Table 6.3) and the desired thickness of the object (Figure 6.9 a). To follow the recommended value of 60 % the number of weld beads can be adjusted. As an example, a number of welds and overlapping percentage will be proposed for two different locations, whose thicknesses are shown in Figure 6.9 a. Thickness of 9.8 mm can be achieved by using two welds with a thickness of 6.9 mm and considering the overlapping of 58 %. In the case of an object thickness of 20.0 mm five weld beads with an overlapping of 53 % can be used. The proposed values are valid for the selected input process parameters (Table 6.2). The selection of different process parameters will change the weld bead dimension, which will have an impact on the required amount of weld beads.

To prove that the proposed design can sustain the applied load, structural validation was done. Stress diagrams are presented in Figure 6.10 a and b. The location of the maximum stresses or the location where yielding is first reached is shown in Figure 6.11. Maximum stresses appear just below where the branch profiles are joined with the connection. The same stress distribution was also reached in the analysis from Chapter 4: Connections where two branched connection was considered, which shows a consistent and coherent outcome of the analysis. From the provided figures it is also clear that the stresses are bigger at the bottom of the connection compared to the top of the connection. This is predictable since forces acting on the bottom part of the connection include compressive normal force, shear force, and compressive moment component, meaning that increased normal force is present. Meanwhile, on the top part of the connection the compressive normal force and tensile moment component are equalizing each other, thus the overall load is smaller.

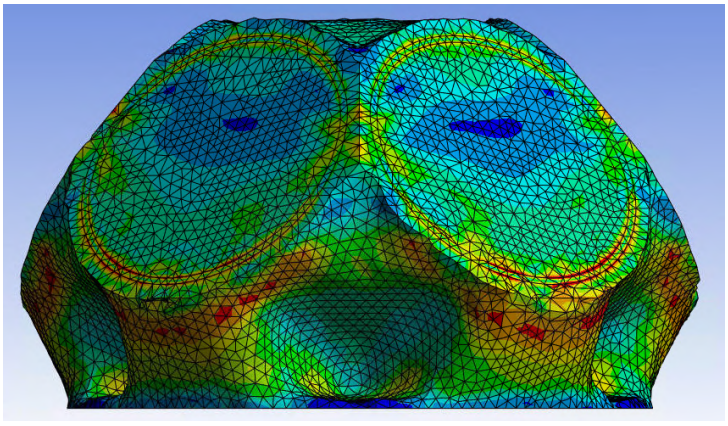

Figure 6.10: Stress diagrams for five branch connection

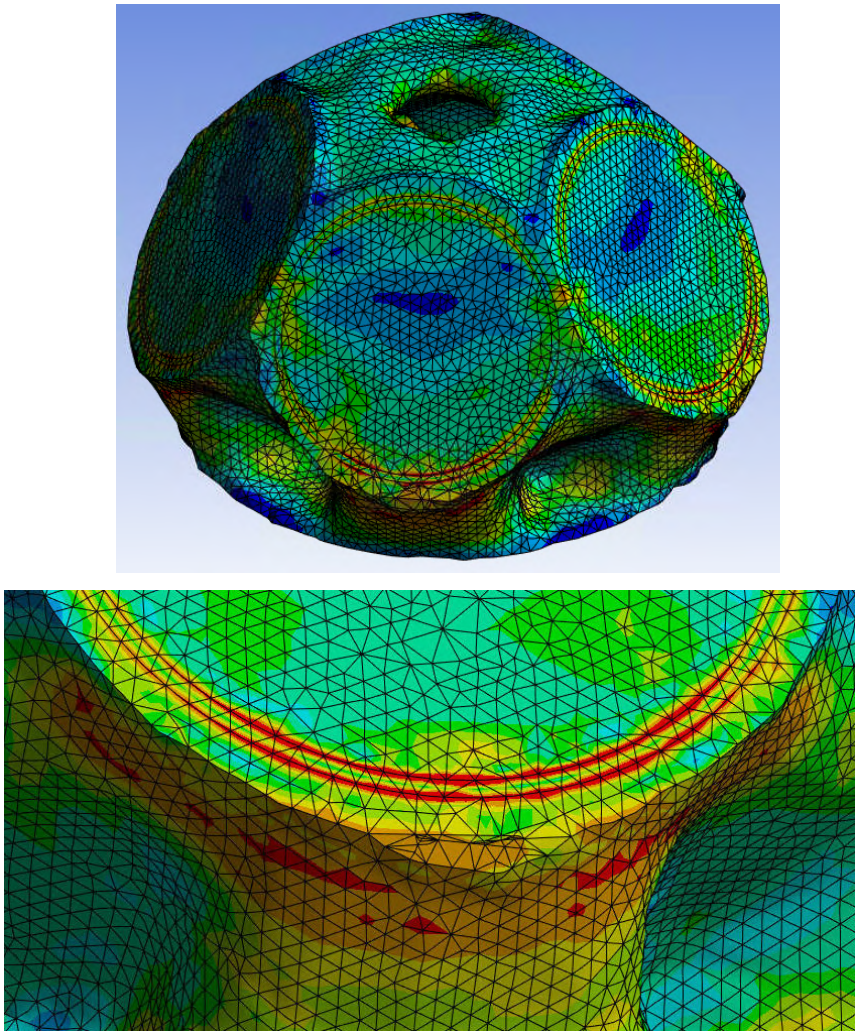

Figure 6.11: Location of the maximum stress in the five branch connection

To verify the performance of the connection load – strain graph was plotted and is presented in Figure 6.12. The graph was plotted for the location where maximum stresses appear as shown in Figure 6.11. It is visible that the nonlinear plastic behaviour of the material starts at exactly 100 % of the applied load. This suggests that a mass retain percentage of 30 % is sufficient and is also the lowest possible mass reduction, which can be applied to the connection. In case of a lower mass retain percentage, the yielding would be reached before the total load is applied.

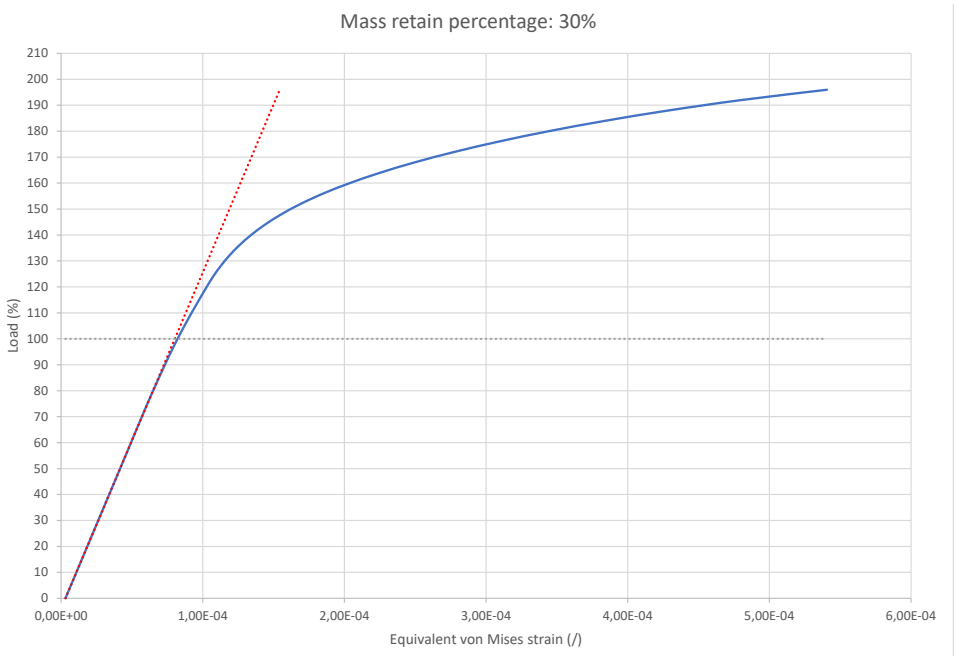

Figure 6.12: Load - strain graph for the location of the maximum stresses in the five branch connection

The onsite assembly of the connection and branch and column profiles is done based on the explanation in Chapter 4.4.3.1 Integration of the designed connection with branch and column profiles and on-site assembly procedure. In the project of 6 Bevis Marks the branch and column profiles are made of steel, therefore they can be directly welded onto the AM connection. Due to the appropriate design, no further modification (sawing) of the profiles is needed. The assembly of the steel profiles and the final design of the connection is presented in Figure 6.13.

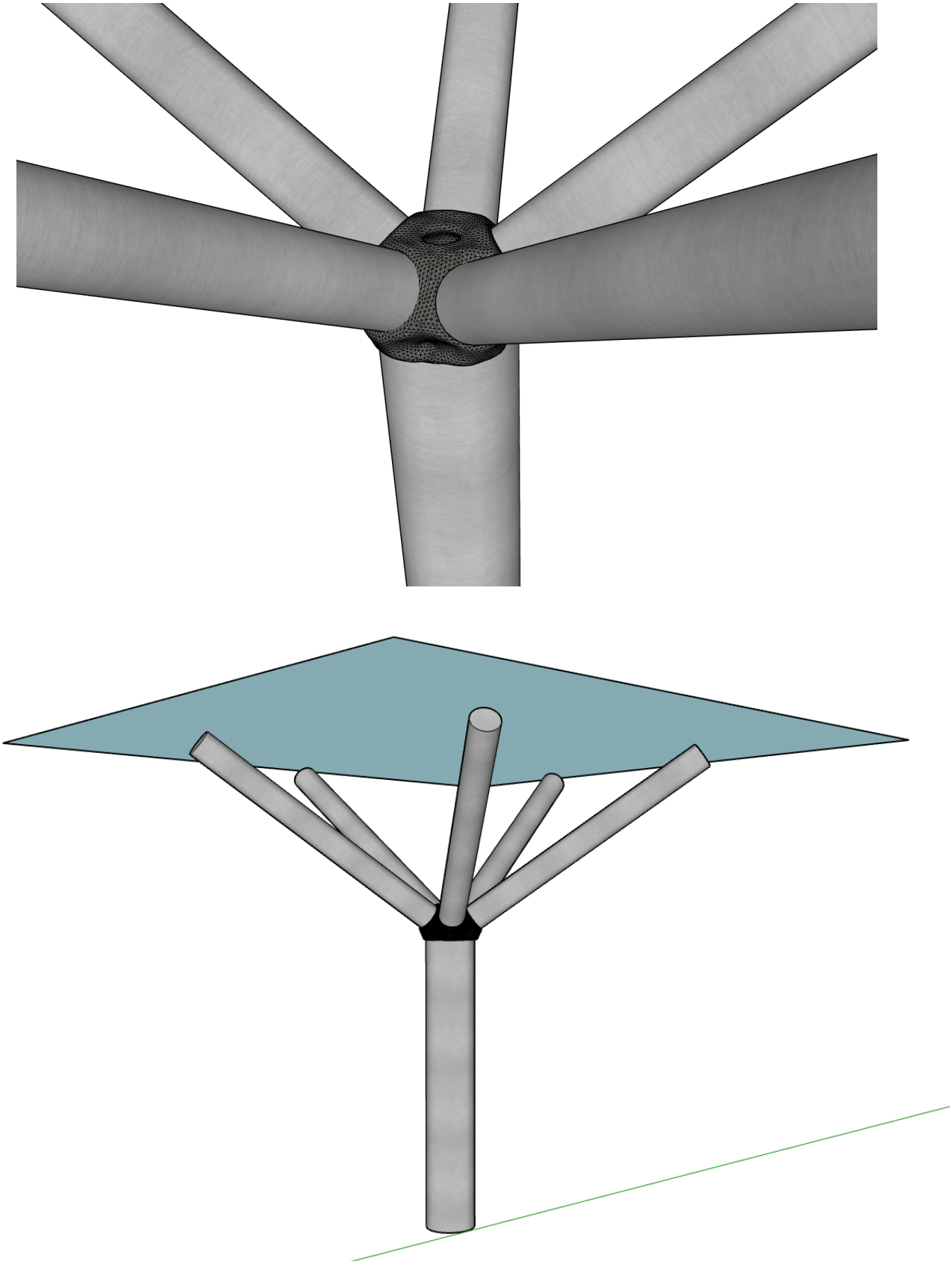

Figure 6.13: Final design of the five branch connection

Alternatively, a special modification to the profiles can be done so that the profiles can be bolted to the connection instead of welded. Welding on construction sites can be challenging due to several reasons. One key factor is the requirement for skilled labor and expertise in welding techniques. Finding highly skilled welders available for on site work can be difficult, and improper welding can compromise structural integrity, posing safety risks. Welding involves high temperatures, electrical equipment, and potentially hazardous fumes. Ensuring a safe welding environment amid various workers and activities on a construction site can be challenging. Logistical challenges further complicate on site welding. Transporting heavy welding machinery and gas tanks to and within construction sites, especially on higher levels can be problematic and time consuming. Additionally, welding requires meticulous preparation, precise execution, and time for cooling before handling. In contrast, bolted connections or prefabricated elements often offer quicker and more manageable assembly on construction sites. These methods are preferred due to their ease of installation, flexibility for modifications, and reduced safety risks compared to welding.

In this specific case study, the TO geometry of the connection includes the opening on the top. The opening serves as a tool so that the screws from the inside of the connection can be reached and thus combine the connection with profiles. A special attachment needs to be designed, which is shown in Figure 6.14 a. The attachment is a steel end plate in the shape of the profile cross section with the preinstalled bolts. The bolts are inserted through the hole in the endplate and then welded in place. By welding the bolts it is guaranteed that they will stay intact and in place during the installation. This is important because the bolts are not accessible through the inner part of the hollow profile. The onsite assembly includes inserting the bolts through the predrilled holes in the printed connection and joining them by nuts from the inside.

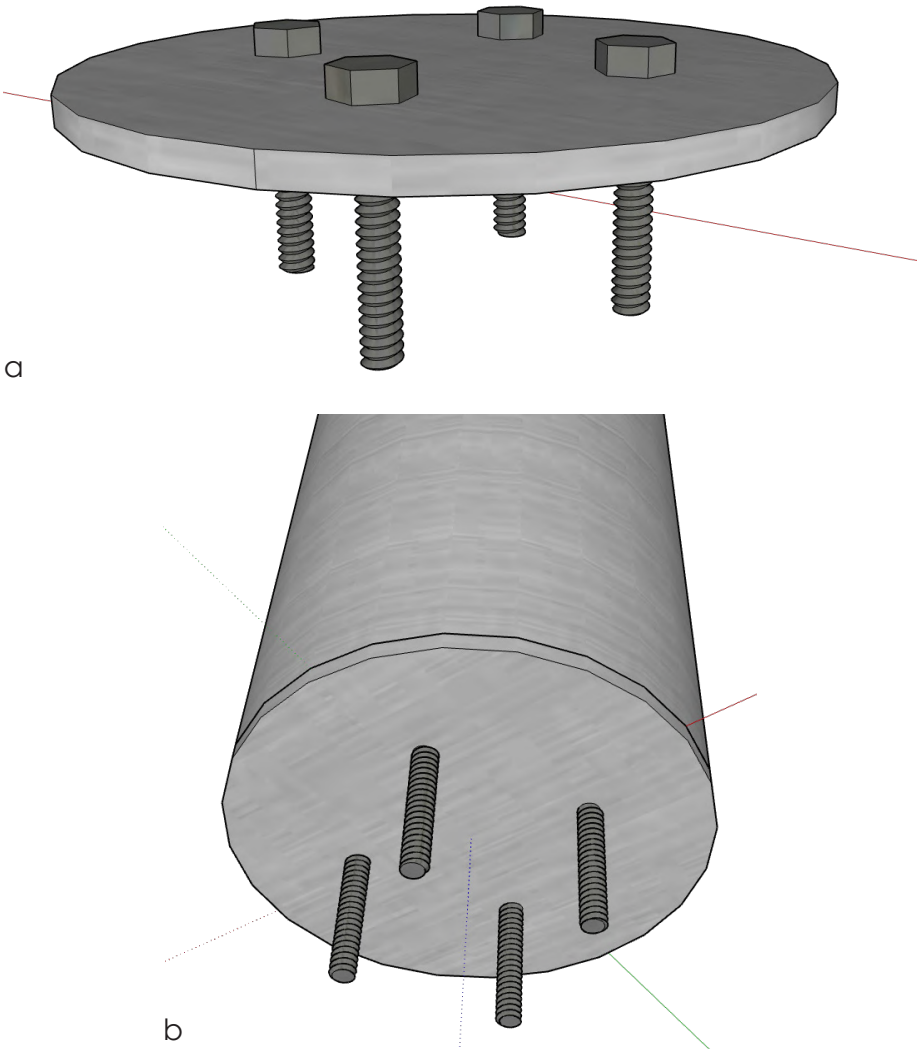

Figure 6.14: a) Designed attachment, b) Modified profile

6.2.1 ADVANTAGES OF THE ADDITIVELY MANUFACTURED CONNECTION

Now that the TO was conducted and the most optimized geometry of the connection was gathered, further analysis can be completed. In the following paragraphs, a comparative analysis between the WAAM connection and the steel plate connection will be done. Both of the two methods will be evaluated based on three key factors: required amount of material, manufacturing time, and manufacturing costs.

a  b 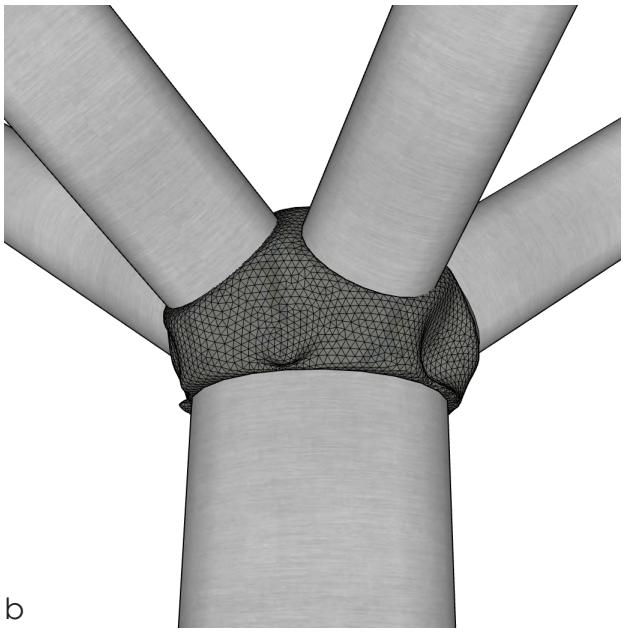

Figure 6.15: a) Steel plate connection [5.2], b) WAAM connection

First, the required material during the manufacturing process will be calculated. Conventional welding processes demand a substantial amount of material in the form of steel plates, welding rods, and other consumables. In contrast, topology optimized connections are engineered to minimize material usage, meaning that the material is distributed only where it's absolutely needed. This said the TO model should experience lower weight and volume compared to conventionally manufactured connection.

Manufacturing time is another crucial aspect to consider. Because traditional welding methods require skilled labour and involve a detailed process, they often have long lead times. On the other hand, TO models, are manufactured with an automated process which can reduce production time.

The costs associated with manufacturing are a major focus from an economic perspective and can be a decisive factor in the selection of the appropriate design. Conventional welding techniques involve multiple steps, including cutting, welding, and post weld inspections, which can be labour intensive and time consuming. The TO connection, on the other hand, streamlines the manufacturing process by reducing the number of components and welding points required. This simplification can lead to cost savings in terms of labour and material usage. There are though some doubts in regard to energy consumption during the WAAM process and the initial price of the WAAM machine. This will further be elaborated on in the following paragraphs.

- **Required material**

The required material for the TO model can be easily obtained from the Ansys software. The total volume of the connection is 10392 cm3, which directly corresponds to 81,5 kg of required welding wire. In the case of steel plate connection, the total volume and thus total required amount of material were assumed based on visual inspection of the connection presented in Figure 6.3. To do so the connection was split into multiple different sections. For each section, the dimensions were assumed upon which the volume could be calculated. The total volume of the conventionally manufactured connection adds up to 17327 cm3. If we assume the steel density of 7850 kg/m3, the total required mass of the connection is 136 kg. Besides steel elements, the connection includes also welds. The total length of welds was assumed to be 30 m, while the weld throat thickness was selected to be 5 mm. Taking this into account the required amount of welding wire adds to 750 cm3 or 5,9 kg. A more detailed presentation of the volume calculation for the conventionally manufactured connection is shown in Appendix C, while the comparison of the two connections is presented in Table 6.4 and Figure 6.16/17.

Table 6.4: Volume and mass values for both connections

	WAAM connection	Steel plate connection
Volume (cm^3)	10392	17327
Mass (kg)	81,5	136

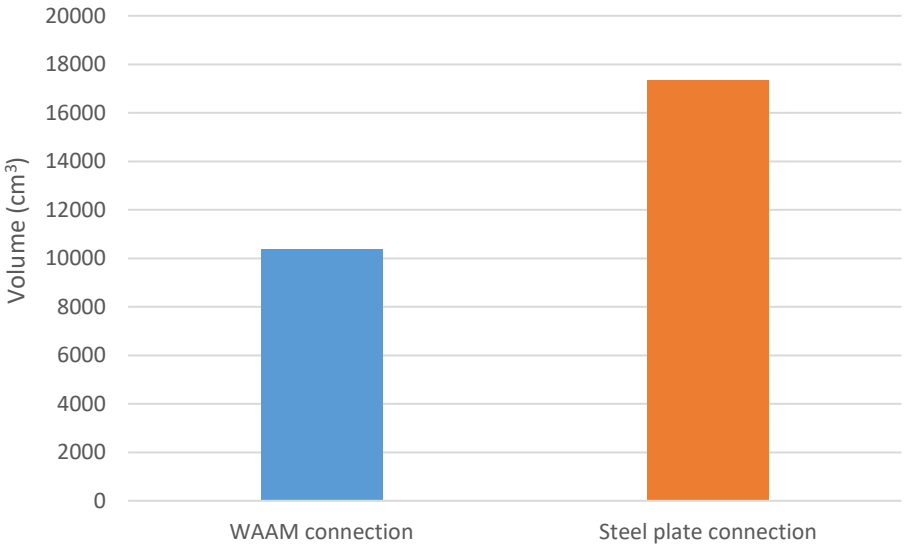

Figure 6.16: Comparison of volume for both connections

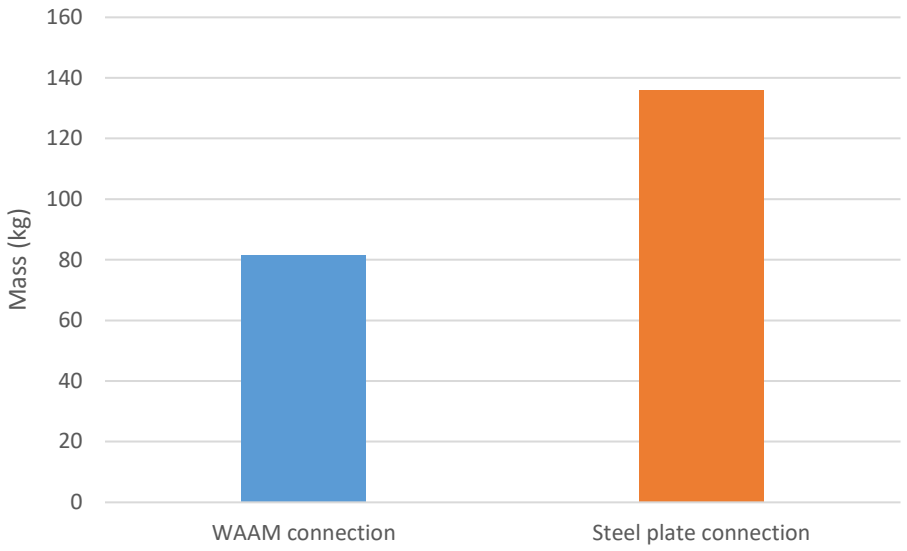

Figure 6.17: Comparison of volume and mass for both connections

- **Manufacturing time**

The manufacturing time of the WAAM connection was calculated based on the model's dimensions and assumed WAAM deposition rate. The deposition rate of 15,7 cm3/min was calculated based on the assumed welding wire diameter (1 mm) and WFS (5 m/min). From the measured volume the printing time can be calculated, which is 661,9 min. Additional manufacturing time was included due to considered pauses during the printing of individual layers. Pausing between layers is essential for controlling heat, managing stresses, and optimizing mechanical properties. This prevents issues like warping and enhances energy efficiency, ensuring the reliability and high performance of the final metal components. Depending on the height of the model and the height of the weld bead, the total number of 103 layers was calculated. With the assumption that between each layer a one minute pause was done, the total manufacturing time adds up to 774,5 min or 12,9 h (including the assumed 10 min preparation time). The more detailed calculation and all relevant data are presented in Appendix D.

The manufacturing time of the steel plate connection was assumed to be 450 min or 7,5 h. The assumption was made based on the required amount of steel and its sawing (250 min) and the required length of welds (200 min).

The comparison between manufacturing time for both connections is presented in Table 6.5 and Figure 6.18. Due to the slower manufacturing process, the total time of WAAM connection is higher. It is important though to take into account the length of the design phase. Due to the higher design complexity of the conventionally manufactured connection, a higher increase in time can be expected. Besides that, the AM is an ''almost'' fully automated process that does not require much intervention during printing. This means that the manufacturing process can continuously take place without pauses, excluding the necessary maintenance.

Table 6.5: Manufacturing time of both connections

	WAAM connection	Steel plate connection
Manufacturing time (h)	12,9	7,5

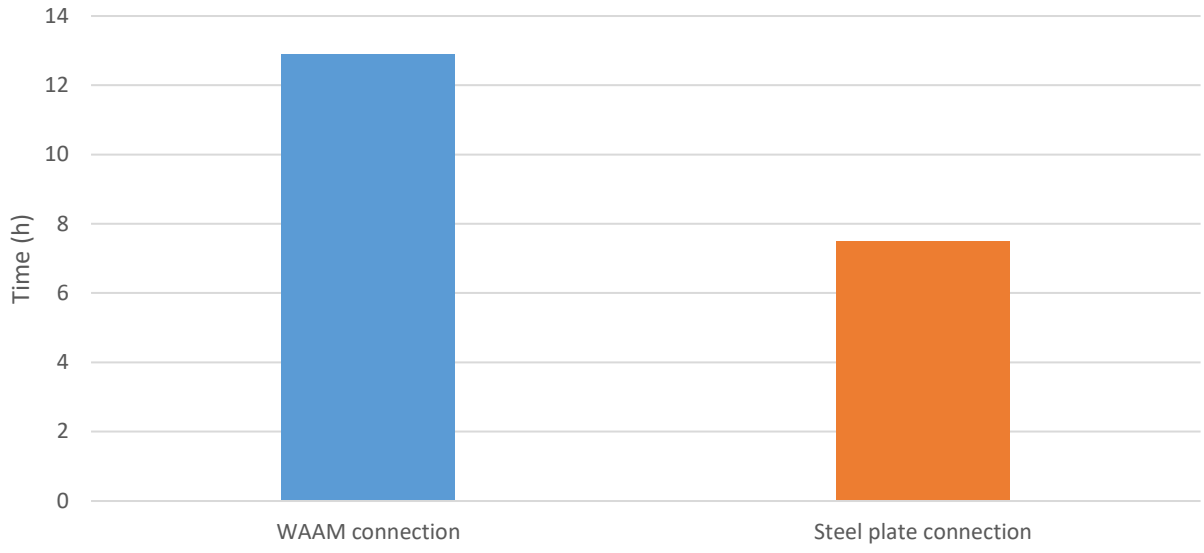

Figure 6.18: Manufacturing time comparison for both connections

- **Manufacturing cost**

To calculate the manufacturing cost of the WAAM connection the procedure proposed in the research paper entitled "Modelling of Wire Arc Additive Manufactured Product Cost" [6.7] was considered. In the calculation, many related activities were considered, for which the relevant input information was either calculated, referenced, or assumed. The total cost was then computed by summing up all the costs of the relevant activities. In the following paragraphs, individual activities and their costs will be explained. The more detailed calculation and all relevant input values are shown in Appendix E.

The first cost that was calculated was the design cost. This phase of the project includes the preparation of the TO model of the connection and programming of the G code for printing. After including the hourly operator rate the total design cost adds up to 81 €.

In the manufacturing phase, the substrate that will be used to print the part on must first be prepared. The substrate used in the WAAM process is assumed to be a mild steel plate. An automatic sawing machine is first used to cut the mild steel plate to the necessary dimensions, while a handheld portable grinder is used to remove the oxide scales from the substrate plate. The build cost includes the required time for the part to be printed and the hourly cost of using WAAM machine. In the stated research paper the hourly rate of the WAAM machine was determined to be 30 €/h. This includes the cost of the machine tool, maintenance cost, tooling cost, electricity cost, shielding gas cost, and operation cost. The machine tool investment for WAAM totaled 300,000 € was used. It was projected that the annual expenses for tooling and maintenance would equate to 3% of the machine tool's cost. Additionally, the electricity costs at a rate of 0.13 €/kWh were considered. In the WAAM process, a shielding gas flow rate of 16 l/ min was utilized, incurring a cost of 2.3 €/m3. The power requirement for WAAM was assumed to be 1.3 kWh. Besides the printing process, the cost of the material used for substrate and printing was calculated. Based on this, the total cost of printing can be calculated by summing up the cost of substrate preparation, build job, and material, which ends up being 1050.13 €.

Throughout the thesis and in this case study the post processing of the printed object was not considered. In case the post processing is included the total manufacturing cost increases. The post processing activities involve CNC machining of the as built WAAM part to achieve the required dimensions, tolerances, and to increase the mechanical properties of the printed material. The contributing factors of the post processing to the total cost are the G code preparation for the CNC machine, the CNC machining itself, and the substrate removal. The total cost of the post processing phase is calculated to be 119,15 €. To determine the hourly rate of the CNC machine (18.5 €/h), the following values were considered. The machine tool investment for CNC is 50,000 €, while the annual expenses for tooling and maintenance equate to 3 % of the machine tool's cost. The power requirement for the CNC machine was assumed to be 1.3 kWh and the electricity cost was 0.13 €/kWh.

Finally, the total manufacturing costs can be calculated. This is done by summing up all the above explained costs, which are design costs, printing costs, and post processing costs, while the inspection costs were also included. The total manufacturing costs are in the case of post processing 1260 €, while if the post processing is not considered 1141 €.

The manufacturing cost of steel plate connection was calculated by following a similar procedure. Step by step calculation is presented in Appendix F. The first step was the calculation of the design cost, which included calculating and dimensioning the CAD model. Based on the assumed design time and the operator's hourly rate the design costs added up to 121,50 €.

The next phase was the preparation of the steel plates which were used in the connection. This includes sawing the plates to the appropriate dimensions and surface cleaning, such as rust, oil, or other contaminants removal. Based on the assumed sawing time and operator hourly rate the costs are 168,75 €. In this part, the price of the required steel was also calculated, which is 136 €.

The cost of welding was calculated by taking into account the required welding time multiplied by welder's hourly rate and the hourly cost of the welding machine. The hourly rate of the welding machine was considered the same as for the WAAM machine, which is 30 €/h. The required amount of welding material was calculated based on the assumed weld length of 30

m and throat thickness of 5 mm. The price of the required welding wire is 94,20 €. This means that the total welding costs are 329,20 €.

To calculate the total costs, the inspection costs were also considered, which are 10,13 €. This means that the total costs of 718 € can be calculated by summing design costs, steel plates sawing costs, welding costs, and inspection costs.

The cost comparison is shown in Table 6.6 and Figure 6.19. It is visible that the AM connection is much more expensive than the conventionally manufactured connection. This is due to the fact that the manufacturing time is also much longer, which significantly increases the total costs. Additionally, the welding wire price per kg is much higher than the price of normal structural steel.

Table 6.6: Manufacturing cost values for both connections

	WAAM connection without post processing	WAAM connection with post processing	Steel plate connection
Manufacturing cost (€)	1141	1260	718

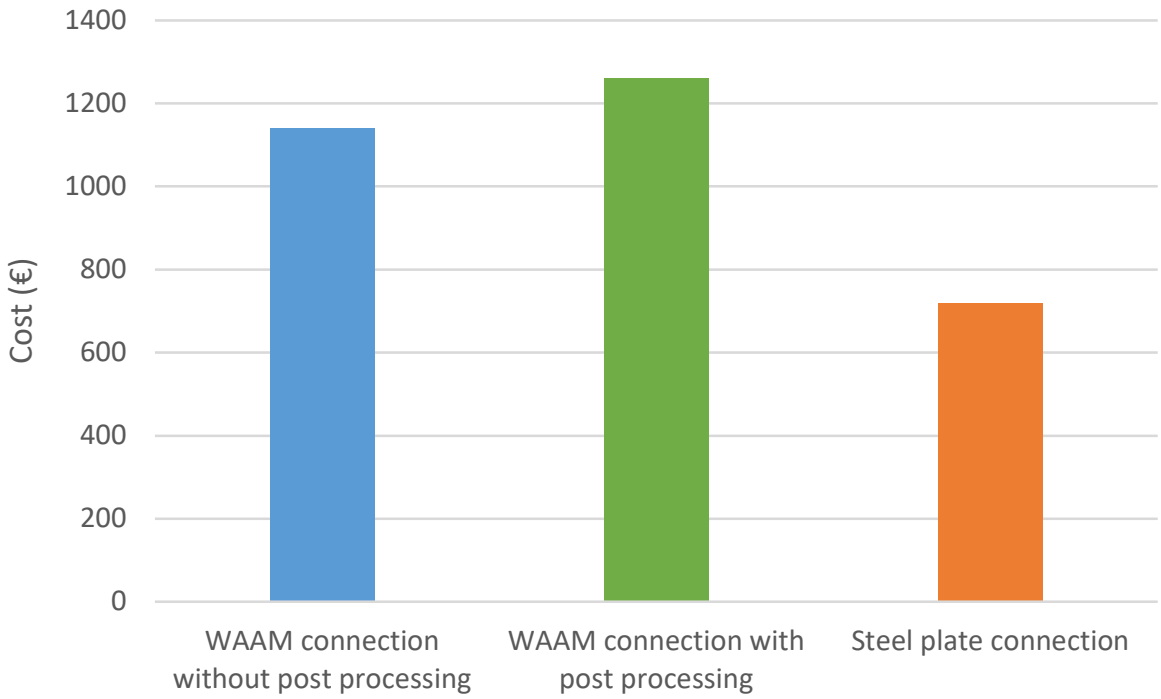

Figure 6.19: Manufacturing cost comparison for both connections

The design of the AM five branch connection achieved the desired and set end objectives. One of the main research questions proposed in the introduction was concerned with the minimization of the used material. Based on the above presented results of the comparative analysis it is visible that by using TO and then printing the geometry with WAAM the required amount of production material can be significantly lowered. Figures 6.15 and 6.16 show that the required volume and its corresponding mass can be almost halved with the implementation the TO in the design. Reducing the quantity of raw materials extracted directly reduces the burden on ecosystems and natural resources. This decrease in extraction decreases the damage that extraction processes cause to the environment. Besides the required amount of material, the manufacturing time and costs were also calculated and compared. Based on Figure 6.17 it is visible that the required manufacturing time for the WAAM manufactured connection is higher than in the case of the steel plate connection. Higher manufacturing time and high welding wire costs contribute to the total manufacturing cost of the WAAM connection, which is 2,3 times higher than in the case of steel plate connection (Figure 6.18).

Material reduction (shadow cost) can be implemented into total cost calculation. Shadow costs represent the often hidden economic and environmental impacts of a product's life cycle. Material reduction directly influences external costs, such as environmental degradation and resource depletion, which traditional accounting methods often overlook. Including these externalities in shadow costs, a more accurate reflection of the actual impact of manufacturing processes on the advantages and limitations can be done. Reducing material consumption impacts not only direct production costs but also the entire supply chain. While there might be upfront investments in innovative technologies or process optimization, the long term benefits in terms of reduced resource consumption, energy usage, and waste generation contribute to a more sustainable and cost effective manufacturing model.

To calculate the additional shadow costs a Life Cycle Assessment (LCA) was done. LCA is an examination of the environmental impact of a material, process, product, or other measurable activity over its whole life. The various interdependent systems that comprise manufacturing processes are modeled by LCA in terms of their effects on the environment. These effects are in the LCA represented as environmental impact categories (EIC). These categories allow for a focused evaluation of different environmental factors by representing specific environmental impact dimensions. Based on Bouwbesluit 2012 [6.10] in the Netherlands in total of 11 basic EIC need to be considered in the calculation of the shadow costs. These categories are considered the most harmful to the environment, people, or animals.

- Abiotic Depletion, non fuel (ADnf)
- Abiotic Depletion, fuel (ADf)
- Global Warming Potential (GWP)
- Ozone Layer Depletion (ODP)
- Photochemical Oxidation Potential (POCP)
- Acidification Potential (AP)
- Eutrophication Potential (EP)
- Human Toxicity Potential (HT)
- Ecotoxicity Potential, Fresh water (FAETP)
- Ecotoxcity Potential, Marine water (MAETP)
- Ecotoxicity Potential, Terrestrial environment (TETP)

In the Bouwbesluit 2012 it is possible to find depending on the type of material, a shadow costs per unit equivalent for each of the EIC. Based on the known total volume of the required material the total shadow costs can be calculated. All relevant input values and the calculation procedure of the total shadow costs are presented in Appendix G. The shadow costs were calculated for the difference in the required material between the WAAM connection and steel plate connection, which is 54,5 kg. This means that the increase of the required material in the steel plate connection will also cause an increase in the total manufacturing costs regarding shadow costs.

The increase of the total manufacturing costs in case of implementation of the shadow costs is shown in Table 6.7, while the comparison between individual costs is done in Figure 6.20. The additional shadow costs are in the graph represented with red colour and amount to 131 €. This means that the total manufacturing cost of the steel plate connection increases to 849 €. By introducing the shadow costs and thus representing the environmental impact that both of these connections will have, the difference between total manufacturing costs is slightly lowered.

Table 6.7: Manufacturing cost values for both connections including shadow costs

	WAAM connection without post processing	WAAM connection with post processing	Steel plate connection
Manufacturing cost (€)	1141	1260	849

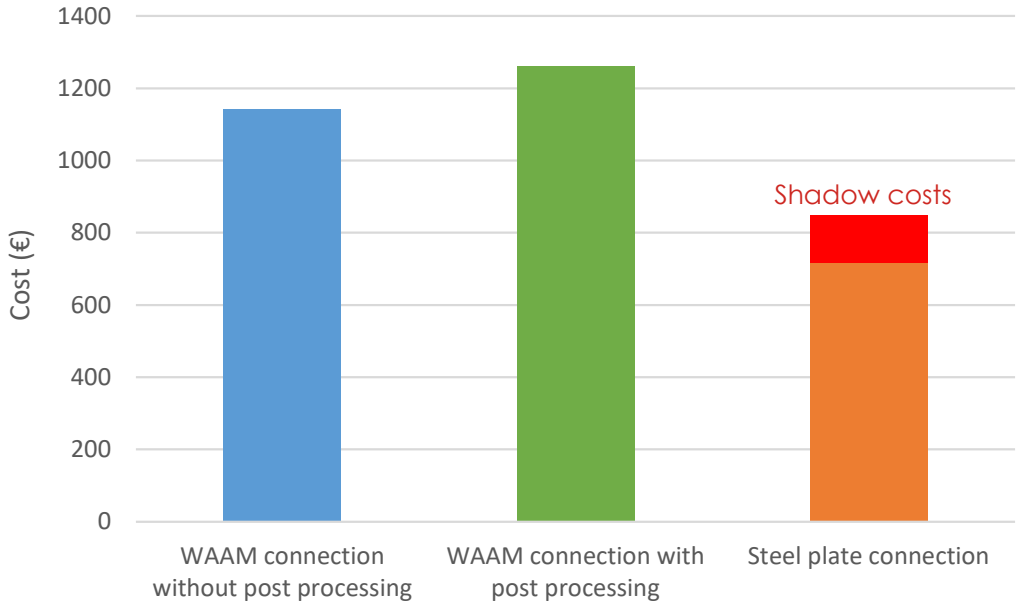

Figure 6.20: Manufacturing cost comparison for both connections including shadow costs (red colour)

6.3 REFERENCES

[6.1] Clayton. L. 2023. BEVIS MARKS – IMPRESSIVE COVERED ETFE ROOF TERRACE. Vector Foiltec. (Accessed on 12.11.2023). Available at: https://www.vector-foiltec.com/projects/6-bevis-marks-roof-garden-3d-printed-structure/

[6.2] Naboni. R., Paoletti. I. 2015. Advanced Customization in Architectural Design and Construction. Springer briefs in applied sciences and technology. (Accessed on 12.11.2023) Available at: https://link.springer.com/book/10.1007/978-3-319-04423-1

[6.3] Foundation reuse creates sustainable landmark. NSC. Vol 21 No.5. Sept/Oct 2013. Available at: https://www.newsteelconstruction.com/wp/

[6.4] Buxton. P. 2014. Feet firmly on the ground. RIBA Journal. (Accessed on 12.11.2023). Available at: https://www.ribaj.com/buildings/feet-firmly-on-the-ground

[6.5] 3D printing: it's the shape of things to come. 2013. Construction Management. (Accessed on 12.11.2023). Available at: https://constructionmanagement.co.uk/3d-printing-shape-things-come/

[6.6] EN-1991-1-1. 2004. Eurocode 1, Actions on Structures—Part 1-1: General Actions —Densities, Self-Weight, Imposed Loads for Buildings. European Committee for Standardization.

[6.7] Kokarea. S., Oliveiraa. J. P., Godinaa. R. 2023. Modelling of Wire Arc Additive Manufactured Product Cost. Procedia Computer Science. Available at: https://doi.org/10.1016/j.procs.2022.12.351

[6.8] Statistica. 2020. Average hourly labor cost in selected European countries in 2020. (Accessed on 12.11.2023). Available at: https://www.statista.com/statistics/1211601/hourly-labor-cost-in-europe/

[6.9] The cost of structural steel per kg in 2023. 2023. Jactio.com. (Accessed on 12.11.2023). Available at: https://jactio.com/en/the-cost-of-structural-steel-per-kg/

[6.10] Bouwbesluit 2012. 2011. Ministerie van Binnenlandse Zaken en Koninkrijksrelaties. (Accessed on 20.12.2023). Available at: https://rijksoverheid.bouwbesluit.com/Inhoud/docs/wet/bb2012

[6.11] Cost of MIG MAG welding wire roll steel ER70S-6. 2024. VECTOR WELDING TECHNOLOGY GmbH. (Accessed on 26.01.2024). Available at: https://www.vector-welding.com/MIG-MAG-welding-wire-roll-steel-ER70S-6-10-1-kg-3x-D100-roll

CONCLUSION AND RECOMMENDATIONS

7. CONCLUSION AND RECOMMENDATIONS

This chapter wraps up the study. It starts by outlining the key discoveries and main contributions that were made throughout the thesis. Following that, it delves into the possible further research options and recommendations for its practical application.

7.1 CONCLUSION

The conclusions presented in this subchapter will be done by answering the research questions proposed in Chapter 1. Before gathering conclusions regarding the main research question (**What strategies and considerations are involved in integrating additive manufacturing into the construction industry, and what specific advantages and limitations characterize its application?**), five additional sub questions need addressing, which are crucial for understanding the purpose and main results of this thesis.

- What kind of additive manufacturing processes and materials are available?

An extensive literature review on the available AM processes with an emphasis on the explanation of their production properties was conducted. It was found that seven processes are frequently employed for industries and commercial usage, namely binder jetting, direct energy deposition, material extrusion, material jetting, powder bed fusion, sheet lamination, and VAT photopolymerization. For the construction industry, the most advantageous process was determined to be direct energy deposition to which group WAAM also belongs. The main reason for choosing WAAM was the ability to print objects with high material properties that can be compared to conventional construction materials. For example, by using carbon steel wire ER70S-6, WAAM elements are capable of reaching YS of about 380 MPa, US of about 500 MPa, and elastic modulus of 214 GPa, showing similarities with S355, which is one of the more commonly used structural steel in the construction industry. Besides good material properties, WAAM is also reasonably cheap compared to other AM processes and has a high deposition rate, which is extremely beneficial in the construction industry where individual objects have in general bigger dimensions.

- Which additive manufacturing limitations need to be consider in the design of the connections?

Considering the limitations of WAAM is crucial for several reasons. Firstly, it helps manage expectations regarding the technology's capabilities, ensuring realistic outcomes. Understanding these limitations aids in refining the design process in the sense of enhancing product quality. Moreover, addressing these constraints fosters innovation by identifying areas for improvement, ultimately advancing the efficacy and applicability of WAAM in various industries.

Throughout the third chapter, three WAAM manufacturing considerations were examined by performing lab tests. Firstly, the input process parameters and their impact on the outcome of the printed object were inspected. Travel speed, wire feed speed, voltage, and current are the four main parameters that need to be determined before the printing can start as they will have an impact on the dimensions of the weld bead and the overall quality of the print. Tests showed that the increase in WFS will increase the weld bead dimensions but will not damage the quality of the weld itself. The decrease of the WFS (under 2 m/min) however presented welds with visible defects (unsmooth surface and discontinuity). TS also has an impact on the dimensions of the

weld bead (reducing the TS will lead to larger weld dimensions, whereas raising the TS will result in smaller dimensions). The second limitation that was considered and perhaps for the design the most relevant one is the overhang. Due to the printing nature of WAAM (printing in layers) proposing the appropriate overhang limitations maintains the accuracy of the final object and prevents potential distortion or collapse during the printing process. Lab tests were performed for the overhang in two directions depending on the direction of the print, namely perpendicular and parallel. The purpose of the lab tests was to determine the biggest allowed offset distance for the selected input process parameters. The results showed that creating the overhang in a perpendicular compared to a parallel direction allows bigger offset distances and thus lower overhang angle. The differences between the two overhang angles were not significant as the perpendicular direction achieved an angle of 43.5°, while the parallel direction 48.2°. A 3D scan of the prints showed the accuracy of both overhangs from which it is seen that the overhang in the perpendicular direction can achieve much higher precision. For the last limitation, the overlapping of the individual weld beads was considered. Considering this limitation ensures proper fusion between layers, maintaining structural integrity and overall print quality. Three builds differing in the overlap percentages were printed, namely 20%, 60%, and 80%. The results of the test showed that the sample with 20% overlapping experienced problems with fusing individual welds, which might result in a nonhomogeneous final part. On the other hand, 80% overlapping meant that weld beads were placed on top of each other, which eventually led to the collapse of the print. The print with 60% overlapping turned out to have high quality with good connectivity between individual welds and a relatively small surface waviness.

- What are the existing applications of additive manufacturing in structural connections within the construction industry?

Over the years, numerous projects exploring the utilization of AM for structural applications have been undertaken. However, the majority of these endeavors have remained in the realm of research rather than finding widespread commercial applications. The AM solutions integrated into real life projects were tailored exclusively for those specific endeavors, lacking a focus on enhancing commercial viability or broader market appeal.

For this thesis, the design of the branch column connection was selected. The selection was made based on the advantages that these structural elements can provide and their limitations which can be solved with the implementation of the AM. The main limitation is the complexity of the design and manufacturing phase, which was solved within the next two research sub questions.

- How to minimize material consumption in the design of the connections?

Material minimization was done through TO with the help of Ansys software. The process finds the most efficient material distribution in a design, removing excess material where it is not needed. It creates lightweight structures without compromising strength or functionality, saving on materials and costs in manufacturing. The outcome of the TO differs depending on the selected input parameters, which consist of TO type, TO objectives, TO constraints, manufacturing constraints, etc. Therefore it is important to carefully determine the most optimal input parameters and thus achieve the highest quality product based on our needs.

In this thesis, the goal of TO was to create the model with the lowest possible mass while still surpassing the required structural performance (no plastic deformation under the proposed load). To do so a variety of models were generated differentiating in the TO input parameters. Four different TO objectives were proposed namely equivalent von Mises stress, compliance, mass, and volume. For each objective, a constraint was implemented, either mass retain percentage or maximum stress concentration. Besides TO constraints the manufacturing constraints were also considered due to limitations of the WAAM process. Manufacturing limitation was considered as a minimum allowed overhang angle, which was determined by lab tests. A comparative analysis showed that using compliance as a TO objective allows to generate a model with the lowest required amount of material while at the same time achieving the desired stress distribution and values. As a comparison, a compliance objective model requires 6 kg of steel, while the stress objective and mass/volume objective require 7.1 kg and 7.5 kg respectively. This can be nicely seen in Figure 4.47 which shows a comparison of models with different TO objectives based on the required amount of material and the average stress in the model. By using an objective of compliance average stress of 91.5 MPa can be achieved, which is lower than in

the case of stress objective (109 MPa) and mass/volume objective (105.4 MPa). Based on these findings it is possible to conclude that for the proposed load distribution, material, manufacturing process, and overall connection setup the most optimal TO input parameters are: the objective of compliance, the constraint of 15 % mass retain percentage, and the manufacturing angle limitation of 45°.

Additionally, sensitivity analysis was performed where the impact of the angle of branches and TO type were examined. The results showed that in the case of steep branches, the overall stresses in the connection are much lower compared to stresses in the case of angles under smaller angles. As a comparison, the average stresses in the connection with the 15° angled branches are approximately 1.5x bigger than in the connection with the branch angle of 75°. Two TO types were examined (density based and level set based) and compared based on the required process time. By using density based TO the analysis time is decreased by about 3.5 times.

- How to lower the complexity of the connection's design and on site assembly?

Another goal of the thesis was to design a connection, which can be easily manufactured and assembled on site. The complexion of the manufacturing phase was solved by using WAAM technology, which allows automated process without a heavy need for human interaction.

The onsite assembly procedure drastically differs depending on the desired material of the column and branch profiles and the geometry of the connection itself. In case the chosen material for profiles is wood, an additional attachment is needed, which joints to the profiles with the connection. The attachment is a hollow steel profile, which is welded onto the connection already in the factory. Wooden profiles are then inserted into the attachment and connected by bolts. The explained principle can be seen in Figures 4.45 and 4.46. For profiles made out of steel, two options are available depending on the geometry of the TO connection. The first option includes a simple welded joint between profiles and a connection (Figure 4.42). This is a very simple method that does not require any additional modification of the profiles or connection. On site welding though demands skilled labor, poses safety risks, and involves logistical challenges with transportation and preparation. As TO in most cases creates irregular shapes the generated geometry might be hollow, which allows for the steel profiles to be joined to the connection by bolts. To do so a special endplate with the in factory inserted bolts is needed to be attached to the profiles (Figure 5.14). In addition, holes need to be drilled into the connection in which the bolts are inserted. Bolted connections offer quicker, safer assembly, with more flexibility and reduced safety concerns compared to welding. The limitation of this method is that it is feasible only in the case of a hollow geometry, which allows for the bolted connection.

The main research question can now be answered. The integration of AM into the construction industry first requires a careful examination of the project's requirements and properties (loads, size of the elements, needed accuracy, available budget, etc.). Based on these criteria, an appropriate AM process and material selection can be done. For the selected AM process a consideration of its manufacturing limitations is needed and their limit values need to be determined. These manufacturing constraints need to be used in the design phase, which will guarantee that the object is printable and can achieve the desired performance. Since one of the main advantages of AM is the capability to manufacture elements with irregular organic shapes, the TO should be introduced into the design. By using TO the total amount of material needed for the design of the connection with sufficient structural performance is lowered. This was presented through a case study where a comparison between a five branch connection manufactured with WAAM and steel plates was done. The results showed that the introduction of AM and TO decreased the required amount of material from 136 kg to 81.5 kg. The comparison between the two connections was done also for the manufacturing time and costs, where the current limitations of the WAAM technology are shown. In both criteria, the WAAM connection achieved higher values compared to the steel plate connection. The manufacturing time increased from 7.5 hours to 12.9 hours, while manufacturing costs more than doubled (going from 765 € to 1793 €).

7.2 RECOMMENDATIONS

In this sub chapter, several recommendations for further research and industry are presented:

- Throughout the thesis all TO models of the branched column connections assumed symmetrical conditions. This means that all branches were evenly spaced around the center, and had the same angle, profile size, and load. The true benefit of branch columns is their adaptability to the specific case and needs, which might include needed asymmetry. It would be interesting to see how asymmetrical conditions impact the geometry and performance of the connection.

- Similarly, the applied loads in the thesis were only symmetrical vertical loads. In reality, horizontal loads like wind and earthquakes should also be considered. Before the connection can be implemented into the real life project it should be tested for all required load combinations proposed by EC.

- Through the thesis, the assumed material mechanical properties were selected for as built samples, thus post processing was not assumed. In the case of post processing the mechanical properties values would increase. It would be interesting to see how increased mechanical properties influence the design of the connection and the additional mass reduction.

- Thesis only included the computational modeling and numerical calculations of the connection. The next step of the research should include the creation of the physical model, printed by WAAM with the parameters proposed throughout the thesis. To verify and complement the presented data a number of structural tests should be conducted. Firstly, the model should be loaded with the proposed load while the deflection is measured. The second test should include gradually increasing the load until the failure of the specimen. This would provide information about the ultimate strength of the model and its failure pattern. Finally, the cycle test should be done representing for example wind loading. From this, information regarding the fatigue strength could be collected. Besides this, the proposed on site assembly procedures could be tested.

- The WAAM industry faces significant limitations highlighted in this thesis: notably, the absence of standardized practices and the elevated manufacturing expenses relative to conventional methods. Future research should prioritize creating standardized design protocols aligned with existing codes. Moreover, efforts within the industry should target reducing the cost of welding wire, a primary contributor to the high manufacturing expenses.

APPENDIX

8. APPENDIX

APPENDIX A

MILD STEEL WIRES

WELD 70S-6 AWS A5.18: ER70S-6

FEATURES

ESAB Weld 70S-6 is a copper-coated AWS ER70S-6 solid wire, suited for general purpose, manual and semiautomatic applications in most industries. It is manufactured under ESAB's Quality Control programs and meets AWS standards.

TYPICAL MECHANICAL PROPERTIES

As Welded GMAW 100% CO_2	
Yield Strength	61 ksi, 424 MPa
Tensile Strength	75 ksi, 518 MPa
Elongation in 2"	28%
As Welded GMAW 75% Ar / 25% CO_2	
Yield Strength	70 ksi, 483 MPa
Tensile Strength	84 ksi, 583 MPa
Elongation in 2"	26%

CLASSIFICATIONS AND APPROVALS

- AWS A5.18: ER70S-6

CHARPY V-NOTCH PROPERTIES

Testing Temperature -20°F (-29°C)	
As Welded GMAW 100% CO_2	
	57 ft-lb, 77 J
As Welded GMAW 75% Ar / 25% CO_2	
	67 ft-lb, 91 J

WELDING PROCESS

- GMAW (MIG)

WELD METAL ANALYSIS

GMAW 100% CO_2	
C	0.073%
Mn	0.97%
Si	0.51%
P	0.009%
S	0.013%
GMAW 75% Ar / 25% CO_2	
C	0.075%
Mn	1.22%
Si	0.67%
P	0.010%
S	0.014%

INDUSTRIES

- Shipbuilding
- Civil Construction
- Mobile Machinery
- General Fabrication
- Automotive

WELD 70S-6 continued

DEPOSITION TABLE - Spray Transfer Welding Parameters							
Diameter in (mm)	Electrode Unit in/lb (m/kg)	Amps	Volts	Wire Feed Speed ipm (cm/min)	Opt. Amps	Opt. Volts	Opt. Wire Feed Speed ipm (cm/min)
.035 (0.9)	3670 (206)	180 - 230	25-27	400 - 550 (1016 - 1397)	200	26	480 (1219)
.045 (1.2)	2220 (124)	260 - 340	25-30	300 - 500 (762 - 1270)	300	27	350 (889)

DEPOSITION TABLE - Shortarc Transfer Welding Parameters							
Diameter in (mm)	Electrode Unit in/lb (m/kg)	Amps	Volts	Wire Feed Speed ipm (cm/min)	Opt. Amps	Opt. Volts	Opt. Wire Feed Speed ipm (cm/min)
.035 (0.9)	3670 (206)	90 - 160	15 - 19	180 - 300 (457 - 762)	130	17	250 (635)
.045 (1.2)	2220 (124)	130 - 200	17 - 19	125 - 200 (318 - 508)	160	18	150 (381)

PART NUMBER / PRODUCT INFORMATION		
Part Number	Description	UPC
321M096700	WELD 70-6 035X33#WB 2376# PLT	662303672812
321M095920	WELD 70-6 035X550# MP 4/PLT	662303672829
321M116700	WELD 70-6 045X33#WB 2376# PLT	662303672836
321M115920	WELD 70-6 045X550# MP 4/PLT	662303672843

APPENDIX B

Topology optimization analysis settings

Details of "Analysis Settings"

Reload Volume Analysis	
Reload Volume Fraction	Off
Definition	
Maximum Number Of Iterations	500,
Minimum Normalized Density	1,e-003
Convergence Accuracy	0,1 %
Initial Volume Fraction	Program Controlled
Penalty Factor (Stiffness)	3,
Region of Manufacturing Constraint	Include Exclusions
Region of Min Member Size	Exclude Exclusions
Region of AM Overhang Constraint	Exclude Exclusions
Filter	Program Controlled
Output Controls	
Export Design Properties	No
Store Results At	All Iterations
Solver Controls	
Solver Type	Program Controlled
Analysis Data Management	
Solver Files Directory	C:\Users\tleban\OneDrive - Del...
Future Analysis	None
Scratch Solver Files Directory	
Save MAPDL db	No
Delete Unneeded Files	Yes
Solver Units	Active System
Solver Unit System	mks
Max Num Of Intermediate Files	All Iterations

Topology optimization objective and constraints

Enabled	Response Type	Goal	Criterion	Formulation	Environment Name	Weight	Multiple Sets	Start Step	End Step	Step	Start Mode	End Mode	Mode
☑	Compliance	Minimize	N/A	Program Controlled	Static Structural	N/A	Enabled	1	1	1	N/A	N/A	N/A

Details of "Response Constraint"

Scope	
Scoping Method	Optimization Region
Optimization Region Selection	Optimization Region
Definition	
Type	Response Constraint
Response	Mass
Define By	Constant
Percent to Retain	15 %
Suppressed	No

Topology optimization region

Details of "Optimization Region"	
Design Region	
Scoping Method	Geometry Selection
Geometry	All Bodies
Exclusion Region	
Define By	Geometry Selection
Geometry	6 Faces
Definition	
Suppressed	No
Optimization Option	
Optimization Type	Topology Optimization - Density Based

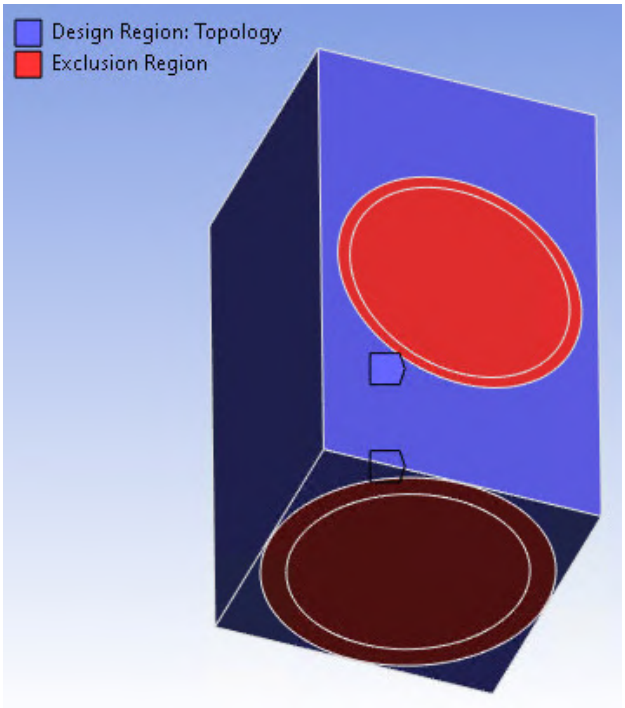

Topology optimization mesh settings and sizing

Details of "Mesh"	
Display	
Display Style	Use Geometry Setting
Defaults	
Physics Preference	Mechanical
Element Order	Program Controlled
Element Size	Default
Sizing	
Use Adaptive Sizing	Yes
Resolution	Default (2)
Mesh Defeaturing	Yes
Defeature Size	Default
Transition	Fast
Span Angle Center	Coarse
Initial Size Seed	Assembly
Bounding Box Diagonal	0,275 m
Average Surface Area	9,6592e-003 m²
Minimum Edge Length	0,1 m
Quality	
Check Mesh Quality	Yes, Errors
Error Limits	Aggressive Mechanical
Target Element Qua...	Default (5,e-002)
Smoothing	Medium
Mesh Metric	None
Inflation	
Use Automatic Inflation	None
Inflation Option	Smooth Transition
Transition Ratio	0,272
Maximum Layers	5
Growth Rate	1,2
Inflation Algorithm	Pre
View Advanced Options	No

Details of "Body Sizing" - Sizing	
Scope	
Scoping Method	Geometry Selection
Geometry	1 Body
Definition	
Suppressed	No
Type	Element Size
Element Size	5,e-003 m
Advanced	
Defeature Size	Default
Behavior	Soft

APPENDIX C

Element	Volume	Quantity	Total Volume (cm^3)	Total mass (kg)
1. Column	1626	1	1625,8	12,76
2. Branch	295,3	5	1476,5	11,59
3. Branch L support	2089	5	10443	81,98
4. Top star	989,8	1	989,8	7,77
5. Top circle	791,8	1	791,8	6,22
6. Rest of the plates	2000	1	2000	15,70
			17326,94	136,02

APPENDIX D

INPUT PARAMETERS		
Object height	19,5	cm
Weld height	0,19	cm
Number of layers	103	/
Volume of object	10392	cm^3
Wire diameter	0,1	cm
WFS	500	cm/min
Deposition rate	15,7	cm^3/min
Deposition rate	123,2	g/min
MANUFACTURING TIME		
Set up time	10	min
Printing time	661,9	min
Pause time	102,6	min
Total time	774,5	min
Total time	12,9	h

APPENDIX E

Parameters	Value	Unit	
BTF_{WAAM}	1	/	assumed
t_{CAD}	60	min	assumed
t_{gcode}	60	min	assumed
$t_{substrate\_preparation}$	5	min	assumed
t_{WAAM}	774,5	min	calculated
t_{gcode_CNC}	30	min	assumed
t_{sawing}	5	min	assumed
$t_{CNC\_machining}$	309,8	min	assumed
$t_{inspection}$	15	min	assumed
m_{wire}	81,5	kg	calculated
$m_{substrate}$	1,5	kg	assumed
m_{part}	81,5	kg	calculated
$C_{operator}$	40,5	€/h	[5.8]
$C_{WAAM\_machine}$	30	€/h	[5.7]
$C_{substrate}$	5	€/kg	[5.7]
C_{wire}	8	€/kg	[5.11]
$C_{CNC\_machine}$	18,50	€/h	[5.7]

WITHOUT POST PROCESSING	
DESIGN COSTS	
$C_{design} = C_{operator} \cdot (t_{CAD} + t_{gcode})$	81,00
MANUFACTURING COSTS	
$C_{substrate\_preparation} = C_{operator} \cdot t_{substrate\_preparation}$	3,38
$C_{build\_job} = C_{WAAM\_machine} \cdot t_{WAAM}$	387,25
$C_{material} = m_{substrate} \cdot C_{substrate} + m_{wire} \cdot C_{wire}$	659,50
$C_{manufacturing}$	1050,125
INSPECTION COSTS	
$C_{inspection} = C_{operator} \cdot t_{inspection}$	10,13
TOTAL COSTS	
$C_{total} = C_{design} + C_{manufacturing} + C_{inspection}$	**1141,25**

WITH POST PROCESSING	
DESIGN COSTS	
$C_{design} = C_{operator} \cdot (t_{CAD} + t_{gcode})$	81,00
MANUFACTURING COSTS	
$C_{substrate\_preparation} = C_{operator} \cdot t_{substrate\_preparation}$	3,38
$C_{build\_job} = C_{WAAM\_machine} \cdot t_{WAAM}$	387,25
$C_{material} = m_{substrate} \cdot C_{substrate} + m_{wire} \cdot C_{wire}$	659,50
$C_{manufacturing}$	1050,13
POST PROCESSING COSTS	
$C_{gcode\_preparation} = C_{operator} \cdot t_{gcode\_CNC}$	20,25
$C_{CNC\_machining} = C_{CNC\_machine} \cdot t_{CNC\_machining}$	95,52
$C_{substrate\_removal} = C_{operator} \cdot t_{sawing}$	3,38
$C_{post\_processing}$	119,15
INSPECTION COSTS	
$C_{inspection} = C_{operator} \cdot t_{inspection}$	10,13
TOTAL COSTS	
$C_{total} = C_{design} + C_{manufacturing} + C_{post\_processing} + C_{inspection}$	**1260,40**

APPENDIX F

Parameters	Value	Unit	
C_{steel}	1	€/kg	[5.9]
C_{wire}	8	€/kg	[5.11]
$C_{welding\_machine}$	30	€/h	[5.7]
C_{welder}	40,5	€/h	[5.8]
$C_{operator}$	40,5	€/h	[5.8]
t_{CAD}	180	min	assumed
t_{sawing}	250	min	assumed
$t_{welding}$	200	min	calculated
travel speed (GMAW)	0,15	m/min	assumed
$t_{inspection}$	15	min	assumed
m_{wire}	5,89	kg	calculated/assumed
m_{steel}	136	kg	calculated/assumed

DESIGN COSTS		
$C_{design} = C_{operator} \cdot t_{CAD}$	121,50	
STEEL PLATES SAWING COSTS		
$C_{sawing} = C_{operator} \cdot t_{sawing}$	168,75	€
$C_{steel\_material} = C_{steel} \cdot m_{steel}$	136,00	€
$C_{steel\_plates\_sawing} = C_{sawing} + C_{steel\_material}$	304,75	
WELDING COSTS		
$C_{weld\_material} = C_{wire} \cdot m_{wire}$	47,10	€
$C_{welding} = C_{welder} \cdot t_{welding} + C_{welding\_machine} \cdot t_{welding}$	235,00	€
$C_{welding\_total}$	282,10	€
INSPECTION COSTS		
$C_{inspection} = C_{operator} \cdot t_{inspection}$	10,13	€
TOTAL COSTS		
$C_{total} = C_{design} + C_{sawing} + C_{welding\_total} + C_{inspection}$	718,48	€

APPENDIX G

Environmental impact category		Indicator eq.	€/kg	Environmental impact / kg	€
Abiotic Depletion, non fuel	(ADnf)	kg Sb eq	0,16	3,50E-06	3,05E-05
Abiotic Depletion, fuel	(ADf)	kg Sb eq	0,16	1,40E-02	1,22E-01
Global Warming Potential	(GWP)	kg CO2 eq	0,05	4,50E+00	1,23E+01
Ozone Layer Depletion	(ODP)	kg CFC-11 eq	30	9,00E-08	1,47E-04
Photochemical Oxidation Potential	(POCP)	kg C2H4 eq	2	1,30E-03	1,42E-01
Acidification Potential	(AP)	kg SO2 eq	4	2,40E-02	5,23E+00
Eutrophication Potential	(EP)	kg PO42- eq	9	8,30E-04	4,07E-01
Human Toxicity Potential	(HT)	kg 1,4-DB eq	0,09	2,30E+01	1,13E+02
Ecotoxicity Potential, Fresh water	(FAETP)	kg 1,4-DB eq	0,03	2,80E-02	4,58E-02
Ecotoxcity Potential, Marine water	(MAETP)	kg 1,4-DB eq	0,0001	6,20E+01	3,38E-01
Ecotoxicity Potential, Terrestrial environment	(TETP)	kg 1,4-DB eq	0,06	2,90E-02	9,48E-02
					131,46